DNA-PROTEIN CROSS-LINKING BY *BIS*-ELECTROPHILES

A DISSERTATION SUBMITTED
TO THE FACULTY OF THE GRADUATE SCHOOL OF THE
UNIVERSITY OF MINNESOTA BY

Rachel Lea Loeber

IN PARTIAL FULFILLMENT OF THE REQUIREMENTS FOR THE DEGREE OF
DOCTOR OF PHILOSOPHY

Dr. Natalia Tretyakova, Advisor

October 2008

ACKNOWLEDGMENTS

I would first like to thank my thesis committee, Dr. Colin Campbell, Dr. Shana Sturla, Dr. Yusuf Abul-Hajj, and my research advisor Dr. Natalia Tretyakova for their guidance and support throughout this project. Secondly, I wish to thank Dr. Karin Musier-Forsyth who served as my co-advisor from 2004-2006 while I was a trainee on the NIH Chemistry- Biology Interface Training Grant (T32-GM08700). I would also like to thank Dr. Daniel Liebler and Dr. Simona Codreanu (Mass Spectrometry Research Center, Vanderbilt University) for their hands-on training in shotgun proteomics, as well as members of the Tretyakova laboratory who contributed to the development of this work, including Mathur Rajesh, Danae Quirk Dorr, Melissa Goggin, Erin Michaleson-Richie, and Brock Matter. I would also like to acknowledge Bob Carlson for help preparing figures for publication, as well as Brian White for his assistance in molecular modeling. Lastly, I could not have completed the requirements for this degree without the support of family and friends, especially my husband Rob, my daughter Allison, and my parents Ray and Linda.

TABLE OF CONTENTS

Chapter **Page**

LIST OF TABLES

LIST OF FIGURES

LIST OF ABBREVIATIONS

5-IdU	5-iododeoxyuracil
6-TG	6-thioguanine
A	adenine
AGT	O^6-alkylguanine DNA alkyltransferase
Arg (or R)	arginine
BCNU	carmustine
BD	1,3-butadiene
BER	base-excision repair
C	cytosine
CCNU	lomustine
CHO	Chinese hamster ovary cell line
CID	collision-induced dissociation
Cys (or C)	cysteine
Cys-Gua-BD	1-(*S*-cysteinyl)-4-(guan-7-yl)-2,3-butanediol
Cys-N7G-EMA	*N*-[2-(*S*-cysteinyl)ethyl]-*N*-[2-(guan-7-yl)ethyl]methylamine
Cys-N7G-PBA	*N*-[2-(*S*-cysteinyl)ethyl]-*N*-[2-(guan-7-yl)ethyl]-*p*-aminophenylbutyric acid
DBE	1,2-dibromoethane
DEB	1,2,3,4-diepoxybutane
dG monoepoxide	N7-(2'-hydroxy-3',4'-epoxybut-1'-yl)-deoxyguanosine
DMSO	dimethylsulfoxide

DPC	DNA-protein cross-link
EB	3,4-epoxy-1-butene
EBD	3,4-epoxy-1,2-butanediol
EF-1α1	elongation factor 1-alpha 1
ESI^+	electrospray ionization, positive mode
EV	empty vector
FA	formaldehyde
FBS	fetal bovine serum
GAPDH	glyceraldehyde-3-phosphate dehydrogenase
GSH	glutathione
Gua (or G)	guanine
hAGT	human recombinant AGT
HAT	hypoxanthine-aminopterin-thymidine
HeLa	human cervical carcinoma cell line
His (or H)	histidine
HPLC	high performance liquid chromatography
***hprt* (and HPRT)**	hypoxanthine phosphoribosyltransferase – *gene and gene product*
HR	homologous recombination
HTH	helix-turn-helix
IR	ionizing radiation
IARC	International Agency for Research on Cancer
Ku	ATP-dependent DNA helicase subunit 2

Lys (or K)	lysine
Lys-N7G-EMA	*N*-[2-[*N*-(lysyl)ethyl]]-*N*-[2-(guan-7-yl)ethyl]methylamine
MS	mass spectrometry
MS/MS	tandem mass spectrometry
N7G-EMA-Cl	*N*-(2-chloroethyl)-*N*-[2-(guan-7-yl)ethyl]methylamine
N7G-PBA-Cl	*N*-(2-chloroethyl)-*N*-[2-(guan-7-yl)ethyl]-*p*-aminophenylbutyric acid
***O*^{6}-BG**	O^6-benzylguanine
***O*^{6}-mG**	O^6-methylguanine
PARP	poly (ADP-ribose) polymerase
Ref-1	DNA-(apurinic or apyrimidinic site) lyase
ROS	reactive oxygen species
SRM	selected reaction monitoring
SSB	single-stranded DNA binding protein
SSBR	single-strand break repair
Thy (or T)	thymine
TFA	trifluoroacetic acid
Tyr (or Y)	tyrosine
XRCC1	X-ray repair cross-complementary protein 1

I. LITERATURE REVIEW

1.1 DNA-Protein Cross-Linking: An Overview

A DNA-protein cross-link (DPC) is a type of DNA lesion that is created when a protein becomes covalently bound to DNA *(1)*. DNA-protein cross-linking generally occurs following exposure to a variety of chemical and physical agents. DPCs can also form as a result of endogenous exposure to reactive oxygen species and aldehydes. Because of the inherent complexity of DPC lesions and the inability to induce DPCs in the absence of other types of DNA damage (e.g. DNA monoadducts and DNA-DNA cross-links), the biological implications of DPCs are not well understood.

1.1.1 DPC Formation

DPCs are ubiquitous lesions formed by a wide variety of cytotoxic, mutagenic, and carcinogenic agents, environmental pollutants, industrial chemicals, physical agents such as IR and UV light, and physiological metabolites *(1)*. The chemistry and biology of DPCs is complex because different agents induce DPCs of varying structures and stability and can include many cellular proteins.

Among all DPC-inducing agents, formaldehyde is perhaps the most widely studied. Formaldehyde (FA) is a genotoxic chemical used in the production of thousands of consumer products, including building materials such as plywood, particle board, paints, carpets, and other textiles. As many of these materials off-gas FA-containing fumes, human exposure is widespread *(2)*. Numerous studies have shown that formaldehyde is mutagenic to mammalian cells, inducing primarily point mutations and

deletions *(3)*. Formaldehyde is reactive towards amine, thiol, hydroxyl, and amide groups present in DNA and proteins, and DPCs are the major class of FA-DNA lesions observed *(4)*. DPC formation by FA involves an initial reaction with an amino group of a DNA base (guanine, adenine, or cytosine) or an amino acid (lysine and arginine) to form a Schiff base, which then reacts with a second biomolecule to produce a cross-linked lesion. *In vivo* studies with rats and monkeys suggest that the rate of DPC formation is proportional to the tissue concentration of formaldehyde, allowing DPCs to serve as a biomarker of FA exposure *(5)*. As the major protein components of chromatin (and their location in close proximity to chromosomal DNA), histones are commonly found to form cross-links to DNA following formaldehyde exposure *(2)*. All five histone proteins, H1, H2A, H2B, H3, and H4, are capable of forming DPCs, with histones H1 and H3 displaying the greatest susceptibility *(4)*. Although the formation of DNA-histone cross-links is strongly correlated with tumorigenesis, the role of DPCs in the carcinogenesis of formaldehyde is unclear *(1;2;6)*.

Various metals and metalloids have also been shown to induce DPCs *(1)*. Exposure to chromium, nickel, and arsenic has been implicated in the induction of several types of cancers, including those of the lung, bladder, and liver *(7-9)*. Analyses of metal ion-induced DPCs demonstrate that they can be produced *via* oxidative mechanisms *(10)*. In addition, chromate can form DNA-protein complexes through a chelatable form of chromium *(8;10)*. At biologically-relevant doses, ~50% of chromium-induced adducts were the DNA-metal-protein complexes involving the side chains of cysteine, histidine, and glutamic acid *(8)*.

Exposure to UV and ionizing radiation (IR) can result in the formation of DPCs in addition to other types of DNA damage, including DNA monoadducts, strand breaks, and DNA-DNA cross-links *(1;11)*. Comparatively speaking, the amounts of DPCs in IR-exposed cells is higher (~150/cell) than the numbers of double-strand DNA breaks (20-40/cell) and DNA-DNA cross-links (~30/cell) *(11)*. When cells are subjected to IR-irradiation, free radicals can form *via* direct oxidation of DNA or proteins. In addition, IR can generate reactive oxygen species (ROS) such as highly reactive hydroxyl radicals *(1)*. Structural analysis of IR-induced DPCs by tandem mass spectrometry suggests covalent bond formation between the methyl group of thymine in DNA and either the C2 or C3 position of a tyrosine ring within a protein *(12)*. IR has been shown to induce DPCs in both aerated and hypoxic mammalian cells, but DPC formation is more prevalent in the absence of oxygen *(13-15)*.

DPCs can also form endogenously as a result of exposure to reactive oxygen species and lipid peroxidation *(16)*. As DNA is surrounded by and tightly associated with proteins that regulate cellular function, oxidation of either DNA or its associated proteins results in the formation of electron-deficient species and ultimately DPCs. ROS-mediated DPCs typically involve guanine residues within DNA and amino acid side chains of lysine, arginine, and tyrosine *(17)*. Burrows and colleagues have reported DPC formation following oxidation of synthetic oligodeoxynucleotides and model proteins, including the identification of a unusual tricyclic [4.3.3.0] lesion between 8-oxoguanosine and tyrosine *(18)*.

Endogenous aldehydes have been shown to induce DPCs *(1)*. Methylglyoxal (pyruvate aldehyde) is a metabolite that readily reacts with nucleic acids and proteins to

form DNA adducts, strand breaks, DNA-DNA cross-links, and DPCs *(19)*. Methylglyoxal-induced mutations in mammalian cells are predominantly deletions, but base-pair substitutions make up a significant portion (50 and 35% respectively). Glyoxal, a related endogenous aldehyde, also induces DPCs. In comparing the two aldehydes, glyoxal produces 10-fold fewer DPCs and 10-fold fewer frameshift mutations, suggesting a role for DPCs in methylglyoxal-mediated mutagenesis *(20)*.

Numerous chemotherapeutic drugs, including cisplatin, mitomycin C, and nitrosoureas, are known for their ability to cross-link biomolecules *(21-23)*. While the antitumor activity of these agents is generally attributed to the formation of DNA inter- and intrastrand cross-links, DPCs have been shown to form following drug treatment and may contribute to the cytotoxic effects of many of these agents. In the current work, the formation of DPCs by two representative types of *bis*-electrophiles was examined – 1,2,3,4-diepoxybutane (DEB) and antitumor nitrogen mustards (*see Section 1.3*).

1.1.2 DPC Repair

If left unrepaired DPCs can result in cytotoxicity and genotoxicity because of their blocking nature. However, DPC repair represents a significant challenge because bulky DPC lesions can block access of DNA repair proteins to the adducted nucleobase. Several types of cellular DPCs have been shown to be relatively long-lived, persisting through several rounds of DNA replication *(1;24;25)*. Thus, DPC-formation could result in permanent DNA damage if left unchecked. However, studies have shown that the majority of DPCs induced by exogenous agents are removed from the genome with time

(1). As described below, the mechanism(s) by which this occurs is highly dependent on the chemistry of the cross-link and on the specific cellular system.

Due to their bulk, many covalent DPCs are likely candidates for nucleotide excision repair (NER) - a pathway known for its ability to repair large, helix-distorting lesions *(26)*. Proteolysis is hypothesized to play a key role in the repair of DPCs by reducing the size of the protein component *via* enzymatic digestion *(27)*. Such proteolytic de-bulking yields a more amenable substrate for NER and other repair pathways *(2;26)*. Homologous recombination (HR) may also be involved in the repair of some types of DPCs *(28)*.

For aldehyde-induced DPCs, cross-linking can be reversed by hydrolysis of the lesion or by active repair *(1;2)*. For example, Quievryn and Zhitkovich examined the repair of formaldehyde-induced DPCs *in vitro* and in treated cells *(2)*. DPCs generated in formaldehyde-treated human cells displayed reduced half-lives as compared to the DPCs formed *in vitro* following incubation of histone H1 with calf thymus DNA, suggesting active repair of formaldehyde-induced DPCs *in vivo*. Further studies showed that the half-lives for formaldehyde-induced DPCs were similar in normal human cells and in human cells deficient in NER, suggesting that NER may not be involved in DPC removal. Interestingly, incubation of both normal and NER-deficient cells with proteasome inhibitor lactacystin resulted in the loss of DPC repair, which is indicative of an active repair process involving proteolytic degradation of formaldehyde-induced DPCs *(2)*.

Nakano *et al.* recently examined the roles of NER and HR in the repair of structurally defined oxidative DPCs *in vitro* and in bacterial cells *(29)*. While NER was

involved in the removal of cross-linked proteins of relatively low molecular weights (<14 kDa), proteolytic degradation of DPCs did not contribute to DPC repair as *E. coli* cells deficient in cytosolic ATP-dependent proteases (counterparts of eukaryotic proteasomes) displayed similar results in terms of cell survival. Instead of NER-coupled proteolysis, repair of DPCs involving oversized proteins (>14 kDa) were processed exclusively by HR *(29)*.

A recent study examining the repair of chromium-induced DNA damage suggests that NER is involved in the removal of this type of DPC *(30)*. However, this study employed a single cysteine residue cross-linked to plasmid DNA following treatment with potassium chromate, leaving a possibility that removal of a cross-linked protein or peptide involves a different mechanism.

The potential role of NER in the repair of IR-induced lesions has been examined by several groups *(31-33)*. Under hypoxic conditions, NER-deficient (XPF^-) hamster cells removed ~20% of their DPCs in a 24 hour period while the corresponding wild-type cells removed ~80% as measured by alkaline elution *(33)*. In contrast, hamster cells deficient in XPB and XPD genes did not display radiosensitivity under hypoxic conditions, suggesting that IR-induced DPCs are not repaired by the NER pathway *(34)*. Further studies are needed to identify the role of NER and other repair mechanisms in the removal of IR-induced DPCs.

Sancar and colleagues proposed a model for the repair of covalent DPCs *(27)*. In this model, DPC repair is coupled to replication-dependent proteolysis of cross-linked proteins. Once a DPC is encountered, a component of the stalled replication machinery sends a signal for proteolysis of the covalently attached protein to a peptide, followed by

recruitment of proteins involved in NER. The resulting DNA-peptide cross-link is then removed *via* nucleotide excision repair. Although this model of repair is supported experimentally for some types of cross-links, it may not apply to all kinds of DPCs. HR is also likely to contribute to the repair/tolerance of DPCs *in vivo (29)*. Further work is needed to better understand how cells protect themselves form these toxic lesions.

1.1.3 Biological Implications of DPC Formation

DPCs are likely to have a negative impact on cell viability because they are bulky, helix-distorting lesions that interfere with crucial cellular processes including DNA replication, transcription, recombination, and chromatin remodeling *(1)*. However, because all known DPC-inducing agents also produce other types of DNA damage, a direct link between DPC formation and carcinogenesis/mutagenesis has not been made *(1)*. Although correlations involving DPC formation and genetic damage have been reported *(5)*, the biological consequences of DPCs remain unclear. In addition to the ill effects of DPCs, lesions resulting from enzymatic repair of DPCs (including DNA strand breaks and abasic sites) could also contribute to their genotoxicity *(6)*.

1.2 Methods of Detecting DNA-Protein Cross-Links

To date, several different approaches have been used in the study of DPCs. While early researchers set out to investigate the association of cellular proteins with DNA following exposure to a given cross-linking agent, more recent work has focused on identifying specific proteins that become cross-linked to DNA. The following sections

discuss some of the methods that have been employed by researchers in the study of DPCs.

1.2.1 Gel-Shift Assay

One of the simplest techniques for detecting DPCs *in vitro* is through the use of gel-shift assays. As the name implies, DPCs are observed as new bands that appear to have "shifted" from their original positions upon one-dimensional separation of protein mixtures on a denaturing gel. In this type of experiment, radiolabeled double-stranded oligodeoxynucleotides are incubated with a protein in the presence or absence of cross-linking agent, and the resulting mixture is separated *via* denaturing gel electrophoresis *(35)*. Following detection of the radio-labeled DNA by autoradiography, oligodeoxynucleotides containing covalently bound proteins migrate slower than free DNA due to the added bulk of the cross-link. These experiments must be performed under conditions that cause dissociation of any non-covalent DNA-protein complexes.

Gel-shift assays have been successfully employed by many different groups in the study of DPC formation by numerous *bis*-electrophiles. Cross-linking of DNA to high mobility group (HMG) proteins, transcription factors, and replicative enzymes by various platinum compounds has been clearly demonstrated using this method *(35;36)*. Similar assays have been used in our own laboratory to detect cross-linking between the DNA repair protein O^6-alkylguanine DNA alkyltransferase (AGT) and ^{32}P-labeled double-stranded oligodeoxynucleotides in the presence of DEB *(37)* and nitrogen mustards *(38)*. Results of these assays can be found in sections 2.4.1 and 3.4.1 respectively.

The greatest disadvantage of the gel-shift assay is that it cannot be used to examine cross-linking in a more complex system (such as cell extracts or drug-treated cells). Furthermore, it does not provide any information regarding the cross-link structure. Nevertheless, this methodology provides a simple and inexpensive way to investigate DPC formation *in vitro*.

1.2.2 Alkaline Elution

During the 1970s, the technique of alkaline elution was developed by Kohn and colleagues to aid in the study of DNA damage *(39)*. In this biophysical technique, measurement of DNA damage is based on the rates at which DNA strands migrate through membrane filters under alkaline conditions. Alkaline elution can be used to study single-strand DNA breaks, alkali-labile sites, interstrand DNA-DNA cross-links, as well as DPCs. Measurement of DPCs using alkaline elution is performed using conditions that favor adsorption of proteins to the filter *(39)*.

In a typical experiment to detect DPCs by alkaline elution, cells are metabolically labeled with [^{14}C]thymidine prior to manipulation *(39)*. Radiolabeling allows for the facile detection of cellular DNA *via* scintillation counting throughout the analysis. Following treatment with a DPC-inducing agent, the cells are exposed to x-rays to produce single-strand DNA breaks. The cells are then deposited onto a membrane filter, lysed using a detergent, and an alkaline solution (pH 12) is pumped slowly through the filter. Fractions are collected to determine the rate with which DNA elutes from the filter. DNA segments with covalently-bound proteins display a higher affinity for the filter and are retained, while unbound DNA strands pass through the filter. From the fraction of

DNA retained on the filter and the single-strand break frequency produced by the x-ray dose, the frequency of DPC formation is calculated.

As several agents that induce DPCs also produce a significant number of DNA-DNA interstrand cross-links, additional experiments are needed to distinguish between the two types of DNA damage by alkaline elution. Like DPCs, interstrand DNA-DNA cross-links pass slowly through the filter due to their increased size. As a result, DPCs and interstrand DNA-DNA cross-links display similar elution profiles. To determine if proteins are present, proteolytic enzymes such as proteinase K can be added to the cell lysate prior to elution *(39)*. If a DPC is present, the addition of a protease should lead to a reduction in DNA retention, since the degraded protein will no longer be able to bind effectively to the filter. DNA-DNA cross-links, on the other hand, will be unaffected by protease treatment and will display similar elution profiles. Kohn and colleagues have demonstrated DPC formation *via* alkaline elution following cellular exposure to several *bis*-electrophiles, including cisplatin, nitrosoureas, and nitrogen mustards *(21;40-42)*. However, all of these agents also induce significant amounts of DNA-DNA cross-links which are more strongly correlated with cytotoxicity.

While alkaline elution is a sensitive method for detecting the formation of DPCs in cells treated with *bis*-electrophiles, this technique does not provide any information regarding the identities of the proteins involved or about the structures of the cross-links. It is also somewhat time-consuming, and thus the number of samples that can be analyzed is limited.

1.2.3 Comet Assay

Comet assay is another biophysical technique that has been successfully employed for the detection of DPCs *(6;43;44)*. Similar to alkaline elution, the comet assay detects the presence of DNA-DNA cross-links and DPCs *via* reduction in DNA migration. For the detection of DPCs using the comet assay, cells are incubated in the presence or in the absence of cross-linking agent. Following γ-irradiation to induce DNA strand breaks, the cells are suspended in agarose and placed on a microscope slide. Following cell lysis, the slide is placed in an alkaline buffer and electrophoresis is performed to separate cellular DNA. The resulting slides are stained with ethidium bromide and visualized using a fluorescent microscope. Intact DNA does not migrate through the agarose, subsequently forming the comet's "head". DNA that has been damaged by exposure to γ-rays (and is thus shorter in length) separates away from the head, forming the comet's "tail". The extent of irradiation-induced DNA migration - referred to as "tail moment" - corresponds to the length of the tail. When a DNA-DNA or DNA-protein cross-link is present, tail movement is reduced. The two types of DNA damage can be distinguished by incorporating a proteolytic step. If a DPC is present, protease treatment prior to electrophoresis should enhance tail moment *(44)*.

Using the comet assay, Speit and colleagues demonstrated DPC formation following cellular exposure to formaldehyde and chromate *(6;43)*. In contrast, the antitumor drugs cisplatin and mitomycin C yielded significant amounts of cross-links which were resistant to protease treatment, indicating that they were mainly DNA-DNA cross-links *(44)*.

For the detection of DPCs in cells, the comet assay is a fast, simple, inexpensive method that is capable of conveying the damaging effects of *bis*-electrophiles at the level of a single cell. Like alkaline elution, a disadvantage of the comet assay is that it does not provide any information about cross-link structure and does not identify the cross-linked proteins.

1.2.4 Potassium-SDS Precipitation

Unlike the previously mentioned techniques which are only capable of detecting DPCs *in vitro* or in cell culture, a breakthrough method was developed in the early 1990's by Costa and colleagues for the detection of DPCs *in vivo (45)*. Through the addition of potassium chloride to cell/tissue lysates containing sodium dodecyl sulfate (SDS), it is possible to selectively separate DPCs from cellular DNA *via* low-speed centrifugation *(45)*. As SDS binds tightly to proteins but not to DNA, all proteins and detergent-resistant DNA-protein complexes co-precipitate, leaving unbound DNA in the supernatant. Thus, the amount of SDS-precipitable DNA directly correlates to DPC formation.

To analyze DPCs using potassium-SDS precipitation, cells/tissues are isolated, washed, and lysed with SDS. The lysates are passed through a syringe needle several times in order to shear the chromosomal DNA, and potassium chloride is added to initiate precipitation. Following a brief incubation at 65 ^{o}C, the lysates are centrifuged to pellet cellular proteins, along with any DPCs. To release protein-bound DNA, the protein pellet is subjected to proteolysis using proteinase K, followed by a final centrifugation step. The supernatant (containing the once protein-bound DNA) is recovered, and the DNA is quantified by UV spectrophotometry or a similar technique.

Potassium-SDS precipitation has been used to detect DPCs induced by chromate, cisplatin, and formaldehyde in cultured cells *(2;45;46)*. It has also proved successful in the study of DPCs formed *in vivo* following environmental exposure to cross-linking agents. Levels of DPCs in human lymphocytes from Bulgarian chrome platers following occupational exposure to hexavalent chromium correlated well with blood chromium levels, suggesting that DPCs can serve as a biomarker of chromate exposure *(8;47)*.

Although potassium-SDS precipitation allows for the detection of DPCs formed *in vivo*, it does not provide any information regarding the structures of the cross-linked lesions and does not identify the proteins involved.

1.2.5 Mass Spectrometry

In recent years, mass spectrometry has proven to be a useful tool for the identification and characterization of DNA-DNA cross-links induced by a variety of bifunctional agents *(48-52)*. As many of these cross-linking agents also induce DPCs, mass spectrometry-based approaches have also been utilized in the study of these conjugates *(53)*. Although the vastly different physico-chemical properties of nucleic acids and peptide entities present in such heteroconjugates make mass spectrometric analysis of these lesions quite challenging, numerous groups have successfully examined a wide variety of DPCs using mass spectrometry.

Wong and colleagues employed UV cross-linking and HPLC-ESI$^-$-MS to identify DNA-protein complexes of M.*Eco*RI and double-stranded oligodeoxynucleotides containing 5-iododeoxyuracil (5-IdU) in place of thymine adjacent to the target adenine in the recognition sequence (5'-GGCG**GAATTC**GCGG-3' → 5'-GGCG**GAA-5-IdU-**

TCGCGG-3') *(54)*. Irradiation of the complex at 313 nm for 1 min resulted in >60% cross-linking, and no protein degradation was observed under these conditions. Upon HPLC-ESI$^-$-MS analysis, unmodified M.*Eco*RI gave rise to an envelope of ions between *m/z* 1150 and 1700, corresponding to the +32 to +23 charge states. In contrast, ESI$^+$-MS analysis of the DNA-M.*Eco*RI complex generated an envelope of ions between *m/z* 1200 and 1800, corresponding to the +35 to +25 charge states. Deconvolution of the mass spectra for M.*Eco*RI and the DNA-M.*Eco*RI complex yielded masses of 37 916 and 42 243 Da respectively. The mass of the DNA-M.*Eco*RI complex was consistent with the presence of M.EcoRI linked to the single-stranded oligodeoxynucleotide 5'-GGCG**GAA-5-IdU-TC**GCGG-3' minus iodine (*M* = 4329.1 Da) *(54)*.

In a more recent study, the same group set out to identify which amino acid residues of M.*Eco*RI were taking part in UV-mediated cross-linking to duplex DNA *(55)*. Upon tryptic digestion, DNA-peptide cross-links were separated from non-cross-linked peptides by anion exchange chromatography, and ESI$^-$-MS analysis revealed the presence of two peptide-oligodeoxynucleotide cross-links with masses of 6450.0 and 6003.8 Da. The major cross-linked species (6450.0 Da) corresponded to tryptic peptide GVSGFIVPEHYELYGTEAR covalently bound to the single-stranded oligodeoxynucleotide 5'-GGCG**GAA-5-IdU-TC**GCGG-3', while the minor species (6003.8 Da) corresponded to the 5-IdU-containing oligodeoxynucleotide cross-linked to the photocleaved peptide IVPEHYELYGTEAR. To confirm amino acid sequences of the cross-linked peptides, the purified cross-linked adducts were subjected to automated peptide sequencing by Edman degradation. Two peptide sequences corresponding to amino acid residues 191-205 and 196-209 of M.*Eco*RI (GVSGFIVPEHYEL**X**G and

IVPEHYEL**X**GTEAR) were identified, where **X** represents the cross-linked amino acid. The cross-linking site was mapped to Tyr^{204}. This ESI-MS method displayed good sensitivity and mass accuracy, identifying ~10-50 pmol of the cross-linked peptide-oligonucleotide adducts.

In a similar study, Steen *et al.* employed four different mass spectrometry-based strategies to characterize UV-mediated cross-links between *E. coli* single-stranded DNA binding protein (SSB) and a 5-iodouracil-containing DNA oligodeoxynucleotide *(56)*. DPC isolation methods were optimized to eliminate the need for sample purification by HPLC or gel electrophoresis prior to MS analysis. Following UV-mediated cross-linking, cross-linking reactions were subjected to either SDS-PAGE, denaturing PAGE, solution digestion with proteinase K, or solution digest with trypsin and phosphodiesterase I. MALDI-TOF analysis of the crude reaction mixture following digestion with proteinase K lead to the identification of two SSB peptides cross-linked to DNA: $T^{52}EWHR^{56}$ and $K^{87}WTDQ^{91}$. Nanospray tandem mass spectrometry of tryptic/nuclease digests was then employed to determine which amino acid residues were involved in photochemical cross-linking to the oligodeoxynucleotide. Using a quadrapole-TOF tandem mass spectrometer, Trp^{54} and Trp^{88} of SSB were identified as the sites of cross-link formation. Although the yields of UV cross-linked DPCs did not exceed 15%, less than 100 pmol of SSB was required for MS/MS analysis *(56)*, a significant improvement in sensitivity over previous methods.

In addition to its use in the study of DNA-protein interactions, mass spectrometry has also been successfully employed to investigate DPCs formed following exposure to bifunctional alkylating agents. Liu *et al.* reported that incubation of human recombinant

O^6-alkylguanine DNA alkyltransferase (AGT) with calf thymus DNA in the presence 1,2-dibromoethane (DBE) resulted in the formation of covalent AGT-DNA complexes *(57)*. To determine which amino acid residue(s) of AGT is/are involved in cross-linking to DNA, the protein was digested with trypsin, and the resulting peptides were analyzed using a MALDI-TOF mass spectrometer. In the MALDI-TOF spectrum, a peak with an *m/z* of 1493 was observed which corresponds to the AGT tryptic peptide $G^{136}NPVPILIPCHR^{147}$ cross-linked to a guanine base. HPLC-ESI^+-MS/MS analysis of a similar reaction mixture in which AGT was incubated with DBE in the presence of a 16-mer double-stranded oligodeoxynucleotide followed by neutral thermal hydrolysis and tryptic digestion revealed the presence of a doubly-charged ion at 746.9 *m/z* corresponding to that same peptide cross-linked to a guanine residue. The CID mass spectrum of this peptide-guanine conjugate yielded *b* and *y* series ions which mapped the cross-linking site to Cys^{145}, the active site residue responsible for alkyl transfer by AGT *(57)*.

More recently, mass spectrometry has been used to detect DPCs in cultured cells. In the early 1990's, Olinski and colleagues reported the formation of DPCs between thymine in DNA and tyrosine residues within proteins in chromatin of γ-irradiated and H_2O_2-treated human cells *(58)*. Chromatin isolated from K562 human chronic myelogenous leukemia cells was hydrolyzed, derivatized with trimethylsilane, and analyzed by gas chromatography/mass spectrometry. Selective ion monitoring analysis of derivatized hydrolysates revealed the presence of 3-[(1,3-dihydro-2,4-dioxopyrimidin-5-yl)-methyl]-L-tyrosine. A linear dose-yield relationship was obtained in the range of 8.7 to 82 Gy ($J \cdot Kg^{-1}$), after which adduct formation reached saturation. Amounts of Thy-Tyr

cross-links in irradiated cells were ~4-fold higher than the background levels. Treatment of cells with H_2O_2 also resulted in the formation of Thy-Tyr cross-links in a dose-dependent manner. Addition of dimethylsulfoxide and *o*-phenanthroline to the culture medium afforded partial inhibition of cross-link formation, while addition of catalase inhibitor potassium cyanide prior to H_2O_2 exposure resulted in an increase in cross-link levels, suggesting that DPC formation in cellular chromatin results from the reaction of thymine and tyrosine radicals *(58)*.

Murray and colleagues at the University of Alberta developed a method for the isolation of DPCs from treated cells (the DNAzol-strip DPC isolation method), which has been successfully coupled to mass spectrometry-based proteomics allowing for the identification of proteins cross-linked to DNA by formaldehyde and IR *(11;59)*. To isolate DPCs using this method, total genomic DNA is first recovered *via* treatment with DNAzol®, a proprietary chaotrope/detergent mixture that lyses cells, hydrolyzes RNA, and dissociates non-covalent DNA-protein complexes *(59)*. The DNA is then further "stripped" of non-covalently bound proteins by washing with SDS, urea, and sodium chloride. Following digestion of DNA with DNAses, the cross-liked proteins are separated by SDS-PAGE, excised from the gel, and digested with trypsin. Upon MS/MS sequencing of tryptic peptides, the resulting spectra are matched against primary sequence data in a protein database using an analytical program such as SEQUEST or MASCOT *(60)*. When a minimum of three unique peptides from a protein have been assigned using, a protein identification is made.

Using the DNAzol-strip DPC isolation method coupled to tandem mass spectrometry, Barker *et al*. identified 29 proteins that had become cross-linked to DNA

following cellular exposure to IR *(11)*. Among the proteins identified by MS were structural proteins, transcription regulators, RNA-splicing components, stress-response proteins, cell cycle regulatory proteins, and GDP/GTP-binding proteins.

Compared to the other DPC detection methods described above, mass spectrometry has many advantages. Not only can MS identify unknown proteins that are cross-linked to DNA, it can also provide information regarding the chemical nature of the cross-link by identifying amino acids and nucleobases involved. Finally, the high sensitivity of MS, especially when coupled to a DPC enrichment technique like the DNAzol-strip method, allows for the detection of DPCs that may not be observed using other methods.

In our laboratory, mass spectrometry has been used extensively for the characterization of AGT-DNA cross-links induced by DEB and antitumor nitrogen mustards (*see Chapters II and III*) *(37;38)*. It has also been employed for the identification of nuclear proteins that cross-link DNA oligonucleotides in the presence of the nitrogen mustard mechlorethamine (*see Section 6.4.1*).

1.3 *Bis*-Electrophiles Examined in this Work

For our studies on DPC formation, cross-linking induced by two different types of agents was investigated: a representative *bis*-epoxide, 1,2,3,4-diepoxybutane (DEB), and representative drugs from the group of antitumor alkylating agents known as nitrogen mustards. The following sections address the reactivity of these compounds towards biomolecules *in vitro* and *in vivo*, as well as their propensity to form DPCs.

1.3.1 1,2,3,4-Diepoxybutane

1,2,3,4-Diepoxybutane (DEB) is the key carcinogenic metabolite of 1,3-butadiene (BD), a flammable, colorless gas used in the production of synthetic rubber and thermoplastic resins *(61)*. BD is obtained through vapor-phase cracking of petroleum at temperatures in excess of 700 °C *(62)*, and several billion pounds of BD are produced in the United States each year *(63)*. It is also present in automobile exhaust *(64)* and cigarette smoke *(65;66)*. Based on epidemiological evidence and the results of animal studies, BD has been classified as a probable human carcinogen by the International Agency for Research on Cancer (IARC) *(67)*. Chronic exposure of industrial workers to BD is believed to result in genotoxic effects *(68-70)* and is correlated with an increased incidence of leukemia *(71;72)*.

During DEB formation upon metabolic activation, BD is initially oxidized by cytochrome P450s CYP2E1 and CYP2A6 to form 3,4-epoxy-1-butene (EB), which can then undergo hydrolysis to form 1-butene-3,4-diol or further epoxidation by CYP2E1 or CYP3A4 to yield DEB (*Scheme 1.1*) *(67;73)*. *R,R*-, *S,S*-, and *meso*-DEB are all produced metabolically from BD, but studies indicate that the *S,S* isomer is the most genotoxic *(74-76)*. Interestingly, *S,S*-DEB is thought to be the active form of Ovastat (L-threitol-1,4-bismethanesulfonate), a drug used clinically for the treatment of advanced ovarian cancer *(77-79)*.

Although DEB is a relatively minor metabolite of BD, experimental evidence suggests that it is responsible for many of the adverse effects associated with BD exposure. Biological studies indicate that DEB is 50 to 100-fold more mutagenic than its monoepoxide analogs *(80;81)*, likely due to DEB's ability to induce DNA-DNA and

Scheme 1.1 Metabolism of 1,3-butadiene to DNA-reactive epoxides

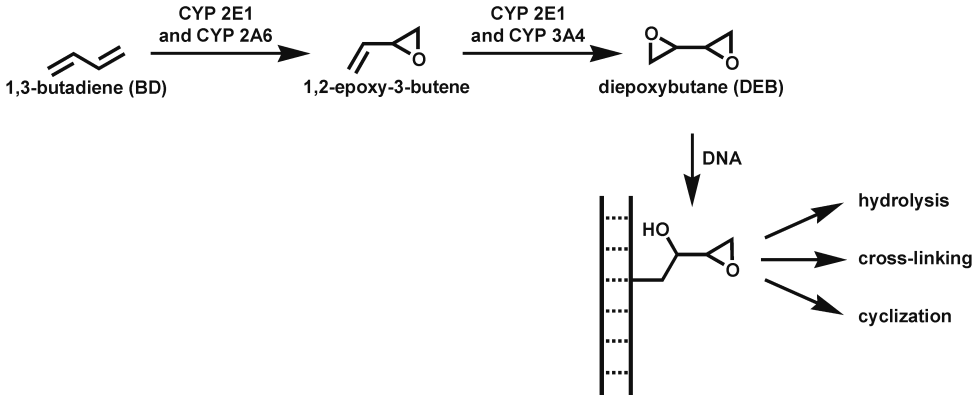

DNA-protein cross-links. DEB-mediated DNA-DNA cross-linking has been extensively studied in our laboratory employing a variety of methods including UV spectrophotometry, NMR spectroscopy, and tandem mass spectrometry to elucidate cross-link structures *(48;82;83)*. Upon exposure of double-stranded DNA to DEB, the major cross-link formed is a guanine-guanine conjugate identified as 1,4-*bis*-(guan-7-yl)-2,3-butanediol *(82;84)*. In addition to reacting at the N7 position of guanine, DEB is has also been shown to alkylate the N1, N3, N7, and N6 positions of adenine to yield a variety of guanine-adenine cross-links *(83)*.

As depicted in *Scheme 1.1*, initial DNA alkylation by DEB produces primarily N7-(2'-hydroxy-3',4'-epoxybut-1'-yl)-guanine monoadducts *(85)*. If not hydrolyzed, the remaining epoxide can react with a second nucleophilic site to form a bifunctional adduct or cyclic lesion *(82;86)*. While the ability of DEB to form both inter- and intrastrand DNA-DNA cross-links has been well established *(48)*, little was known regarding its propensity to cross-link DNA to protein. Thus, the ability of DEB to induce DPCs *in vitro* was investigated in our laboratory (*see Chapters II and IV*).

1.3.2 Antitumor Nitrogen Mustards

Among all cytostatic drugs, alkylating agents still rank as some of the most valuable chemotherapeutics in the treatment of cancer *(87)*. Chemically, alkylating agents are divided into five different groups: nitrogen mustards, ethylenimines, alkyl sulfonates, triazenes, and nitrosoureas *(87)*. Due to their relevance in the current work, the remainder of this section will focus on nitrogen mustards.

During World War I, it was observed that victims of mustard gas often exhibited leucopenia in addition to other symptoms, suggesting enhanced biological activity of alkylating agents in rapidly proliferating tissues *(88)*. In World War II, nitrogen mustards were developed as part of a program to design new and improved chemical warfare agents. Since the 1940s, nitrogen mustards have been a mainstay in cancer chemotherapy *(89)*.

Biological efficacy of nitrogen mustards is closely related to the reactivity of the two chloroethyl groups, which is in turn linked to the basicity of the corresponding amine *(87)*. Substitution of electrophilic groups at the amino nitrogen reduces its basicity, thus reducing the drug's reactivity and increasing its half-life.

The mechanism by which nitrogen mustards exert their cytotoxic effects is through the alkylation of biomolecules and is believed to include a two-step process (*Scheme 1.2*). Nucleophilic displacement of chloride by the amine nitrogen forms a highly reactive aziridinium ion, which can then react with nucleophilic sites in DNA and proteins. The aziridinum ion also reacts readily with water and glutathione (GSH) to yield hydrolysis products and GSH conjugates *(87;90;91)*.

Mechlorethamine (*Figure 1.1*), the first nitrogen mustard drug developed, has been used clinically for the treatment of cancer for the past 60 years *(89)*. Mechlorethamine is delivered intravenously in combination with other drugs primarily for the treatment of advanced Hodgkin's disease *(87)*. Because of its high reactivity and the resulting off-target toxicity, analogs based upon the structure of mechlorethamine have been developed that display a reduced reactivity and an increased selectivity towards tumor cells. By replacing the methyl group of mechlorethamine with a

Scheme 1.2 Reactivity of nitrogen mustards towards cellular nucleophiles

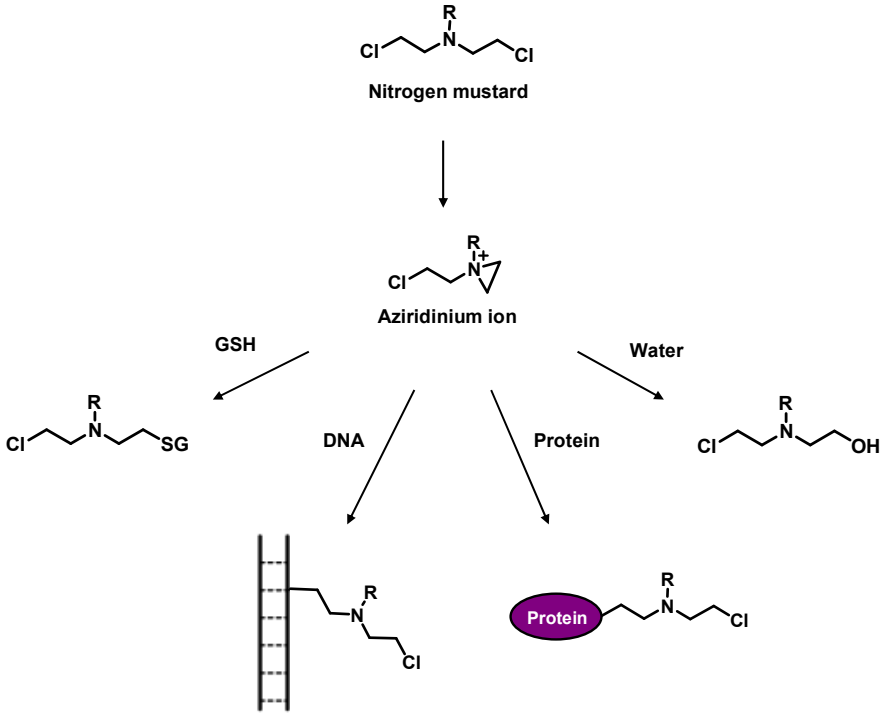

Figure 1.1 Chemical structures of nitrogen mustards

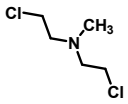

Mechlorethamine

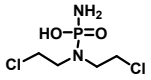

Phosphoramide mustard

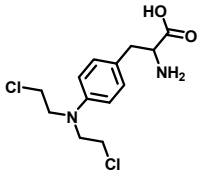

Melphalan

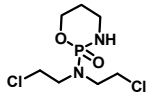

Cyclophosphamide

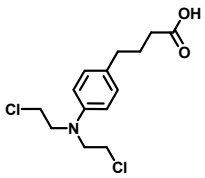

Chlorambucil

substituted benzene ring, the drug chlorambucil (*Figure 1.1*) was developed which displays reduced a reactivity/toxicity *(87)*. Chlorambucil is used alone and in combination therapy for the treatment of chromic lymphocytic leukemia, malignant non-Hodgkin's lymphomas, and advanced Hodgkin's disease *(87)*.

Melphalan (also known as phenylalanine mustard) is the L-isomer of the phenylalanine derivative of mechlorethamine (*Figure 1.1*) *(87)*. Designed to resemble phenylalanine (an amino acid precursor of melanin), it was hoped that it would selectively target melanoma cells. Today, melphalan is used mainly for the treatment of multiple myeloma and ovarian carcinoma. Unlike chlorambucil which enters cells primarily *via* passive diffusion *(92)*, melphalan is actively transported into cells by two different systems that normally engage in the shuttling of amino acids *(93)*. As a result, intracellular concentrations of melphalan are typically much higher as compared to chlorambucil.

In further attempts to target nitrogen mustard compounds to tumor cells, cyclophosphamide was developed (*Figure 1.1*). Although it was originally hoped that cyclophosphamide would be specifically activated by tumor enzymes, it was later found to be activated mainly through hydroxylation by hepatic cytochrome P450s belonging to the 2B and 2C families *(87;94)*. Following hydroxylation of cyclophosphamide to yield 4-hydroxycyclophosphamide, this hydroxylated species equilibrates with the ring-opened aldophosphamide which spontaneously decomposes to phosphoramide mustard (*Figure 1.1*) and acrolein. While phosphoramide mustard possesses DNA-alkylating activity and is considered the therapeutically-relevant metabolite of cyclophosphamide, it cannot readily enter cells. Thus, it is believed that 4-hydroxycyclophosphamide acts as a carrier

molecule to transport phosphoramide mustard across cell membranes *(95)*. Clinically, cyclophosphamide is used in the treatment of a variety of neoplastic conditions, including Hodgkin's disease, malignant lymphomas, leukemia, multiple myeloma, neuroblastoma, retinoblastoma, as well as ovarian and breast carcinomas *(87)*.

As each of the nitrogen mustard drugs mentioned above contains two reactive chloroethyl groups, these compounds are all capable of reacting with two nucleophilic sites within DNA or proteins, giving rise to DNA-DNA and DPCs *(96)*. DNA-DNA cross-linking by nitrogen mustards has been well characterized and is believed largely responsible for their antitumor effects. Like DEB, nitrogen mustards react primarily with the N7 position of guanine residues in duplex DNA *(96-99)*. However, they are also capable of reacting at the N1, N3, N^6, and N7 positions of adenine to form a variety of inter- and intrastrand guanine-guanine, guanine-adenine, and adenine-adenine cross-links *(50)*.

In contrast to DNA monoadducts and DNA-DNA cross-links, very little is known regarding the potential contribution of DNA-protein cross-linking in nitrogen mustard-mediated cytotoxicity. Although previous work has demonstrated DPC formation following cellular exposure to mechlorethamine and melphalan *via* alkaline elution, no information was obtained in regards to cross-link structure or protein identities *(41;100)*. In the current work, the ability of nitrogen mustards to form DPCs was examined *in vitro* using gel-shift assays, tandem mass spectrometry, and Western blot analysis (*see Chapters III, IV, and VI*).

1.4 O^6-Alkylguanine DNA Alkyltransferase: A Probable Target for DNA-Protein Cross-Linking

O^6-Alkylguanine DNA Alkyltransferase (AGT) is a DNA repair protein responsible for the removal of alkyl lesions from the O^6-position of guanine *(101)*. Through the irreversible transfer of the O^6-alkyl group to an active site cysteine, AGT prevents mutations and apoptosis resulting from alkylation damage to guanines by environmental toxins and chemotherapeutic agents *(102-106)*. Since AGT expression can result in tumor resistance to commonly used anti-cancer drugs, inhibitors of AGT are in development *(107)*.

1.4.1 Structure of AGT Protein

Human AGT is a relatively small protein (~21,600 Da) comprised of two distinct domains – an N-terminal domain (residues 1-85) and a C-terminal domain (residues 86-207). As indicated by the crystal structure of human AGT *(108)*, the N-terminal domain consists of a four-stranded anti-parallel β-sheet, a single α-helix, and a 3_{10}-helix to form an α/β-roll. Compared to Ada (the AGT homolog in *E. coli*) *(109)*, the human protein contains a solvent-exposed and disordered loop immediately following β3 (residues 36-44) which corresponds to the first α-helix of Ada. A zinc ion with tetrahedral coordination to Cys^5, Cys^{24}, His^{29}, and His^{85} lies on the active site face, bridging three of the four strands of the anti-parallel β-sheet. Located ~20 Å from catalytic Cys^{145}, the presence of this zinc atom is thought to help stabilize the interface between the N- and C-terminal domains *(108)*.

The C-terminal domain of AGT consists of a short two-stranded parallel β-sheet and five α-helicies that houses the protein's active site and DNA-binding motif *(108)*. Near the bottom of a solvent-accessible grove lies catalytic Cys^{145}, which is part of the active site sequence IPCHRV and is highly conserved between species. Adjacent to the active site pocket is the DNA-binding domain which interacts with double-stranded DNA *via* a helix-turn-helix (HTH) motif. Other DNA-binding proteins with the HTH motif are often found to bind duplex DNA through the major groove. AGT, however, has been shown to bind DNA through the minor groove in an unprecedented mechanism *(110)*. As observed in the crystal structure of wild-type AGT cross-linked to a double-stranded oligodeoxynucleotide by means of the mechanism-based inhibitor N^1O^6-ethanoxanthosine (*Figure 1.2*), the second recognition helix (Ala^{127}-Gly^{136}) of the HTH binds deep within the minor groove while the first recognition helix (Tyr^{114}-Ala^{121}), while the preceding helix (Phe^{94}-Val^{105}) interacts with the phosphate backbone through helix dipoles *(110)*. Upon binding to DNA, the structure of AGT is essentially unchanged. Instead, DNA structure is significantly affected. AGT binding results in the widening of the minor groove by ~3 Å and bending of the DNA ~15^o away from the protein. As discussed below, these structural changes facilitate the anzymatic activity of AGT by flipping the alkylated nucleotides out of the DNA stack to enter the protein active site.

1.4.2 Biological Function of AGT

Within the cell, repair of O^6-alkylguanine lesions occurs almost entirely through the action of the AGT protein *(111)*. AGT has been conserved over the course of

Figure 1.2 Crystal structure of human AGT bound to DNA (PDB 1T39) *(110)*. A recognition helix of AGT (residues 127-136, shown in aqua) binds deep within the minor groove allowing the side chain of Arg^{128} (shown in white) to intercalate into the helix. Along with Tyr^{114} (green), the substrate guanine is flipped out of the base stack and into the protein's active site where Cys^{145} (yellow) is ideally placed to carry out alkyl transfer. This figure was generated using the molecular modeling environment Maestro.

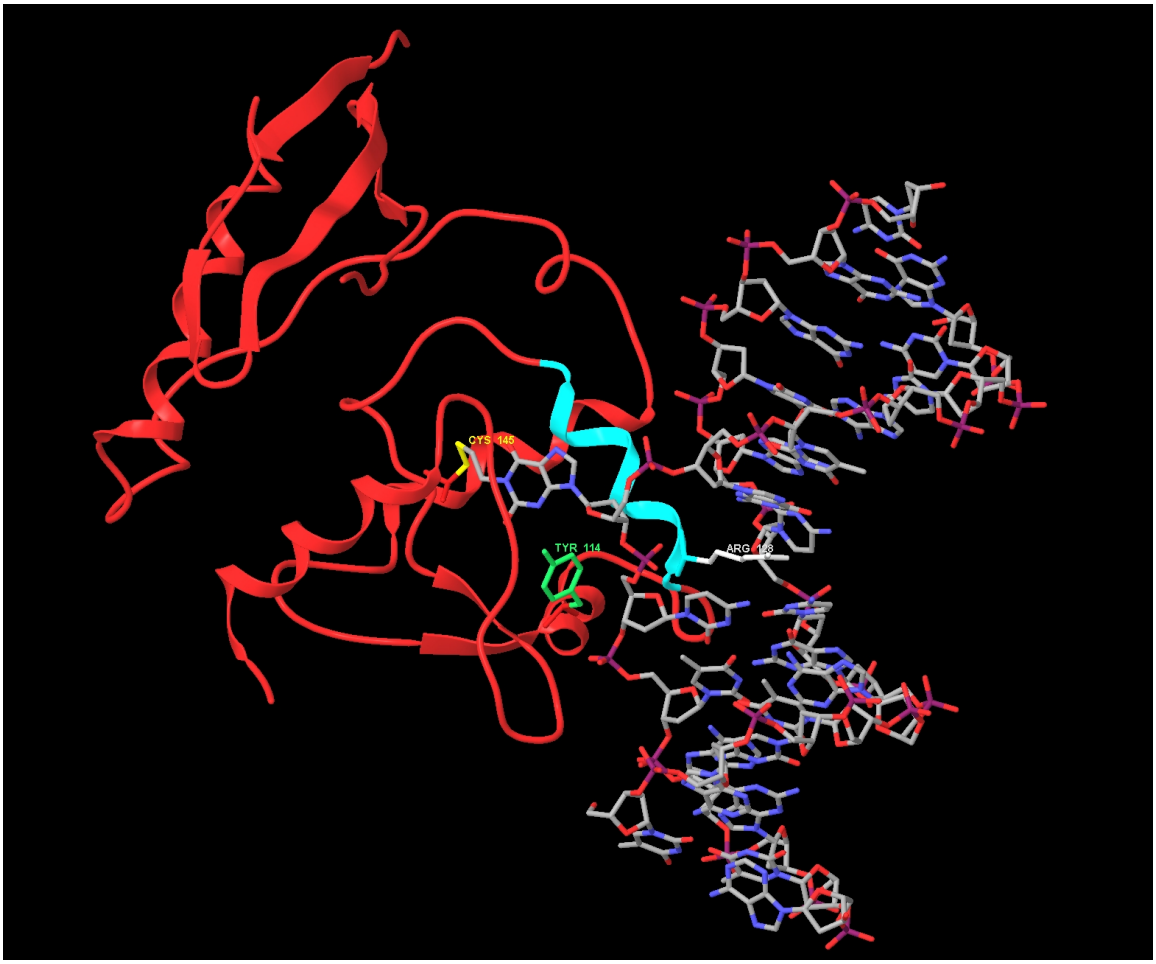

evolution, and is present in all species from bacteria to humans *(111)*. Repair is mediated by the transfer of the O^6-alkyl lesion to a highly-conserved active site cysteine within the protein's active site. The substrate O^6-alkyl guanine is placed in close proximity to the cysteine nucleophile *via* nucleotide flipping *(110)*.

Binding of AGT to DNA markedly widens the DNA minor groove, reducing the stability of local base pairs. Arg^{128}, which is located at the beginning of the recognition helix, is positioned inside the DNA duplex where it promotes flipping of nucleotides out of the base stack and into the protein's active site (*Figure 1.2*). Intercalating through the DNA minor groove, Arg^{128} helps to stabilize the extrahelical conformation of flipped out nucleotides by stacking interactions with the bases that flank the substrate nucleotide and forming hydrogen bonds with the orphaned cytosine. The importance of this "arginine finger" in the repair of O^6-alkylguanine lesions is supported by mutation studies in which substitution of this amino acid led to a dramatic decrease in AGT activity *(108)*.

Another amino acid residue, Tyr^{114}, is believed to play an important role in AGT-mediated repair by promoting the flipping of the substrate guanine nucleotide into the protein's active site (*Figure 1.2*). As demonstrated in the crystal structures of AGT bound to DNA *(110)*, the 3' phosphate of the target nucleotide is turned inward, with the oxygen atoms facing the center of the DNA helix. The close proximity of Tyr^{114} in the AGT-DNA complex facilitates rotation of the phosphate, presumably due to both charge and steric effects. Studies with Y114F and Y114A AGT mutants displayed reduced activity as compared with the wild-type protein (30- and 600-fold respectively), suggesting the importance of this residue in DNA repair *(112)*.

Within the AGT active site, hydrogen bonding and geometric exclusion provide some selectivity for 2'-deoxyguanosine nucleotides *(110)*. The carbonyls of Cys^{145} and Val^{148} accept hydrogen bonds from the exocyclic amine of guanine, while the side chain hydroxyl of Tyr^{114} and the amino group of Ser^{159} donate hydrogen bonds to the N3 and O^6 positions of guanine. When flipped out of the base stack, the substrate guanine is packed within a hydrophobic cleft defined by Met^{134} and an active site loop (Val^{155}-Gly^{160}). This hydrophobic pocket is able to accommodate O^6-alkyl lesions of various shapes and sizes and yields preferential binding of alkylated guanines *via* hydrophobic interactions *(110)*.

To facilitate alkyl transfer, the O^6-position of the substrate guanine is positioned ~3 Å opposite the thiolate nucleophile,an ideal location for in-line displacement *(110)*. A Glu-His-water-Cys hydrogen bond network (similar to the Asp-His-Ser catalytic triad of serine proteases) is thought to enhance the nucleophilicity of Cys^{145} (*Figure 1.3*). In this mechanism, His^{146} acts as a water-mediated general base to deprotonate Cys^{145}, the residue which serves as the nucleophile for alkyl transfer. Proton transfer through this network is likely to generate a thiolate anion, explaining the low pKa and high reactivity of this residue *(113)*.

In its search for DNA damage, AGT is believed to bind DNA and to scan individual bases for evidence of O^6 alkylation *(114)*. As AGT has been shown to bind both single- and double-stranded DNA with a high cooperativity, the recruitment of several AGT molecules to the same region of DNA may facilitate the search for DNA damage through localization *(110;115)*. Repair of O^6-alkylgunaine lesions by AGT is

Figure 1.3 Alkyl transfer mechanism of AGT *(110)*

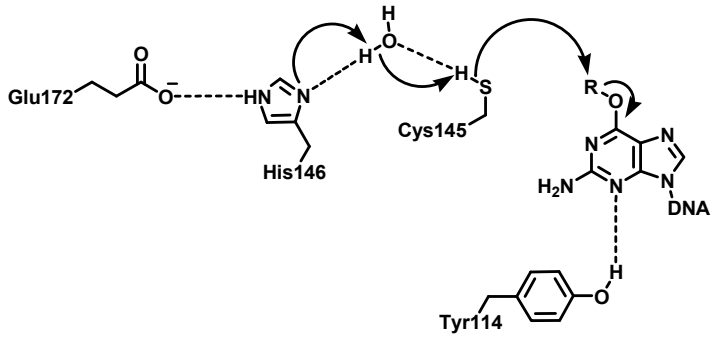

rapid, with the rate-limiting step being the alkyl transfer reaction, rather than adduct recognition *(116)*.

In contrast to other DNA repair proteins, AGT lacks dealkylation activity and is irreversibly inactivated following a single alkyl transfer reaction *(117)*. Prior to alkylation, AGT is relatively long-lived (half-life of 24 h *in vivo*). However, cellular exposure to alkylating agents results in a rapid disappearance of AGT *(111)*. In eukaryotic cells, alkylated AGT is ubiquitinated and transferred to the cytoplasm where it is degraded by the 26S proteasome *(118)*. AGT alkylation has been shown to disrupt the protein's native fold and is therefore thought to act as a signal for ubiquitination *(117)*.

1.4.3 Implications of AGT in Cancer Therapy and Drug Resistance

Numerous alkylating agents used in the treatment of cancer exert their cytotoxic effects through alkylation of the O^6 position of guanine *(107)*. Methylating agents including procarbazine, temozolomide, streptozotocin, and dacarbazine (*Figure 1.4*) form O^6-methylgunaine (O^6-mG) lesions that disrupt hydrogen bonding between the adducted guanine and its cytosine base pair. Although O^6-mG adducts do not significantly distort the DNA helix, the presence of these lesions interferes with DNA synthesis. As O^6-alkylated guanine forms base pairs preferentially with thymidine, these O^6-mG:T mispairs result in G to A point mutations during subsequent rounds of DNA replication *(119;120)*. Chloroethylating agents (*Figure 1.4*) such as carmustine (BCNU) and lomustine (CCNU) initially alkylate the O^6 position of guanine, followed by attack at the N1 position to yield the cyclic intermediate, N^1,O^6-ethanoguanine. Due to its inherent instability, this structure rearranges to form an interstrand cross-link with cytosine in the

Figure 1.4 Chemical structures of therapeutic methylating and chloroethylating agents

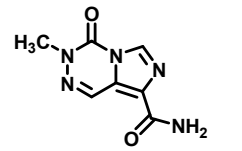

Temozolomide

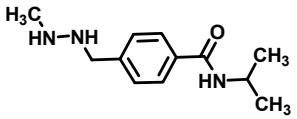

Procarbazine

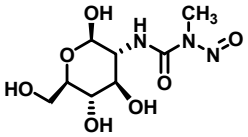

Streptozotocin

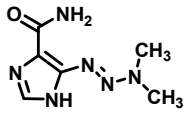

Dacarbazine

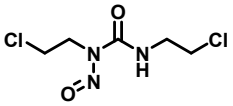

Carmustine

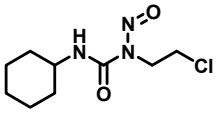

Lomustine

opposite DNA strand *(121)*. Methylating agents and chloroethylnitrosoureas are active against a number of malignacies including glioma (temozolomide and BCNU), Hodgkin's disease (procarbazine), melanoma (dacarbazine and temozolomide), and non-Hodgkin's lymphoma (BCNU) *(107)*.

Because AGT is capable of repairing DNA damage induced by these commonly used antitumor drugs, overexpression of AGT in tumor cells can result in drug resistance *(106)*. AGT is ubiquitously expressed in all tissues, with protein levels varying considerably between organs and individuals. In most species, the liver has the highest AGT activity, closely followed by the kidney and the lung. AGT expression is often enhanced in malignant tissues, with high levels observed in colon cancer *(122;123)*, melanoma *(124;125)*, pancreatic carcinoma *(126)*, lung cancer *(127)*, gliomas *(128-130)*, breast cancer, non-Hodgkin's lymphoma, and myeloma *(106;131)*. AGT expression in tumor cells can be heterogeneous due to abnormal promoter methylation *(132-135)*.

In an attempt to combat AGT-mediated drug resistance, inhibitors of AGT protein have been developed. First introduced in 1990, O^6-benzylguanine (O^6-BG) is a potent, non-toxic inhibitor of AGT with an IC_{50} of 0.5 μM against the human protein *(136)*. O^6-BG effectively inactivates AGT *via* covalent transfer of the benzyl group to the active site cysteine. It took only five years for O^6-BG to reach clinical trials *(137-139)*, and during these trials the dose of O^6-BG required to completely inhibit human AGT was determined as 120 mg/m^2. Pharmacokinetic analysis of O^6-BG suggests that it has a very short half-life (~40 min) due to a rapid conversion to the active metabolite O^6-benzyl-8-oxoguanine *(140)*. Cytochrome P450s 1A1 and 1A2 are responsible for O^6-BG oxidation and debenzylation to 8-oxoguanine, the later accounting for the longer half-life of O^6-benzyl-

8-oxoguanine (3.5-4 h) compared to O^6-BG *(141)*. Although O^6-BG is credited with the initial inactivation of tumor AGT, O^6-benzyl-8-oxoguanine is believed to uphold inhibition. Human studies indicate that both O^6-BG and O^6-benzyl-8-oxoguanine cross the blood-brain barrier *(142)*.

Due to its ability to induce drug resistance in tumor cells, the *MGMT* gene which encodes AGT has emerged as an attractive target for the protection of haematopoietic stem cells during cancer chemotherapy *(106)*. In addition to their activity against tumor cells, nitrosoureas are haematopoietic stem cell toxins, causing dose-limiting cumulative myelosuppression and have been implicated in treatment-related leukemias and myelodysplastic syndromes *(143)*. Because AGT is capable of protecting against nitrosourea-induced DNA damage, transduction of *MGMT* into marrow cells would likely prevent these undesirable effects. In recent years, point mutations in the human *MGMT* gene have been genetically engineered which render the resulting gene product resistant to O^6-BG while maintaining variable levels of reactivity towards chemotherapy-induced O^6-alkylguanine lesions *(144;145)*. Because of their resistance to O^6-BG, these AGT mutants are ideal candidates for gene therapy. Of the mutants identified, two have been expressed from viral vectors and transduced into haematopoietic progenitor cells, G156A-*MGMT* (60-fold resistance to O^6-BG) and P140K-*MGMT* (500-fold resistance to O^6-BG) *(146-149)*. These studies revealed that expression of G156A or P140K *MGMT* in haematopoietic cells results in an increased tolerance towards O^6-BG, BCNU, and temozolomide *(150-152)*.

1.4.4 AGT-DNA Cross-Linking by *Bis*-Electrophiles

While AGT typically protects cells against the mutagenic, carcinogenic, and cytotoxic effects of alkylating agents, recent studies have shown that cellular expression of AGT can enhance the cytotoxicity and mutagenicity of several *bis*-electrophiles *(57;153;154)*. For example, the cytotoxicity and mutagenicity of 1,2-dibromoethane (DBE) are increased in *E. coli* cells expressing human recombinant AGT, while the expression of a catalytically-inactive AGT mutant (C145A) had no effect on DBE-induced toxicity *(153)*. Following the mass spectrometric identification of a DBE-induced peptide-guanine cross-link at Cys^{145}, it was proposed that AGT increases the cytotoxic and mutagenic effects of DBE by reaction of the dihaloalkane with the active site cysteine to form a half-mustard which can react with DNA to form an AGT-DNA cross-link *(57)*. Analysis of DBE-induced mutants in the *RpoB* gene revealed that the majority of AGT-mediated mutations were G to A transitions, while ~20% were G to T transversions, the later of which potentially result from depurination of AGT-N7-guanine adducts.

Further investigations identified additional *bis*-electrophiles that displayed enhanced cytotoxic and mutagenic profiles in bacterial cells expressing human recombinant AGT *(154)*. In the current work, we set out to structurally characterize AGT-DNA cross-links induced by DEB and nitrogen mustard drugs *in vitro* (*Chapters II and III*) and to examine the effect of AGT on DEB- and nitrogen mustard-induced cytotoxicity and mutagenicity in Chinese hamster ovary (CHO) cells expressing the human protein (*Chapter V*).

II. CROSS-LINKING OF HUMAN RECOMBINANT O^6-ALKYLGUANINE DNA ALKYLTRANSFERASE TO DNA BY 1,2,3,4-DIEPOXYBUTANE

2.1 Abstract

A key carcinogenic metabolite of the important industrial chemical 1,3-butadiene (BD), DEB is a bifunctional alkylating agent capable of reacting with both DNA and proteins. Initial DNA alkylation by DEB produces N7-(2'-hydroxy-3',4'-epoxybut-1'-yl)-guanine monoadducts, which can then react with a second nucleophilic site to form cross-linked adducts. A recent report revealed a strong correlation between expression of the human DNA repair protein AGT in bacteria and the cytotoxic and mutagenic activity of DEB (J. G. Valadez *et al.*, *Chem. Res. Toxicol.* 17 (2004) 972-982). As AGT expression appeared to enhance the toxic effects of this *bis*-electrophile, the authors proposed that DEB induces AGT-DNA cross-links. The purpose of our study was to structurally characterize DEB-induced AGT-DNA conjugates and to identify amino acid residues within the protein involved in cross-linking. DNA-protein cross-link formation was first detected by SDS-PAGE when ^{32}P-labeled double-stranded oligodeoxynucleotides were exposed to DEB in the presence of both wild-type AGT or a C145A AGT mutant. Capillary HPLC-electrospray ionization mass spectrometry (ESI-MS) analysis of AGT that had been treated with N7-(2'-hydroxy-3',4'-epoxybut-1'-yl)-deoxyguanosine (dG monoepoxide) revealed the ability of the protein to form either one or two butanediol- dG cross-links, corresponding to mass shifts of +353 and +706 Da, respectively. HPLC-ESI$^+$-MS/MS sequencing of tryptic peptides obtained from dG monoepoxide-treated AGT indicated that the two cross linking sites were located at the alkyl acceptor site, Cys^{145}

and a neighboring active site residue, Cys^{150}. The same two active site cysteines became cross-linked to DNA following DEB treatment. Modification of Cys^{145} was further confirmed by HPLC-ESI^+-MS/MS analysis of dG monoepoxide-treated synthetic peptide GNPVPILIPCHR which represents the active site tryptic fragment of AGT (C = Cys^{145}). Replacement of the catalytic cysteine residue with alanine (C145A AGT) abolished DEB-induced cross-linking at this site, while the formation of conjugates *via* neighboring Cys^{150} was retained. The exact chemical structure of the cross-linked lesion was established as 1-(*S*-cysteinyl)-4-(guan-7-yl)-2,3-butanediol by HPLC-ESI^+-MS/MS analysis of the amino acids resulting from total digestion of modified AGT analyzed in parallel with an authentic standard. Based upon these results, the formation of AGT-DNA cross-links is a likely mechanism to explain the enhanced cytotoxicity of DEB in cells expressing this important repair protein.

2.2 Introduction

The DNA repair protein AGT transfers the O^6-alkyl group from promutagenic O^6-alkylguanine lesions in DNA to an active site cysteine (Cys^{145} in human protein), restoring normal guanine and preventing mutagenesis *(101)*. Crystal structures of DNA-bound AGT support a repair mechanism involving protein binding to the minor groove of double-stranded DNA and subsequent "flipping" of nucleotides out of the base stack into the AGT active site *(110)*. This conformational change places O^6-alkylguanine group <3 Å from the side chain of Cys^{145} within the active site. Cys^{145} is activated to a thiolate anion because of its interactions with a bound Zn (II) cation and the formation of a Glu-His-water-Cys H-bond network *(108)*. Nucleophilic attack of Cys^{145} at the O^6-alkyl lesion

results in the formation of a thioether at Cys^{145} and restores intact dG within DNA. Because alkylation of the catalytic residue of AGT is irreversible, this repair process is non-enzymatic in nature, consuming a molecule of AGT in each alkyl transfer reaction *(117)*. Cys^{145} alkylation destabilizes the native fold of AGT, targeting the protein for ubiquitination and subsequent degradation by the 26S proteasome *(117;155)*.

AGT can repair a wide variety of O^6-alkylguanines, including those resulting from exposure to anticancer chemotherapeutics (dacarbazine, temozolomide, *bis*-chloroethyl-nitrosourea). AGT overexpression in tumors can be responsible for the acquired resistance of cancer cells to DNA-alkylating agents *(156;157)*. A reversal of AGT-mediated drug resistance can be achieved by co-administration of O^6-benzylguanine, an AGT substrate that inactivates the protein *via* transfer of the O^6-benzyl group to Cys^{145} *(156-158)*.

In a sharp contrast with the protective effects of AGT against alkylation damage by many DNA alkylating agents, AGT expression in cell culture enhances the cytotoxic and mutagenic effects of DEB *(154;159)*. DEB is the suspected carcinogenic metabolite of BD, a major industrial chemical used in the manufacturing of rubber and plastics and a recognized human carcinogen *(160;161)*. The metabolic activation of BD to DEB is catalyzed by CYP2E1 and CYP2A6 monooxygenases. The first epoxidation step yields *(R)*- and *(S)*-EB *(73;162)*, which can then be hydrolyzed to 1-butene-3,4-diol or can undergo a second oxidation to yield *R,R; S,S;* and *meso*-DEB *(163)*. Although DEB is a relatively minor metabolite, available experimental evidence suggests that it is responsible for many of the adverse effects of BD. Biological studies indicate that DEB is 50 to 100-fold more genotoxic and mutagenic than its monoepoxide analogues, EB and

3,4-epoxy-1,2-butanediol *(80;81)*. Efficient metabolism of BD to DEB in target tissues of laboratory mice is thought to be responsible for susceptibility of this species to BD carcinogenesis *(164)*.

The enhanced biological activity of DEB in the presence of AGT may result from chemical cross-linking of AGT to DNA, by analogy with other *bis*-alkylating agents (*Scheme 2.1*) *(57;154)*. DEB is a bifunctional electrophile capable of sequentially alkylating two nucleophilic sites within DNA and/or proteins *(48;82;83)*. Evidence for the formation of DNA-protein cross-links of DEB *in vivo* has been provided by alkaline elution assays *(165)*, however, no structural information for these lesions was available. The goal of the present work was to investigate the molecular mechanisms of AGT-mediated cytotoxicity and mutagenicity of DEB by determining DNA-AGT cross-link structures and identifying the amino acid residues within AGT involved in cross-linking.

2.3 Materials and Methods

Chemicals and Reagents. Racemic DEB was purchased from Sigma-Aldrich (Milwaukee, WI), 2'-deoxyguanosine was obtained from TCI (Tokyo, Japan). L-cysteine and Boc-L-cysteine were purchased from Fluka (Buchs, Switzerland). Adenosine 5'-[γ-^{32}P]triphosphate was purchased from Perkin-Elmer (Boston, MA), and T4 polynucleotide kinase was obtained from New England Biolabs (Beverly, MA). Trypsin, carboxypeptidase Y, and proteinase K were purchased from Worthington Biochemical Corporation (Lakewood, NJ). Synthetic DNA oligodeoxynucleotides and the peptide GNPVPILIPCHR corresponding to positions 136-147 of human AGT were prepared at the University of Minnesota's Microchemical Facility (Minneapolis, MN). Human

Scheme 2.1 DNA-AGT cross-linking by dihaloethanes and DEB

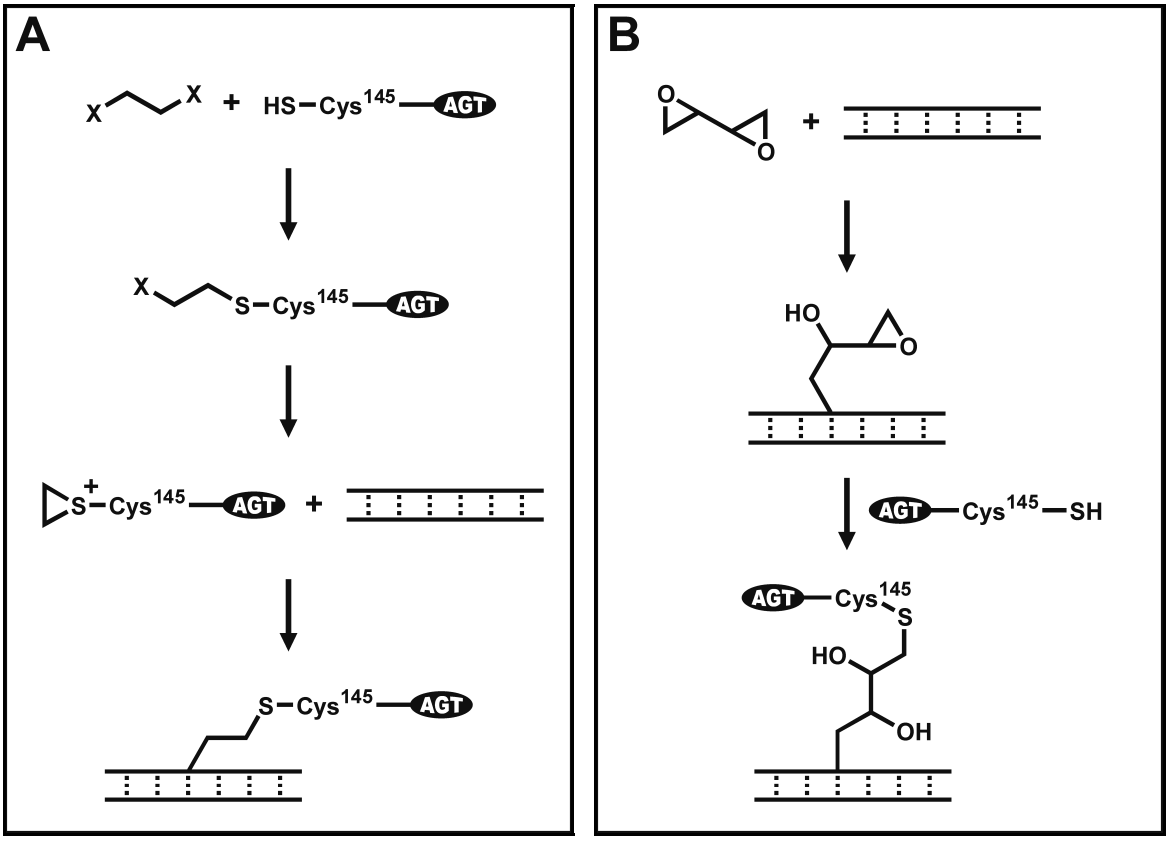

recombinant C-terminal histidine-tagged wild-type AGT and an N-terminal histidine-tagged C145A AGT mutant (*Tables 2.1 and 2.2*) were prepared as previously described *(166;167)*.

Detection of DEB-Induced AGT- DNA Cross-Links by SDS-PAGE. DNA 18-mer 5'-GGA GCT GGT GGC GTA GGC-3' (+ strand) and the complimentary (-) strand were purified using an Agilent Technologies HPLC system (model 1100) incorporating a UV diode array detector and a semi-micro UV cell. A Supelcosil LC-18-DB semipreparative column (25 cm x 10 mm, 5 μm) was eluted with 100 mM TEAA, pH 7.0 (A) and 50% acetonitrile in 100 mM TEAA, pH 7.0 (B) at a flow rate of 3 mL/min. The gradient program began at 7.5% B, followed by a linear increase to 26% B in 42 min, and further to 60% B in 28 min. Under these conditions, DNA 18-mers eluted as sharp peaks around 40 min. HPLC pure (+) strand (200 pmol) was 5'-end labeled with ^{32}P in the presence of [γ-^{32}P]ATP/T4 polynucleotide kinase *(168)*. The resulting [γ-^{32}P] 5'-end labeled oligodeoxynucleotides were purified by 8% denaturing PAGE and desalted by SPE using Waters SepPak C18 cartridges. Once spiked with the corresponding unlabeled DNA (12 nmol), the radiolabeled (+) strand was annealed to its complimentary strand (12.2 nmol) in AGT buffer (50 mM TRIS (pH 7.6) and 0.1 mM EDTA). The ^{32}P-labeled duplex (0.93 nmol) was incubated with human recombinant AGT (hAGT, 2.0 μg, 0.093 nmol) in the presence of 100, 500, and 3000 molar equivalents of racemic DEB (9.3 nmol, 46.5 nmol, and 279 nmol respectively). In a separate experiment, C145A AGT (2.0 μg, 0.087 nmol) was incubated with 3000 molar equivalents of racemic DEB. Following 3 h incubation at

Table 2.1 HPLC-ESI$^+$-MS analysis of AGT tryptic peptides

Position	Peptide	$[M + H]^+_{calculated}$	$[M + 2H]^{2+}_{calculated}$	Observed Ions
1-9	MDKDCEMKR	1156.4	578.7	1156.7, 578.9
10-18	TTLDSPLGK	931.5	466.3	931.7, 466.3
19-32	LELSGCEQGLHEIK	1555.8	778.4	778.8
33-36	LLGK	430.3	215.7	430.4, 215.6
37-96	GTSAADAVEVPAPAAVLGG PEPLMQCTAWLNAYFHQP EAIEEFPVPALHHPVFQQES FTR	6469.2	3235.1	ND
97-101	QVLWK	673.4	337.2	673.5
102-104	LLK	373.3	187.1	373.3, 187.1
105-107	VVK	345.3	173.1	ND
108-125	FGEVISYQQLAALAGNPK	1906.0	953.5	953.5
126-128	AAR	317.2	159.0	317.2
129-135	AVGGAMR	661.4	331.2	661.4, 331.2
136-147	GNPVPILIPCHR	1315.7	658.4	1315.7, 658.6
148-165	VVCSSGAVGNYSGGLAVK	1667.8	834.4	834.6
166-175	EWLLAHEGHR	1247.6	624.3	1247.7, 624.5
176-193	LGKPGLGGSSGLAGAWLK	1668.9	835.0	1669.0, 835.2
194-207	GAGATSGSHHHHHH	1429.6	715.3	1429.6, 715.4

Table 2.2 HPLC-ESI$^+$-MS analysis of C145A AGT tryptic peptides

Position	Peptide	$[M + H]^+$ calculated	$[M + 2H]^{2+}$ calculated	Observed Ions
1-9	MRGSHHHHHHGSMDKDCEMKR	2553.1	1277.1	ND
10-18	TTLDSPLGK	931.5	466.3	931.6, 466.3
19-32	LELSGCEQGLHEIK	1555.8	778.4	778.4
33-36	LLGK	430.3	215.7	430.4
37-96	GTSAADAVEVPAPAAVLGG PEPLMQCTAWLNAYFHQP EAIEEFPVPALHHPVFQQES FTR	6469.2	3235.1	ND
97-101	QVLWK	673.4	337.2	673.5
102-104	LLK	373.3	187.1	373.4
105-107	VVK	345.3	173.1	ND
108-125	FGEVISYQQLAALAGNPK	1906.0	953.5	953.6
126-128	AAR	317.2	159.0	ND
129-135	AVGGAMR	661.4	331.2	661.4
136-147	GNPVPILIPAHR	1283.8	642.4	1283.8, 642.5
148-165	VVCSSGAVGNYSGGLAVK	1667.8	834.4	834.4
166-175	EWLLAHEGHR	1247.6	624.3	1247.6, 624.5
176-193	LGKPGLGGSSGLAGAWLK	1668.9	835.0	1669.1, 835.4
194-207	GAGATSGSPPAGRN	1199.6	600.4	1199.7, 600.6

Note: Numbering begins at M.

37 °C, the reaction mixtures were separated by 12% SDS-PAGE, and the radiolabeled products were visualized using a Bio-Rad Molecular Imager FX. DEB-induced DNA-protein cross-links were quantified by volume analysis employing Bio-Rad Quantity One Software, with cross-linking efficiency determined by the intensity ratio of the low-mobility cross-link band versus the band corresponding to single-stranded DNA.

Preparation of dG Monoepoxide. 2'-Deoxyguanosine (59.0 mg, 0.22 mmol) was suspended in 3 mL of 10 mM TRIS-HCl buffer (pH 7.2), and 34 μL (0.44 mmol) of racemic DEB was added. The resulting mixture was incubated overnight at 37 °C. N7-(2'-hydroxy-3',4'-epoxybut-1'-yl)-deoxyguanosine (dG monoepoxide) was purified by semipreparative HPLC on an Agilent 1100 HPLC system. A Supelcosil LC-18-DB column (25 cm x 10 mm, 5 μm) was eluted with a gradient of water (A) and acetonitrile (B) at a flow rate of 3 mL/min. Solvent composition was changed linearly from 3 to 7 % B in 8 min, further to 8% B in 3 min, and held at 8% B for 9 min. Under these conditions, dG monoepoxide eluted as a broad peak at ~16 min. dG monoepoxide was characterized by tandem mass spectrometry (ESI^+-MS/MS: *m/z* 354.0 $[M + H]^+ \rightarrow$ 238.0 $[M + H - dR]^+$, 152.0 $[Gua + H]^+$). UV absorption spectrum of dG monoepoxide (λ_{max} = 274 nm at pH 7.0) was reminiscent of other N7-alkylguanosines, including N7-methyl dG. Thus, the extinction coefficient for N7-methyl dG (ε_{274} = 9,000 at pH 7.0) was used to estimate standard solution concentrations of HPLC-purified dG monoepoxide. dG monoepoxide was stable in an aqueous solution at -20 °C for up to a month as determined by ESI^+-MS analysis.

Preparation of Cys-Gua-BD. 2'-Deoxyguanosine (29.5 mg, 0.11 mmol) was combined with racemic DEB (17 μL, 0.22 mmol) in 1 mL of 10 mM TRIS-HCl buffer (pH 7.2), and the resulting mixture was incubated overnight at 37 °C. Boc-L-cysteine (24.4 mg, 0.11 mmol) was added, and the mixture was left for an additional 48 h at 37 °C. The reaction mixture was then centrifuged at 1,000 x *g* for 2 min, and the supernatant was dried in a speed-vac concentrator. The resulting white powder was dissolved in 200 μL of TFA and allowed to stand at room temperature for 15 min to remove the Boc protecting group. The structure of 1-(*S*-cysteinyl)-4-(guan-7-yl)-2,3-butanediol (Cys-Gua-BD) was confirmed by HPLC-ESI$^+$-MS/MS (*m/z* 359.7 $[M + H]^+ \rightarrow$ 208.0 $[M+ H – Gua]^+$, 190.0 $[M+ H – Gua – H_2O]^+$).

Modification of synthetic peptide GNPVPILIPCHR with dG monoepoxide. Synthetic peptide GNPVPILIPCHR representing positions 136-147 of human AGT (40.0 μg, 30.42 nmol) was reacted with 5 molar equivalents of dG monoepoxide in 400 μL of 10 mM TRIS-HCl buffer, pH 7.2. The mixture was incubated under argon at 37 °C for 3 h, and the resulting peptide-guanine DEB conjugate was isolated *via* HPLC using an Agilent 1100 HPLC system. A Supelcosil LC-18-DB column (25 cm x 4.6 mm, 5 μm) was eluted with 0.1% TFA in water (A) and 0.1% TFA in acetonitrile (B) at a flow rate of 0.2 mL/min. The solvent composition began at 5% B and was changed linearly to 80% B in 45 min. Under these conditions, the peptide-guanine cross-link eluted as a broad peak at ~13 min.

dG Monoepoxide-Induced Cross-Linking of AGT for MS Analysis. Human recombinant AGT (77.6 μg, 3.55 nmol) or C145A AGT (77.5 μg, 3.37 nmol) was incubated with 50 molar equivalents of dG monoepoxide in 200 μL of 10 mM TRIS-HCl buffer (pH 7.2) under argon for 3 h at 37 °C. Following incubation, the proteins were isolated by HPLC using an Agilent 1100 HPLC system. A Zorbax 300 SB-C3 column (2.1 mm x 150 mm, 5 μm) was eluted with 0.05% TFA in water (A) and 0.05% TFA in acetonitrile (B) at a flow rate of 0.2 mL/min. The elution program began at 30% B and was increased to 80% B in 30 min. Under these conditions, both native and alkylated proteins eluted as a single peak at 27 min. The collected protein fractions were dried, dissolved in 0.05% TFA, and aliquots were taken for HPLC-ESI$^+$-MS analysis. To identify the residues of AGT and C145A AGT involved in cross-linking to guanine, dG monoepoxide-treated protein samples (~70 μg each) were dried, dissolved in 200 μL of 100 mM ammonium bicarbonate buffer (pH 7.9), and trypsin (7.0 μg, 0.30 nmol) was added to initiate proteolytic digestion. The resulting solutions were incubated at 37 °C for 24 h. The proteolytic mixtures were then dried, reconstituted in 50 μL of 0.5% formic acid/0.01% TFA in water, and subjected to HPLC-ESI$^+$-MS/MS analysis as described below. To confirm the structures of dG monoepoxide-induced cross-links, AGT and C145A AGT tryptic peptides were subjected to total digestion to amino acids. AGT and C145A AGT tryptic peptides (from ~50 μg protein) were dissolved in 100 μL of water and filtered through Microcon YM-10 membrane filters to remove trypsin, followed by a 24 h incubation of the filtrate with carboxypeptidase Y (1.0 μg, 16.4 pmol) and proteinase K (1 μg, 34.6 pmol) at room temperature. Once dried, the samples were reconstituted in 40 μL water and analyzed by HPLC-ESI$^+$-MS/MS.

dG Monoepoxide-Induced Cross-Linking of AGT in the Presence of L-Cysteine. hAGT (20.0 μg, 0.914 nmol) was treated with 50 equivalents of racemic dG monoepoxide (45.7 nmol, 0.23 mM) in the presence of 0, 500, 1250, and 2500 equivalents of L-cysteine (2.3, 5.7, and 11.4 mM respectively) in 200 μL of 10 mM TRIS-HCl buffer, pH 7.2. Following a 3 h incubation under argon at 37 °C, the samples were acidified via addition of 50 μL 1.0% formic acid and directly analyzed by HPLC-ESI$^+$-MS.

DEB-Induced Cross-Linking of AGT to Double-Stranded Oligodeoxynucleotides for MS Analysis. The DNA 18-mer (5'-GGA GCT GGT GGC GTA GGC-3') (+ strand) and the complementary (-) strand (5'-GCC TAC GCC ACC AGC TCC-3') were prepared by standard phosphoramidite chemistry on a DNA synthesizer. To obtain double-stranded DNA, (+) and (-) strand (20 nmol each) were combined, dried under vacuum, and dissolved in 10 mM TRIS-HCl buffer, pH 7.2. The solution was heated to 90 °C and allowed to slowly cool to room temperature to anneal the complementary strands. AGT (44.0 μg, 2.01 nmol) or C145A AGT (46.0 μg, 2.00 nmol) was incubated under argon for 3 h at 37 °C with 10 nmol of double-stranded DNA in 10 mM TRIS-HCl buffer (pH 7.2) containing racemic DEB (1 μmol, 2.5 mM). Following incubation, the samples were heated to 70 °C for 1 h to release N7-alkylated guanines. Once dry, the samples were dissolved in 100 mM ammonium bicarbonate buffer (pH 7.9), trypsin (5 μg, 0.21 nmol) was added, and the samples were digested overnight at 37 °C. The resulting peptides were dried, reconstituted in 50 μL 0.5% formic acid/0.01% TFA in water, and analyzed by HPLC-ESI$^+$-MS/MS.

Capillary HPLC-ESI$^+$-MS/MS Analysis of dG Monoepoxide and DEB-Induced AGT-Guanine Cross-Links. HPLC-ESI$^+$-MS analysis of AGT and C145A AGT proteins was performed using an Agilent 1100 capillary HPLC-ion trap MS system operated in the ESI$^+$ mode. The spectra were obtained by performing full scan MS within the *m/z* range of 100-1500. Chromatographic separation was achieved with an Agilent Zorbax 300 SB-C3 column (150 mm x 0.5 mm, 5 um) eluted at a flow rate of 15 uL/min. The mobile phase consisted of 0.05% TFA in water (A) and 0.05% TFA in acetonitrile (B). The elution program started at 30% B for 5 min, followed by a linear increase to 80% B in 25 min. Under these conditions, AGT and C145A AGT (both native and alkylated) eluted as sharp peaks at ~16 min. Deconvolution of the resulting charge envelopes was performed using the Agilent ion trap deconvolution software.

HPLC-ESI$^+$-MS/MS analysis of AGT and C145A AGT tryptic peptides was performed using the same Agilent 1100 capillary HPLC-ion trap MS system. Operating in ESI$^+$ mode, Auto MS^2 was used to select and fragment the following doubly-charged ions: *m/z* 658.4 (unmodified peptide G^{136}NPVPILIPCHR^{147}); *m/z* 776.9 (G^{136}NPVPILIPCHR^{147} peptide cross-linked to guanine); *m/z* 710.4 (G^{136}NPVPILIPCHR^{147} peptide containing a DEB-induced trihydroxybutyl adduct); *m/z* 834.4 (unmodified peptide V^{148}VCSSGAVGNYSGGLAVK^{165}); *m/z* = 952.9 (V^{148}VCSSGAVGNYSGGLAVK^{165} peptide cross-linked to guanine); *m/z* 886.4 (V^{148}VCSSGAVGNYSGGLAVK^{165} peptide containing a DEB-induced trihydroxybutyl adduct); and *m/z* 642.4 (unmodified peptide G^{136}NPVPILIPAHR^{147} from C145A hAGT).

Chromatographic separation of tryptic peptides was achieved using an Agilent Zorbax SB-C18 column (150 mm x 0.5 mm, 5 μm) eluted at a flow rate of 15 μL/min.

The mobile phase consisted of 0.5% formic acid/0.01% TFA in water (A) and 0.5% formic acid/0.01% TFA in acetonitrile (B). The solvent composition began at 3% B and was held constant for the first 3 min. The gradient was then increased to 5% B in 7 min, held at 5% B for 10 min, increased to 35% B in 95 min, and further to 75% B in 10 min. Full scan MS spectra obtained from these and control experiments was used in the identification of other AGT tryptic peptides. This same method was employed for the analysis of synthetic peptide GNPVPILIPCHR containing a dG monoepoxide-induced cross-link to guanine and for DEB-induced AGT-DNA cross-links.

HPLC-ESI$^+$-MS/MS analysis of the amino acids present in total digests of alkylated AGT was performed with an Agilent 1100 capillary HPLC-ion trap MS system. Operating in positive ion mode, Auto MS^2 was used to isolate and fragment the following singly-charged ions: *m/z* 359.1 (1-(*S*-cysteinyl)-4-(guan-7-yl)-2,3-butanediol); *m/z* 420.1 (1-(*O*-tyrosyl)-4-(guan-7-yl)-2,3-butanediol); *m/z* 385.4 (1-(*N*-lysyl)-4-(guan-7-yl)-2,3-butanediol); *m/z* 413.4 (1-(*N*-arginyl)-4-(guan-7-yl)-2,3-butanediol); and *m/z* 393.4 (1-(*N*-histidyl)-4-(guan-7-yl)-2,3-butanediol). Chromatographic separation was achieved using a Phenomenex Synergi C18 column (250 mm x 0.5 mm, 4 um) eluted at a flow rate of 10 uL/min. The mobile phase consisted of 15 mM ammonium acetate, pH 5.0 in water (A) and 3:1 methanol/acetonitrile (B). The solvent composition was changed from 2-8% B in 10 min, increased to 12% B in 22 min, and further to 30% B in 10 min. Under these conditions, Cys-Gua-BD eluted as a sharp peak at ~15 min.

2.4 Results

2.4.1 SDS-PAGE Analysis of DEB-Induced AGT-DNA Cross-Links

The ability of DEB to induce AGT-DNA cross-links was first examined by SDS-PAGE (*Figure 2.1*). DNA duplexes comprised of the 5'-^{32}P-end labeled 18-mer 5'-GGA GCT GGT GGC GTA GGC-3' (+ strand) and its complement (5'-GCC TAC GCC ACC AGC TCC-3') were incubated with recombinant human AGT in the presence of increasing amounts of racemic DEB (100, 500, or 3000 molar equivalents). SDS-PAGE separation of the resulting reaction mixtures provided evidence for the formation of AGT-DNA conjugates as indicated by the appearance of a new DNA band with reduced mobility compared to the free 18-mer (*Figure 2.1*). This slowly moving band was absent in control experiments lacking AGT, DEB, or the DNA duplex (*lanes 1-3 in Figure 2.1*). The degree of DEB-induced AGT-DNA cross-linking was dose-dependent, increasing from 1.5 to 3% (*lanes 4-6*). Interestingly, AGT-DNA complex formation was also observed with the C145A AGT mutant (*lane 7*), suggesting that AGT-DNA cross-linking by DEB can take place at a site other than Cys^{145}.

2.4.2 HPLC-ESI$^+$-MS Analysis of dG Monoepoxide-Treated AGT: Whole Protein MS

A mass spectrometry based strategy was employed to identify the cross-linking sites within AGT and to determine the covalent structures of DEB-induced DNA-AGT conjugates (*Scheme 2.2*). Initial DNA alkylation by DEB is known to produce N7-(2'-hydroxy-3',4'-epoxybut-1'-yl)-guanine (dG monoepoxide) adducts, which result from the nucleophilic attack of N7-guanine at the terminal carbon of DEB (> 90% of total adducts)

Figure 2.1 12% SDS-PAGE analysis of ^{32}P-end labeled DNA duplexes (5'-GGA GCT GGT GGC GTA GGC-3', (+) strand) following incubation with DEB and AGT (lanes 4-6) or C145A AGT (lane 7).

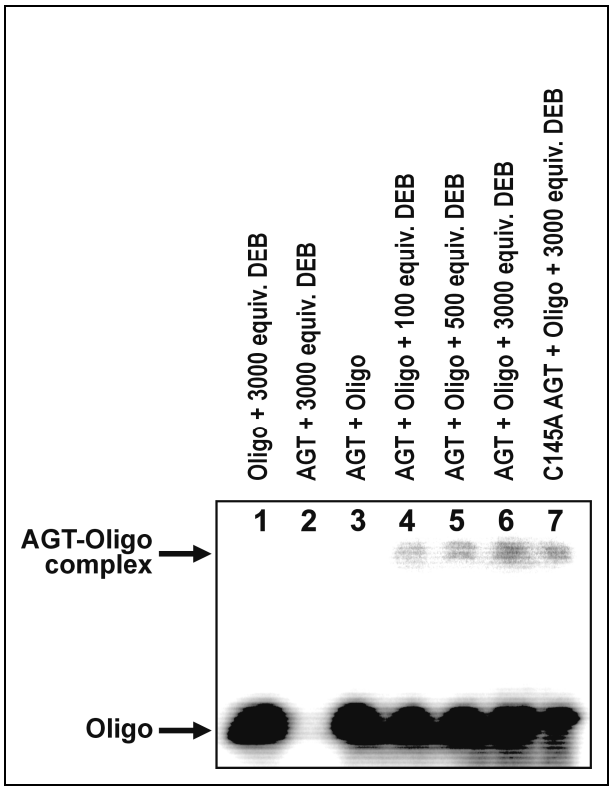

Scheme 2.2 Mass spectrometric analysis of DEB-induced AGT-DNA conjugates

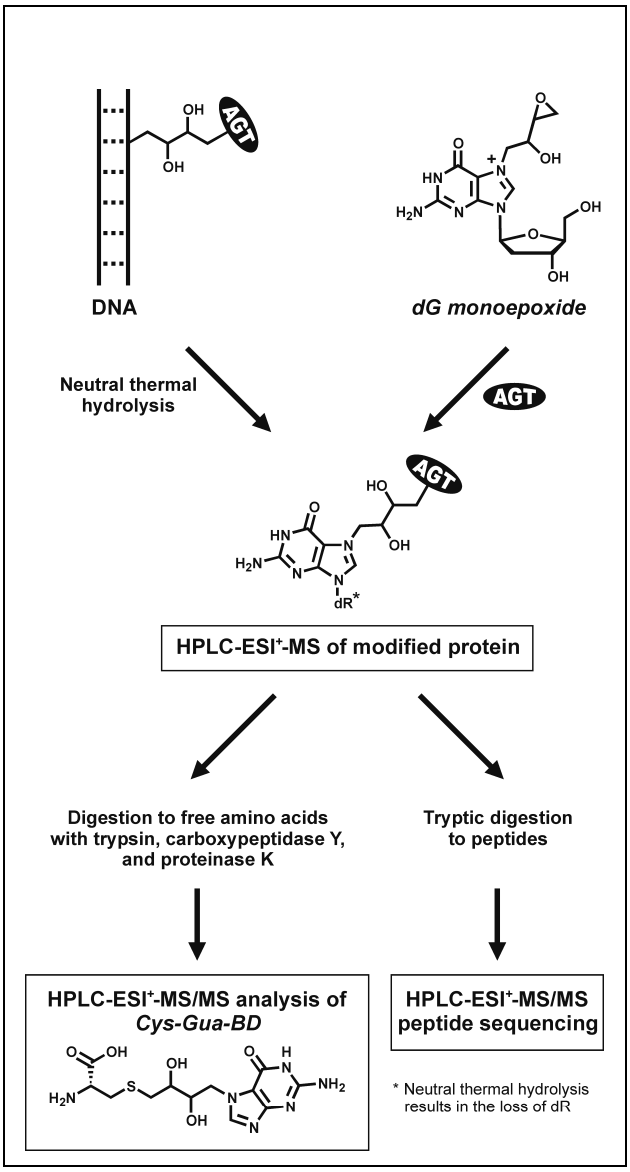

(169). Therefore, initial studies of DNA-protein cross-linking by DEB employed synthetic N7-(2'-hydroxy-3',4'-epoxybut-1'-yl)-deoxyguanosine as a model for monoalkylated DNA (*Scheme 2.2, right*). We then went on to investigate AGT cross-linking to double-stranded DNA in the presence of DEB (*Scheme 2.2, left*). In DNA experiments, N7-alkylguanine residues were released from the DNA backbone by neutral thermal hydrolysis to facilitate mass spectral analysis (*Scheme 2.2*).

HPLC-ESI$^+$-MS analysis of native AGT on an ion trap mass spectrometer reveals a single protein peak eluting at 16.6 min (*Figure 2.2, panel A*). The ESI$^+$ spectrum across this peak contains *m/z* signals corresponding to multiple charge states (+18 to +30) of a protein with a mass of 21 880 Da, consistent with the calculated molecular weight of 21 876 Da (*Table 2.1*). HPLC-ESI$^+$-MS analysis of AGT following incubation with dG monoepoxide reveals the presence of native AGT (M = 21 877 Da), as well as monoalkylated protein containing a single butanediol-dG cross-link (calculated M = 22 229 Da, observed M = 22 230 Da) and a protein containing two butanediol cross-links to dG (calculated M = 22 582 Da, observed M = 22 586 Da) (*Figure 2.2, panel B - inset*). For each additional adduct, a mass increase of ~353 Da is observed, corresponding to the addition of a molecule of dG monoepoxide. dG monoepoxide-induced modification of AGT was not blocked by the presence of free L-cysteine (*Table 2.3*). Over 1000-fold molar excess of L-cysteine was required to achieve a small decrease of AGT-dG conjugate yields, accompanied by the formation of disulfide adducts between the free L-cysteine and cysteine residues within the protein (*Table 2.3*). These experiments suggest that free cysteine cannot prevent the formation of DNA-protein cross-links by DEB,

Figure 2.2 Whole protein MS of dG monoepoxide-induced butanediol cross-links to AGT. (**A**) HPLC-ESI$^+$-MS of untreated AGT. *Top*: Total ion chromatogram; *Bottom*: ESI$^+$ mass spectrum of the 16.6 min protein peak; *Inset*: Deconvoluted mass spectrum of the 16.6 min peak (observed M = 21 880 Da, calculated M = 21 876 Da). (**B**) HPLC-ESI$^+$-MS of AGT following incubation with 50 molar equivalents dG monoepoxide. *Top*: Total ion chromatogram; *Bottom*: ESI$^+$ mass spectrum of the 16.3 min protein peak; *Inset*: Deconvoluted mass spectrum of the 16.3 min peak: A = AGT containing a single cross-link to dG (observed M = 22 230 Da, calculated M = 22 229 Da); B = double cross-link to dG (observed M = 22 586 Da, calculated M = 22 582 Da); C = unmodified AGT (observed M = 21 877 Da, calculated M = 21 876 Da).

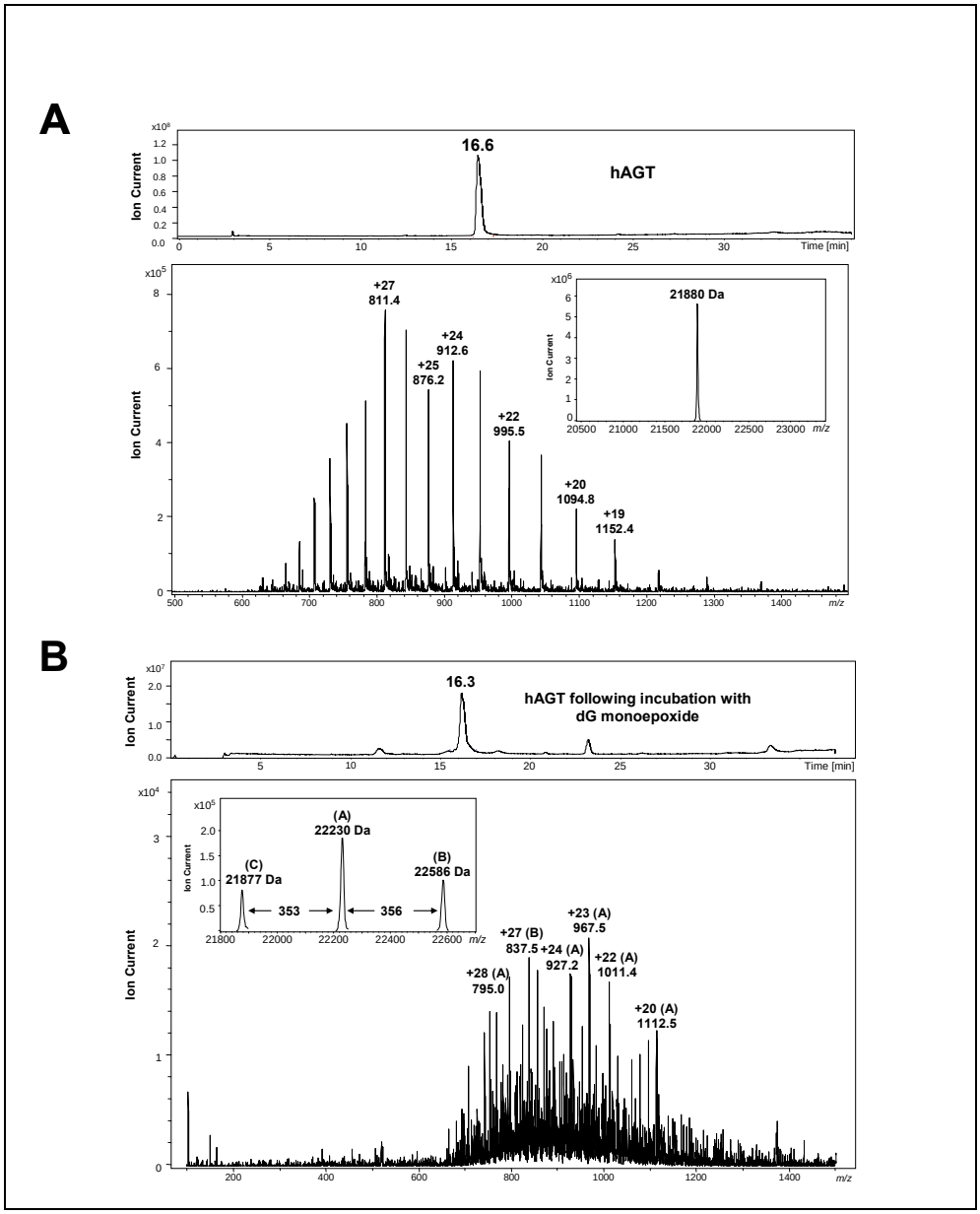

Table 2.3 Inhibition of dG monoepoxide-induced modification of AGT in the presence of L-cysteine

Equivalents L-Cysteine	% Unmodified AGT *M* = 21877.7 ± 0.2 Da	% AGT Butanediol Cross-Link to dG *M* = 22229.9 ± 0.9 Da	% AGT-Cysteine Disulfide *M* = 21996.5 ± 0.1 Da
0	78.9	21.1	0
500	81.3	18.7	0
1250	77.6	11.5	10.9
2500	80.5	5.4	14.1

consistent with our previous data which revealed a lack of reactivity between glutathione and DEB under physiological conditions.

Similar analyses were conducted with the C145A AGT active site mutant. In this protein, the Cys^{145} alkyl acceptor site is replaced with alanine, eliminating the possibility of cross-linking through this position. The calculated molecular weight of the C145A AGT variant is 23 012 Da due to the addition of an N-terminal histidine tag (MRGSHHHHHHGS) (*Table 2.2*). HPLC-ESI^+-MS analysis of C145A AGT prior to treatment reveals a single protein species with a deconvoluted mass of 23 015 Da, consistent with the theoretical value (*Figure 2.3, panel A*). HPLC-ESI^+-MS analysis of dG monoepoxide-treated C145A AGT provides evidence of cross-linking at a single site (observed M = 23 367, mass increase of 353 Da), suggesting that one of the cross-linking sites observed within the wild-type protein, namely Cys^{145}, has been removed (*Figure 2.3, panel B*). The residual ability of C145A mutant to form butanediol conjugates to dG is consistent with our SDS-PAGE results, which support C145A AGT cross-linking to DNA in the presence of DEB (*Figure 2.1, lane 7*). Unfortunately, it was not possible to perform MS analysis on AGT-guanine cross-links formed upon reaction of AGT with double-stranded oligodeoxynucleotides in the presence of DEB due to protein solubility issues.

2.4.3 HPLC-ESI^+-MS Analysis of dG Monoepoxide-Treated AGT: Peptide Mapping

Our whole protein MS results for dG monoepoxide-treated AGT variants (*Figures 2.2 and 2.3*) are consistent with the presence of two distinct cross-linking sites within the

Figure 2.3 Whole protein MS of C145A AGT protein following treatment with dG monoepoxide. (**A**) HPLC-ESI$^+$-MS of untreated C145A AGT. *Top*: Total ion chromatogram; *Bottom*: ESI$^+$ mass spectrum of the 16.2 min protein peak; *Inset*: Deconvoluted mass spectrum of the 16.2 min peak (observed M = 23 015 Da, calculated M = 23 012 Da). (**B**) HPLC-ESI$^+$-MS of C145A AGT mutant following incubation dG monoepoxide. *Top*: Total ion chromatogram; *Bottom*: ESI$^+$ mass spectrum of the 16.1 min protein peak; *Inset*: Deconvoluted mass spectrum of the 16.1 min peak: A = C145A AGT containing a single cross-link to dG (observed M = 23 367 Da, calculated M = 23 365 Da); B = unmodified protein (observed M = 23 014 Da, calculated M = 23 012 Da).

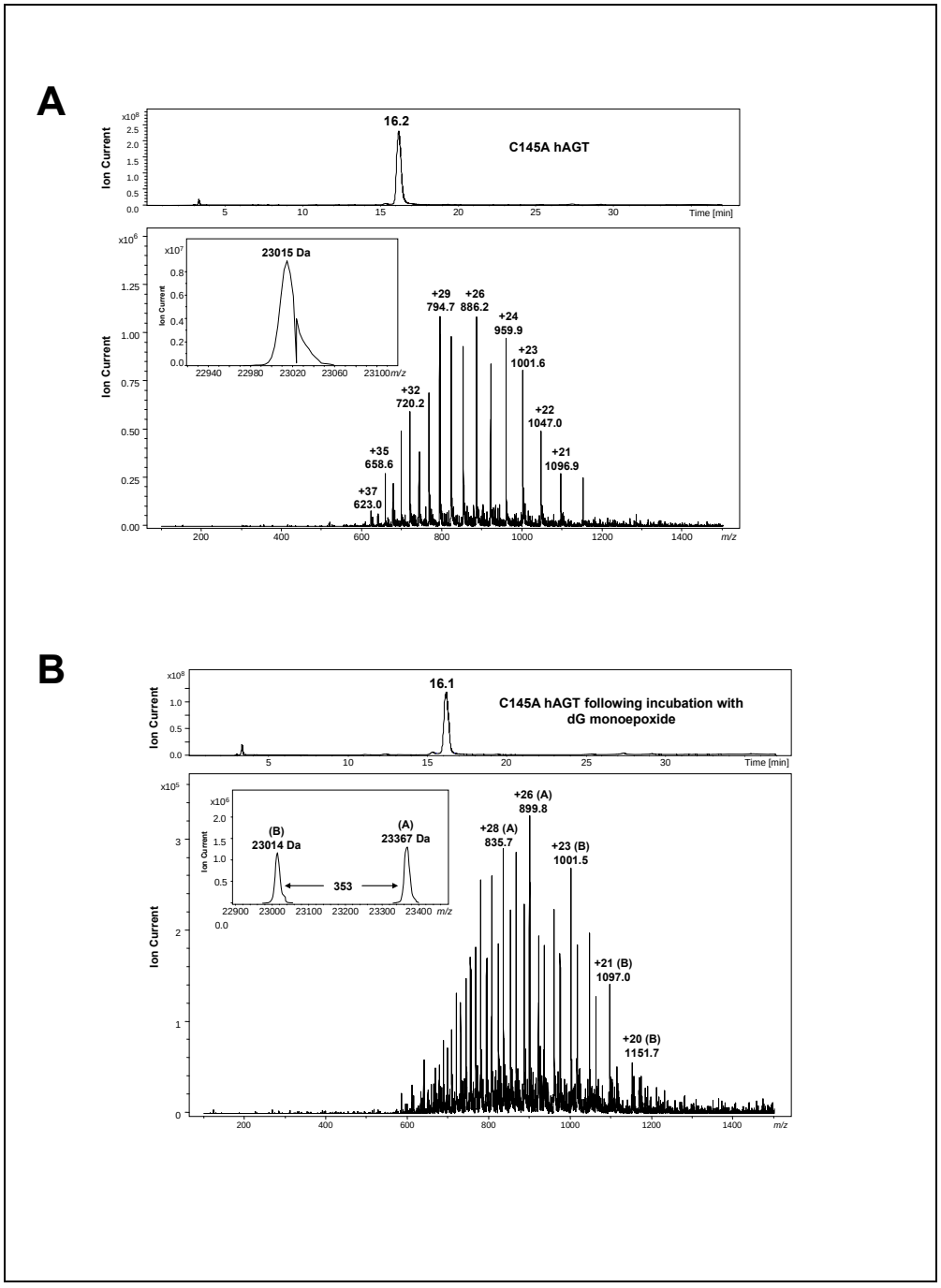

wild-type protein, one of which involves the alkyl acceptor site, Cys^{145}. Further insight into the identities of AGT amino acids responsible for reaction with dG monoepoxide was provided by HPLC-ESI^+-MS/MS analysis of tryptic digests of alkylated protein.

Proteolytic digestion with trypsin provided good sequence coverage for both protein variants (*Tables 2.1 and 2.2*). For wild-type AGT, 14 of the 16 possible tryptic peptides were observed, including the doubly charged active site peptide G^{136}NPVPILIPC*HR^{147} (C* = Cys^{145}) at 658.4 *m/z* (calculated *M* = 1314.7 Da). HPLC-ESI^+-MS/MS analysis of the tryptic digest of dG monoepoxide-treated hAGT detected a prominent doubly charged peptide (*m/z* 777.9 $[M + 2H]^{2+}$) corresponding to a butanediol conjugate between G^{136}NPVPILIPCHR^{147} and a free guanine base (calculated *M* = 1551.7 Da, ΔM = 237 Da) (*Figure 2.4*). As expected, the deoxyribose originating from dG monoepoxide was released by spontaneous hydrolysis of the N7-alkylated dG during tryptic digestion of the cross-linked protein. When this peptide was subjected to collision induced dissociation (CID) in the ion trap mass spectrometer, it produced MS/MS spectrum consistent with the presence of a butanediol-guanine adduct at C* (Cys^{145}) (*Figure 2.4*). The masses of b_4-b_8 ions were in agreement with theoretical values for unmodified peptide, while the mass of the b_{11} fragment was increased by 237 Da (observed *M* = 1377.9 Da *vs.* calculated *M* = 1141.6 Da for the unmodified peptide), suggesting that the adduct resides between the 9^{th} and 11^{th} residue of the peptide (PC*H). The y_4-y_9 ions carry the butanediol-Gua adduct as indicated by a +237 Da mass shift, consistent with modification at the C-terminus (PC*HR). Taken together, these results are consistent with butanediol-guanine cross-linking to Cys^{145} (C*). Further proof of modification at this site was obtained by HPLC-ESI^+-MS/MS analysis of synthetic

Figure 2.4 MS/MS analysis of AGT tryptic peptide $G^{136}NPVPILIPCHR^{147}$ containing a dG monoepoxide-induced butanediol cross-link between Cys^{145} and guanine. *Top:* Extracted ion chromatogram of *m/z* 777.0 $[M + 2H]^{2+}$; *Bottom:* MS/MS spectrum. Modified fragment ions are indicated by "*".

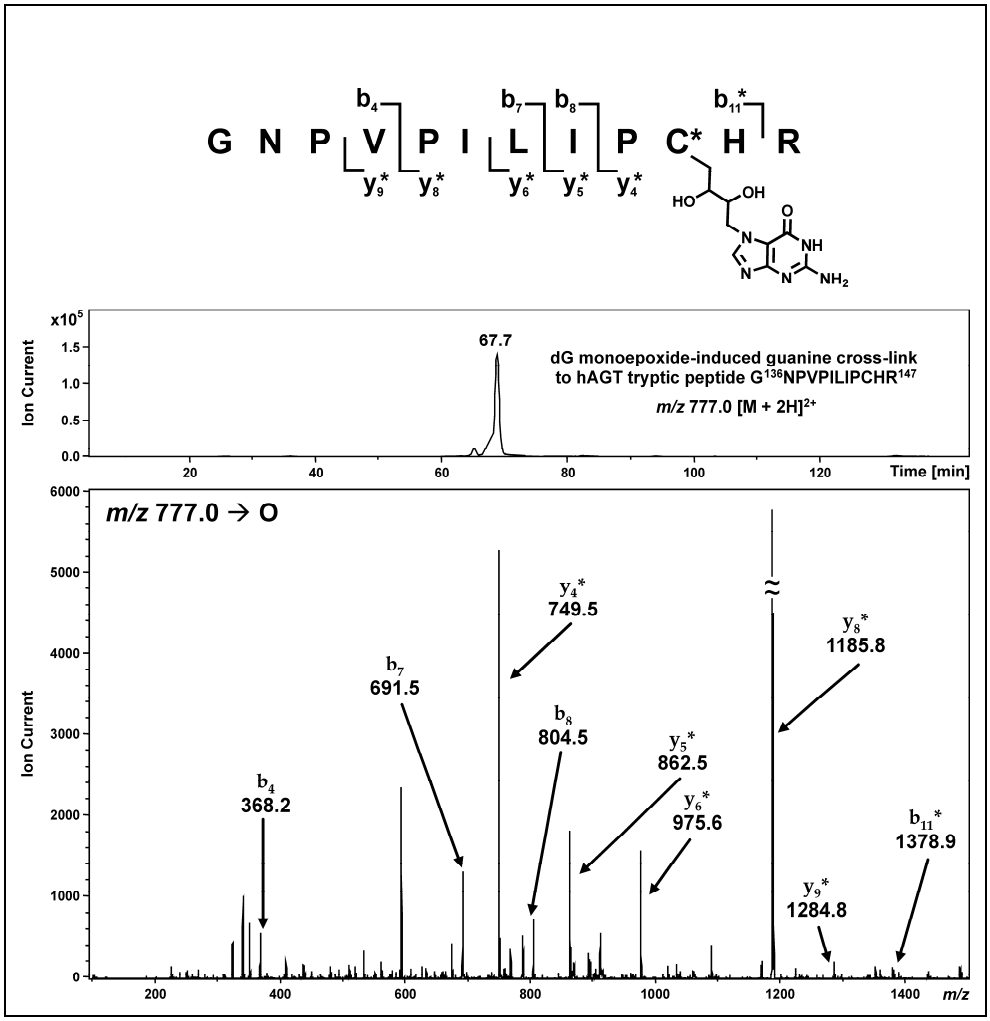

peptide GNPVPILIPCHR containing a dG monoepoxide-induced butanediol cross-link to guanine (*m/z* 777.1 $[M + 2H]^{2+}$) which displayed similar HPLC retention time and MS/MS fragmentation as the AGT derived cross-link (*Figure 2.5*). Finally, the C145A mutant has lost the ability to form conjugates within this protein region, supporting a critical role of Cys^{145} in the cross-linking reaction (see below).

The second cross-linking site was located upon further analysis of the tryptic fragments originating from dG monoepoxide-treated wild-type AGT. HPLC-ESI^+-MS/MS signal corresponding to the peptide V^{148}VC*SSGGAVGNYS GGLAVK^{165} containing a single butanediol-guanine adduct was detected (*m/z* 953.6 $[M + 2H]^{2+}$; calculated *M* = 1903.8) (*Figure 2.6*). The cross-linking site was mapped to Cys^{150} (C*) based on the MS/MS fragmentation patterns, especially the diagnostic b_3 and y_{15} ions at 593.3 and 1366.8 *m/z*, respectively. The y_{15} ion mass matched the theoretical value, while the b_3 ion experienced a +237 Da mass shift, suggesting that cross-linking took place within the C-terminal region of the peptide (VVC), probably at Cys^{150}. HPLC-ESI^+-MS/MS analysis of the tryptic digests of the C145A AGT mutant detected 12 of the 16 expected tryptic fragments, including the active site peptides G^{136}NPVPILIPAHR^{147} (*m/z* 624.5 $[M + 2H]^{2+}$) and V^{148}VC*SSGGAVGNYSG GLAVK^{165} (*m/z* 834.8 $[M + 2H]^{2+}$) (*Table 2.2*). Mass spectral analysis of the dG monoepoxide-treated C145A mutant detected an adducted peptide V^{148}VC*SSGGAVGNY SGGLAVK^{165} containing a butanediol cross-link to guanine (*m/z* 953.4 $[M + 2H]^{2+}$). This peptide adduct displayed the same HPLC retention time and CID fragmentation pattern as the product observed in wild-type AGT exposed to dG monoepoxide, suggesting that these two peptide cross-links were identical. In contrast, no cross-linking to peptide G^{136}NPVPILIPAHR^{147} was

Figure 2.5 Synthetic peptide GNPVPILIPCHR containing dG monoepoxide-induced butanediol cross-link between Cys and guanine. *Top:* Extracted ion chromatogram of *m/z* 777.0 $[M + 2H]^{2+}$; *Bottom:* MS/MS spectrum. Modified fragment ions are indicated by "*".

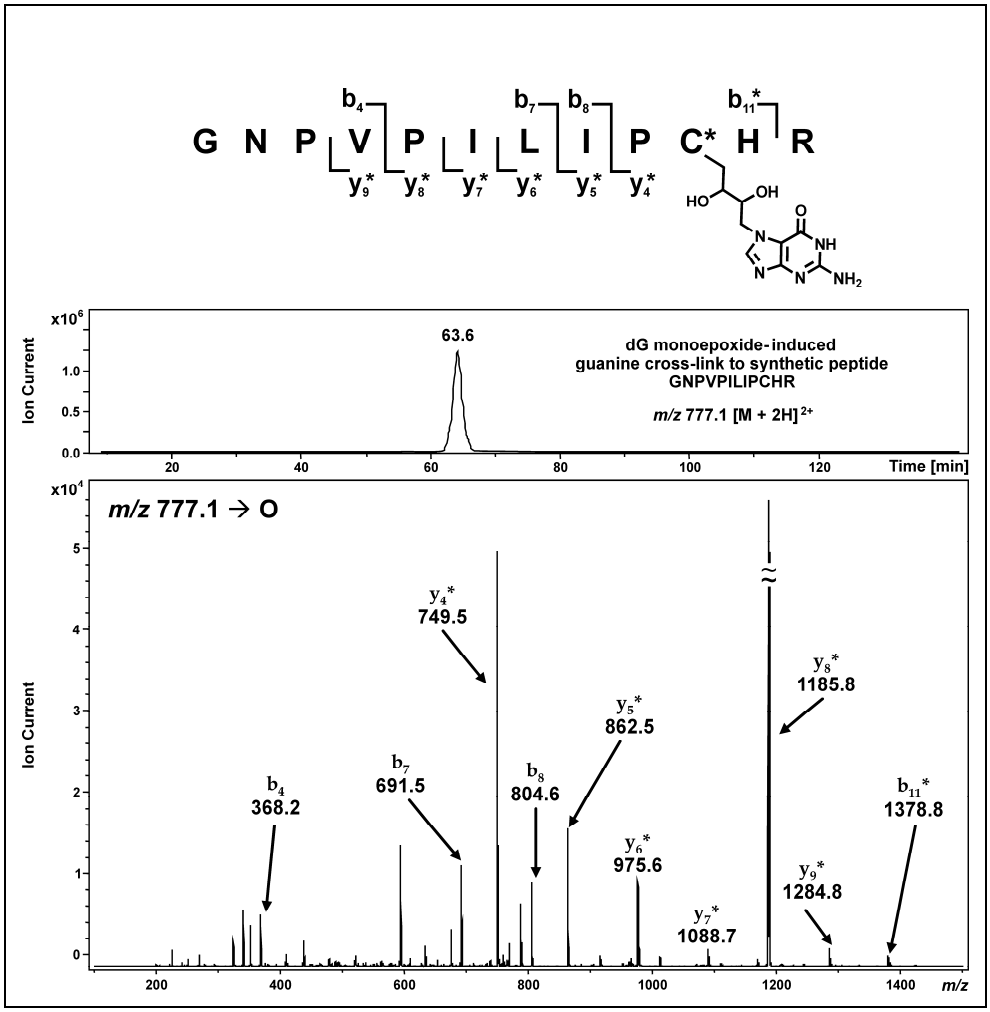

Figure 2.6 MS/MS analysis of AGT tryptic peptide V^{148}VCSSGGAVGNYSG GLAVK^{165} containing dG monoepoxide-induced butanediol cross-link between Cys^{150} and guanine. *Top:* Extracted ion chromatogram of *m/z* 953.6 $[M + 2H]^{2+}$; *Bottom*: MS/MS spectrum. Modified fragment ions are indicated by "*".

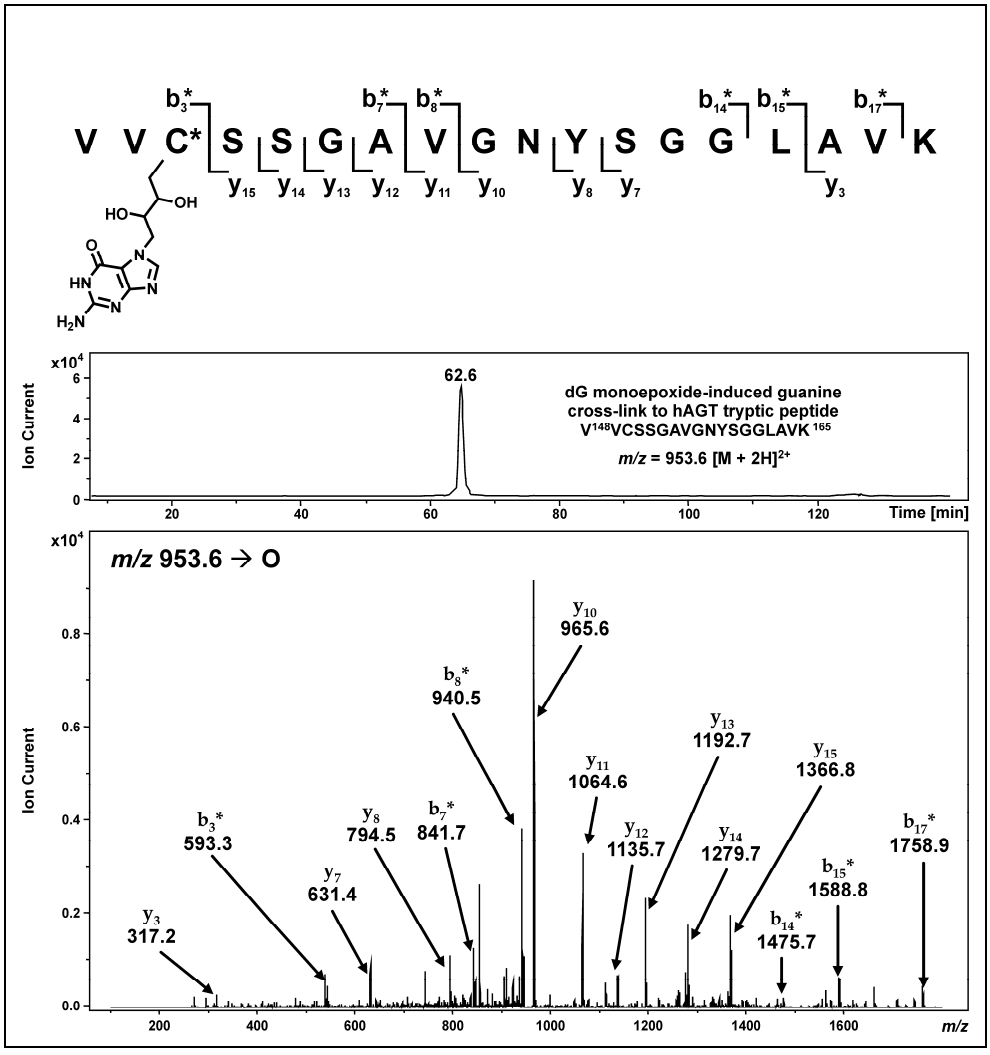

observed for C145A mutant protein in which the key cysteine residue was replaced with alanine (A), confirming that C^{145} participates in cross-linking to DNA.

2.4.4 HPLC-ESI$^+$-MS/MS Analysis of DEB-Induced AGT Cross-Links to Double-Stranded DNA.

Although our peptide mapping results using a model system composed of AGT protein and pre-formed dG monoepoxide (*Scheme 2.2, right*) are consistent with the formation of butanediol conjugates involving active site cysteines 145 and 150 (*Figures 2.3-2.6*), the cross-linking specificity of DEB can potentially be altered upon AGT binding to double-stranded DNA. Furthermore, protein modification by DEB may take place prior to DNA binding as proposed for dihaloethanes *(57)*. Therefore, an additional series of experiments was conducted to map the locations of DEB-induced cross-links of AGT to double-stranded DNA. In these studies, AGT or C145A AGT proteins were incubated under physiological conditions with oligodeoxynucleotide duplexes (5'- GGA GCT GGT GGC GTA GGC-3', (+) strand) in the presence of excess racemic DEB (500 molar equivalents). Samples were subjected to thermal hydrolysis to release N7-alkylated guanines, followed by enzymatic digestion with trypsin and mass spectral analysis (*Scheme 2.2, left*).

HPLC-ESI$^+$-MS/MS analysis of the tryptic digest of wild-type AGT which had been incubated with DEB in the presence of double stranded DNA revealed the presence of butanediol cross-links to G^{136}NPVPILIPC*HR^{147} and V^{148}VC*SSGGAVGNYSGGLA VK^{165}, with CID fragmentation patterns supporting modifications at Cys^{145} and Cys^{150}

Figure 2.7 AGT tryptic peptide $G^{136}NPVPILIPCHR^{147}$ containing a DEB-induced butanediol cross-link to guanine. *Top:* Extracted ion chromatogram (*m/z* 776.9 $[M + 2H]^{2+}$); *Bottom:* MS/MS mapping the cross-link to Cys^{145}. Modified fragment ions are indicated by "*".

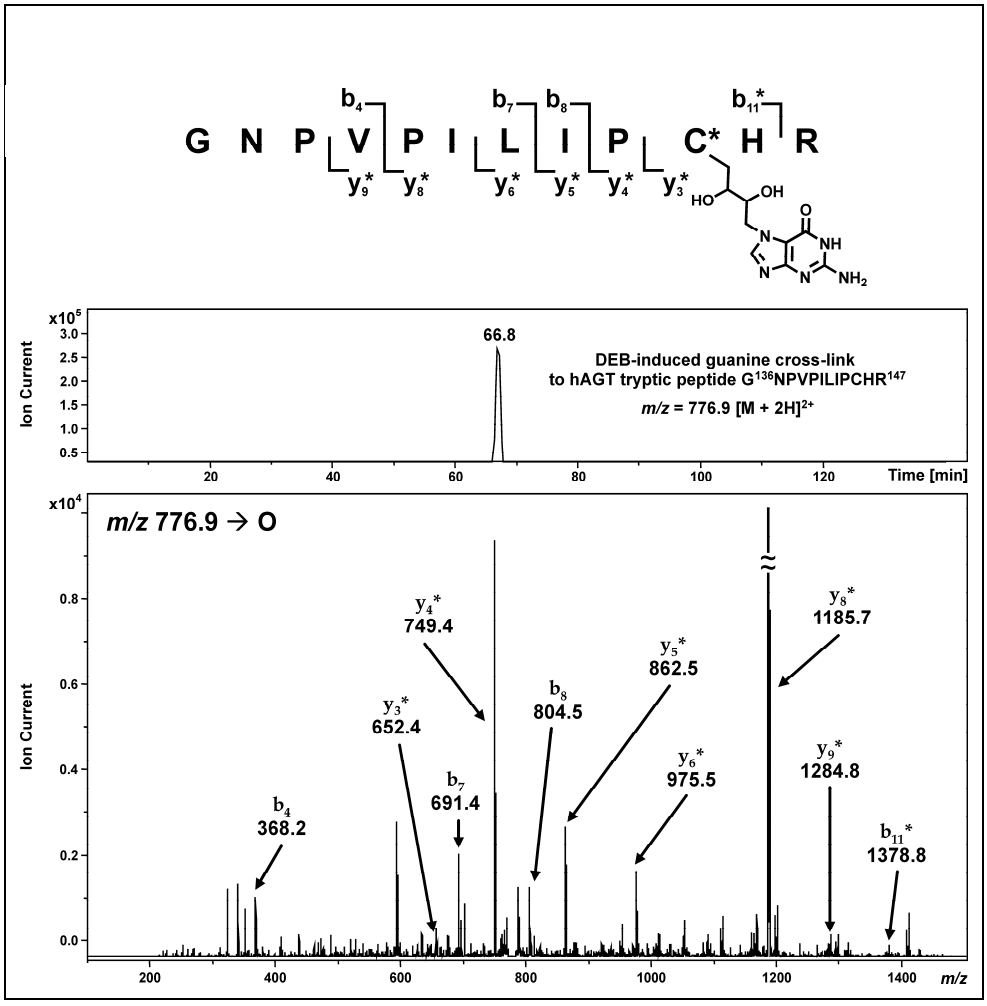

Figure 2.8 AGT tryptic peptide V^{148}VCSSGGAVGNYSGGLAVK^{165} containing a DEB-induced butanediol cross-link to guanine. *Top:* Extracted ion chromatogram (*m/z* 952.9 $[M + 2H]^{2+}$); *Bottom:* MS/MS spectrum mapping the cross-link to Cys^{150}. Modified fragment ions are indicated by "*".

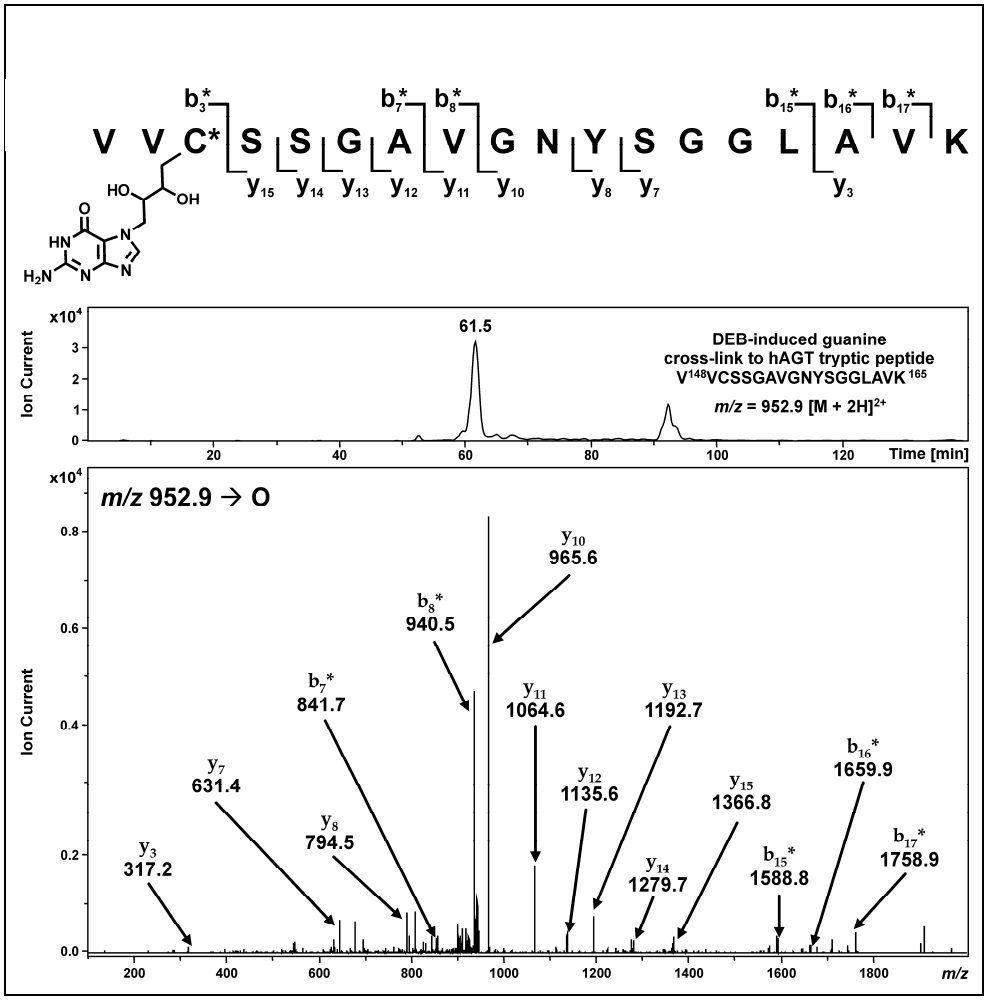

(*Figures 2.7 and 2.8*). In addition, DEB-induced trihydroxybutyl adducts were detected at Cys^{145} (*m/z* 710.4 $[M + 2H]^{2+}$) and Cys^{150} (*m/z* 886.4 $[M + 2H]^{2+}$) (*Figures 2.9 and 2.10*). The latter products likely originate from the reactions of cysteine residues of AGT with DEB to form (2'-hydroxy-3',4'-epoxybut-1'-yl)-cysteine intermediates, followed by spontaneous hydrolysis to the corresponding 2',3',4'-trihydroxybutyl species.

Tryptic digests of the C145A mutant subjected to DEB treatment in the presence of DNA contained $V^{148}V\underline{C}SSGGAVGNYSGGLAVK^{165}$ butanediol cross-links to guanine (*m/z* 952.9 $[M + 2H]^{2+}$), which displayed the same HPLC retention time and CID fragmentation patterns as the corresponding product originating from the wild-type protein (*Figure 2.8*). In contrast, no cross-links to the active site peptide $G^{136}NPVPILIP\underline{A}HR^{147}$ were formed for C145A AGT, supporting the direct participation of Cys^{145} in DNA-protein cross-linking.

In general, our results for AGT cross-linking to double-stranded DNA in the presence of DEB were analogous to those obtained upon AGT treatment with pre-formed dG monoepoxide. One noticeable difference involved the relative reactivity of Cys^{145} and Cys^{150} residues. While both cysteines were modified with similar efficiency in dG monoepoxide treated AGT, Cys^{145} formed three times more AGT-guanine cross-links in DNA experiments. As the formation of DEB-mediated trihydroxybutyl adducts was comparable at these two cysteines, this suggests that cross-linking specificity of DEB is altered by DNA-protein interactions between AGT and double stranded oligodeoxynucleotides.

Figure 2.9 AGT tryptic peptide G[136]NPVPILIPCHR[147] containing a DEB-induced 2',3',4'-trihydroxybut-1'-yl adduct to active site Cys[145]. *Top:* Extracted ion chromatogram (*m/z* 710.4 $[M + 2H]^{2+}$); *Bottom*: MS/MS spectrum mapping the lesion to Cys[145]. Modified fragment ions are indicated by "*".

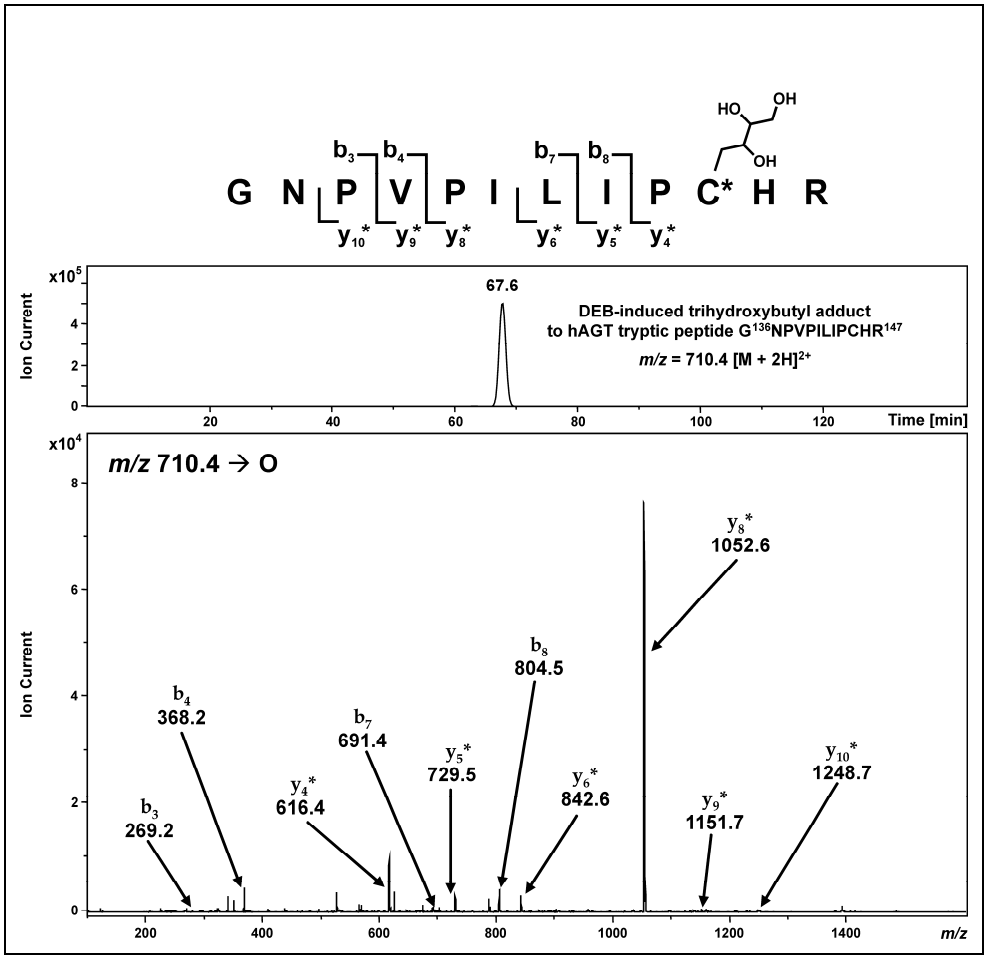

Figure 2.10 AGT tryptic peptide $V^{148}VCSSGGAVGNYSGGLAVK^{165}$ containing a DEB-induced 2',3',4'-trihydroxybut-1'-yl adduct to cysteine 150. *Top:* Extracted ion chromatogram (*m/z* 886.4 $[M + 2H]^{2+}$); *Bottom*: MS/MS spectrum mapping the lesion to Cys^{150}. Modified fragment ions are indicated by "*".

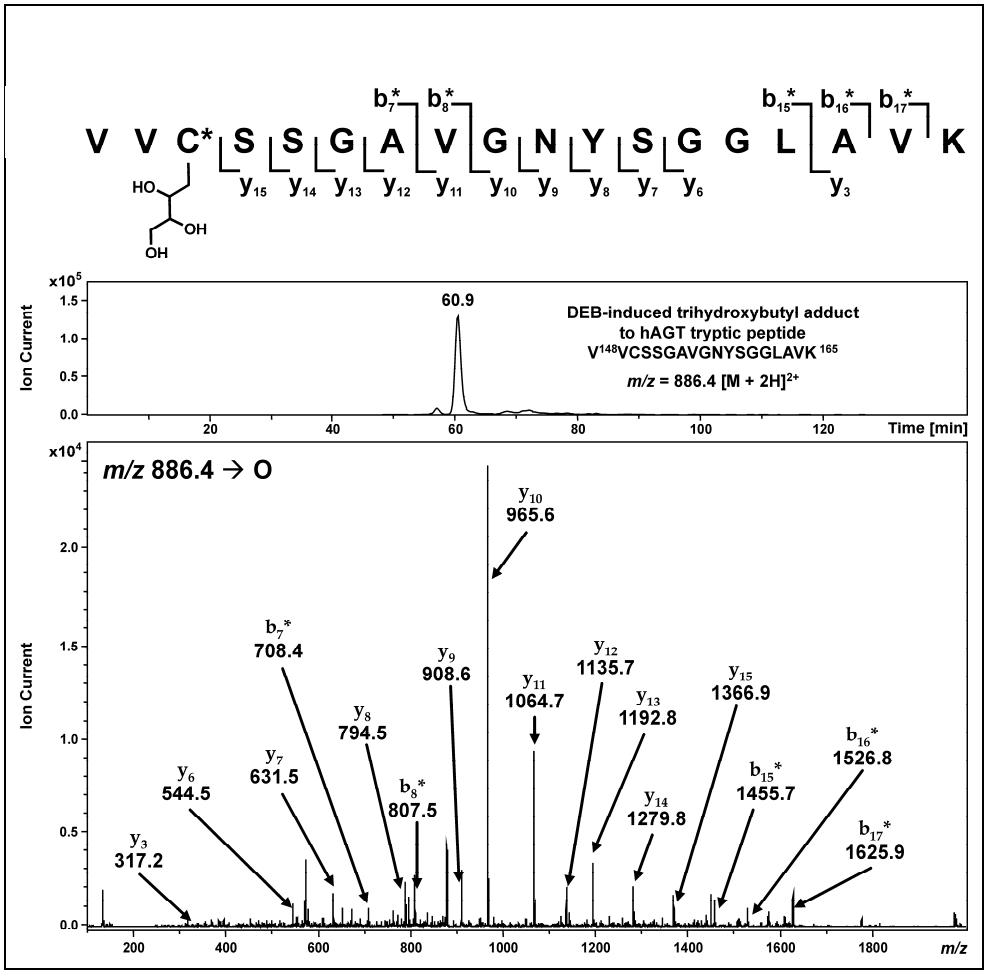

2.4.5 HPLC-ESI$^+$-MS Analysis of Total Digests of dG Monoepoxide-Treated AGT and DEB-Induced AGT-DNA Cross-Links

In order to confirm that AGT-DNA cross-linking by DEB took place exclusively at the cysteine residues within the protein, HPLC-MS/MS analysis of the total enzymatic digests of alkylated proteins was performed. Following the cross-linking reaction, AGT proteins were subjected to complete digestion in the presence of carboxypeptidase Y and proteinase K, followed by HPLC-ESI$^+$-MS/MS analysis of the resulting amino acids. The mass spectrometer was set up to monitor the formation of 1-(*S*-cysteinyl)-4-(guan-7-yl)-2,3-butanediol (*m/z* 359.1), 1-(*O*-tyrosyl)-4-(guan-7-yl)-2,3-butanediol (*m/z* 420.1), 1-(*N*-lysyl)-4-(guan-7-yl)-2,3-butanediol (*m/z* 385.4), 1-(*N*-arginyl)-4-(guan-7-yl)-2,3-butanediol (*m/z* 413.4), and 1-(*N*-histidyl)-4-(guan-7-yl)-2,3-butanediol (*m/z* 393.4). HPLC-ESI$^+$-MS/MS of a digest of dG monoepoxide treated AGT detected a prominent peak co-eluting with the authentic standard of 1-(*S*-cysteinyl)-4-(guan-7-yl)-2,3-butanediol (Cys-Gua-BD, *m/z* 359.7 $[M + H]^+$) (*Figure 2.11, panel A*). MS/MS fragmentation of *m/z* 359.7 yielded the product ions corresponding to the loss of guanine (*m/z* 208.0 $[M + H - Gua]^+$) and the removal of guanine and a molecule of water (*m/z* 190.0 $[M + H - Gua - H_20]^+$). This compound had the same MS/MS fragmentation pattern and HPLC retention time as synthetically prepared standard of Cys-Gua-BD. In contrast, no amino acid-guanine cross-links involving other nucleophilic residues (Lys, Arg, His, Tyr) were detected (results not shown). Similar results were obtained for the C145A AGT mutant (*Figure 2.11, panel B*) and for AGT-DNA cross-linking in the presence of DNA, confirming that the cross-linking reaction is specific for cysteine residues within the protein.

Figure 2.11 HPLC-ESI$^+$-MS/MS analysis of 1-(*S*-cysteinyl)-4-(guan-7-yl)-2,3-butanediol (Cys-Gua-BD) in total digests of AGT proteins treated with dG monoepoxide. (**A**) Extracted ion chromatogram of Cys-Gua-BD (*m/z* 359.7 [M + H]$^+$) resulting from the total digestion of dG monoepoxide-treated AGT; *Inset*: MS/MS fragmentation of Cys-Gua-BD. (**B**) Extracted ion chromatogram of Cys-Gua-BD (*m/z* 359.4 [M + H]$^+$) resulting from the total digestion of dG monoepoxide-treated C145A AGT; *Inset*: MS/MS fragmentation of Cys-Gua-BD.

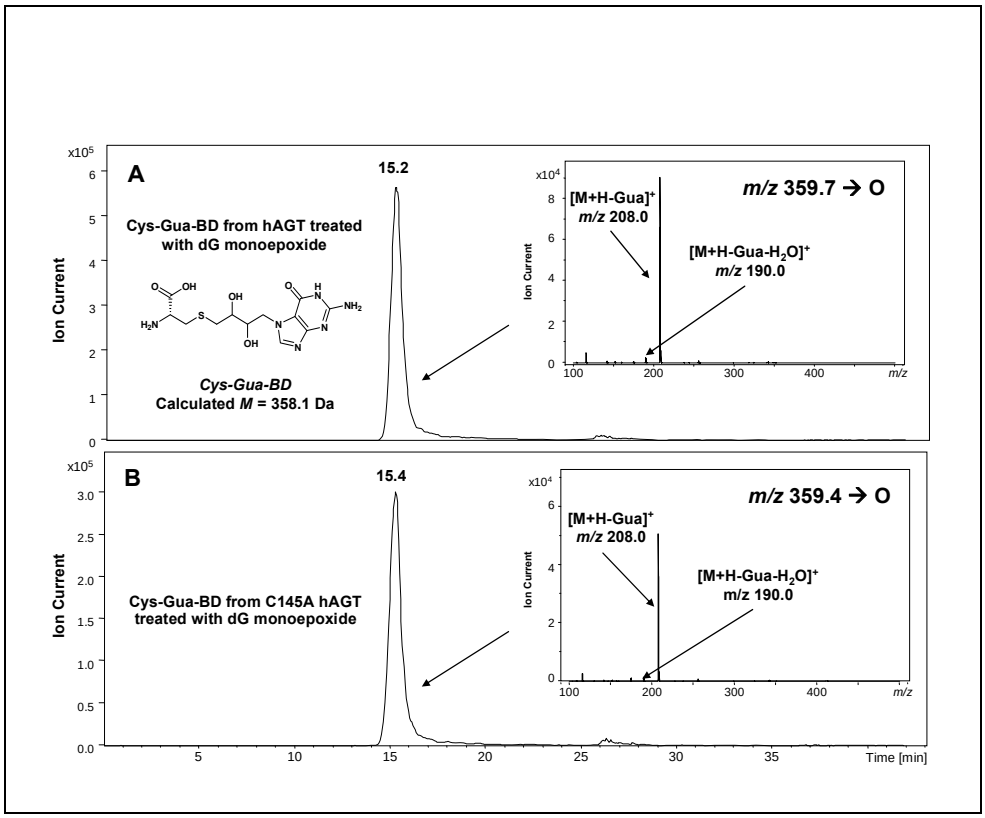

2.5 Discussion

Our results presented above provide direct evidence for AGT-DNA cross-linking by DEB. The resulting AGT-DNA conjugates involve the side chain sulfhydryls of Cys^{145} or Cys^{150} within the active site of AGT and the N7 position of guanine in duplex DNA and have the structure of 1-(*S*-cysteinyl)-4-(guan-7-yl)-2,3-butanediol.

As indicated by the crystal structure of human AGT, this protein contains two distinct domains – an N-terminal domain (residues 1-85) and a C-terminal domain (residues 86-207) *(108)*. The N-terminal domain is comprised of a four-stranded anti-parallel β-sheet packed against a single α-helix (Helix 1). The C-terminal domain, which contains both the O^6-alkylguanine-binding channel and helix-turn-helix DNA-binding motif, is made up of a short two-stranded parallel β-sheet and five α-helicies. Human AGT contains a total of five cysteine residues: Cys^5, Cys^{24}, Cys^{62}, Cys^{145}, and Cys^{150}. Cysteines 145 and 150 are located in the protein's C-terminal domain within the active site, with Cys^{145} directly participating in the alkyl transfer reaction (*Figure 2.12*). In contrast, Cys^5, Cys^{24}, and Cys^{62} are all located in N-terminal domain, far removed from the site of DNA binding.

Our results indicate that there are two distinct sites within human AGT that can form cross-links to DNA in the presence of DEB (*Figures 2.2 and 2.3*), and that AGT-DNA cross-linking by DEB is specific for active site cysteines 145 and 150 (*Figures 2.4-2.6*). In contrast, no cross-linking was detected at Cys^5, Cys^{24}, or Cys^{62}. The apparent inability of these three residues to cross-link DNA can be explained by the fact that Cys^5 and Cys^{24} (along with His^{29} and His^{85}) are involved in coordination with Zn (II) and that

Cys^{62} is located in Helix 1 of the N-terminal domain which does not appear to be solvent-accessible *(108;110)*.

The preferential alkylation of Cys^{145} is not unexpected because of its unusually low pK_a (4 - 5) and high reactivity towards electrophiles *(113)*. Previous studies examining DNA-AGT cross-linking by dibromoethane and other dihaloethanes suggest that these compounds first alkylate the side chain thiol of Cys^{145} to afford a half-mustard, which then reacts with nucleophilic sites in DNA to form a covalent DNA-AGT complex (*Scheme 2.1, panel A*) *(159)*. The reactivity of dihaloethanes towards DNA without AGT-induced activation to an episulfonium ion is minimal.

Unlike dihaloalkanes, DEB also produces a large number of cross-links at Cys^{150}. The AGT mutant in which Cys^{145} was replaced with alanine (C145A) was capable of forming conjugates with DNA in the presence of DEB by utilizing the side chain of Cys^{150} (*Figures 2.1 and 2.3*). This is in contrast with dibromoethane, which participated in cross-linking to Cys^{150} only under extensive treatment conditions *(57;153)*. A likely explanation for a greater contribution of Cys^{150} to cross-linking to DNA by DEB involves a different sequence of events leading up to cross-link formation (*Scheme 2.1*). In contrast with dihaloalkanes, DEB has a high reactivity towards the N7 position of guanine in DNA *(82;169)*, giving rise to N7-(2'-hydroxy-3',4'-epoxybut-1'-yl)-guanine monoadducts (*Scheme 2.1, panel B*). AGT binding to a double stranded DNA substrate brings Cys^{150} in close proximity to DNA *(110)*. In the crystal structure of AGT bound to a double-stranded oligonucleotide (*Figure 2.12*), Cys^{150} is located on the outer perimeter of the active site pocket adjacent to residues Ser^{151} and Tyr^{114}, both of which directly contact the DNA backbone *(110)*. Upon binding to duplex DNA, Cys^{150} may

Figure 2.12 Locations of AGT active site cysteines in relationship to DNA *(110)*. Catalytic Cys^{145} and neighboring Cys^{150} are shown in yellow. This figure was generated using the molecular modeling environment Maestro.

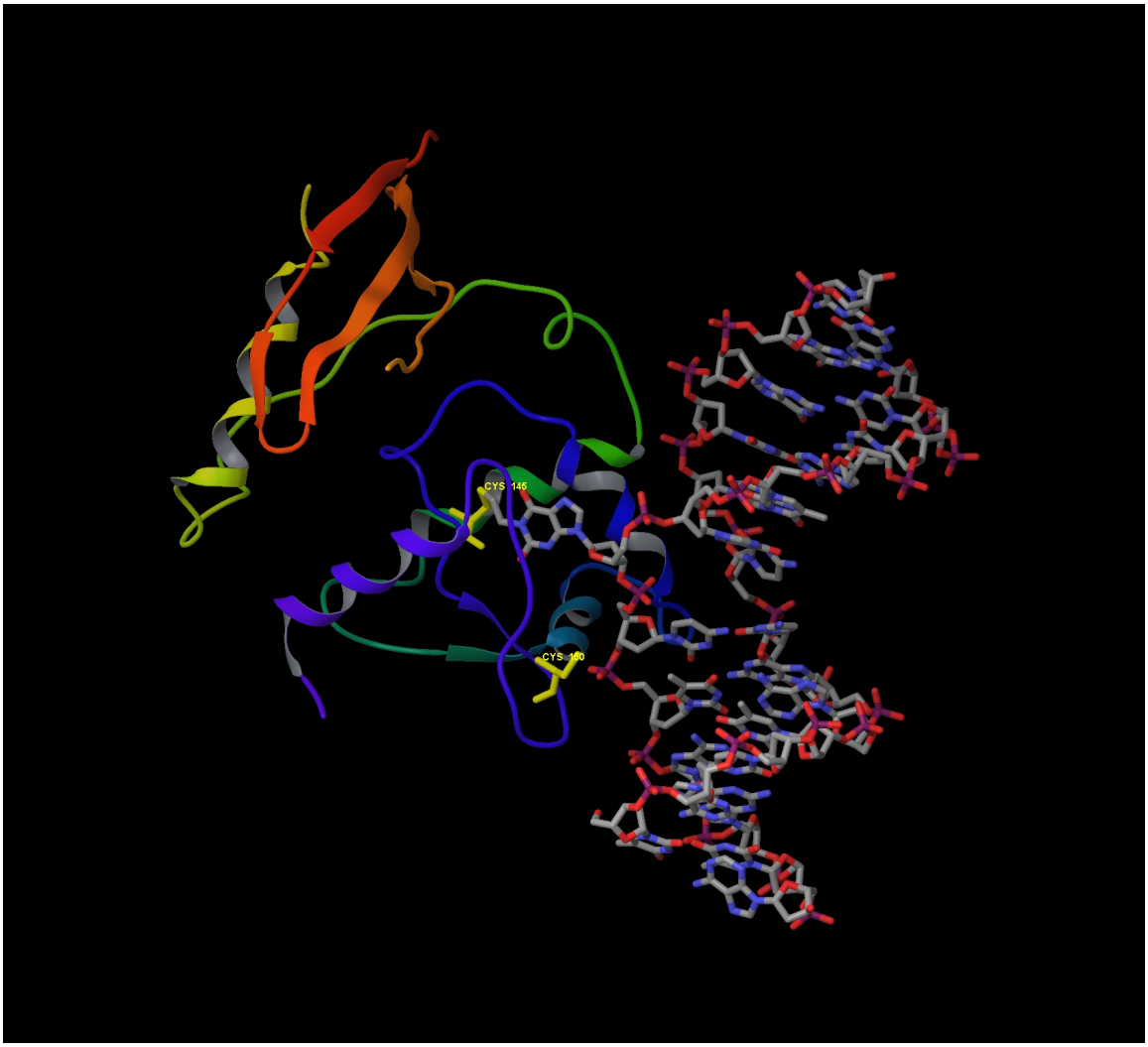

nucleophilically attack DEB-induced N7-(2'-hydroxy-3',4'-epoxybut-1'-yl)-guanine monoepoxide lesions to form DNA-protein adducts (*Scheme 2.1, panel B*). A similar specificity for cross-linking to DNA *via* Cys^{150} and Cys^{150} is observed for antitumor nitrogen mustards, another group of bifunctional electrophiles with high reactivity towards guanine in DNA (*see Chapter III*). However, initial alkylation of AGT protein by DEB cannot be presently ruled out. Both Cys^{145} and Cys^{150} can be directly alkylated by DEB as demonstrated by the formation of (2',3',4'-trihydroxybut-1'-yl) adducts at these sites (*Figures 2.9 and 2.10*). These lesions may originate as 2'-hydroxy-3',4'-epoxybut-1'-yl monoadducts, followed by spontaneous hydrolysis of the epoxide in the presence of water.

Although our study employed a large excess of DEB to afford the levels of cross-linking detectible by HPLC-ESI^+-MS, these results may still hold biological significance because the bulky DNA-protein cross-links are likely to cause significant disruption of cellular processes, including DNA replication and transcription. Studies are currently underway to further elucidate the mechanisms of AGT-DNA cross-link formation and to develop sensitive and specific methodology to enable their detection *in vivo*. These experiments will help explain the enhanced cytotoxicity and mutagenicity of DEB observed in cells expressing the AGT protein *(154)*.

III. CROSS-LINKING OF HUMAN RECOMBINANT O^6-ALKYLGUANINE DNA ALKYLTRANSFERASE TO DNA BY ANTITUMOR NITROGEN MUSTARDS

3.1 Abstract

The antitumor activity of chemotherapeutic nitrogen mustards including chlorambucil, cyclophosphamide, and melphalan, is commonly attributed to their ability to induce DNA-DNA cross-links by consecutive alkylation of two nucleophilic sites within the DNA duplex. DNA-protein cross-linking by nitrogen mustards is not well characterized, probably because of its inherent complexity and the insufficient sensitivity of previous methodologies. If formed, DNA-protein conjugates are likely to contribute to both target and off-target cytotoxicity of nitrogen mustard drugs. Here we show that the human DNA repair protein AGT can be readily cross-linked to DNA in the presence of nitrogen mustards. Both chlorambucil and mechlorethamine induced the formation of covalent conjugates between ^{32}P-labeled double-stranded oligodeoxynucleotides and recombinant human AGT protein, which were detected by SDS-PAGE. Capillary HPLC-electrospray ionization mass spectrometry (ESI-MS) analysis of hAGT that had been treated with guanine half-mustards of chlorambucil or mechlorethamine revealed the ability of the protein to form either one or two cross-links to guanine. C145A AGT – a variant containing a single point mutation in the protein's active site – was found capable of forming a single guanine conjugate, while cross-linking was virtually abolished upon treatment of the C145A/C150S AGT double mutant with the guanine half-mustards. HPLC-ESI$^+$-MS/MS sequencing of the tryptic peptides obtained from the wild type AGT that had been treated with nitrogen mustard in the presence of DNA confirmed that the

cross-linking took place between the N7 position of guanine in DNA and two active site residues within the AGT protein (Cys^{145} and Cys^{150}). The exact chemical structures of AGT-DNA cross-links induced by chlorambucil and mechlorethamine were identified as *N*-(2-[*S*-cysteinyl]ethyl)-*N*-(2-[guan-7-yl]ethyl)-*p*-aminophenylbutyric acid and *N*-(2-[*S*-cysteinyl]ethyl)-*N*-(2-[guan-7-yl]ethyl)methylamine, respectively, based upon HPLC-MS/MS analysis of protein hydrolysates in parallel with the corresponding amino acid conjugates prepared synthetically. Because AGT is overexpressed in many tumor types, further investigations of potential role of AGT-DNA cross-linking in the antitumor and mutagenic activity of antitumor nitrogen mustards is warranted.

3.2 Introduction

Nitrogen mustard drugs are broadly used in the clinic against a variety of neoplastic conditions, including lymphoma (cyclophosphamide, uramustine), leukemia (cyclophosphamide), multiple myeloma, and ovarian carcinoma (melphalan), as well as autoimmune diseases (cyclophosphamide) *(170)*. Spontaneous cyclization of the 2-(chloroethyl) groups of nitrogen mustards under physiological conditions produces highly reactive aziridinium ions, which alkylate cellular biomolecules (*Scheme 3.1*). Initial DNA alkylation leads to the formation of N7-guanine half mustards, which retain one of the chloroethyl groups (*Scheme 3.1*). These monoadducts can then react with another nucleophilic site within DNA or in a neighboring protein, giving rise to DNA-DNA cross-links and DPCs. If not repaired, the resulting bifunctional lesions can cause the blockage of the replication fork, accumulation of mutations, and the induction of protective genes involved in pro-apoptotic processes *(1)*.

Scheme 3.1. Chemical structures of nitrogen mustards and guanine half-mustards

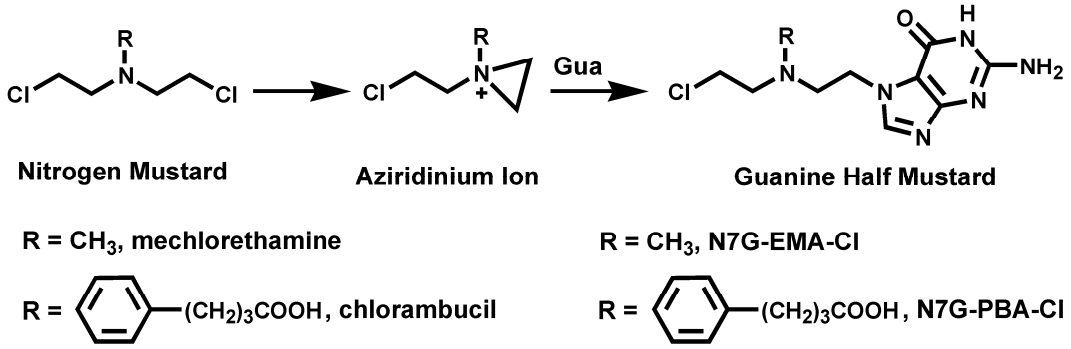

DNA-DNA cross-linking by nitrogen mustards is well characterized and is thought to be largely responsible for their cytotoxic effects *(50;85;98;170;171)*. In contrast, little is known about the identities of the corresponding DNA-protein conjugates. DNA binding proteins (histones, DNA repair proteins, and transcription factors) are known to become chemically linked to DNA in the presence of various oxidants and numerous *bis*-electrophiles including DBE, DEB, platinum drugs, and dialhehydes *(11;153;170;172;173)*. If formed as a result of nitrogen mustard chemotherapy, the resulting DNA-protein adducts are likely to be strongly blocking and poorly repaired *(27)*, mediating their biological activity in target and non-target cells.

We recently employed a mass spectrometry based strategy to demonstrate that AGT, an important DNA repair protein, forms cross-links to the N-7 guanine within DNA in the presence of DEB *(37)*. The normal physiological function of AGT protein is to transfer the O^6-alkyl group from promutagenic O^6-alkylguanine lesions in DNA to an active site cysteine (Cys^{145} in the human protein), restoring normal guanine and preventing mutagenesis *(101)*. Crystal structures of DNA-bound AGT protein support a repair mechanism involving protein binding to the minor groove of double-stranded DNA and subsequent "flipping" of nucleotides out of the base stack into the AGT active site *(110)*. This conformational change places O^6-alkylguanine group <3 Å from the side chain of Cys^{145} within the active site. Cys^{145} is activated to a thiolate anion because of its interactions with a bound Zn (II) cation and the formation of a Glu-His-water-Cys H-bond network *(108;117)*. Nucleophilic attack of Cys^{145} at the O^6-alkyl lesion results in the formation of a thioether at Cys^{145} and restores intact dG within DNA. Because alkylation of the catalytic residue of AGT is irreversible, this repair process is non-

enzymatic in nature, consuming a molecule of AGT in each alkyl transfer reaction *(117)*. Cys^{145} alkylation destabilizes the native fold of AGT, targeting the protein for ubiquitination and subsequent degradation by the 26S proteasome *(155)*. Most tumor cells overexpress AGT, leading to resistance against alkylating agents that target the O^6 position of guanine, such as BCNU *(111)*. Potent irreversible inhibitors of AGT have been developed in an attempt to sensitize tumor cells to the alkylating drugs *(157;174)*.

In a sharp contrast with protective effects of AGT against DNA monoalkylating agents, AGT expression in bacterial cell culture has been shown to enhance the cytotoxic and mutagenic effects of simple *bis*-electrophiles, including DBE and DEB *(57;153;154)*. As described in *Chapter II*, our previous studies have shown that DEB forms covalent AGT-DNA conjugates involving the side chain sulfhydryls of Cys^{145} or Cys^{150} within the active site of human recombinant AGT and the N7 position of guanine in duplex DNA *(37)*. We therefore hypothesized that antitumor nitrogen mustards can similarly induce the formation of AGT-DNA cross-links. Our present study employed a combination of mass spectrometry, site specific mutagenesis, and proteomics techniques to demonstrate that chlorambucil and mechlorethamine readily cross-link hAGT to DNA *via* two active site cysteine residues. The exact structures of amino acid-nucleobase conjugates were established by capillary HPLC-ESI-MS/MS of protein digests in comparison with synthetic standards prepared by an independent route.

3.3 Materials and Methods

Chemicals and Reagents. The nitrogen mustards used in this study, mechlorethamine hydrochloride and chlorambucil, were purchased from Sigma-Aldrich (Milwaukee, WI).

Boc-Cys-OH was obtained from Fluka (Buchs, Switzerland) and Boc-Lys-OMe was purchased from Bachem (King of Prussia, PA). 2'-Deoxyguanosine was obtained from TCI America (Portland, OR). Adenosine 5'-[γ-^{32}P]triphosphate was purchased from Perkin-Elmer (Boston, MA), and T4 polynucleotide kinase was obtained from New England Biolabs (Beverly, MA). Trypsin, carboxypeptidase Y, and proteinase K were purchased from Worthington Biochemical Corporation (Lakewood, NJ). Synthetic peptide GNPVPILIPCHR (which corresponds to positions 136-147 of hAGT) and all synthetic DNA oligodeoxynucleotides were prepared at the University of Minnesota Microchemical Facility (Minneapolis, MN). Human recombinant AGT proteins (C-terminal histidine-tagged wild-type and N-terminal histidine-tagged C145A and C145A/C150S mutants, *Table 3.1*) were prepared as described previously *(166;167)*.

Detection of Nitrogen Mustard-Induced DNA-Protein Cross-Links by Denaturing PAGE. DNA 18-mer, 5'-GGA GCT GGT GGC GTA GGC-3' (200 pmol), was 5'-end labeled with ^{32}P in the presence of [γ-^{32}P]ATP/T4 polynucleotide kinase. The resulting [γ-^{32}P] 5'-end labeled oligodeoxynucleotide was purified by 12% denaturing PAGE and desalted by SPE using Waters SepPak C18 cartridges. Upon spiking with the corresponding unlabeled DNA (12 nmol), the radiolabeled (+) strand was annealed to its complimentary strand (12.2 nmol) and dissolved in AGT buffer (50 mM TRIS - pH 7.6, and 0.1 mM EDTA). The ^{32}P-labeled duplex (0.93 nmol) was incubated with hAGT (2.0 μg, 0.093 nmol) in the presence of 50, 100, and 200 molar equivalents of mechlorethamine or chlorambucil (4.7, 9.3, and 18.6 nmol respectively). Following a 3 h incubation at 37 °C, the reaction mixtures were separated by 12% SDS-PAGE and the radiolabeled products

Table 3.1 Amino acid sequences of human recombinant AGT and its variants

Wild-type hAGT with C-Terminal His Tag			
MDKDCEMKRT	TLDSPLGKLE	LSGCEQGLHE	IKLLGKGTSA
ADAVEVPAPA	AVLGGPEPLM	QCTAWLNAYF	HQPEAIEEFP
VPALHHPVFQ	QESFTRQVLW	KLLKVVKFGE	VISYQQLAAL
AGNPKAARAV	GGAMRGNPVP	ILIPCHRVVC	SSGAVGNYSG
GLAVKEWLLA	HEGHRLGKPG	LGGSSGLAGA	WLKGAGATSG
SHHHHHH			

MW (average mass): 21876 Da / MW (monoisotopic mass): 21862 Da

C145A hAGT with N-Terminal His Tag			
MRGSHHHHHH	GSMDKDCEMK	RTTLDSPLGK	LELSGCEQGL
HEIKLLGKGT	SAADAVEVPA	PAAVLGGPEP	LMQCTAWLNA
YFHQPEAIEE	FPVPALHHPV	FQQESFTRQV	LWKLLKVVKF
GEVISYQQLA	ALAGNPKAAR	AVGGAMRGNP	VPILIPAHRV
VCSSGAVGNY	SGGLAVKEWL	LAHEGHRLGK	PGLGGSSGLA
GAWLKGAGAT	SGSPPAGRN		

MW (average mass): 23012.40 Da / MW (monoisotopic mass): 22997.79 Da

C145A/C150S hAGT with N-Terminal His Tag			
MRGSHHHHHH	GSMDKDCEMK	RTTLDSPLGK	LELSGCEQGL
HEIKLLGKGT	SAADAVEVPA	PAAVLGGPEP	LMQCTAWLNA
YFHQPEAIEE	FPVPALHHPV	FQQESFTRQV	LWKLLKVVKF
GEVISYQQLA	ALAGNPKAAR	AVGGAMRGNP	VPILIPAHRV
VSSSGAVGNY	SGGLAVKEWL	LAHEGHRLGK	PGLGGSSGLA
GAWLKGAGAT	SGSPPAGRN		

MW (average mass): 22996.34 Da / MW (monoisotopic mass): 22981.81 Da

were visualized using a Bio-Rad Molecular Imager FX. Nitrogen mustard-induced DNA-protein cross-linking was quantified by volume analysis employing Bio-Rad Quantity One Software, with cross-linking efficiency determined by the intensity ratio of the low-mobility cross-link band versus the band corresponding to single-stranded DNA.

Synthesis of Guanine Half-Mustards of Chlorambucil and Mechlorethamine. Guanine half-mustards of chlorambucil and mechlorethamine (*Scheme 3.1*) were prepared by reacting dG with 0.9 equivalents of the mustard in triflouroethanol at 37 ^{o}C for 72 h under anhydrous conditions. The reaction mixture was dried under nitrogen and used without further purification. Following reaction of dG with chlorambucil, the desired *N*-(2-chloroethyl)-*N*-[2-(guan-7-yl)ethyl]-*p*-aminophenylbutyric acid (N7G-PBA-Cl) was obtained in ~ 80% yield. The resulting N7G-PBA-Cl product was characterized by tandem mass spectrometry and UV spectrophotometry. UV: λ_{max} = 246 nm, λ_{min} = 275 nm (pH 4.9); ESI$^+$-MS/MS: *m/z* 419.1 $[M + H]^+ \rightarrow$ *m/z* 268.1 $[M + H - Gua]^+$. The desired mechlorethamine half-mustard, *N*-(2-chloroethyl)-*N*-[2-(guan-7-yl)ethyl]methylamine (N7G-EMA-Cl), was obtained in ~ 60% yield and the chemical structure was confirmed by tandem mass spectrometry and UV spectrophotometry. UV: λ_{max} = 246 nm, λ_{min} = 275 nm (pH 4.9); ESI$^+$-MS/MS: *m/z* 271.1 $[M + H]^+ \rightarrow$ *m/z* 120.1 $[M + H - Gua]^+$. Concentrations of N7G-PBA-Cl and N7G-EMA-Cl were estimated from HPLC-UV peak areas (250 nm) using standard curves generated by injecting known amounts of N7-(2',3',4'-trihydroxybut-1'-yl)-guanine *(82)*.

Synthesis of Amino Acid-Guanine Conjugates: N-(2-[S-cysteinyl]ethyl)-N-(2-[guan-7-yl]ethyl)-p-aminophenylbutyric acid (Cys-N7G-PBA). N7G-PBA-Cl in DMSO was combined with 0.8 equivalents of Boc-Cys-OH in water, and the pH of the reaction mixture was raised to ~ 9 with ammonium hydroxide. The reaction mixture was incubated at 37 °C for 18 h, filtered, and isolated by semi preparative HPLC using a Supelcosil LC-18-DB column (25 cm x 10 mm, 5 µm). The column was eluted with a linear gradient of acetonitrile (B) in 20 mM ammonium acetate, pH 4.9 (A). The solvent composition was changed from 15 to 34 % B in 22 minutes and further to 50% in 4 min. Under these conditions, Boc-protected Cys-N7G-PBA eluted as a sharp peak at 18.6 min. ESI^+-MS/MS: *m/z* 604.3 $[M + H]^+ \rightarrow$ *m/z* 504.2 $[M + H - Boc]^+$ and *m/z* 353.2 $[M + H - Boc - Gua]^+$. HPLC-purified Boc-Cys-N7G-PBA in TFA was incubated at room temperature for 45 min. The deprotected cross-link was purified by semi-preparative HPLC as described previously. Under these conditions, Cys-N7G-PBA eluted as a sharp peak at 9.3 min (~ 1% yield). UV: λ_{max} 256 nm, λ_{min} 280 nm (pH 4.9); ESI^+-MS/MS: *m/z* 504.2 $[M + H]^+ \rightarrow$ *m/z* 353.1 $[M + H - Gua]^+$; ^1H NMR 600 MHz δ (DMSO-d_6, *Table 3.2*): 7.87 (1H, s, H-8), 7.15 (1H, s, NH-1), 6.98 (1H, s, NH_2-8'), 7.06 (1H, s, NH_2-8'), 6.94 (2H, d, CH-2", CH-6", J = 8.4 Hz), 6.72 (2H, d, CH-3", CH-5", J = 8.4 Hz), 6.15 (2H, s, NH_2-2), 4.28 (2H, t, CH_2-1', J = 7.2, 13.8 Hz), 3.65 (2H, t, CH_2-2', J = 6.6, 13.2 Hz), 3.37 (2H, m, CH_2-4', J = 6.0 Hz), 2.98 (2H, m, CH_2-5', J = 4.2, 6.6 Hz), 2.70 (2H, t, CH_2-7', J = 6.0 Hz), 2.42 (2H, t, CH_2-7", J = 7.2 Hz), 2.15 (2H, t, CH_2-9", J = 7.2 Hz), 1.70 (2H, m, CH_2-8", J = 7.2 Hz).

Table 3.2 ^{1}H NMR characterization of synthetic Cys-N7G-PBA in DMSO-d_6 using a 600 MHz Varian Inova NMR spectrometer

	Chemical Shift	^{1}H NMR
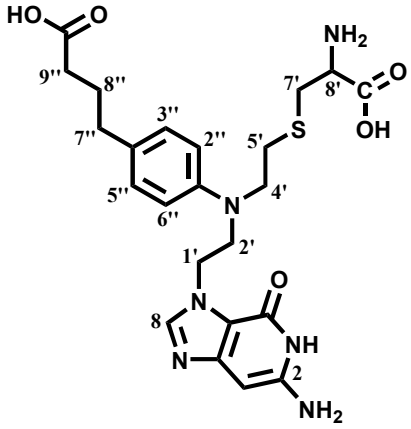	7.87 ppm, s, 1H	**H**-8
	7.15 ppm, s, 1H	N**H**-1
	7.01 ppm, ss, 2H	N**H**$_2$-8'
	6.94 ppm, d, 2H	C**H**-2", C**H**-6"
	6.72 ppm, d, 2H	C**H**-3", C**H**-5"
	6.15 ppm, s, 2H	N**H**$_2$-2
	4.28 ppm, t, 2H	C**H**$_2$-1'
	3.65 ppm, t, 2H	C**H**$_2$-2'
	3.37 ppm, m, 2H	C**H**$_2$-4'
	2.98 ppm, m, 2H	C**H**$_2$-5'
	2.70 ppm, m, 2H	C**H**$_2$-7'
Cys-N7G-PBA	2.42 ppm, t, 2H	C**H**$_2$-7"
	2.15 ppm, t, 2H	C**H**$_2$-9"
	1.70 ppm, m, 2H	C**H**$_2$-8"

Synthesis of Amino Acid-Guanine Conjugates: N-[2-(cysteinyl)ethyl]-N-[2-(guan-7-yl)ethyl]methylamine (Cys-N7G-EMA). Boc-Cys-OH was combined with 2 equivalents N7G-EMA-Cl in DMSO/water (1:1). The pH of the reaction mixture was adjusted to ~9 by the addition of ammonium hydroxide, and the reaction mixture was stirred at 37 °C for 72 h. The insoluble product was isolated by filtration and further purified by semi-preparative HPLC on a Supelcosil LC-18-DB column (25 cm x 10 mm, 5 μm) eluted with a linear gradient of acetonitrile (B) in 20 mM ammonium acetate, pH 4.9 (A). The solvent composition was changed from 0 to 24% B in 24 min and further to 60% in 6 min. Under these conditions, Boc-protected Cys-N7G-EMA eluted as a sharp peak at 20.9 min. ESI^+-MS/MS: *m/z* 456.2 $[M + H]^+ \rightarrow$ *m/z* 356.1 $[M + H - Boc]^+$ and *m/z* 205.0 $[M + H - Boc - Gua]^+$. Following HPLC purification, Boc-protected Cys-N7G-EMA was dissolved in TFA and incubated at room temperature for 45 min. The deprotected Cys-N7G-EMA was purified by HPLC using the same method described above. Under these conditions, Cys-N7G-EMA eluted as a sharp peak at 10.4 min (0.2% yield). UV: λ_{max} 280 nm, λ_{min} 246 nm (pH 4.9); ESI^+-MS/MS: *m/z* 356.1 $[M + H]^+ \rightarrow$ *m/z* 205.0 $[M + H - Gua]^+$; ^1H NMR 600 MHz δ (DMSO-d_6, *Table 3.3*): 8.30 (1H, s, H-8), 4.66 (2H, d, NH_2-8'), 4.06 (2H, t, CH_2-1'), 3.69 (1H, s, NH-1), 3.54 (2H, s, NH_2-2), 3.28 (2H, t, CH_2-2'), 3.00 (2H, m, CH_2-4'), 2.90 (2H, m, CH_2-5'), 2.83 (2H, m, CH_2-7'), 2.75 (3H, s, CH_3-1"), 2.5 (1H, s, H-8').

Synthesis of Amino Acid-Guanine Conjugates: N-[2-[N-(lysyl)ethyl]-N-[2-(guan-7-yl)ethyl]methylamine (Lys-N7G-EMA). Equimolar amounts of Boc-Lys-OMe and N7G-EMA-Cl were combined in water, and ammonium hydroxide was added to increase the

Table 3.3 ^{1}H NMR characterization of synthetic Cys-N7G-EMA in DMSO-d_6 using a 600 MHz Varian Inova NMR spectrometer

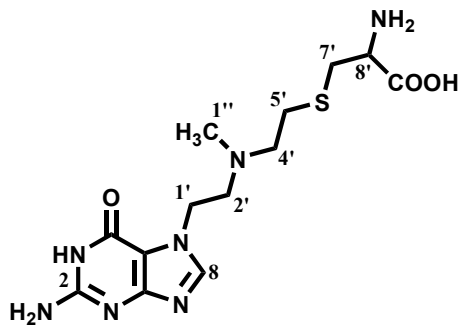

Cys-N7G-EMA

Chemical Shift	^{1}H NMR
8.30 ppm, s, 1H	H-8
4.66, ppm, d, 2H	NH_2-8
4.06, ppm, t, 2H	CH_2-1'
3.69 ppm, s, 1H	NH-1
3.54 ppm, s, 2H	NH_2-2
3.28 ppm, t, 2H	CH_2-2'
3.00 ppm, m, 2H	CH_2-4'
2.90 ppm, m, 2H	CH_2-5'
2.83 ppm, m, 2H	CH_2-7'
2.75 ppm, s, 3H	CH_3-1''
2.50 ppm, s, 1H	H-8'

pH of solution to ~ 9 prior to overnight incubation at 37 °C. The Boc-protected lysine-guanine conjugate was isolated from the reaction supernatant by semi-preparative HPLC using a Supelcosil LC-18-DB column (25 cm x 10 mm, 5 μm) eluted with 20 mM ammonium acetate, pH 4.9 (A) and acetonitrile (B) at a flow rate of 3 mL/min. The solvent composition was changed linearly from 0-40% B in 30 min. Under these conditions, Boc-Lys-OMe-N7G-EMA eluted as a sharp peak at 27 min. ESI^+-MS/MS: *m/z* 495.0 $[M + H]^+ \rightarrow$ *m/z* 395.0 $[M + H - Boc]^+$. Removal of the Boc protecting group was achieved by incubation of Boc-Lys-OMe-N7G-EMA with TFA at room temperature for 45 min. ESI^+-MS/MS: *m/z* 395.0 $[M + H]^+ \rightarrow$ *m/z* 244.0 $[M + H - Gua]^+$. Hydrolysis of the methyl ester was achieved *via* incubation of Lys-OMe-N7G-EMA with 0.1N NaOH at room temperature for 3 h. The desired Lys-N7G-EMA conjugate was isolated by semi-preparative HPLC using a Supelcosil LC-18-DB column (25 cm x 10 mm, 5 μm) eluted with 20 mM NH_4OAc, pH 4.9 (A) and acetonitrile (B). The solvent composition was changed from 1-20% B in 60 min. Under these conditions, Lys-N7G-EMA eluted as a sharp peak at 18.4 min. UV: λ_{max} 280 nm, λ_{min} 246 nm (pH 4.9); ESI^+-MS/MS: *m/z* 381.2 $[M + H]^+ \rightarrow$ *m/z* 363.1 $[M + H - H_2O]^+$ and m/z 230.1 $[M + H - Gua]^+$.

Reaction of Synthetic Peptide GNPVPILIPCHR with Guanine Half-Mustards. Synthetic peptide GNPVPILIPCHR, representing residues 136-147 of wild-type hAGT (76.1 nmol), was reacted with 5 equivalents of N7G-PBA-Cl or N7G-EMA-Cl (380.5 nmol) in 10 mM TRIS-HCl buffer, pH 7.2. The samples were incubated at 37 ^oC for 2 h, followed by direct HPLC-ESI^+-MS/MS analysis.

Treatment of hAGT with Chlorambucil, Mechlorethamine, and Their Guanine Half-Mustards. Wild-type hAGT (75.0 μg, 3.4 nmol) or its variants (C145A hAGT and C145A/C150S hAGT) were incubated with 10 molar equivalents of chlorambucil or mechlorethamine (34.0 nmol) and with 25 molar equivalents of N7G-PBA-Cl or N7G-EMA-Cl (85.8 nmol) in 10 mM TRIS-HCl buffer (pH 7.2) for 3 hours at 37 ^{o}C. Following incubation, the proteins were either analyzed directly by HPLC-ESI^{+}-MS or isolated *via* offline HPLC using a Zorbax 300 SB-C3 column (2.1 x 150 mm, 5 μm) eluted at a flow rate of 0.2 mL/min with 0.05% TFA in water (A) and 0.05% TFA in acetonitrile (B). The solvent composition was held at 30% B for the first 5 min, followed by a linear increase to 80% B in 25 min. Under these conditions, alkylated hAGT co-eluted with unmodified protein as a sharp peak at 25 min. The collected protein fractions were dried, reconstituted in 0.05% TFA in water, and aliquots were set aside for HPLC-ESI^{+}-MS analysis. To asses the ability of the guanine half-mustards to alkylate hAGT in the presence of a competing nucleophile, wild-type hAGT was incubated N7G-PBA-Cl or N7G-EMA-Cl (85.8 nmol) in the presence of 100 and 500 molar equivalents $_{L}$-cysteine (0.34 and 1.7 μmol respectively) in 10 mM TRIS-HCl buffer (pH 7.2) at 37 ^{o}C for 3 h prior to MS analysis.

Tryptic Digestion of Alkylated hAGT. Control or alkylated hAGT (~ 70 μg) was dissolved in 100 mM ammonium bicarbonate buffer (pH 7.9) and digested with trypsin (7.0 μg) for 24 h at 37 ^{o}C. Samples were dried, re-dissolved in 50 μL of 0.5% formic acid/0.01% TFA for analysis by HPLC-ESI^{+}-MS/MS.

Total Digestion of Alkylated hAGT to Amino Acids. hAGT tryptic peptides (from ~50 μg protein) were dried, reconstituted in deionized water, and filtered through Microcon YM-10 membrane filters to remove trypsin. Carboxypeptidase Y (1.0 μg) and proteinase K (1.0 μg) were added to the filtrate, and proteolysis proceeded at room temperature for 24 h. Once dried, the samples were reconstituted in 15 mM ammonium acetate buffer (pH 5.0) and analyzed by HPLC-ESI$^+$-MS/MS.

AGT Cross-Linking to Double-Stranded Oligodeoxynucleotides in the Presence of Chlorambucil and Mechlorethamine. The DNA 18-mer (5'-GGA GCT GGT GGC GTA GGC-3') (+ strand) and the complementary (-) strand (5'-GCC TAC GCC ACC AGC TCC-3') were prepared by standard phosphoramidite chemistry on a DNA synthesizer. To obtain double-stranded DNA, 20 nmol of the (+) and (-) strands were combined, dried under vacuum, and dissolved in 10 mM TRIS-HCl buffer (pH 7.2). The solution was heated to 90 ^{o}C and slowly cooled to room temperature. hAGT (45 μg, 2.1 nmol) was incubated for 3 h at 37 ^{o}C with 10 nmol of double-stranded DNA in 10 mM Tris-HCl buffer (pH 7.2) containing 200 nmol of either mechlorethamine hydrochloride or chlorambucil. Following incubation, the samples were heated to 70 ^{o}C for 1 h to release N7-alkylated guanines. Once dried, the samples were dissolved in 100 mM ammonium bicarbonate buffer (pH 7.9), and trypsin (4.5 μg) was added to initiate proteolysis. The samples were allowed to digest overnight at 37 ^{o}C. Following digestion, the samples were dried, reconstituted in 0.5% formic acid/0.01% TFA in water, and directly analyzed by HPLC-ESI$^+$-MS/MS.

Mass Spectrometric Analysis of Cross-Linked AGT: HPLC-ESI$^+$-MS Analysis of Intact Protein Following Alkylation with Chlorambucil, Mechlorethamine, and Their Guanine Half-Mustards. Analysis of alkylated AGT was performed using an Agilent 1100 capillary HPLC-ion trap MS system operated in the ESI$^+$ mode. Spectra were obtained by performing full scan MS within the *m/z* range of 100-1500. Separation was achieved with an Agilent Zorbax 300 SB-C3 column (150 mm x 0.5 mm, 5 um) eluted at a flow rate of 15 μL/min. The column temperature was held at 25 ^{o}C, and the mobile phase consisted of 0.05% TFA in water (A) and 0.05% TFA in acetonitrile (B). The elution program began at 30% B and was held at 30% B for the first 3 min. This was followed by a linear increase to 80% B in 20 min, and further to 90% B in 5 min. Under these conditions, alkylated and native hAGT co-eluted as a broad peak at ~ 16 min. Deconvolution of the MS charge envelope was performed using the Agilent ion trap deconvolution software.

HPLC-ESI$^+$-MS/MS Analysis of hAGT Peptides. Mass spectrometric analysis of chlorambucil, mechlorethamine, and guanine half-mustard treated synthetic peptide GNPVPILIPCHR and hAGT tryptic peptides was performed using an Agilent 1100 capillary HPLC-ion trap MS system. The mass spectrometer was operated in ESI$^+$ mode, and Auto MS^2 was used to select and fragment the doubly-charged ions at *m/z* 658.4 (unmodified peptide G^{136}NPVPILIPCHR^{147}), *m/z* 849.6 (chlorambucil-induced guanine cross-link to G^{136}NPVPILIPCHR^{147}), *m/z* 775.4 (mechlorethamine-induced guanine cross-link to G^{136}NPVPILIPCHR^{147}), *m/z* 834.4 (unmodified peptide V^{148}VCSSGAVGNYSGGLAVK^{165}), *m/z* 1025.9 (chlorambucil-induced guanine cross-link to V^{148}VCSSGAVGNYSGGLAVK^{165}), and *m/z* 951.4 (mechlorethamine-induced

guanine cross-link to V^{148}VCSSGAVGNYSGGLAVK^{165}). Chromatographic separation was achieved using an Agilent Zorbax SB-C18 column (150 mm x 0.5 mm, 5 μm) eluted at a flow rate of 15 μL/min. The mobile phase consisted of 0.5% formic acid/0.01% TFA in water (A) and 0.5% formic acid/0.01% TFA in acetonitrile (B). The column temperature was held at 25 ^{o}C and a slow gradient was employed to maximize peptide separation. The solvent composition was held at 3% B for the first 3 min, followed by a linear increase to 5% B in 7 min. The composition was held at 5% B for 10 min, increased to 35% B in 95 min, and further to 75% B in 10 min. Full scan data obtained from these and control experiments was used to identify the remaining unmodified hAGT tryptic peptides.

HPLC-ESI^{+}-MS/MS Analysis of Amino Acid-Guanine Conjugates. Mass spectrometric analysis of amino acid-guanine cross-links present in half-mustard treated hAGT total digests was performed using an Agilent 1100 capillary HPLC-ion trap MS system operated in ESI^{+} mode. Auto MS^{2} was used to isolate and fragment the following singly-charged ions: *m/z* 504.2 (*N*-(2-[*S*-cysteinyl]ethyl)-*N*-(2-[guan-7-yl]ethyl)-*p*-aminophenylbutyric acid, Cys-N7G-PBA), *m/z* 356.2 (*N*-(2-[*S*-cysteinyl]ethyl)-*N*-(2-[guan-7-yl]ethyl)methylamine, Cys-N7G-EMA), and the corresponding conjugates to lysine, arginine, histidine, and tyrosine. Chromatographic separation of amino acids and guanine half-mustard induced amino acid conjugates was achieved using a Phenomenex Synergi C18 column (250 mm x 0.5 mm, 4 μm) eluted at a flow rate of 10 μL/min. The mobile phase consisted of 15 mM ammonium acetate, pH 5.0 in water (A) and acetonitrile (B). Chlorambucil-induced amino acid-guanine conjugates were

chromatographically separated employing a linear gradient of 2-65% B over the course of 30 min. To improve peak shape, the column was cooled to 10 ^{o}C. Under these conditions, Cys-N7G-PBA eluted as a sharp peak at 19.5 min. For the separation of mechlorethamine-mediated amino acid-guanine cross-links, the column temperature was held at 25 ^{o}C and the gradient program began with an isocratic elution of 2% B for 15 min, followed by a linear increase to 30% B over the next 15 min. Under these conditions, Cys-N7G-EMA eluted as a broad peak ~12 min and Lys-N7G-EMA eluted at ~ 23 min.

3.4 Results

3.4.1 AGT-DNA Cross-Links Induced by Nitrogen Mustards as Detected by Denaturing PAGE

The ability of human recombinant AGT protein to form cross-links to DNA in the presence of nitrogen mustards was first detected by denaturing gel electrophoresis. SDS-PAGE analysis of 5'-^{32}P-end labeled DNA duplex (5'-GGA GCT GGT GGC GTA GGC-3' (+ strand)/5'-GCC TAC GCC ACC AGC TCC-3' (- strand) that had been incubated with hAGT protein in the presence of increasing amounts of mechlorethamine or chlorambucil revealed the presence of an additional slow-moving band corresponding to AGT-DNA conjugates (*Figure 3.1*). This band was absent in control experiments lacking AGT or oligonucleotide, as well as those without *bis*-electrophile (*lanes 2 and 7*). Cross-linking of hAGT to DNA by mechlorethamine was quite efficient and displayed concentration dependence, increasing linearly from 15 to 25% (*lanes 3-5*). Compared to mechlorethamine, chlorambucil was not as effective at cross-linking hAGT to DNA (2-5

Figure 3.1 Detection of nitrogen mustard-induced AGT-DNA cross-links by SDS-PAGE. Recombinant human AGT protein and radioactive duplex oligodeoxynucleotide (see Materials and Methods) were incubated in the presence of 50 (lanes 3 and 8), 100 (lanes 4 and 9) or 200 (lanes 5 and 10) equivalents of mechlorethamine (lanes 3-5) or chlorambucil (lanes 8-10) and subsequently resolved by 12% SDS-PAGE. Free duplex DNA (labeled 'Oligo') migrated to the bottom of the gel, whereas DNA cross-linked to AGT (labeled 'AGT-Oligo complex') displayed a substantially reduced mobility. The mobility of the higher-order complex of drug and AGT is indicated by an asterisk (see text).

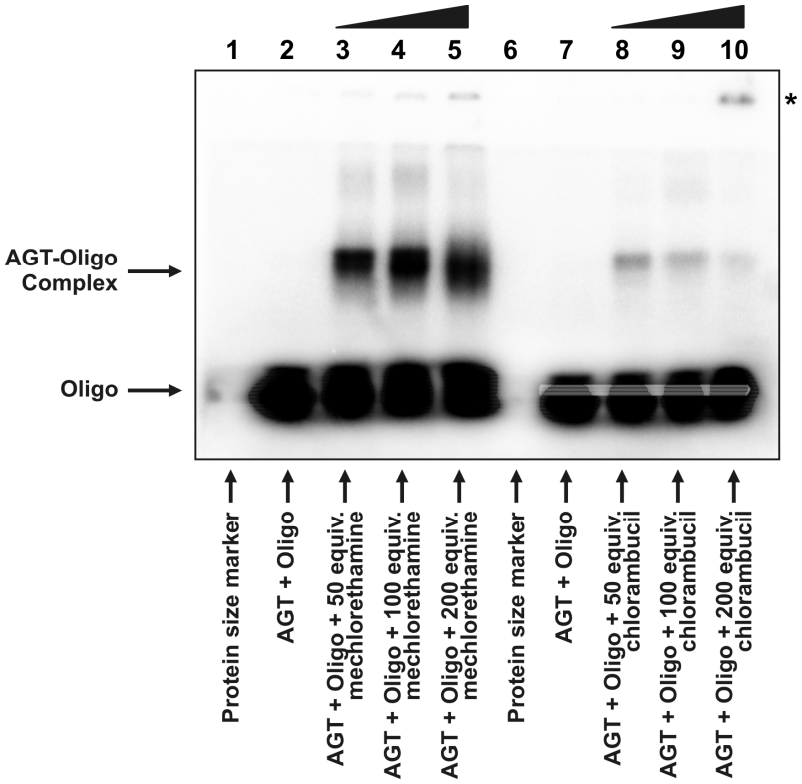

% cross-linking, *lanes 8-10*). Furthermore, an increase in chlorambucil concentration coincided with the appearance of additional high molecular weight bands (*lane 10, top of gel*), likely the result of multiple molecules of protein binding to the same DNA molecule.

3.4.2 HPLC-ESI$^+$-MS Analysis of Half-Mustard Induced AGT-Guanine Cross-Links: Whole Protein MS

Initial DNA alkylation by mechlorethamine and chlorambucil leads to the formation of N7-guanine half-mustards, which retain one of the chloroethyl groups (*Scheme 3.1*). These monoadducts can then react with a nucleophilic site within a neighboring protein, giving rise to DNA-protein cross-links. To gain insight into the nature of the nitrogen mustard-induced AGT-DNA linkages, recombinant AGT protein or its variants were incubated with synthetic guanine half-mustards of mechlorethamine or chlorambucil as models of monoalkylated DNA, followed by capillary HPLC-ESI$^+$-MS analysis of modified proteins (*Scheme 3.2*). When the experiment was performed with the wild-type protein, deconvoluted mass spectra of the reaction mixture revealed three protein species: unreacted hAGT (M = 21 880 Da), hAGT containing a single chlorambucil cross-link to guanine (M = 22 263 Da), and a double chlorambucil cross-link to guanine (M = 22 646 Da) (*Figure 3.2, panel A*). The presence of a large molar excess of L-cysteine (100-500 equivalents) did not inhibit alkylation of hAGT by N7G-PBA-Cl, suggesting that this low molecular weight thiol does not protect against the formation of DNA-protein cross-links upon exposure to nitrogen mustards. These results

Scheme 3.2 Mass Spectrometry-based approach used to characterize AGT-DNA cross-links of antitumor nitrogen mustards

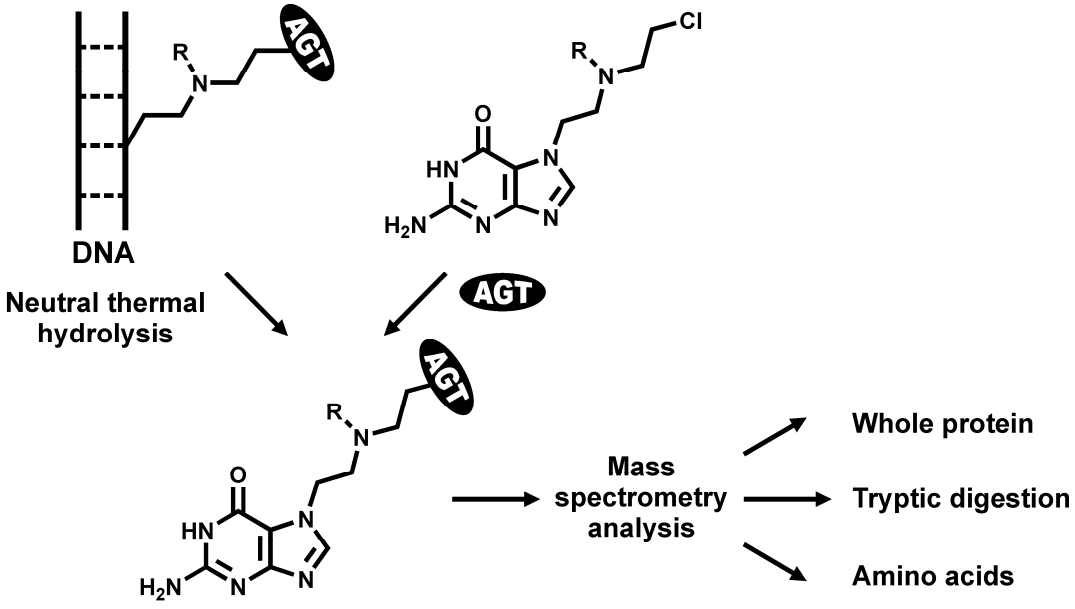

Figure 3.2 ESI$^+$-MS spectra and deconvoluted spectra (inset) of N7G-PBA-Cl and N7G-EMA-Cl treated AGT and its variants. (**A**) Wild type protein: *A* = unmodified hAGT (calculated *M* = 21 876 Da, observed *M* = 21 880 Da), *B* = hAGT containing a single chlorambucil cross-link to guanine (calculated *M* = 22 259 Da, observed *M* = 22 263 Da), *C* = hAGT containing two chlorambucil cross-links to guanine (calculated *M* = 22 642 Da, observed *M* = 22 646 Da). (**B**) C145A AGT variant: *A* = unmodified C145A hAGT (calculated *M* = 23 015 Da, observed *M* = 23 017 Da), *B* = C145A hAGT containing a single chlorambucil cross-link to guanine (calculated *M* = 23 398 Da, observed *M* = 23 401 Da). (**C**) C145A/C150S variant: *A* = unmodified C145A/C150S hAGT (calculated *M* = 22 996 Da, observed *M* = 23 001 Da), *B* = C145A/C150S hAGT containing a single chlorambucil cross-link to guanine (calculated *M* = 23 379 Da, observed *M* = 23 384 Da). (**D**) Wild type protein: *A* = unmodified hAGT (calculated *M* = 21 876 Da, observed *M* = 21 876 Da), *B* = hAGT containing an intramolecular mechlorethamine cross-link (calculated *M* = 21 959 Da, observed *M* = 21 959 Da), *C* = hAGT containing a single mechlorethamine cross-link to guanine (calculated *M* = 22 110 Da, observed *M* = 22 110 Da), *D* = hAGT containing two mechlorethamine cross-links to guanine (calculated *M* = 22 344 Da, observed *M* = 22 345 Da).

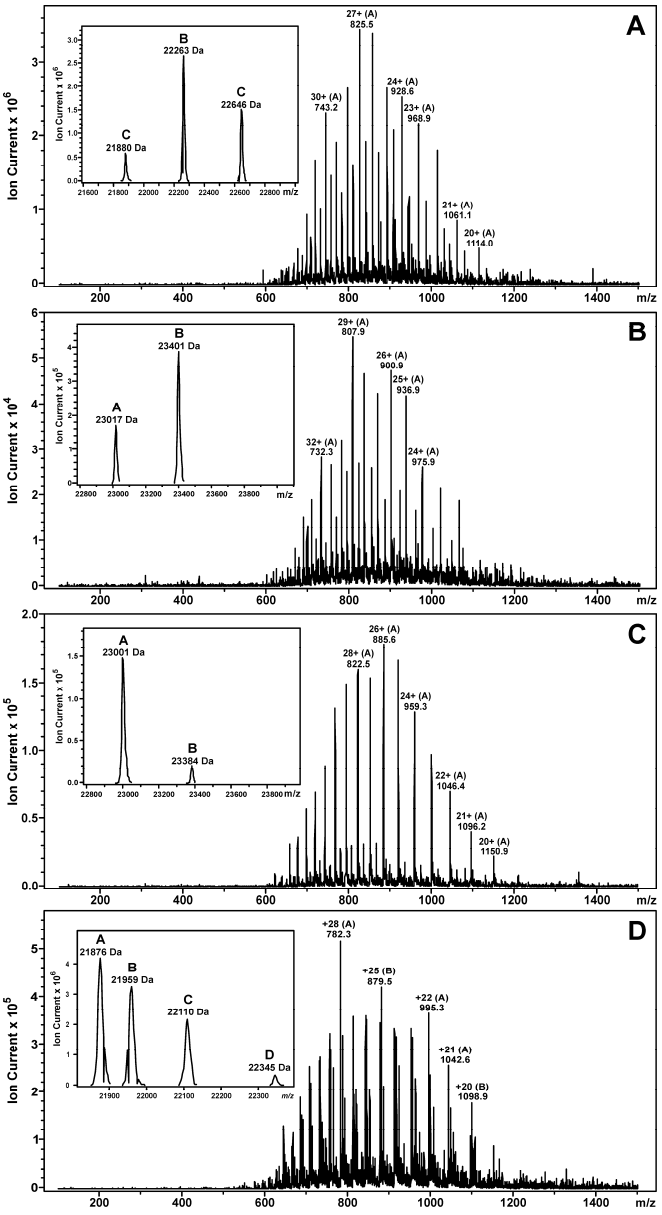

were consistent with a previous study in which L-cysteine and glutathione did not prevent the formation of DEB-mediated AGT-DNA cross-links *(37)*.

When the same experiment was conducted with a variant form of AGT in which cysteine 145 was replaced by an alanine residue, a single half-mustard modified species was apparent (M = 23 401, mass increase of ~ 384 Da) (*Figure 3.2, panel B*), suggesting that one of the cross-linking sites observed within the wild-type protein, namely Cys^{145}, had been removed. Incubation of a third variant of AGT protein in which cysteine residues 145 and 150 had both been mutated (C145A/C150S) with chlorambucil half-mustard yielded only trace amounts of cross-linked protein (*Figure 3.2, panel C*). The significant differences between the observed molecular weights of the C145A and C145A/C150S AGT variants (M = 23 017 Da and M = 23 001 Da) and the wild-type protein (M = 21 880) are due to the presence of an N-terminal histidine tag (MRGSHHHHHHGS).

Similar results were obtained following reaction of wild-type hAGT with the guanine half-mustard of mechlorethamine (*Figure 3.2, panel D*), with both single (M = 22 110 Da) and double (M = 22 345 Da) cross-links to guanine observed. A third species of alkylated AGT was also identified (M = 21 959 Da), corresponding to a mechlorethamine-induced intramolecular cross-link involving two amino acid residues within the protein. Taken together, these results support the interpretation that chlorambucil and mechlorethamine cross-link AGT to DNA *via* cysteine residues 145 and 150.

3.4.3 HPLC-ESI$^+$-MS/MS Analysis of Half-Mustard Induced AGT-Guanine Cross-Links: Peptide Mapping

Further evidence for nitrogen mustard-mediated cross-linking of hAGT to DNA involving active site cysteines within the protein was obtained through MS/MS sequencing of peptides resulting from proteolytic digestion of alkylated hAGT. Tryptic digestion of native hAGT resulted in the positive identification of 14 of the 16 possible tryptic fragments (*Table 3.4*), including the doubly-charged peptide $G^{136}NPVPILIP\underline{C}HR^{147}$ at 658.6 *m/z* (calculated *M* = 1314.7 Da) containing catalytic Cys^{145} and *m/z* 834.8 $[M + 2H]^{2+}$ corresponding to peptide $V^{148}V\underline{C}SSGGAVGNYSGGLAVK^{165}$ containing Cys^{150} (calculated *M* = 1666.8 Da). HPLC-ESI$^+$-MS/MS analysis of a tryptic digest of N7G-PBA-Cl-treated hAGT detected a prominent doubly-charged ion at 850.1 *m/z* corresponding to a chlorambucil-induced conjugate involving peptide $G^{136}NPVPILIP\underline{C}HR^{147}$ and a guanine base (calculated *M* = 1697.8 Da, t_R = 86.2 min). When subjected to collision induced dissociation in the ion trap mass spectrometer, the resulting MS/MS spectrum was consistent with the presence of a chlorambucil-mediated guanine adduct located at either Cys^{145} or His^{146} (*Figure 3.3, panel A*). While the masses of product ions b_3-b_8 were in agreement with the theoretical values for the unmodified peptide, the mass of b_{11} was increased by 383 Da (observed *M* = 1523.2 Da versus calculated *M* = 1140.5 Da for the unmodified peptide). The y_4-y_9 ions also contained the chlorambucil-induced guanine cross-link as indicated by the 383 Da mass shift. MS^3 analysis of the y_8* fragment ion ($P^{140}ILIP\underline{C}HR^{147}$, *m/z* 1331.0 $[M + H]^+$) yielded product ions corresponding to b_6, b_7, y_5, and y_4 + 383 Da, mapping the site of modification to Cys^{145} (*Figure 3.3, panel B*). Further proof of modification at this site was

Table 3.4 HPLC-ESI$^+$-MS analysis of AGT tryptic peptides

Position	Peptide	$[M + H]^+_{calculated}$	$[M + 2H]^{2+}_{calculated}$	Observed Ions
1-9	MDKDCEMKR	1156.4	578.7	1156.7, 578.9
10-18	TTLDSPLGK	931.5	466.3	931.7, 466.3
19-32	LELSGCEQGLHEIK	1555.8	778.4	778.8
33-36	LLGK	430.3	215.7	430.4, 215.6
37-96	GTSAADAVEVPAPAAVLGG PEPLMQCTAWLNAYFHQP EAIEEFPVPALHHPVFQQES FTR	6469.2	3235.1	ND
97-101	QVLWK	673.4	337.2	673.5
102-104	LLK	373.3	187.1	373.3, 187.1
105-107	VVK	345.3	173.1	ND
108-125	FGEVISYQQLAALAGNPK	1906.0	953.5	953.5
126-128	AAR	317.2	159.0	317.2
129-135	AVGGAMR	661.4	331.2	661.4, 331.2
136-147	GNPVPILIPCHR	1315.7	658.4	1315.7, 658.6
148-165	VVCSSGAVGNYSGGLAVK	1667.8	834.4	834.6
166-175	EWLLAHEGHR	1247.6	624.3	1247.7, 624.5
176-193	LGKPGLGGSSGLAGAWLK	1668.9	835.0	1669.0, 835.2
194-207	GAGATSGSHHHHHH	1429.6	715.3	1429.6, 715.4

Figure 3.3 MS/MS (**A**) and MS^3 spectrum (**B**) of AGT tryptic peptide G^{136}NPVPILIPCHR^{147} containing a N7G-PBA-Cl-induced guanine cross-link at Cys^{145}. Modified fragment ions are indicated by "*".

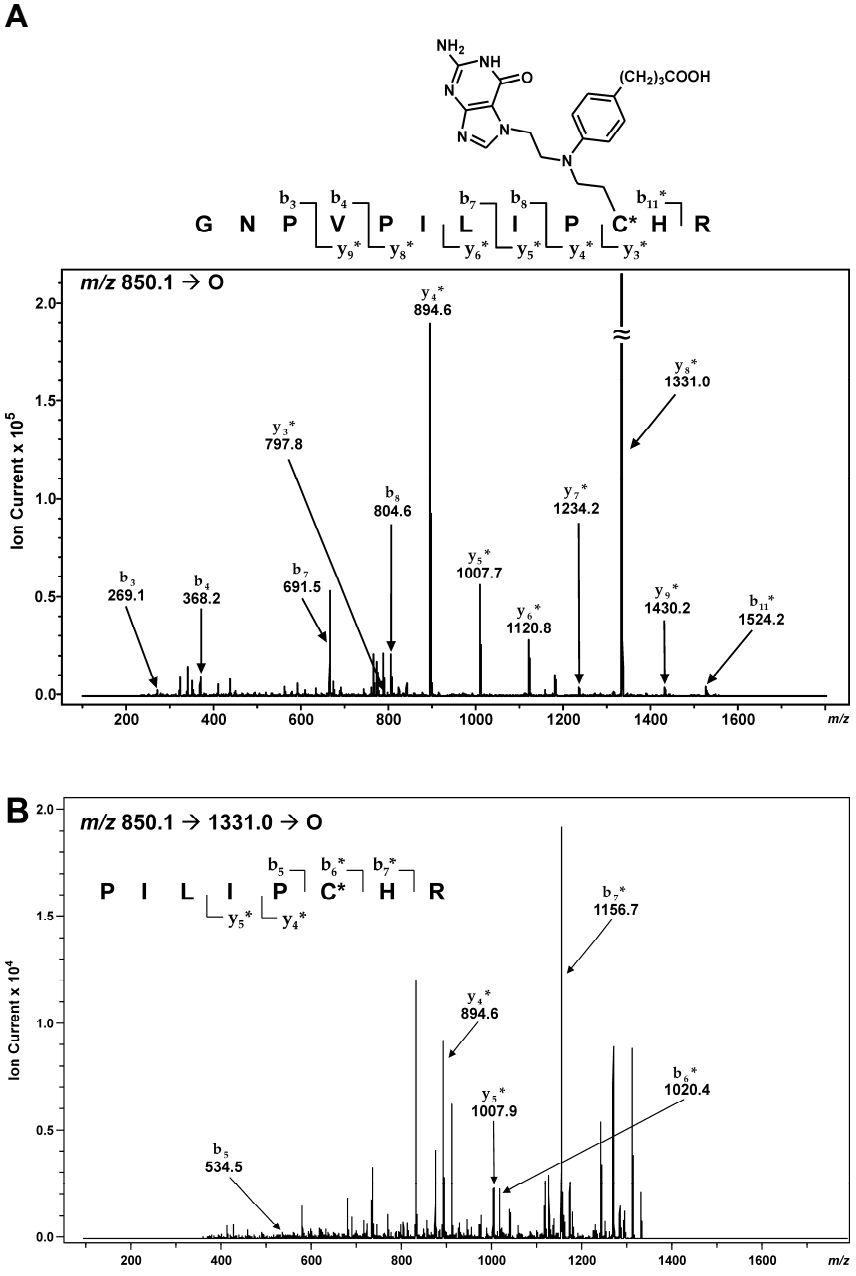

obtained upon analysis of synthetic peptide GNPVPILIPCHR containing a chlorambucil cross-link to guanine (*m/z* 849.7 $[M + 2H]^{2+}$) which displayed a similar HPLC retention time and MS/MS fragmentation as the hAGT-derived peptide-guanine cross-link (*Figure 3.4*).

The second cross-linking site was found to reside on peptide V^{148}VCSSGGAVGNYSGGLAVK^{165} based upon the detection of a doubly-charged ion at 1026.1 *m/z* (calculated *M* = 2049.8 Da) corresponding to a peptide-guanine conjugate of PBA (*Figure 3.5*). The cross-linking site was then mapped to the N-terminal region (VVC) based upon MS/MS fragmentation patterns, most notably the diagnostic b_8 and y_{15} ions. The y_{15} ion mass matched the theoretical value (calculated *M* = 1366.7 Da, observed *M* = 1366.7 Da) while the mass of the b_8 ion was increased by 383 Da (observed *M* = 1086.6 Da versus calculated *M* = 703.4 Da for the unmodified peptide). Although MS/MS data alone could not establish the exact modification site, similar studies with the C145A/C150S hAGT mutant revealed that the same peptide was no longer modified, confirming that C^{150} was the site of cross-link formation.

Similar results were obtained upon analysis of tryptic fragments resulting from proteolytic digestion of N7G-EMA-Cl-treated hAGT. As shown in *Figure 3.6*, HPLC-ESI^+-MS/MS afforded a doubly-charged ion at 775.9 *m/z* corresponding to a mechlorethamine-induced cross-link between guanine and peptide G^{136}NPVPILIPCHR^{147} (calculated *M* = 1548.7 Da). When subjected to CID, the resulting MS/MS spectrum was consistent with the presence of a guanine adduct at the C-terminus (PCH), most likely involving Cys^{145} as the alkyl acceptor. Subsequent analysis of synthetic peptide GNPVPILIPCHR following incubation with N7G-EMA-Cl resulted in the identification

Figure 3.4 Synthetic peptide GNPVPILIPCHR containing a N7G-PBA-Cl-induced cross-link to guanine. *Top*: Extracted ion chromatogram of *m/z* 849.7 $[M + 2H]^{2+}$; *Bottom*: MS/MS spectrum of the 86.4 min peak mapping the cross-link to Cys (C*). Modified fragment ions are indicated by "*".

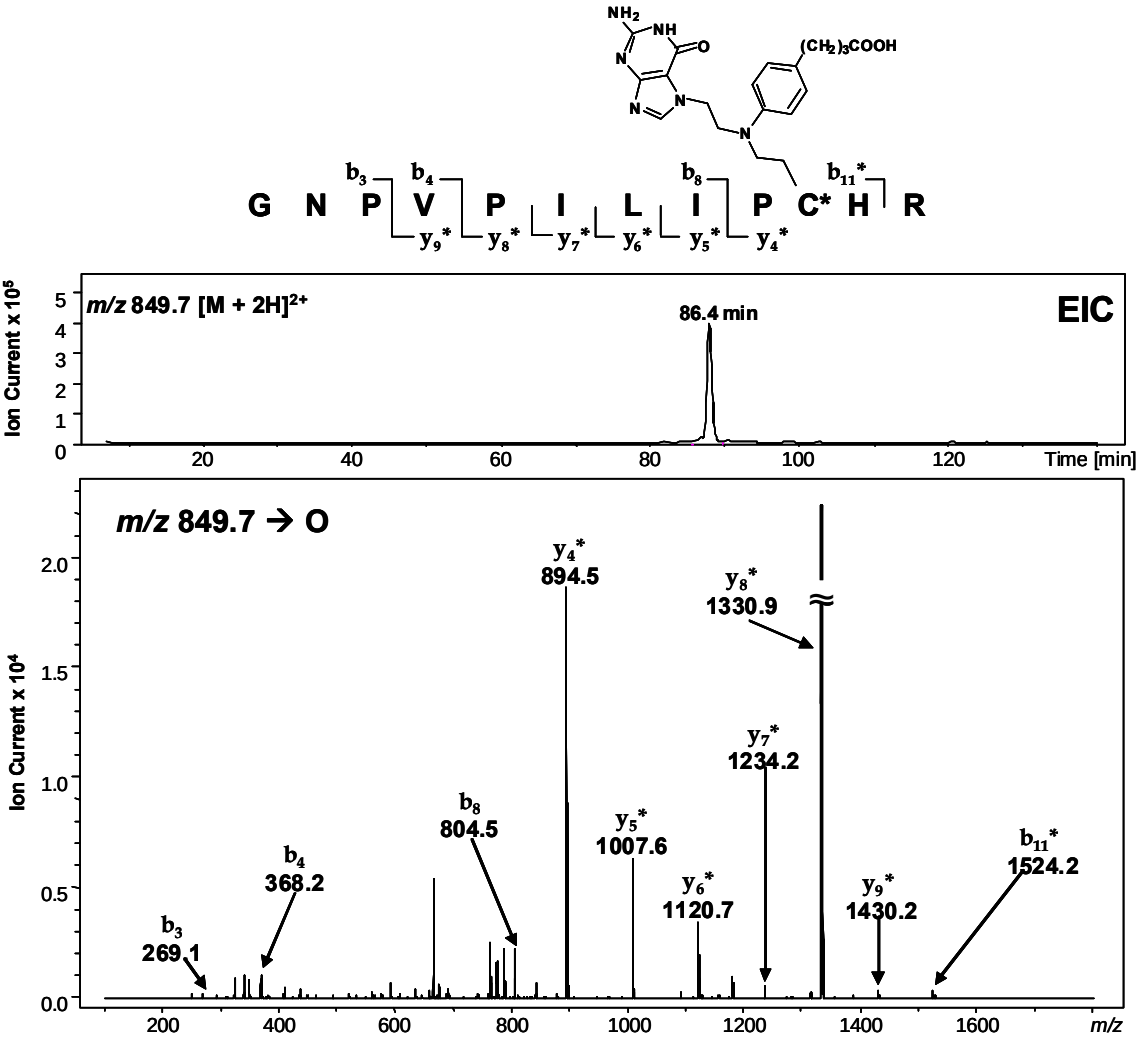

Figure 3.5 AGT tryptic peptide $V^{148}VCSSGAVGNYSGGLAVK^{165}$ containing a N7G-PBA-Cl-induced cross-link to guanine. *Top:* Extracted ion chromatogram of *m/z* 1026.1 $[M + 2H]^{2+}$; *Bottom:* MS/MS spectrum of adducted peptide $V^{148}VCSSGAVGNYSGGLAVK^{165}$ mapping the cross-link to Cys^{150}. Modified fragment ions are indicated by "*".

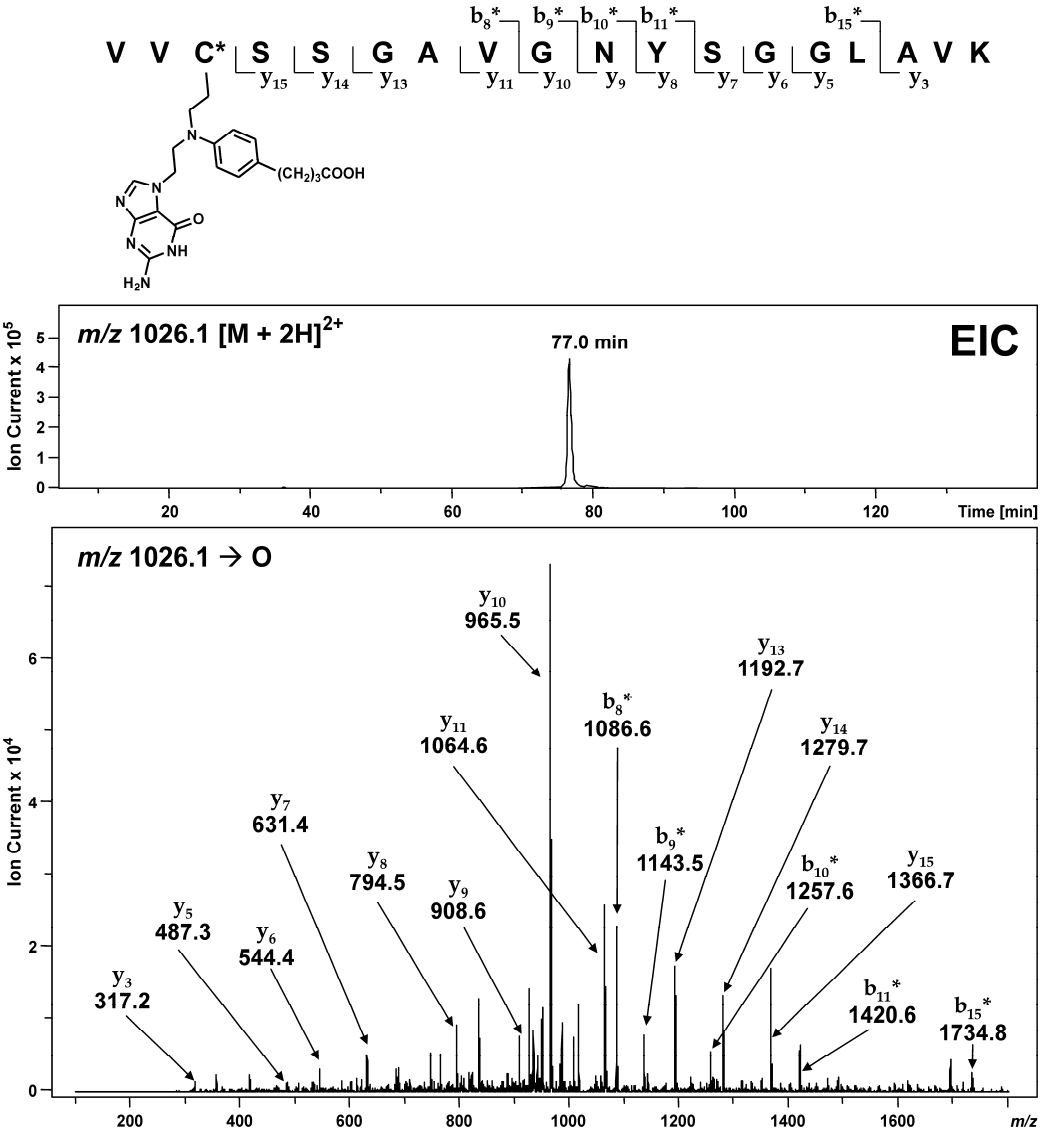

Figure 3.6 AGT tryptic peptide G[136]NPVPILIPCHR[147] containing a N7G-EMA-Cl-induced cross-link to guanine. *Top*: Extracted ion chromatogram of *m/z* 775.9 $[M + 2H]^{2+}$; *Bottom*: MS/MS spectrum of the 62.5 min peak mapping the cross-link to Cys[145]. Modified fragment ions are indicated by "*".

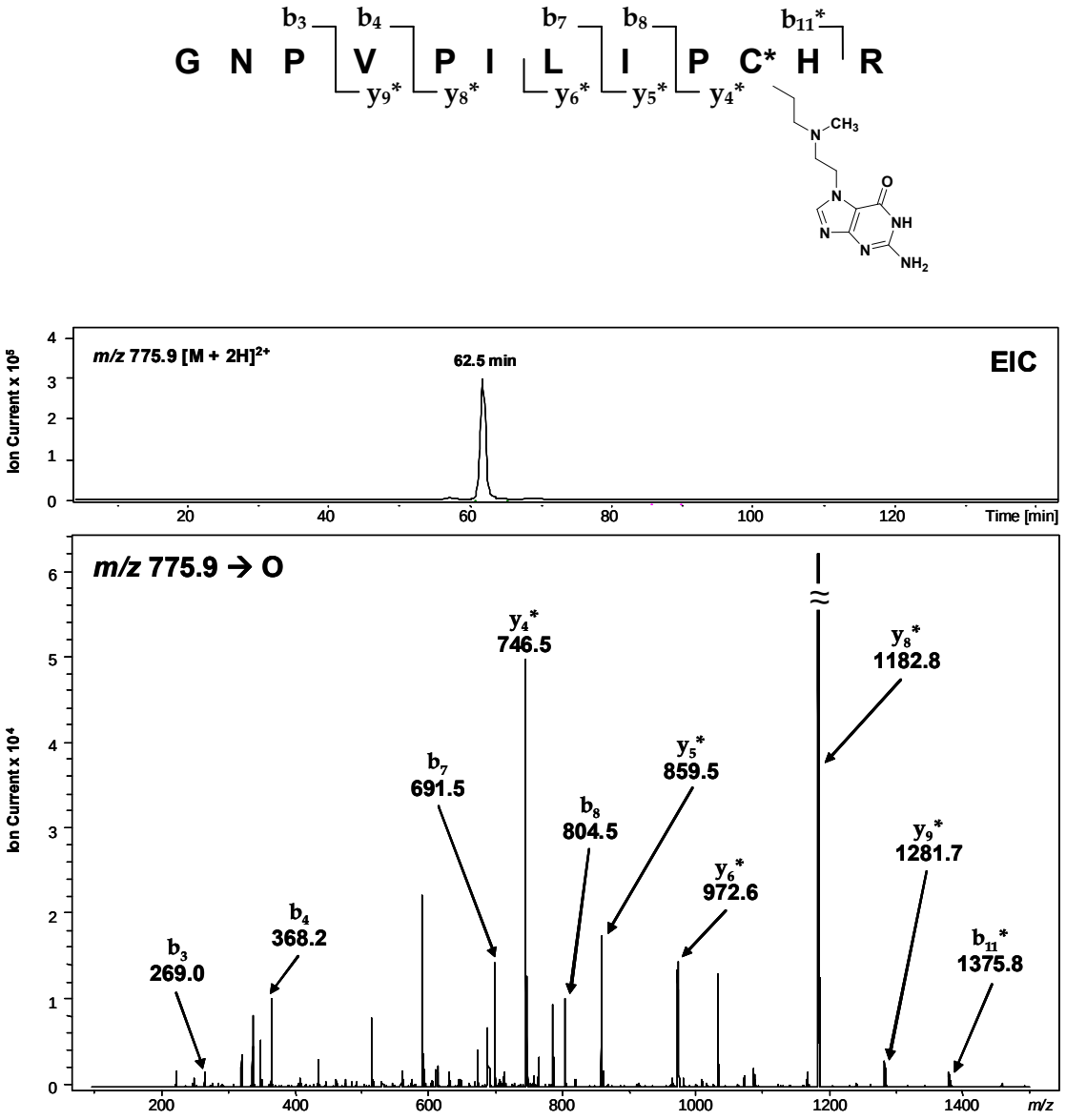

of a peptide guanine cross-link (*m/z* 775.7 $[M + 2H]^{2+}$) which exhibited a similar HPLC retention time and CID spectrum as the hAGT-derived peptide-guanine cross-link. The MS/MS spectrum of the alkylated synthetic peptide yielded characteristic fragments corresponding to the b_{10} and y_3 ions, thus mapping the cross-link site to the lone cysteine residue (*Figure 3.7*). Peptide $V^{148}V\underline{C}SSGGAVGNYSGGLAVK^{165}$ was also found to contain a mechlorethamine-mediated guanine lesion (*m/z* 951.5 $[M + 2H]^{2+}$, calculated *M* = 1900.8 Da) on the N-terminus (VV<u>C</u>), most likely at Cys^{150} (*Figure 3.8*). No other peptides were found to contain guanine half-mustard-induced lesions, suggesting that nitrogen mustard-mediated cross-linking is confined to cysteines 145 and 150 of the protein.

3.4.4 HPLC-ESI$^+$-MS/MS Analysis of AGT Total Digests

To establish the exact molecular structures of AGT-DNA conjugates, half-mustard-treated hAGT protein was subjected to total hydrolysis to amino acids followed by HPL-ESI$^+$-MS/MS analysis. Synthetic cysteine-guanine conjugates, *N*-(2-[*S*-cysteinyl]ethyl)-*N*-(2-[guan-7-yl]ethyl)-*p*-aminophenylbutyric acid and *N*-(2-[*S*-cysteinyl]ethyl)-*N*-(2-[guan-7-yl]ethyl)methylamine, which had undergone structural characterization by mass spectrometry, UV spectrophotometry, and NMR spectroscopy (*Tables 3.2 and 3.3*), were used as authentic standards in these analyses. HPLC-ESI$^+$-MS/MS analysis of protein digests detected a prominent peak at *m/z* 504.2 which had the same retention time, MS/MS fragmentation pattern, and UV spectrum as synthetic *N*-(2-[*S*-cysteinyl]ethyl)-*N*-(2-[guan-7-yl]ethyl)-*p*-aminophenylbuyric acid (*Figure 3.9*). In contrast, no HPLC-ESI$^+$-MS/MS signals were observed in the ion channels

Figure 3.7 Synthetic peptide GNPVPILIPCHR containing a N7G-EMA-Cl-induced cross-link to guanine. *Top*: Extracted ion chromatogram of *m/z* 775.7 $[M + 2H]^{2+}$; *Bottom*: MS/MS spectrum of the 62.3 min peak mapping the cross-link to Cys (C*). Modified fragment ions are indicated by "*".

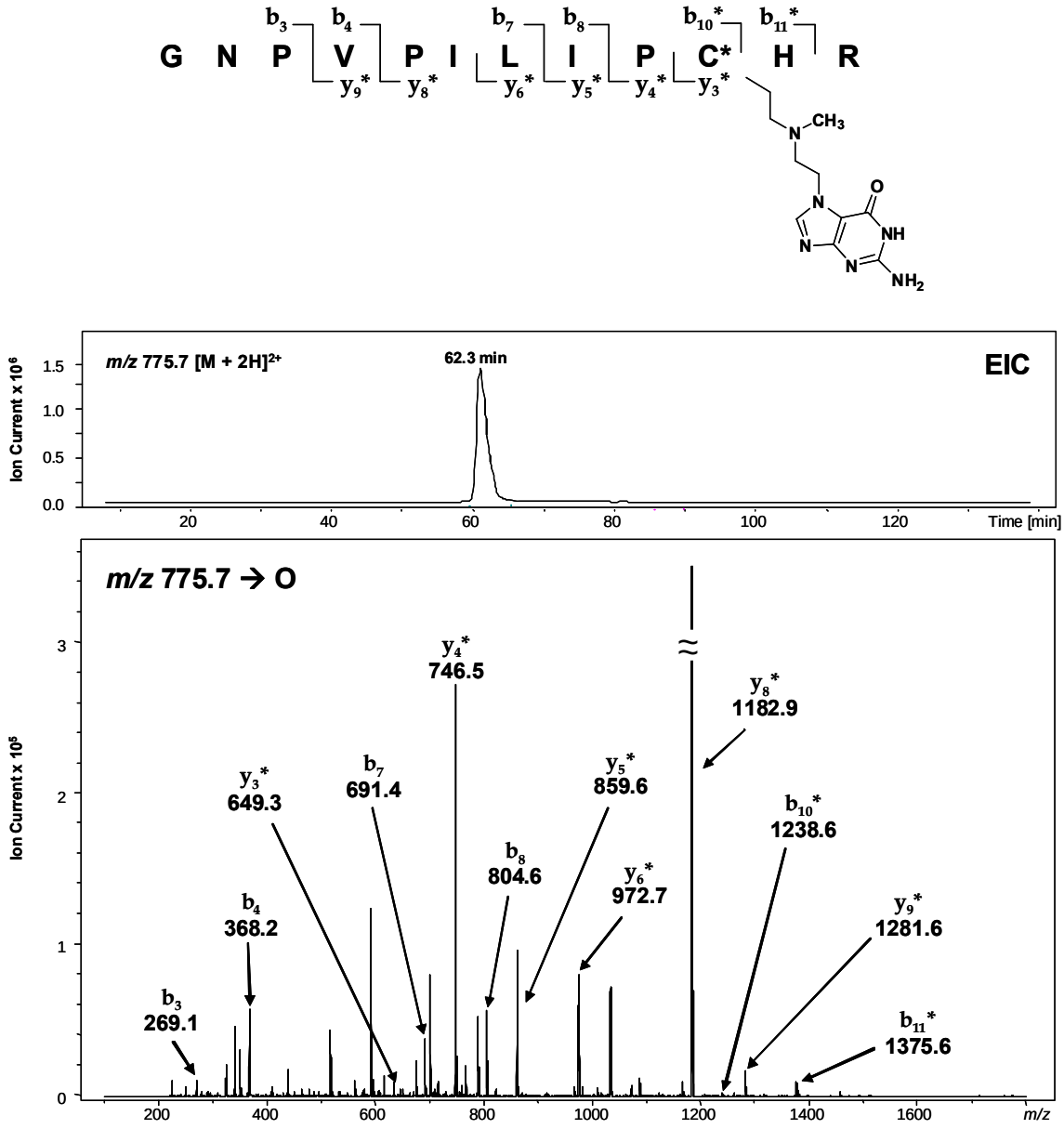

Figure 3.8 AGT tryptic peptide $V^{148}VCSSGAVGNYSGGLAVK^{165}$ containing N7G-EMA-Cl-induced cross-link to guanine. *Top*: Extracted ion chromatogram of *m/z* 951.5 $[M + 2H]^{2+}$; *Bottom*: MS/MS spectrum of the 58.2 min peak mapping the cross-link to Cys^{150}. Modified fragment ions are indicated by "*".

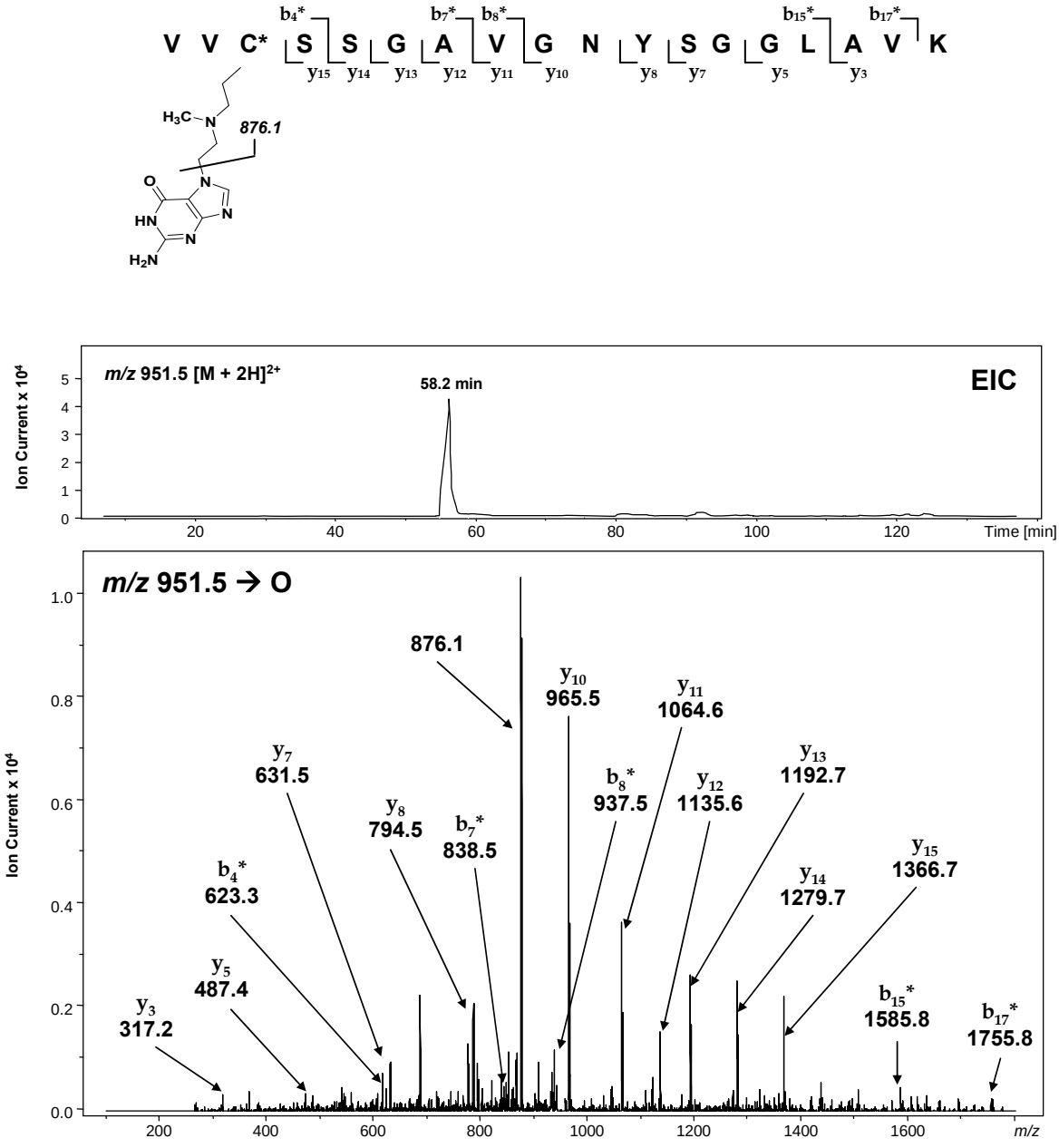

Figure 3.9 HPLC-ESI$^+$-MS/MS analysis of amino acid-guanine conjugates of chlorambucil. **(A)** Extracted ion chromatogram of synthetic Cys-N7G-PBA (*m/z* 356.2 $[M + H]^+$); *Inset*: MS/MS fragmentation and UV spectrum. **(B)** Extracted ion chromatogram of AGT-derived Cys-N7G-PBA (*m/z* 356.2 $[M + H]^+$; *Inset:* MS/MS fragmentation and UV spectrum.

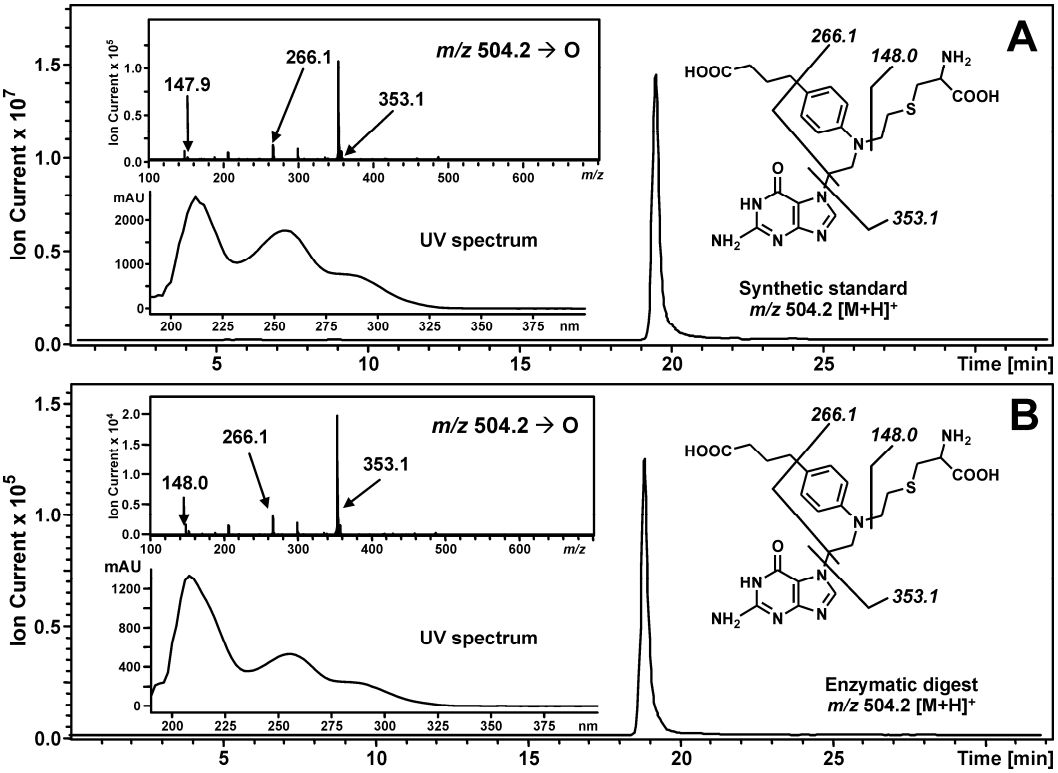

corresponding to nitrogen mustard-guanine conjugates to other nucleophilic residues (Lys, Arg, His, Tyr). Similar results were observed for mechlorethamine (*Figures 3.10 and 3.11*). Combined with the ESI^+-MS data from treated protein and the MS/MS data from tryptic digests, our results indicate that nitrogen mustard-mediated cross-linking is specific for two cysteine residues within the active site of hAGT – Cys^{145} and Cys^{150} and establish the covalent structures of amino acid-nucleobase conjugates as *N*-(2-[*S*-cysteinyl]ethyl)-*N*-(2-[guan-7-yl]ethyl)-*p*-aminophenylbutyric acid (Cys-N7G-PBA) and *N*-(2-[*S*-cysteinyl]ethyl)-*N*-(2-[guan-7-yl]ethyl)methylamine (Cys-N7G-EMA).

3.4.5 HPLC-ESI^+-MS/MS Analysis of AGT-Guanine Cross-Links Induced by Nitrogen Mustards in the Presence of DNA

To demonstrate that AGT is capable of forming nitrogen mustard-mediated cross-links to guanine involving active site cysteines in the presence of duplex DNA, additional experiments were performed in which hAGT protein was incubated with chlorambucil or mechlorethamine in the presence of double-stranded oligodeoxynucleotides (*Scheme 3.2*). Analysis of tryptic digests detected alkylation of the same two cysteine residues - Cys^{145} and Cys^{150} - suggesting that they are inherently reactive towards nitrogen mustard-derived aziridinium ions (*Figures 3.12 and 3.13*).

HPLC-ESI^+-MS/MS analysis of hAGT tryptic peptides following exposure to nitrogen mustards in the presence double-stranded DNA also resulted in the detection of ions corresponding to peptides G^{136}NPVPILIP<u>C</u>HR^{147} and $V^{148}V\underline{C}SSGGAVGNYSGGLAVK^{165}$ containing hydrolyzed monoadducts of chlorambucil (+ 250 Da mass shift, *Figures 3.14 and 3.15*) and mechlorethamine (+ 102

Figure 3.10 HPLC-ESI$^+$-MS/MS analysis of Cys-N7G-EMA conjugates: (**A**) Synthetic Cys-N7G-EMA (*m/z* 356.2 $[M + H]^+$) *Inset*: MS/MS fragmentation and UV spectrum of the authentic standard; (**B**) Cys-N7G-EMA present in enzymatic digests of wild type AGT treated with mechlorethamine half mustard (*m/z* 356.2 $[M + H]^+$) *Inset*: MS/MS fragmentation and UV spectrum of AGT-derived Cys-N7G-EMA.

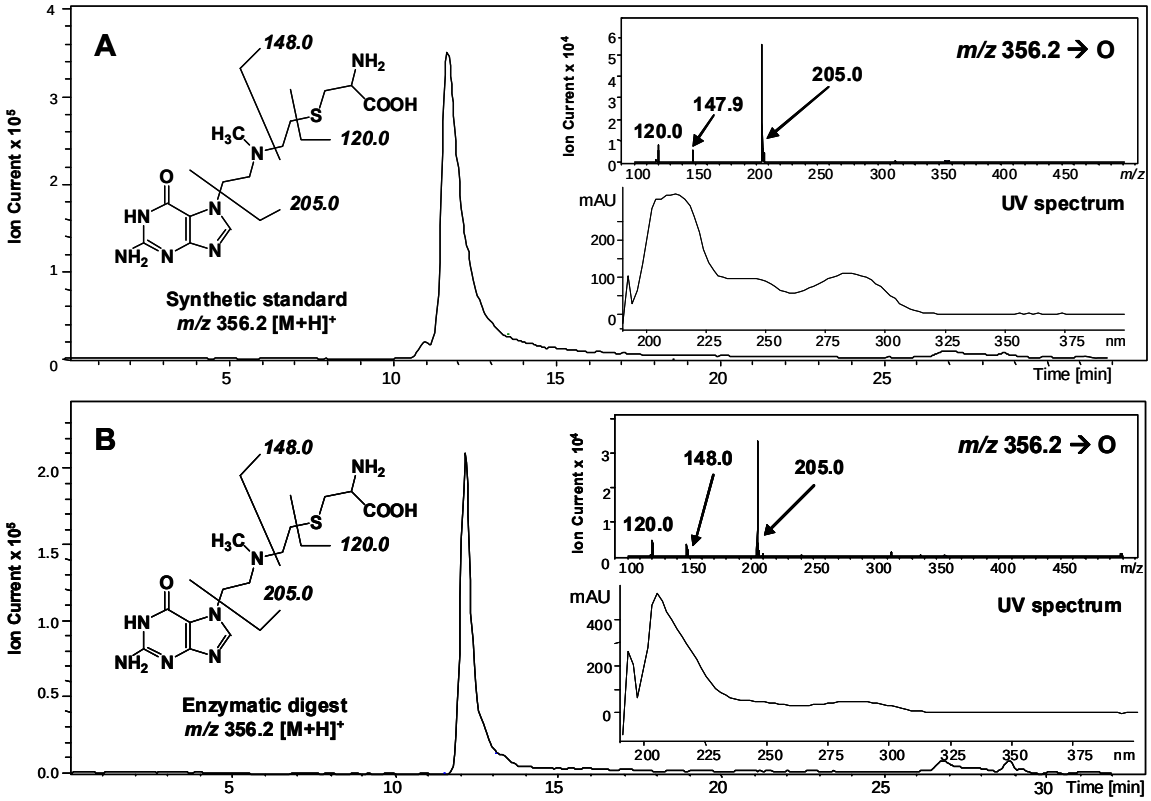

Figure 3.11 HPLC-ESI$^+$-MS/MS analysis of Lys-N7G-EMA (*m/z* 381.2 $[M + H]^+$): (**A**) Synthetic standard; *Inset*: MS/MS fragmentation and UV spectrum of Lys-N7G-EMA. (**B**) HPLC-ESI$^+$-MS/MS analysis of the total digests of AGT treated with mechlorethamine in the presence of DNA.

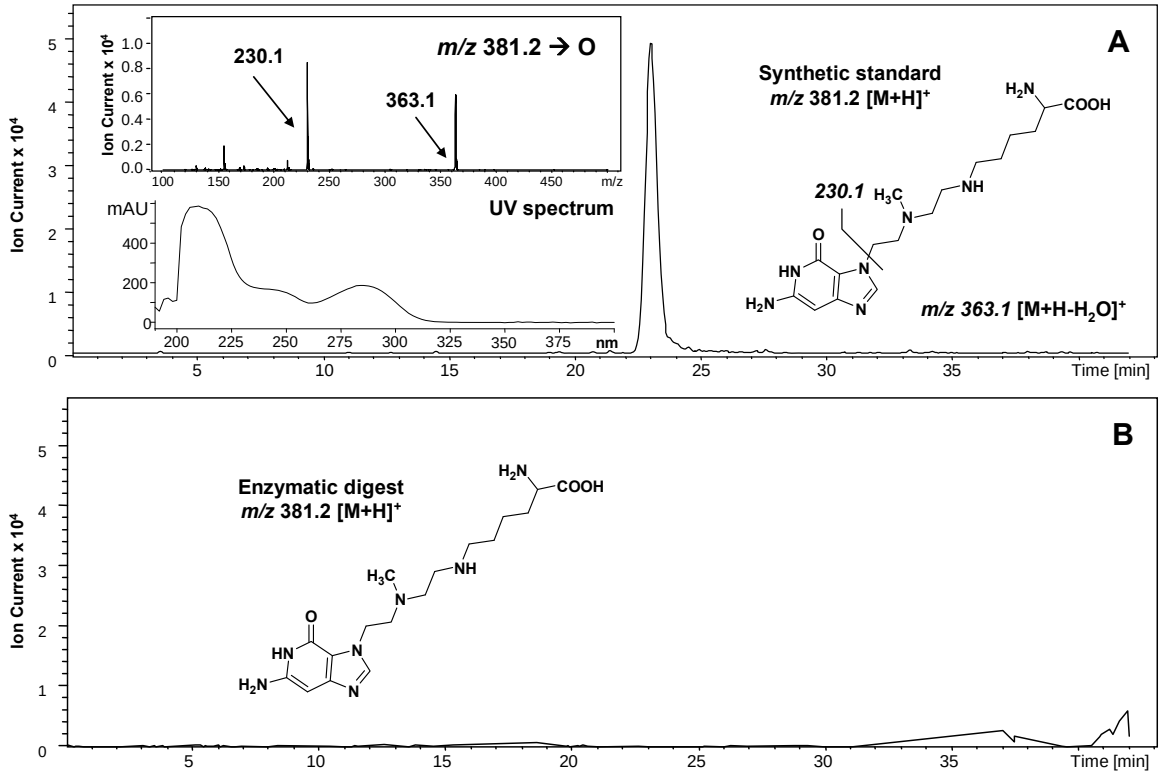

Figure 3.12 AGT tryptic peptides G[136]NPVPILIPCHR[147] (**A**) and V[148]VCSSGAVGNYSGGLAVK[165] (**B**) containing chlorambucil-mediated cross-links to guanine obtained from chlorambucil treatments of AGT-DNA mixtures. Modified fragment ions are indicated by "*".

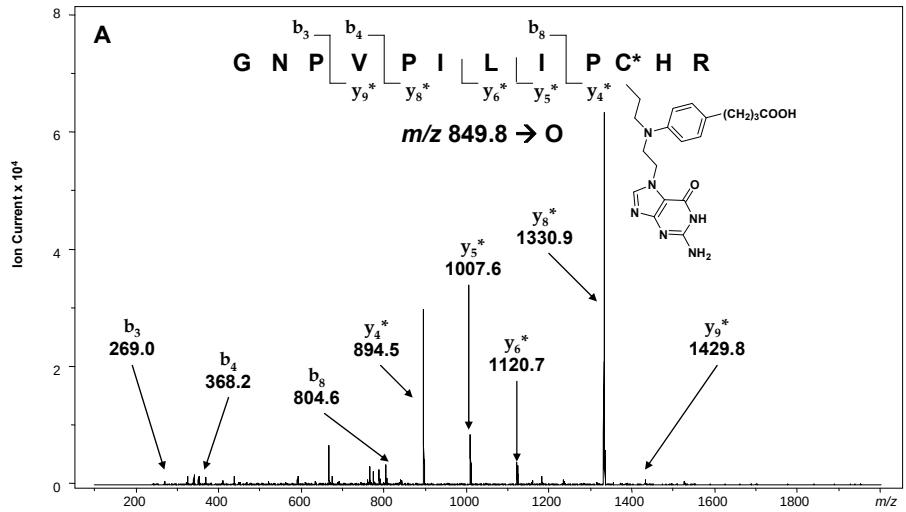

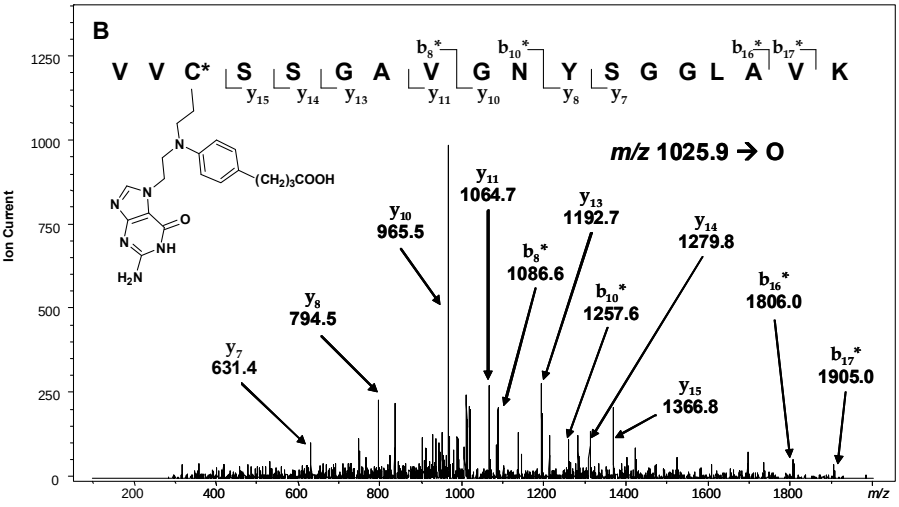

Figure 3.13 AGT tryptic peptides G[136]NPVPI LIPCHR[147] (**A**) and V[148]VCSSGAVGNYSGGLAVK[165] (**B**) containing mechlorethamine-mediated cross-links to guanine obtained from mechlorethamine treatment of AGT-DNA mixtures. Modified fragment ions are indicated by "*".

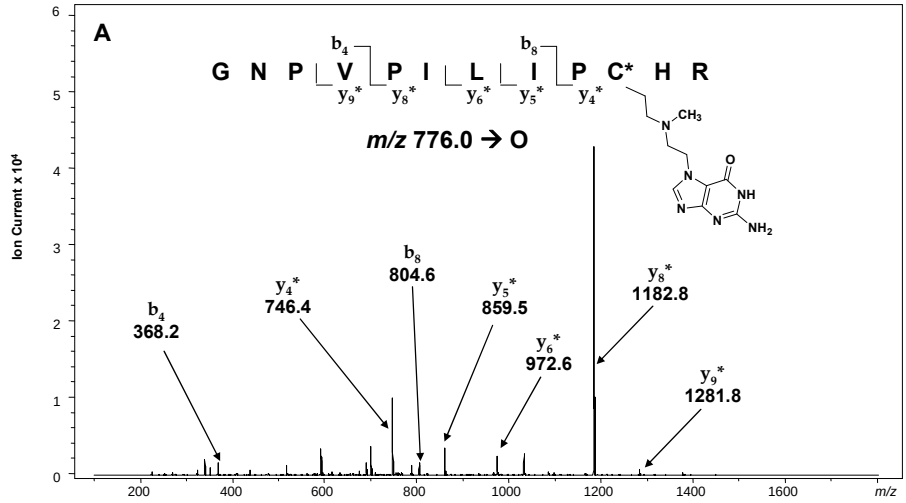

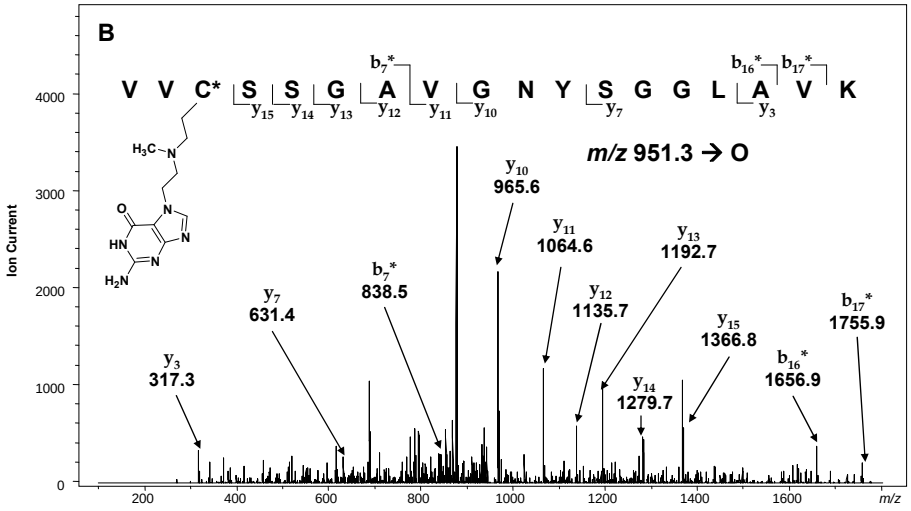

Figure 3.14 AGT tryptic peptide G[136]NPVPILIPCHR[147] containing a hydrolyzed chlorambucil monoadduct. *Top*: Extracted ion chromatogram of *m/z* 783.0 $[M + 2H]^{2+}$; *Bottom*: MS/MS spectrum of the 81.6 min peak mapping the adduct to Cys[145]. Modified fragment ions are indicated by "*".

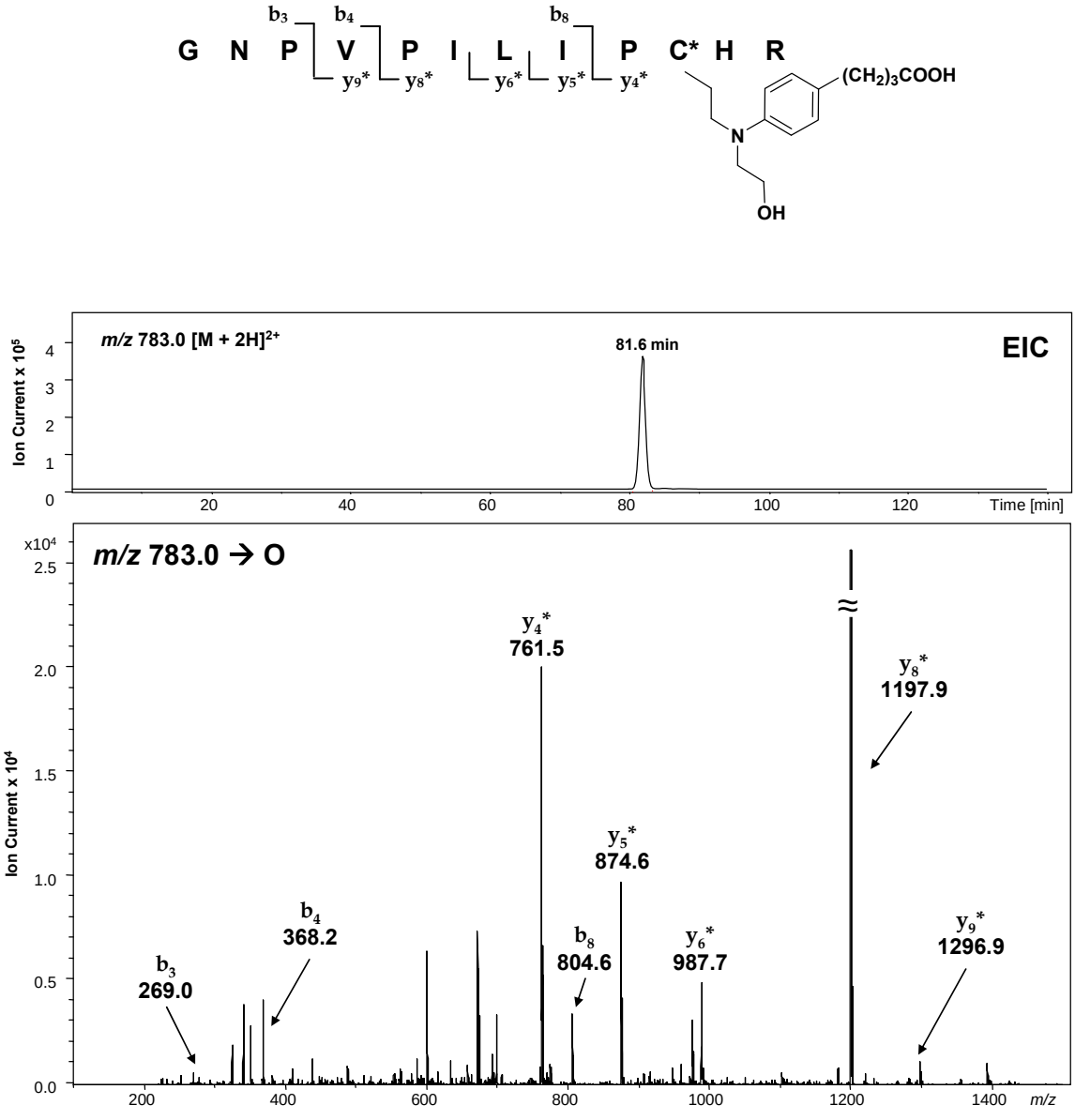

Figure 3.15 AGT tryptic peptide V[148]VCSSGAVGNYSGGLAVK[165] containing a hydrolyzed chlorambucil monoadduct. *Top*: Extracted ion chromatogram of *m/z* 960.0 $[M + 2H]^{2+}$; *Bottom*: MS/MS spectrum of the 70.1 min peak mapping the adduct to Cys[150]. Modified fragment ions are indicated by "*".

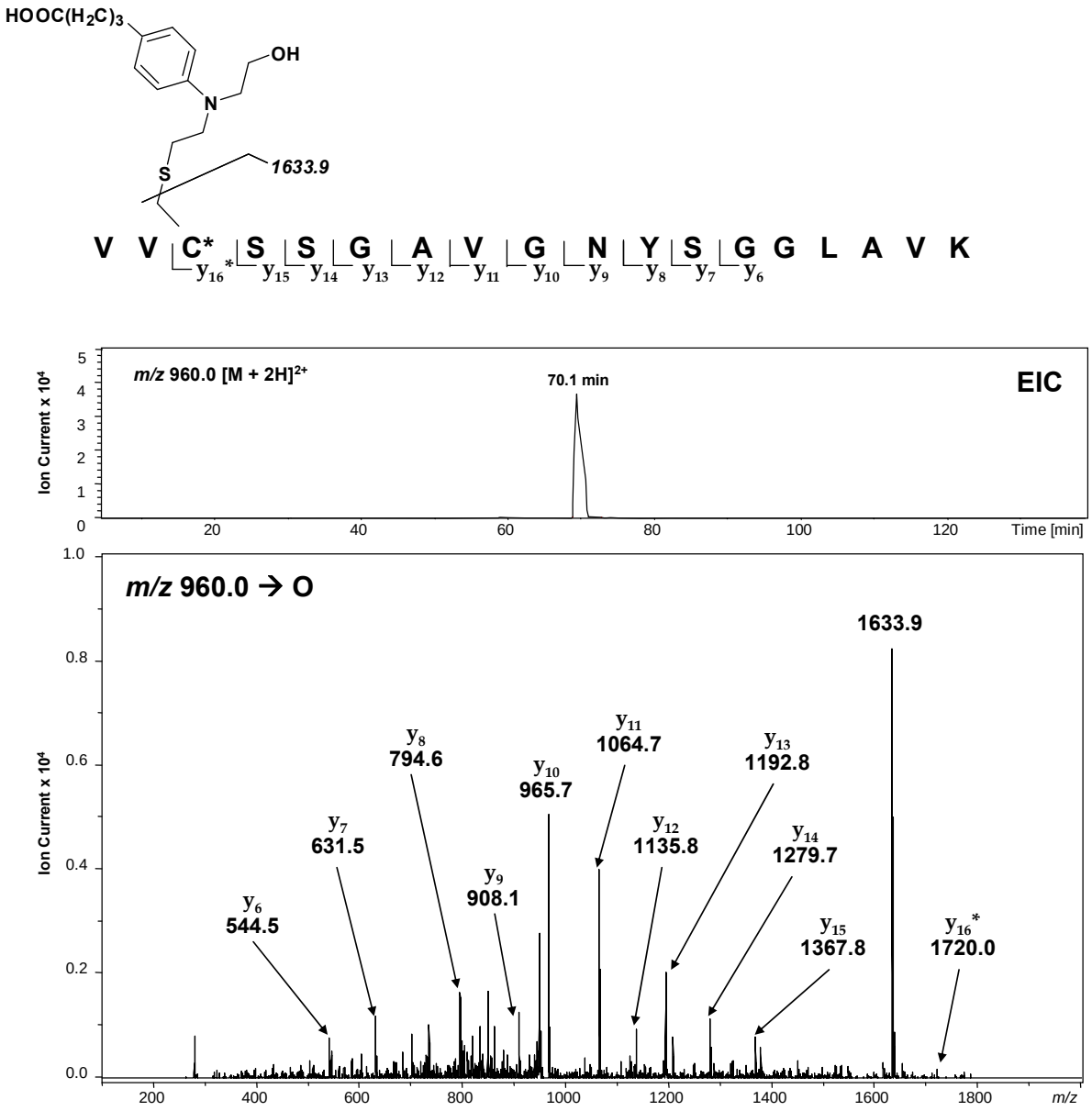

Da mass shift, *Figures 3.16 and 3.17*), with *b* and *y* fragment ions suggesting alkylation of Cys^{145} and Cys^{150}. These results were consistent with the ESI^{+}-MS whole protein data which indicated that there were two residues of hAGT capable of becoming alkylated in the presence of chlorambucil and mechlorethamine (*Figures 3.18 and 3.19* respectively). The formation of hydrolyzed monoadducts can be attributed to initial protein alkylation followed by hydrolytic displacement of the second chloride, or by direct alkylation by a nitrogen mustard that has already lost one of its reactive groups to spontaneous hydrolysis.

In addition to DPCs and monoadducts, exposure of hAGT to mechlorethamine afforded an intramolecular AGT cross-link involving AGT tryptic peptides G^{136}NPVPILIP<u>C</u>HR^{147} and V^{148}V<u>C</u>SSGGAVGNYSGGLAVK^{165} (*Figure 3.20*). While MS/MS sequencing could not confirm that the side chain sufhydryls of cysteines 145 and 150 were involved in cross-linking these two peptides, MS analysis of mechlorethamine-treated AGT mutants lacking one or both active site cysteines yielded no evidence of intramolecular cross-link formation. Taken together, this data suports the sequential reaction of Cys^{145} and Cys^{150} with mechlorethamine to form an unprecedented AGT lesion.

3.5 Discussion

Historically, DPCs have received less attention than other types of DNA lesions. As a result, the biological consequences and cellular mechanisms for the repair of DPCs are not fully understood. As bulky, helix-distorting lesions, DPCs can block the binding and progression of protein complexes, potentially interfering with crucial cellular

Figure 3.16 AGT tryptic peptide G[136]NPVPILIPCHR[147] containing a hydrolyzed mechlorethamine monoadduct. *Top*: Extracted ion chromatogram of *m/z* 708.9 $[M + 2H]^{2+}$; *Bottom*: MS/MS spectrum of the 63.6 min peak mapping the cross-link to Cys[145]. Modified fragment ions are indicated by "*".

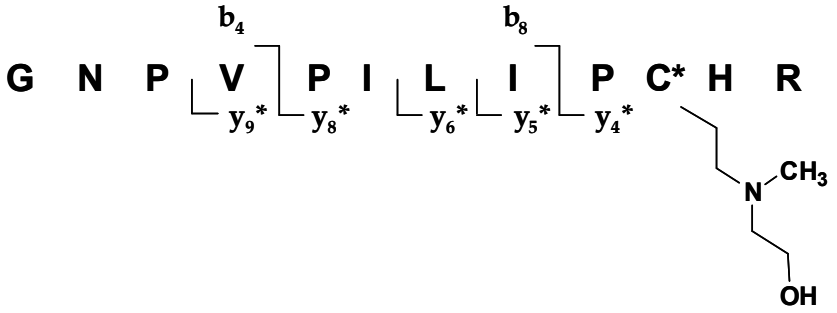

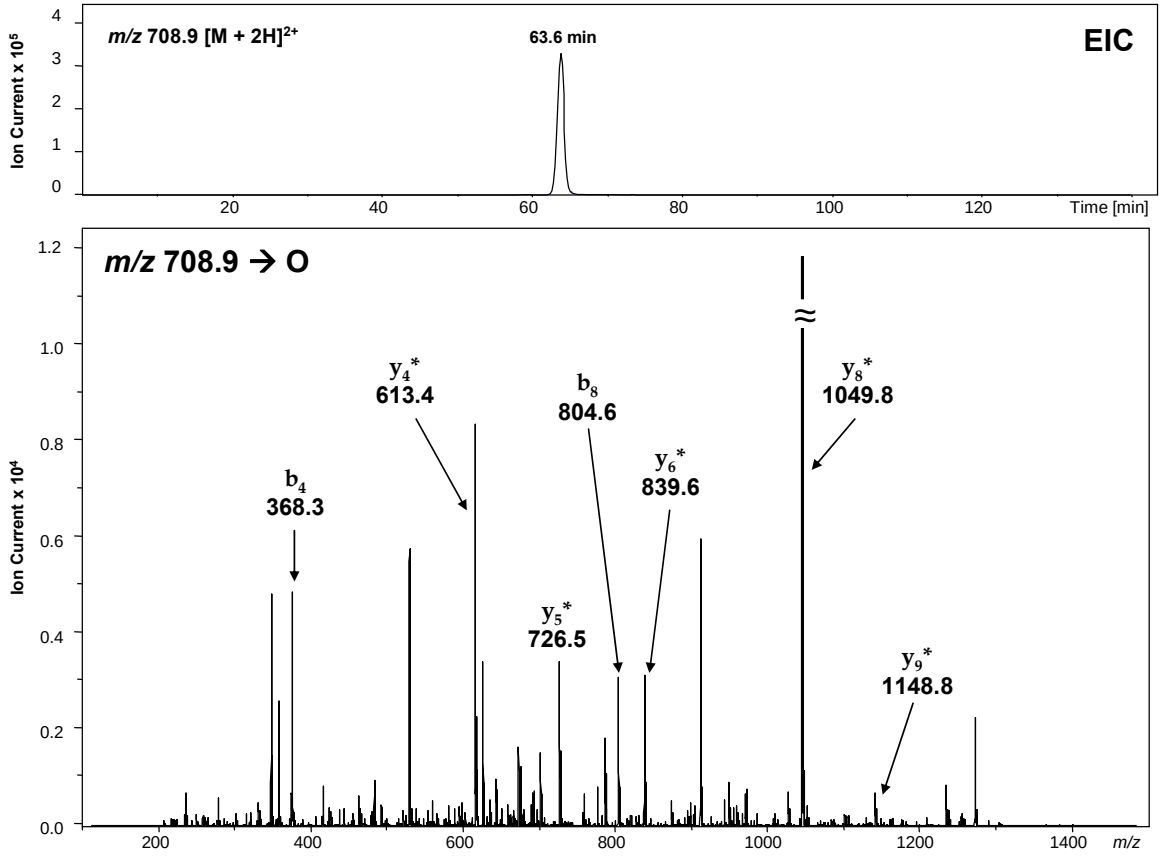

Figure 3.17 AGT tryptic peptide $V^{148}VCSSGAVGNYSGGLAVK^{165}$ containing a hydrolyzed mechlorethamine monoadduct. *Top*: Extracted ion chromatogram of *m/z* 885.0 $[M + 2H]^{2+}$; *Bottom*: MS/MS spectrum of the 57.2 min peak mapping the cross-link to Cys^{150}. Modified fragment ions are indicated by "*".

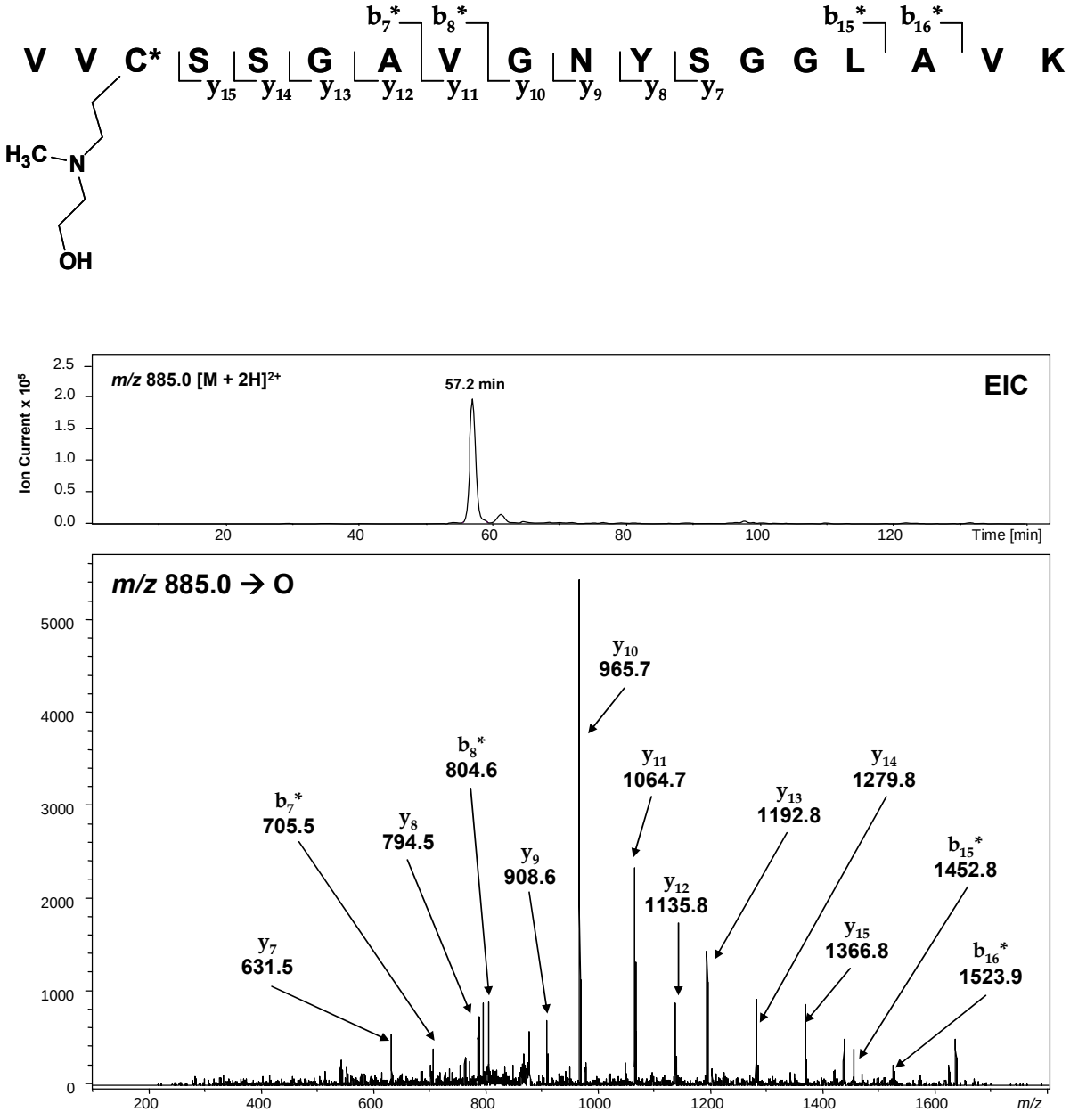

Figure 3.18 Whole protein MS analysis of hAGT following incubation with chlorambucil. *Top*: Total ion chromatogram; *Bottom:* ESI^+ mass spectrum of 17.3 min protein peak; *Inset:* Deconvoluted mass spectrum of the 17.3 min peak: The observed mass of 22 379 Da corresponds to WT AGT containing two hydrolyzed chlorambucil adducts (calculated M = 22 376 Da).

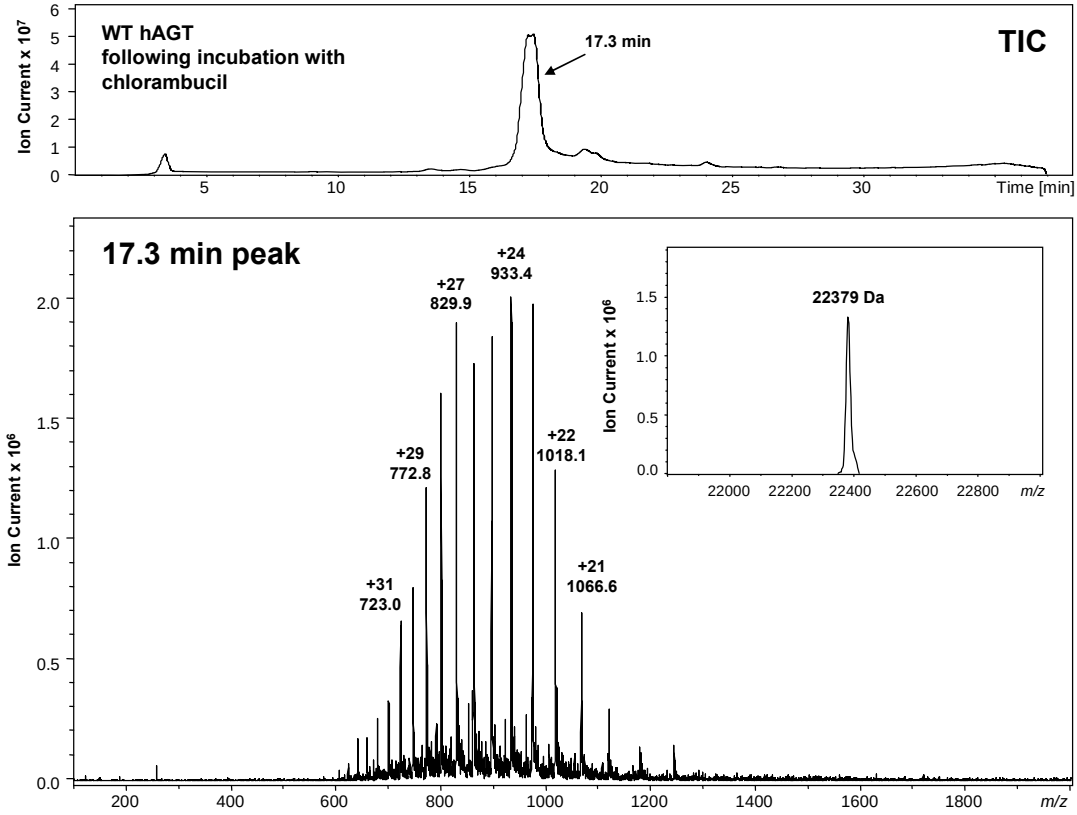

Figure 3.19 Whole protein MS analysis of AGT following incubation with mechlorethamine. *Top*: Total ion chromatogram; *Bottom:* ESI^+ mass spectrum of 17.6 min protein peak; *Inset:* Deconvoluted mass spectrum of the 17.6 min peak: *A* = WT AGT containing an intramolecular mechlorethamine cross-link (calculated *M* = 21 959 Da, observed *M* = 21 964 Da), *B* = WT AGT containing a single hydrolyzed mechlorethamine adduct (calculated *M* = 21 978 Da, observed *M* = 21 981 Da), *C* = AGT containing two hydrolyzed mechlorethamine adducts (calculated *M* = 22 080 Da, observed *M* = 22 084 Da).

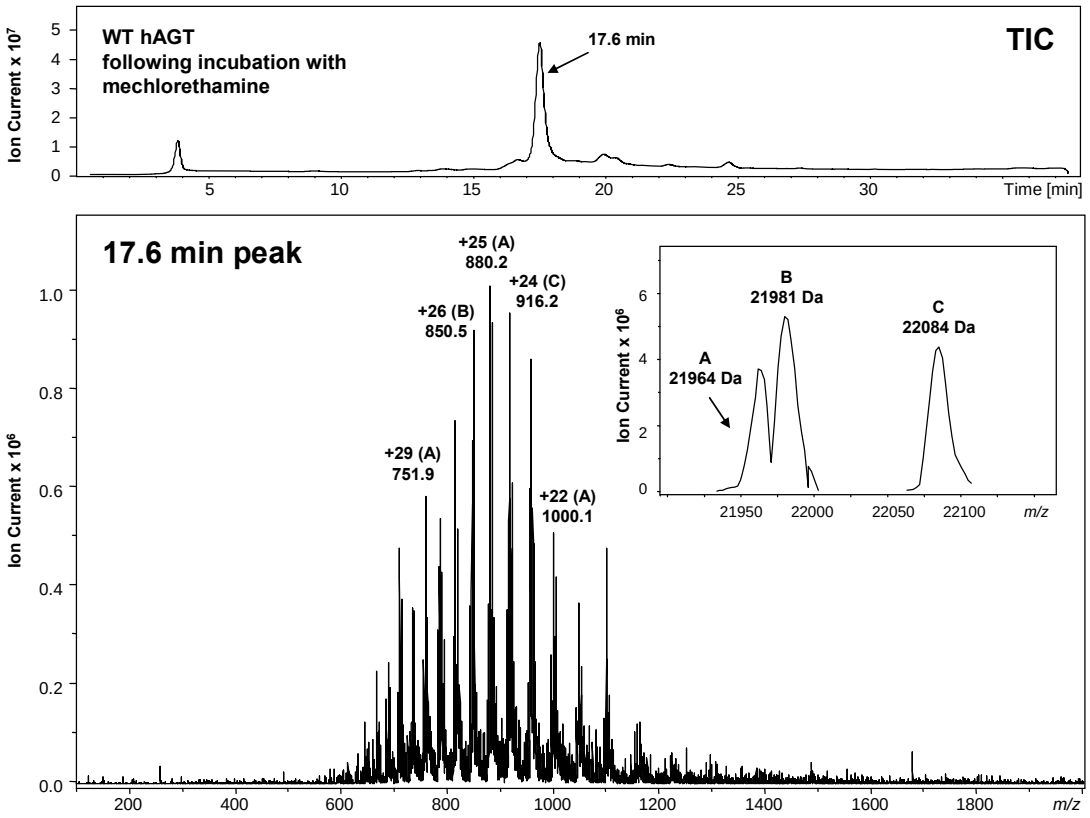

Figure 3.20 MS/MS analysis of AGT tryptic peptides G[136]NPVPILIPCHR[147] and V[148]VCSSGAVGNYSGGLAVK[165] cross-linked by mechlorethamine.

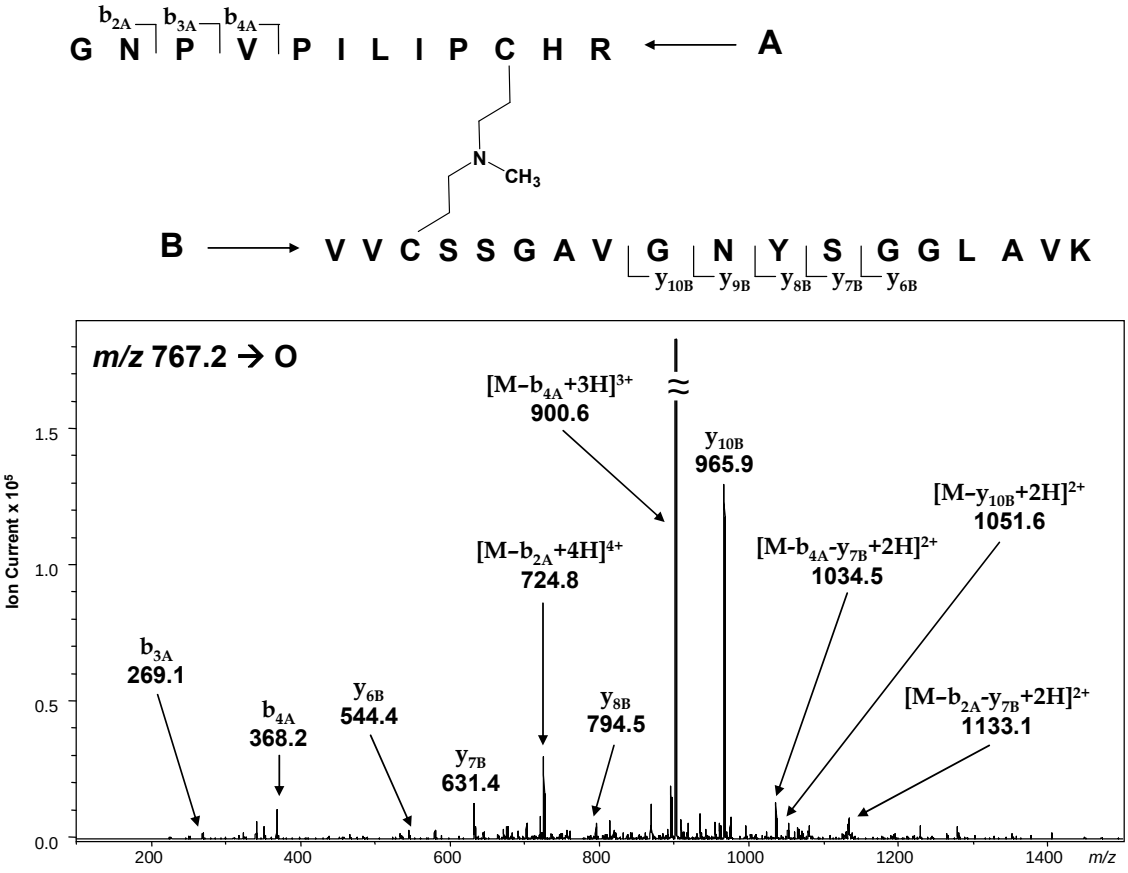

processes including DNA replication, transcription, DNA repair, recombination, and chromatin remodeling *(1)*. The formation of DPCs can occur upon exposure to a variety of cytotoxic, mutagenic, and carcinogenic agents, including ionizing radiation *(11)*, metals *(8)*, endogenous and exogenous aldehydes *(19)*, and chemotherapeutic drugs *(36;100)*. Because certain types of DNA-protein cross-links have been shown to persist through several cycles of DNA replication due to lack of repair *(1)*, DNA-protein cross-linking could play an important role in the cytotoxic activity of many antitumor drugs traditionally known for cross-linking DNA, including the nitrogen mustards.

We present the first evidence for the cross-linking of a specific DNA repair protein, O^6-alkylguanine DNA alkyltransferese, to DNA in the presence of antitumor nitrogen mustards. Denaturing gel electrophoresis detected a concentration-dependent formation of AGT-DNA conjugates following incubation of human recombinant AGT protein with ^{32}P-labeled oligonucleotides in the presence of nitrogen mustards (*Figure 3.1*). Mass spectrometry analysis of recombinant human AGT that had been incubated with guanine half-mustards as models for monoalkylated DNA confirmed these findings and revealed that cross-linking can take place at two different sites within the protein (*Figure 3.2, panels A and D*). Mutagenesis studies indicated that the two observed cross-linking sites reside at the active site cysteine residues, Cys^{145} and Cys^{150}, since their replacement with Ala and Ser, respectively, blocked cross-linking (*Figure 3.2, panels B and C*). These results were fully supported by HPLC-ESI^+-MS/MS sequencing of tryptic peptides obtained from AGT treated with guanine half-mustards (*Figures 3.3-3.8*) or with mustards in the presence of double stranded DNA (*Figures 3.12-3.13*). The exact structures of the cross-links were established as *N*-(2-[*S*-cysteinyl]ethyl)-*N*-(2-[guan-7-

yl]ethyl)-*p*-aminophenylbutyric acid and *N*-[2-[*S*-cysteinyl]ethyl]-N-[2-(guan-7-yl)ethyl]methylamine for chlorambucil and mechlorethamine, respectively, based on HPLC-ESI$^+$-MS/MS analysis of amino acid-nucleobase conjugates in total protein digests in comparison with the corresponding synthetic standards (*Figures 3.9 and 3.10*).

In comparing the overall AGT-DNA cross-linking ability of the two nitrogen mustards used in this study, several interesting observations were made. For reactions in which cross-linking was initiated between double-stranded oligodeoxynucleotides and AGT *via* the addition of free drug, mechlorethamine displayed greater cross-linking efficiency (*Figure 3.1*). This is not surprising since nitrogen mustard derivatives based upon the structure of mechlorethamine (including chlorambucil) were specifically designed to afford compounds with reduced reactivity/toxicity for chemotherapeutic applications *(175)*. However, reactions in which cross-linking was achieved upon incubation of AGT with the synthetically-prepared guanine half-mustards, chlorambucil appeared to be a more efficient cross-linker (*Figure 3.2*). Higher affinity of N7G-PBA-Cl with its aromatic substituent for the primarily hydrophobic active site pocket of AGT is one possible explanation its superior cross-linking ability *(110)*. Another possible explanation could involve competing alkylation of AGT by N7G-EMA-Cl and mechlorethamine due to the formation of an AGT intramolecular cross-link (*Figure 3.2, panel D*).

Our results support nitrogen mustard-induced AGT-DNA cross-linking involving two active site cysteine residues (Cys^{145} and Cys^{150}), despite the presence of three other cysteines within the protein. These same two sites were also directly modified by

chlorambucil and mechlorethamine (*Figures 3.14-3.20*), suggesting selective reactivity of these residues towards nitrogen mustards.

As nitrogen mustard-mediated DNA-protein cross-linking displays selectivity for two active site cysteine residues of AGT, questions are raised regarding the role of this important repair protein in the cellular response to bifunctional alkylating agents. Within the cell, AGT is responsible for the irreversible transfer of promutagenic O^6-alkylguanine lesions in DNA to an active site cysteine residue, Cys^{145}, restoring normal guanine and preventing mutagenesis. Levels of AGT expression are highly variable between different tissues and tumor types, opening the possibility that it may mediate the biological effects of DNA alkylating drugs. Previous studies have yielded conflicting reports on the possible role of AGT in mediating cytotoxicity of nitrogen mustards, specifically cyclophosphamide and chlorambucil. Several papers provide evidence that AGT partially protects against the toxicity and mutagenicity of cyclophosphamide metabolites and imparts resistance to treatment of tumor xenografts *(176)*. In CHO cells, expression of human AGT was found to protect against the toxic and mutagenic effects of cyclophosphamide, and that the metabolite acrolein was responsible for generating the lesions in which AGT afforded protection *(177)*. Although the idea that AGT may be acting as a molecular scavenger was proposed, a more recent study has shown that DNA binding is required for AGT-mediated protection against acrolein toxicity, suggesting that the active site thiol is not simply sequestering this reactive metabolite *(178)*. However, in other studies in cultured cells, survival was not affected by AGT activity *(179)*, and a comparison of the therapeutic response of 23 tumor xenografts showed no correlation with AGT levels *(180)*. The presence of AGT renders *E. coli* strains more sensitive to

killing by chlorambucil *(181)* but no effect of AGT status on drug sensitivity was seen in a studies of HeLa or CHO cells (*see Chapter V*) *(179)*. Clinical studies have also yielded conflicting results on the role of AGT levels in the outcome of therapy with cyclophosphamide [reviewed *(178)*]. Recently, it was shown that MGMT does not protect against mutations induced by cyclophosphamide in mice *(182)*.

The present results showing that AGT can be cross-linked to DNA by nitrogen mustards adds another factor that must be considered in the overall effect of AGT levels to the response to treatment. This cross-linking could increase the toxicity, and the extent to which this is balanced or exceeded by the ability to repair other adducts may determine the overall biological response.

IV. CROSS-LINKING OF O^6-ALKYLGUANINE DNA ALKYLTRANSFERASE TO DNA IN THE PRESENCE OF OTHER CELLULAR PROTEINS

4.1 Abstract

Studies described in *Chapters II* and *III* demonstrated cross-linking of the human DNA repair protein AGT to double-stranded DNA in the presence of DEB and antitumor nitrogen mustards. By the use of tandem mass spectrometry in combination with NMR spectroscopy and UV spectrophotometry, the exact chemical structures of DEB- and nitrogen mustard-induced AGT-DNA cross-links have been elucidated. While the formation of AGT-DNA cross-links occurs readily upon incubation of the purified recombinant protein with DNA in the presence of *bis*-electrophiles, the propensity of DEB and nitrogen mustards to selectively induce AGT-DNA cross-links is unclear. In the present study, the ability of AGT to cross-link DNA in the presence of other nuclear proteins was examined by tandem mass spectrometry and immunological techniques. Using a commercially-available antibody against the human protein, AGT-DNA cross-linking was detected following incubation of mammalian nuclear extract proteins with double-stranded oligodeoxynucleotides in the presence of mechlorethamine and DEB. In all cases, AGT-DNA cross-linking displayed concentration-dependence with little to no protein detected in samples lacking *bis*-electrophile. The involvement of AGT in cross-linking was confirmed by mass spectrometric identification of AGT tryptic peptides. The ability of *bis*-electrophiles to cross-link AGT to DNA is likely to contribute to their cytotoxicity and mutagenicity *in vivo*.

4.2 Introduction

The genotoxicity of numerous chemical agents is tightly correlated to their ability to induce chromosomal damage *via* direct alkylation of DNA nucleobases *(170)*. While generally known for its negative connotations regarding the carcinogenic potential of environmental toxins, DNA alkylation can also prove beneficial for the treatment of cancer. The majority of clinically-useful alkylating drugs are electrophiles that modify cellular macromolecules, giving rise to a wide variety of lesions. Although all alkylating agents are capable of producing DNA lesions which can lead to cytotoxicity and/or the induction of mutations, bifunctional alkylating agents are unique in that they can react with two sites within biomolecules to form a cross-linked lesion. While interstrand DNA-DNA cross-links are thought to represent the most toxic of all DNA lesions (as their formation results in seizure of the replication fork), the biological consequences of DPCs are less clear.

Due to their close proximity to DNA, DNA binding proteins have a high probability of becoming chemically linked to DNA in the presence of *bis*-electrophiles. In particular, DNA repair proteins are at high risk of becoming covalently bound to their DNA substrate *via* active site residues upon encountering a monoalkylated nucleobase lesion containing a reactive group. The resulting DPC could potentially contribute to the cytotoxicity of these agents by further blocking DNA replication and depleting cellular pools of DNA repair proteins.

Previous studies in our laboratory have shown that AGT readily formed cross-links to DNA in the presence of DEB and nitrogen mustard drugs *(37;38)*. Using a variety of analytical techniques, the chemical structures of DEB- and nitrogen mustard-

induced AGT-DNA cross-links were identified as involving the side chain sulfhydryls of cysteines 145 and 150 of AGT and the N7 position of guanine in duplex DNA. However, as AGT-DNA cross-linking in these studies was examined using a rather simplified system containing purified human recombinant AGT incubated with double-stranded oligodeoxynucleotides in the presence of *bis*-electrophile, it is possible that other cellular proteins may influence/interfere with AGT-DNA cross-linking *in vivo*. In this work, we examined AGT-DNA cross-linking in the presence of other cellular proteins in cell-free extracts. Employing a novel affinity enrichment strategy which effectively isolates AGT-DNA cross-links prior to detection by tandem mass spectrometry and immunological techniques, we demonstrate that mechlorethamine- and DEB-mediated AGT-DNA cross-linking does occur in the presence of other cellular proteins.

4.3 Materials and Methods

Cell Culture. Chinese hamster ovary cells expressing human recombinant O^6-alkylguanine DNA alkyltransferase (CHO-AGT) and their wild-type/empty vector equivalent (CHO-EV) were obtained from Dr. Anthony Pegg (Pennsylvania State University) and maintained as exponentially growing monolayer cultures in α-MEM supplemented with 9% FBS and G418 (1 mg/mL) in a humidified incubator at 37 ^{o}C with 5% CO_2 *(183)*. Human cervical carcinoma (HeLa) cells were a gift from Dr. Jonathan Marchand (University of Minnesota). Like the CHOs, the HeLa cells were maintained as exponentially growing monolayer cultures in Dulbecco's Modification of Eagle's Medium **(**DMEM) supplemented with 9% FBS.

Preparation of Nuclear Protein Extracts. Nuclear extracts from each cell line were prepared as previously described *(184)*. Cells were harvested (~ 10^8 cells/preparation), washed with phosphate-buffered saline (140 mM NaCl/3 mM KCl/8 mM NaH_2PO_4/1 mM K_2HPO_4/1 mM $MgCl_2$/1 mM $CaCl_2$), and resuspended in hypotonic buffer (10 mM TRIS-HCl - pH 7.4/10 mM $MgCl_2$/10 mM KCl/1 mM dithiothreitol) containing phenylmethylsulfonyl fluoride (1 mM). The cells were broken by 20 strokes in a Dounce homogenizer, and the resulting mixture was centrifuged at 2,600 rpm for 8 min. Following centrifugation, the pelleted nuclei were resuspended in hypotonic buffer containing 350 mM NaCl. Upon addition of a cocktail of protease inhibitors (including pepstatin, leupeptin, aprotinin, and phenylmethylsulfonyl fluoride), the nuclei were incubated at 0 ^oC for 1 h. The extracted nuclei were centrifuged at 70,000 rpm at 4 °C for 30 min, and the clear supernatant was adjusted to 10% glycerol/10 mM β-mercaptoethanol and stored at -80 °C. Prior to use in cross-linking reactions, the nuclear extracts were dialyzed overnight at 4 ^oC against 10 mM TRIS-HCl (pH 7.4) using Slide-A-Lyzer dialysis cassettes from Pierce Biotechnology (3.5 kDa molecular weight cut-off, Rockford, IL). Protein concentrations were determined *via* colorimetric assay *(185)*.

Detection of AGT-DNA Cross-Links: Slot Blot Analysis. 5'-Biotinylated double-stranded oligodeoxynucleotides (5'-GGA GCT CGT GGC CTA-3' (+) strand, 6.25 nmol) were combined with CHO-AGT nuclear extract (1 mg) in 10 mM TRIS-HCl – pH 7.4 in the presence of excess mechlorethamine (1.5, 3.0, or 6.0 mM). The reaction mixtures were incubated at 37 ^oC for 2 h to induce cross-linking. Reactions lacking either mechlorethamine or DNA served as negative controls, as did mechlorethamine treatment

of CHO-EV nuclear extracts (which do not express AGT). Treatment of hAGT (10 μg) and hAGT-spiked CHO-EV nuclear extract (10 μg hAGT/1 mg extract) with 6.0 mM mechlorethamine in the presence of biotinylated oligonucleotide served as positive controls. Following the capture of biotinylated DNA/AGT-DNA cross-links with Streptavidin Sepharose High Performance beads (GE Healthcare, Piscataway, NJ), the beads were washed with 0.1% SDS and 1 M NaCl to remove any non-covalently bound proteins. Biotinylated DNA/AGT-DNA cross-links were then released from the beads upon overnight treatment with 0.5 M formic acid/25% ACN at 4 ^{o}C. To detect AGT-DNA cross-links, the eluates were adhered to a nitrocellulose membrane *via* vacuum using a Bio-dot® Microfiltration apparatus (Bio-Rad, Hercules, CA). Once the AGT-DNA cross-links were bound, the membrane was blocked in Tris-buffered saline containing 5% bovine serum albumin, followed by a 2 h incubation with anti-MGMT, clone MT3.1 (Millipore, Temecula, CA) at room temperature. After rinsing three times with Tris-buffered saline, the membrane was incubated with the corresponding secondary antibody (alkaline phosphatase-conjugated anti-mouse IgG, Sigma, St. Louis, MO, 1:10,000 dilution) for 1 h at room temperature. Following three more rinses with Tris-buffered saline to remove unbound antibodies, the blot was developed using SIGMA Fast BCIP/NBT (Bio-Rad, Hercules, CA). The finished blot was scanned as an image file and the optical densities of the bands in the resulting image file were quantified using the ImageJ software/shareware available free of charge from the NIH (www.ncbi.nlm.nih.gov). The amount of AGT present in the eluate following biotin capture was determined by direct comparison of AGT band intensity to known amounts

of hAGT. Cross-linking efficiency was determined by dividing the amount of AGT present in the eluate by the total amount of AGT present in the reaction mixture.

Detection of AGT-DNA Cross-Links: Western Blot Analysis. Double-stranded oligodeoxynucleotides containing a 5' biotin tag (5'-GGAGCTCGTGGCCTA-3' (+) strand, 3.12 nmol) were incubated with CHO-AGT or HeLa nuclear extract proteins (0.5 mg) in 10 mM TRIS-HCl – pH 7.4 in the absence and presence of mechlorethamine (100-1000 uM) at 37°C for 3 h to induce cross-linking. Biotinylated DNA with any bound proteins was captured using streptavidin beads, and the beads were washed with 0.1% SDS, 4 M urea, and 1 M NaCl to remove any non-covalently attached proteins. Biotinylated DNA containing covalently bound proteins was released from the beads upon the addition of 4X SDS-PAGE loading buffer and heating to 90°C for 15 min. DNA-protein cross-links present in the elutes were separated by 10 or 12% SDS-PAGE, and the presence of AGT was detected using anti-MGMT, clone MT3.1 (1:500 dilution) and alkaline phosphatase-conjugated anti-mouse IgG (1:10,000 dilution). The amount of AGT cross-linked to DNA was determined by direct comparison of the band intensity to that of known AGT standards analyzed in parallel. Percent cross-linking was determined by dividing the amount of AGT present in the biotin capture by the total amount of AGT in the reaction mixture. Analogous experiments were carried out in the presence and absence of DEB (0-25 mM).

Mass Spectrometric Identification of Cross-Linked AGT. For mass spectrometric identification of cross-linked AGT, SDS-PAGE gels were stained with SimplyBlue

SafeStain (Invitrogen, Carlsbad, CA), and sample lanes were cut into 10 slices comprising the entire molecular weight range. Upon further dicing of the gel pieces into 1 mm pieces and washing with 100 mM ammonium bicarbonate, each fraction was subjected to reduction with dithiothreitol and alkylation with iodoacetaminde as previously described *(186)*. Gel pieces were dehydrated with acetonitrile, dried under vacuum, and reconstituted in 25 mM ammonium bicarbonate containing mass spectrometry grade trypsin (~1 μg). The samples were digested overnight at 37°C. Tryptic peptides were extracted from the gel pieces using 0.1% aqueous formic acid/60% acetonitrile, evaporated to dryness, and resuspended in 0.1% aqueous formic acid. HPLC-ESI^+-MS/MS analyses were performed on a Thermo LTQ linear ion trap MS system equipped with a Thermo Surveyor solvent delivery system and a microelectrospray source. Tryptic peptides were resolved on a 100 μm x 11 cm fused silica capillary column packed with 5 μm, 300 Å Jupiter C18 (Phenomenex, Torrence, CA) eluted at 0.6 μL/min with 0.1 formic acid in water (A) and 0.1% formic acid in acetonitrile (B). Solvent composition was kept at 2% B for the first 15 min, followed by a linear increase to 25% B over the next 35 min and further to 90% B in the next 15 min, and held at 90% B for 10 min. MS/MS spectra of peptides were acquired using data-dependent scanning in which a single full MS spectrum (400-2000 *m/z*) was followed by four MS/MS spectra. Spectra were recorded using dynamic exclusion of previously analyzed precursors for 60 s. The MS/MS spectra were searched against human and *Cricetulus griseus* (Chinese hamster) database sequences using the SEQUEST algorithm *(60)*. *S*-Carboxamidomethylation at cysteine (+57 Da), oxidation of methionine (+16 Da), and mechlorethamine-induced

alkylation at cysteine (hydrolyzed monoadduct: +102 Da, guanine cross-link: +234 Da) were specified as dynamic modifications to identify spectra of adducted peptides.

4.4 Results

4.4.1 Immunological Detection of AGT-DNA Cross-Links Induced by Mechlorethamine in Mammalian Nuclear Extracts

To determine whether AGT-DNA cross-linking can occur in the presence of other cellular proteins, an affinity based approach was developed (*Scheme 4.1*). Nuclear protein extracts were prepared from transgenic CHO expressing human recombinant AGT and from CHO cells transfected with an empty vector, which do not express the AGT protein. Extracts were also prepared from HeLa cells which endogenously express AGT. Protein extracts were incubated with synthetic DNA duplexes containing a 5' biotin tag (5'-GGAGCTGGTGGCGTAGGC-3', (+) strand) in the presence and absence of *bis*-electrophile. Streptavidin beads were employed to capture any proteins chemically cross-linked to the biotinylated DNA. Following stringent washing procedures to remove non-covalently bound proteins, biotinylated DNA (along with any covalently attached protein) was eluted from the beads, DPCs were thermally hydrolyzed to release alkylated guanines from the DNA backbone, and the cross-linked proteins were analyzed by immunological techniques and HPLC-ESI$^+$-MS/MS.

To ensure that the biotin capture strategy was working properly, numerous positive and negative controls were included in initial studies. As human recombinant AGT had previously been shown to cross-link DNA in the absence of other proteins, a reaction in which purified hAGT protein was incubated with mechlorethamine in the

Scheme 4.1 Biotin capture assay for AGT-DNA cross-links

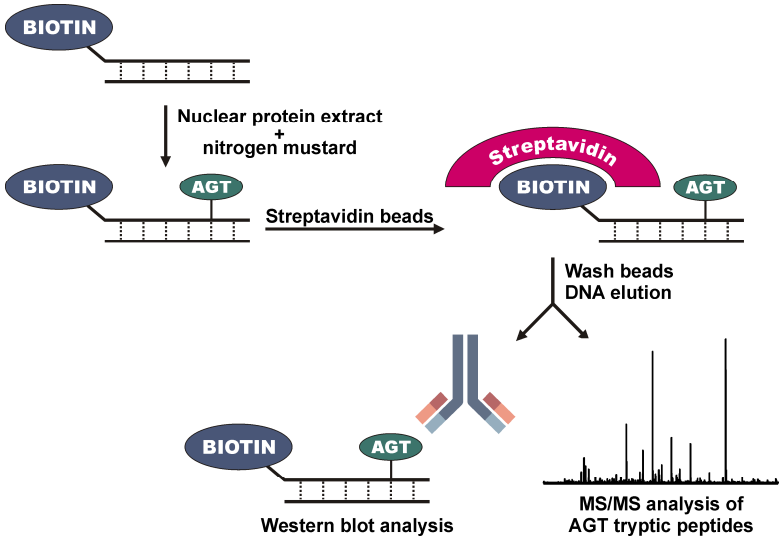

presence of 5'-biotinylated oligodeoxynucleotides served as a positive control, whereas reactions lacking AGT, DNA, or mechlorethamine served as negative controls.

Immunological detection *via* slot blot analysis employing anti-MGMT (*Figure 4.1*) revealed a concentration-dependent formation of drug-induced AGT-DNA cross-links in nuclear protein extracts from the AGT-expressing Chinese hamster ovary cell line (*column 1 - rows B-D*), but not in protein extracts from the control cell line (*column 1 – row H*). Between 0.1 and 2.0% of AGT became cross-linked to DNA as the mechlorethamine concentration was increased from 1.5 to 6.0 mM based upon signal comparison to known AGT amounts (*column 2 - rows A-H*). Negative control experiments detected little to no AGT in the biotin capture of reactions lacking mechlorethamine, DNA, or AGT (*column 1 - rows A, G, and H respectively*) while positive controls obtained by reacting purified recombinant AGT (*column 1 – row E*) and AGT-spiked CHO-EV nuclear extract (*column 1 – row F*) with 5'-biotinylated DNA in the presence of drug exhibited more intense AGT signals.

Due to weak signal intensity, relatively low cross-linking efficiency, and very high concentrations of mechlorethamine required for the detection of CHO-AGT cross-links, it appeared that we were losing protein during biotin capture enrichment – most likely during DNA elution. After further experimentation, the acidic DNA elution protocol was replaced with one in which biotinylated DNA was released from the streptavidin beads upon heating in SDS-PAGE loading buffer. Unlike acid elution where the samples had to be dried prior to analysis, the new elution technique allowed for immediate analysis by SDS-PAGE/Western blotting.

Figure 4.1 Representative slot blot of AGT-DNA cross-links resulting from biotin capture. Exposure of CHO-AGT nuclear extract proteins to increasing amounts of mechlorethamine in the presence of 5'-biotinylated DNA duplexes (5'-GGAGCTGGTGGCGTAGGC-3' (+) strand) afforded AGT-DNA cross-links in a dose-dependant manner (*column 1, rows B-D*). Reactions lacking mustards or containing DNA without the 5'-biotin tag served as negative controls (*column 1, rows A and G*), as did nitrogen mustard treatment of CHO-EV nuclear extracts (which contain no AGT, *column 1, row H*). Treatment of hAGT and hAGT-spiked CHO-EV nuclear extract with mechlorethamine in the presence of biotinylated oligonucleotide served as positive controls (*column 1, rows E-F*). Known amounts of hAGT (*column 2, rows A-G*) were analyzed in parallel for quantitative purposes. Botinylated DNA and AGT-DNA cross-links were captured using streptavidin sepharose high performance beads, washed with buffers containing SDS and NaCl to remove non-covalently bound proteins, and eluted with acid. The presence of AGT in the biotin capture fractions following DNA elution was detected using a monoclonal antibody against AGT.

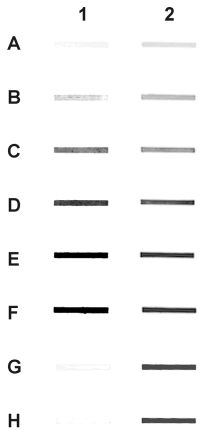

Column 1 – Biotin Capture

A: CHO-AGT – *No Mechlorethamine*
B: CHO-AGT + 1.5 mM Mechlorethamine
C: CHO-AGT + 3.0 mM Mechlorethamine
D: CHO-AGT + 6.0 mM Mechlorethamine
E: hAGT + 6.0 mM Mechlorethamine
F: CHO-EV + hAGT + 6.0 mM Mechlorethamine
G: CHO-AGT + 6.0 mM Mechlorethamine – *No 5'-Biotin DNA*
H: CHO-EV + 6.0 mM Mechlorethamine – *No AGT*

Column 2 – hAGT Standards

A: 1 ng
B: 5 ng
C: 10 ng
D: 20 ng
E: 50 ng
F: 100 ng
G: 200 ng
H: 500 ng

Western blot analysis of CHO-AGT nuclear protein extracts following incubation with 5'-biotinylated DNA in the presence of 0, 100, 250, 500, 750, and 1000 μM mechlorethamine revealed a concentration-dependent formation of drug-induced AGT-DNA cross-links (*Figure 4.2, lanes 2-6*). Cross-linking of AGT to DNA increased from ~ 2.0% to 10.0% as the mechlorethamine concentration increased from 100 to 1000 uM based upon signal comparison to known AGT standards. Very little AGT was detected in the biotin capture of reactions lacking mechlorethamine (*Figure 4.2, lane 1*).

In comparing the Western blot results (*Figure 4.2*) to those obtained *via* slot blot analysis (*Figure 4.1*), detection of AGT-DNA cross-links was vastly improved upon DNA elution with SDS-PAGE loading buffer following biotin capture enrichment. We were able to reduce the amount of protein used per cross-linking reaction without a loss of signal. Thus, DNA elution *via* heating in SDS-PAGE loading buffer was implemented in all subsequent experiments.

Mechlorethamine-induced AGT-DNA cross-linking also occurred following incubation of biotinylated oligodeoxynucleotides with HeLa nuclear extract proteins containing endogenous AGT (*Figure 4.3*). Unlike the CHO-AGT cell line which is genetically engineered to over-express human AGT, HeLa cells exhibit endogenous AGT expression (~0.01% of total nuclear protein). In the presence of 500 and 1000 μM of mechlorethamine, AGT-DNA cross-linking was detected (*lanes 2 and 3*). In contrast, little to no AGT was observed in the untreated control (*lane 1*).

Figure 4.2 Mechlorethamine induces AGT-DNA cross-links in nuclear protein extracts as indicated by Western blotting. Biotinylated double-stranded oligodeoxynucleotides (5'-GGAGCTCGTGGCCTA-3' (+) strand) were incubated with nuclear protein extracts from Chinese hamster ovary cells (CHO) expressing human AGT in the absence (*lane 1*) or presence of increasing amounts of mechlorethamine (*lanes 2-6*). Botinylated DNA and AGT-DNA cross-links were captured using streptavidin sepharose high performance beads, washed with buffers containing SDS, urea, and NaCl to remove non-covalently bound proteins, and eluted *via* heating in SDS-PAGE loading buffer. The presence of AGT in the biotin capture fractions following DNA elution was detected by Western blot analysis using a monoclonal antibody against AGT.

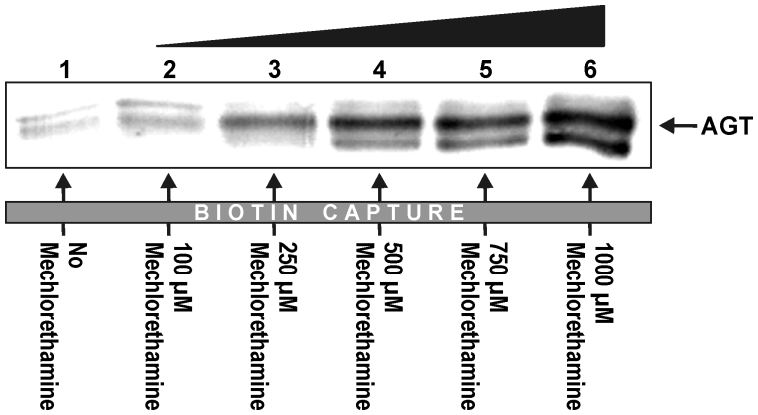

Figure 4.3 Mechlorethamine induces AGT-DNA cross-links in nuclear protein extracts derived from human cells with endogenous AGT expression. Biotinylated double-stranded oligodeoxynucleotides (5'-GGAGCTCGTGGCCTA-3' (+) strand) were incubated with nuclear protein extracts from human cervical carcinoma (HeLa) cells in the absence (*lane 1*) and presence of mechlorethamine (*lanes 2 and 3*). Botinylated DNA and AGT-DNA cross-links were captured using streptavidin sepharose high performance beads, washed with buffers containing SDS, urea, and NaCl to remove non-covalently bound proteins, and eluted *via* heating in SDS-PAGE loading buffer. The presence of AGT in the biotin capture fractions following DNA elution was detected by Western blot analysis using a monoclonal antibody against AGT. A known amount of nuclear extract was analyzed in parallel to determine relative cross-linking efficiency.

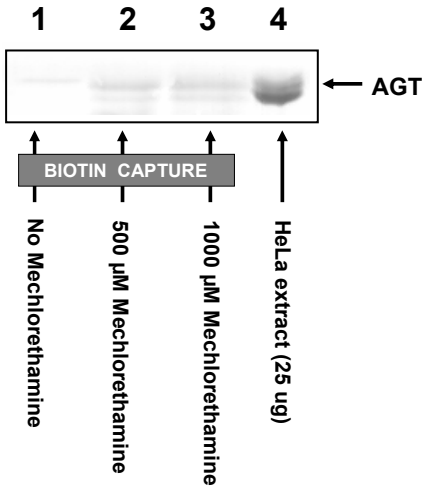

4.4.2 HPLC-ESI$^+$-MS/MS Analysis of Mechlorethamine-Induced AGT-DNA Cross-Links: Protein Identification

Identification of AGT-DNA cross-links by Western blot was further confirmed by mass spectrometry of tryptic digests (*Scheme 4.1*). Protein mixtures eluted from streptavidin beads were separated by SDS-PAGE (*Figure 4.4*), protein bands encompassing the entire molecular weight range were excised, and the resulting proteins were subjected to in-gel tryptic digestion. Upon HPLC-ESI$^+$-MS/MS analysis of peptides present in the biotin capture of the mechlorethamine-treated sample, three distinct AGT tryptic peptides were identified: F^{108}GEVISYQQLAALAGNPK^{125} (*Figure 4.5*), V^{148}VCSSGAVGNYSGGLAVK^{165}, and L^{176}GKPGLGGSSGLAGAWLK^{193}. In contrast, no AGT peptides were detected in the biotin capture from the control reaction lacking mechlorethamine (*Figure 4.4*). Although we were unable to observe the AGT tryptic peptides containing cysteines 145 and 150 or map the cross-linking site *via* MS/MS sequencing of peptides, we hypothesize that these two active site residues are responsible for cross-link formation based upon our previous work (*see Chapters II and III*).

4.4.3 Detection of DEB-Induced AGT-DNA Cross-Links by Western Blot Analysis

Like the nitrogen mustard mechlorethamine, DEB has been shown to induce AGT-DNA cross-links in the absence of other proteins *(37)*. To determine the ability of DEB to induce AGT-DNA cross-links in a more complex/biologically-relevant system, AGT- DNA cross-linking in the presence of other cellular proteins was examined by Western blotting (*Figure 4.6*). Incubation of CHO-AGT nuclear extract proteins with 5'-biotinylated double-stranded oligodeoxynucleotides in the presence of excess DEB

Figure 4.4 SDS-PAGE separation of mechlorethamine-induced DNA-protein cross-links following biotin capture. Biotinylated double-stranded oligodeoxynucleotides (5'-GGAGCTCGTGGCCTA-3' (+) strand) were incubated with CHO-AGT nuclear protein extracts in the presence of 0 (**A**) or 500 μM (**B**) mechlorethamine. Botinylated DNA and AGT-DNA cross-links were captured using streptavidin beads, washed with buffers containing SDS, urea, and NaCl to remove non-covalently bound proteins, and eluted by heating in SDS-PAGE loading buffer. Cross-linked proteins were resolved by SDS-PAGE, stained, and subjected to in-gel tryptic digest. The resulting peptides were analyzed by HPLC-ESI$^+$-MS/MS.

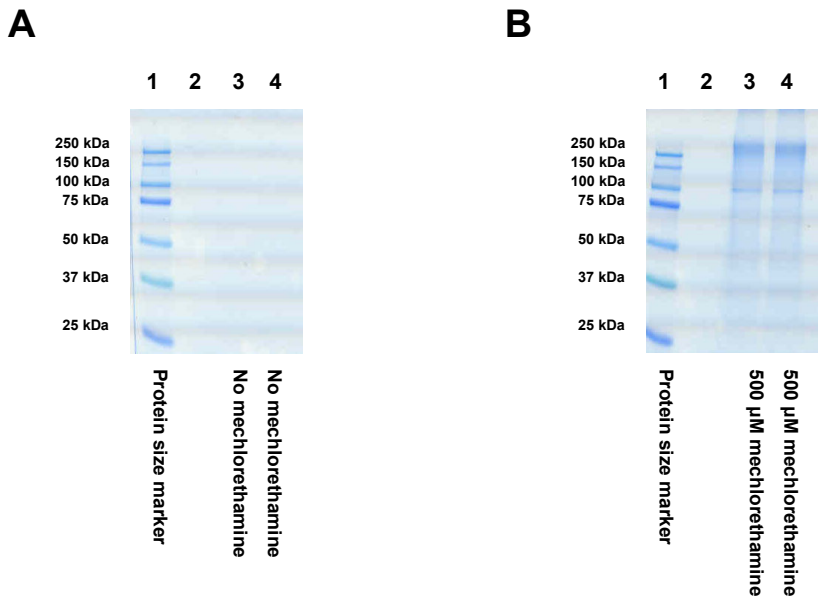

Figure 4.5 HPLC-ESI$^+$-MS/MS identification of AGT tryptic peptide F^{108}GEVISYQQLAALAGNPK^{125} resulting from biotin capture of mechlorethamine-induced AGT-DNA cross-links. Biotinylated double-stranded oligodeoxynucleotides (5'-GGAGCTCGTGGCCTA-3' (+) strand) were incubated with nuclear protein extracts from Chinese hamster ovary cells (CHO) expressing human AGT in the presence of 500 μM mechlorethamine. Botinylated DNA and AGT-DNA cross-links were captured using streptavidin beads, washed with buffers containing SDS, urea, and NaCl to remove non-covalently bound proteins, and eluted by heating in SDS-PAGE loading buffer. Cross-linked proteins were resolved by SDS-PAGE, subjected to in-gel tryptic digest, and the resulting peptides were analyzed by HPLC-ESI$^+$-MS/MS.

Seq	#	b	y	
F	1	148.1	1906.0	18
G	2	205.1	1758.9	17
E	3	**334.1**	1701.9	16
V	4	**433.2**	1572.9	15
I	5	**546.3**	**1473.8**	14
S	6	**633.3**	**1360.7**	13
Y	7	**796.4**	**1273.7**	12
Q	8	**924.4**	**1110.6**	11
Q	9	**1052.5**	**982.6**	10
L	10	**1165.6**	**854.5**	9
A	11	**1236.6**	**741.4**	8
A	12	**1307.7**	**670.4**	7
L	13	**1420.7**	**599.4**	6
A	14	**1491.8**	**486.3**	5
G	15	**1548.8**	**415.2**	4
N	16	**1662.8**	**358.2**	3
P	17	1759.9	244.2	2
K	18	1888.0	147.1	1

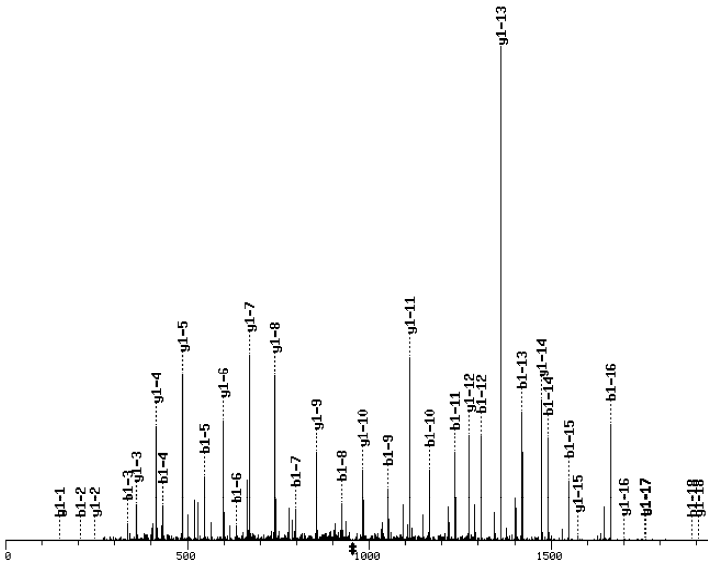

Figure 4.6 Detection of DEB-induced AGT-DNA cross-links by Western blot analysis. Biotinylated double-stranded oligodeoxynucleotides (5'-GGAGCTCGTGGCCTA-3' (+) strand) were incubated with nuclear protein extracts from Chinese hamster ovary cells (CHO) expressing human AGT in the absence (*lane 3*) or presence of increasing amounts of DEB (*lanes 4-6*). Botinylated DNA and AGT-DNA cross-links were captured using streptavidin beads, thoroughly washed to remove non-covalently bound proteins, and eluted *via* heating in SDS-PAGE loading buffer. The presence of AGT in the biotin capture fractions following DNA elution was detected using a monoclonal antibody against AGT.

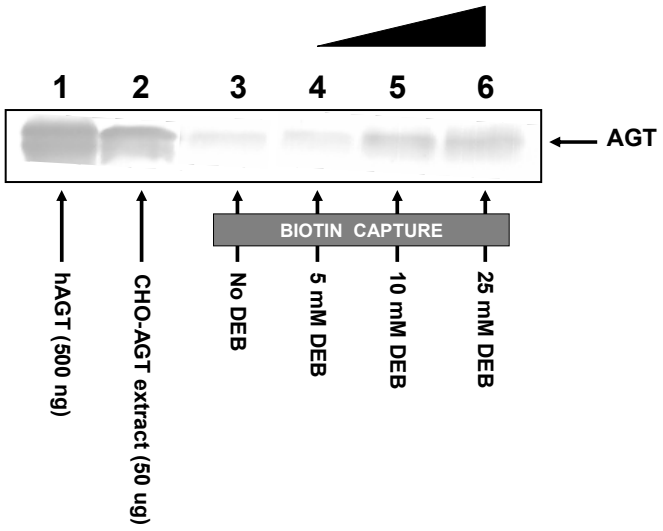

yielded detectable levels of AGT-DNA cross-links at the two highest concentrations (7-9%, *lanes 5 and 6*) with little to no cross-links observed in the sample exposed to 5 mM DEB and the untreated control (*lanes 4 and 3 respectively*).

4.5 Discussion

Cellular expression of AGT is fundamental for maintaining genomic integrity *(107)*. Encoded by the gene *MGMT*, AGT repairs alkyl lesions at the O^6 position of guanine and is responsible for protecting both tumor and normal cells from the damaging effects of alkylating agents *(106)*. While AGT is ubiquitously expressed in normal human tissues, increased levels of this important DNA repair protein have been observed in a variety of malignancies, including tumors of the colon, lung, breast, pancreas, brain, and blood *(131;187)*. As a result, expression of AGT can lead to drug resistance to alkylating agents used in cancer chemotherapy *(107)*.

While AGT is capable of protecting tumors from alkylating drugs which act upon the O^6 position of guanine (temozolomide, procarbazine, and BCNU) *(188;189)*, recent studies have shown that AGT expression can actually enhance the cytotoxic effects of *bis*-electrophiles, likely through the formation of AGT-DNA cross-links *(57)*.

Using a novel biotin/streptavidin enrichment strategy in combination with immunodetection and tandem mass spectrometry, AGT-DNA cross-linking in the presence of other cellular proteins was established. Upon incubation of 5'-biotinylated oligodeoxynucleotides with nuclear proteins from AGT-expressing CHO cells (in which AGT comprises ~ 0.5% of total protein), AGT-DNA cross-linking was detected using a commercially-available antibody. Early experiments indicated that AGT-DNA cross-

linking did occur in the presence of mechlorethamine (*Figure 4.1*), but cross-linking efficiency was lower than expected. Following optimization of the DNA elution step of the biotin capture assay (*Scheme 4.1*), Western blot analysis revealed the dose-dependent formation of AGT-DNA cross-links, with cross-linking increasing from 2 to 10% as the mechlorethamine concentration increased from 100-1000 uM (*Figure 4.2*). Similar results were obtained in HeLa nuclear extracts (*Figure 4.3*), a cell line with endogenous expression of AGT.

To further confirm the involvement of AGT in DNA-protein cross-linking by mechlorethamine, proteins recovered from biotin capture were separated by SDS-PAGE (*Figure 4.4*), subjected to in-gel tryptic digestion, and analyzed by HPLC-ESI$^+$-MS/MS. Through matching of the resulting MS/MS spectra to peptide sequences in both human and Chinese hamster protein databases using the SEQUEST algorithm, three peptides corresponding to human AGT were identified in mechlorethamine-treated samples (*Figure 4.5*), confirming the involvement of AGT in cross-linking.

Similar results were obtained upon Western blot analysis of DEB-induced AGT-DNA cross-links (*Figure 4.6*). While AGT-DNA cross-linking was evident at the highest two DEB concentrations tested, the amounts of DEB required to achieve comparable cross-linking efficiency to mechlorethamine were 25-fold greater (*Figure 4.2*), consistent with a lower reactivity of DEB towards cellular biomolecules.

Although these studies employed large excesses of mechlorethamine and DEB to afford levels of cross-linking detectable by Western blotting/HPLC-ESI$^+$-MS/MS, these results may still hold biological relevance as even small numbers of AGT-DNA cross-links can cause significant disruption to normal cellular processes. Every day a human

cell is riddled with DNA damage, including ~50,000 single-strand breaks, 10,000 depurination events, 2000 oxidative lesions, and 10 interstrand DNA-DNA cross-links *(190)*. Despite their low numbers, it is estimated that as few as 40 interstrand cross-links are sufficient to induce cell death by interfering with crucial cellular processes *(191)*. Similar to a DNA-DNA cross-link, the presence of a bulky AGT-DNA lesion would likely block the binding and progression of protein complexes involved in DNA replication and repair, transcription, recombination, and chromatin remodeling *(1)*. The formation of AGT-DNA cross-links could also result in decreased AGT activity due to sequestration of the protein. This could ultimately lead to greater susceptibility to alkylation damage by agents which alkylate the O^6 position of guanine, which could prove beneficial in the treatment of tumors with AGT-mediated drug resistance.

Based on the results of this work, we hypothesize that AGT-DNA cross-linking can contribute to the cytotoxic and mutagenic effects of *bis*-electrophiles. By demonstrating that mechlorethamine and DEB induce AGT-DNA cross-links in the presence of other nuclear proteins, we have provided further support for this hypothesis. Future studies will focus on the isolation and detection of AGT-DNA cross-links in intact cells (*see Chapter VIII*).

V. EFFECTS OF O^6-ALKYLGUANINE DNA ALKYLTRANSFERASE ON CYTOTOXICITY AND MUTAGENICITY OF *BIS*-ELECTROPHILES IN MAMMALIAN CELLS

5.1 Abstract

AGT is a DNA repair protein responsible for the removal of alkyl lesions from the O^6 position of guanine, restoring normal guanine and preventing mutagenesis. Ironically, AGT has also been shown to form cross-links to DNA in the presence of *bis*-electrophiles, including DBE, DEB, and antitumor nitrogen mustards, resulting in enhanced cytotoxicity and mutagenicity in bacterial cells expressing human AGT. To determine whether AGT expression in mammalian cells enhances the cytotoxic effects of *bis*-electrophiles, AGT-mediated toxicity and mutagenicity of mechlorethamine, chlorambucil, and DEB was examined in CHO cells expressing human AGT. Unlike previous results in *E. coli*, no differences in cytotoxicity of *bis*-electrophiles were observed between the cell line expressing AGT and the empty vector control cell line. There was also no significant difference in mutation frequency at the *hprt* locus following exposure to mechlorethamine in the presence and absence of O^6-benzylguanine, a potent inactivator of AGT. We conclude that AGT expression in CHO cells does not significantly alter the cytotoxic and mutagenic effects of *bis*-electrophiles.

5.2 Introduction

As discussed in *Chapter I*, the AGT protein is capable of reversing DNA damage caused by agents which alkylate the O^6 position of guanine *(101)*. Through the

stoichiometric transfer of the alkyl lesion to an active site cysteine residue (Cys^{145} in the human protein), guanine is restored and alkylated AGT is promptly degraded by the 26S proteosome *(110;118;192)*. Because numerous chemotherapeutic agents exert their antitumor effects through alkylation of guanine at the O^6 position, AGT expression in tumor cells has been linked to drug resistance *(106)*.

AGT affords protection against the damaging effects of drugs commonly used in cancer chemotherapy, including streptozotocin, temozolomide, procarbazine, dacarbazine, carmustine, and lomustine *(107)*. As numerous tumors possess increased levels of this repair protein, AGT-mediated drug resistance is yet another factor that needs to be considered prior to starting a treatment regimen. When given in combination with inhibitors of AGT (such as O^6-BG), the antitumor activity of the abovementioned alkylating agents is restored *(193)*.

While better known for its ability to protect cells from environmental toxins and chemotherapeutic agents, AGT expression in bacterial cells has been shown to paradoxically enhance the cytotoxic and mutagenic effects of *bis*-electrophiles *(153;154)*. Based upon *in vitro* data, this enhancement is attributed to the formation of covalent AGT-DNA cross-links involving active site cysteine residues and the N7 position of gunanine in duplex DNA *(37;38;57)*. In the present work, the effect of AGT expression on nitrogen mustard and DEB-mediated cytotoxicity and mutagenicity in Chinese hamster ovary cells was examined using clonogenic assays along with analysis of *hprt* mutants.

5.3 Materials and Methods

Cell Culture. CHO-AGT and CHO-EV cell lines were obtained from Dr. Anthony Pegg (Pennsylvania State University) and maintained as exponentially growing monolayer cultures in α-MEM supplemented with 9% FBS and G418 (1 mg/mL) in a humidified incubator at 37 ^{o}C with 5% CO_2 *(183)*.

Assay for Cell Survival. The effect of AGT expression on nitrogen mustard- and DEB-induced cytotoxicity was determined *via* clonogenic assay as previously described *(183)*. CHO-AGT and CHO-EV cells were plated in α-MEM containing 9% FBS and penicillin/streptomycin at a density of 500 cells/6 cm dish and allowed to adhere overnight. The following morning cultures (in triplicate) were exposed to *bis*-electrophile (0.2-1.0 μM mechlorethamine, 10-50 μM chlorambucil, and 10-50 μM DEB) or vehicle for 1 h at 37 ^{o}C. After replacing the media, the cultures were placed back at 37 ^{o}C for 8-10 days. Colonies were counted following staining with crystal violet, and colony-forming efficiency was expressed as a percentage of the number of cells surviving treatment with *bis*-electrophile relative to untreated controls.

Assay for Mutation Frequency. The effect of mechlorethamine on mutation frequency at the hypoxanthine guanine phosphoribosyltransferase (*hprt*) gene was determined *via* selection of $HPRT^-$ mutants *(183)*. To eliminate cells from the population which lacked HPRT expression, both CHO-AGT and CHO-EV stock cultures were grown in α-MEM containing hypoxanthine (100 μM), aminopterin (0.4 μM) and thymidine (16 μM) for 2 weeks prior to use *(194)*. Cells were plated (10^6 cells/10 cm dish) and treated with

mechlorethamine (0-0.5 μM) for 1 h at 37 ^{o}C in the presence and absence of O^6-benzylguanine (100 μM). Following replacement of the drug-containing α-MEM with fresh media supplemented with 9% FBS and penicillin/streptomycin, the cultures were placed at 37 ^{o}C overnight. The next day, cells were counted and plated (in triplicate) at a density of 500 cells/6 cm dish to determine cytotoxicity/cloning efficiency. The remaining cells were maintained as exponentially growing monolayers for an additional 7 days. Following trypsinization, 0.75 x 10^6 cells were plated onto 15 cm culture dishes (5 dishes/concentration) and cultured in α-MEM containing 9% FBS, penicillin/streptomycin, and 6-thioguanine (5 μg/mL). The cultures were placed in the 37 ^{o}C incubator for 10 days to allow for the formation of colonies. Mutation frequency was calculated as follows and expressed as the number of 6-thioguanine resistant colonies per 10^6 surviving cells:

cloning efficiency = colonies counted/total seeded cells

mutation frequency = total 6-TG resistant colonies/(total seeded cells)(cloning efficiency)

5.4 Results

5.4.1 Effect of AGT Expression on the Cytotoxicity of *Bis*-Electrophiles

Expression of human AGT in bacterial cells had previously been shown to enhance the cytotoxicity of numerous *bis*-electrophiles, including DBE and DEB *(154)*. The goal of this work was to determine whether a similar effect is observed in a mammalian system. Cytotoxicity mediated by mechlorethamine, chlorambucil, and DEB was assessed in Chinese hamster ovary cells expressing human recombinant AGT or in control cells transfected with an empty vector (*Figure 5.1*). As described below, no

Figure 5.1 Effect of AGT expression on the cytotoxicity induced by mechlorethamine (**A**), chlorambucil (**B**), and DEB (**C**). CHO-AGT (*blue*) or CHO-EV (*pink*) cells (500 cells/dish) were treated in triplicate with mechlorethamine (0-1.0 μM), chlorambucil (0-50 μM), or DEB (0-50 μM) for 1 h. The plots contain data obtained from three separate experiments.

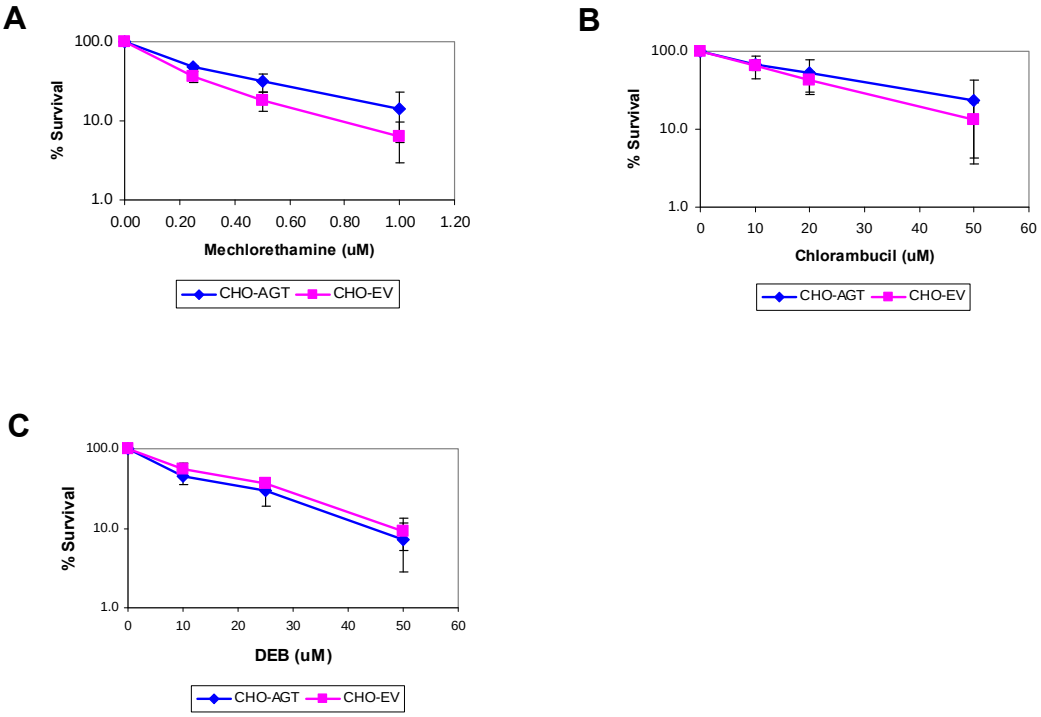

significant difference in cell viability was observed between the two cell lines, suggesting that AGT expression does not significantly influence the cytotoxicity of *bis*-electrophiles in a mammalian cell system.

5.4.2 Effect of AGT Expression on Mutation Frequency at the *hprt* Locus

We next investigated mutagenic effects of nitrogen mustards in CHO-AGT and CHO-EV cell lines using endogenous hypoxanthine phosphoribosyltransferase (*hprt*) gene as a target *(195)*. The gene product of *hprt*, HPRT, is a phosphoribose transferase enzyme involved in the purine salvage pathway for nucleotide biosynthesis. 6-Thioguanine (6-TG) – a cytostatic antimetabolite commonly used in the treatment of myelogenous leukemia – is bioactivated by HPRT to the corresponding ribonucleotide mono-, di-, and triphosphate derivatives, which are incorporated into the DNA and RNA resulting in toxicity *(196)*. The monophosphate metabolite of 6-TG inhibits several enzymes involved in purine biosynthesis, including PRPP amidotransferase, IMP dehydrogenase, and ATP:GMP phosphotransferase. *hprt* gene mutations render the gene product non-functional, resulting in a loss of 6-TG activation and leading to drug resistance/cell survival. In this assay, we examined the spontaneous and mechlorethamine-induced *hprt* mutation frequencies in CHO cells by assessing cell survival in the presence of 6-TG.

To reduce background levels of spontaneous mutations in the CHO cell lines, cultures were maintained in HAT-containing media (hypoxanthine-aminopterin-thymidine) for 2 weeks prior to experimental use. Mechanistically, aminopterin blocks DNA synthesis by inhibiting dihydrofolate reductase *(197)*. However, cells that possess

HPRT and thymidine kinase can bypass this inhibition *via* utilization of the purine salvage pathway in the presence of hypoxanthine and thymidine *(196)*. Thus, HAT pre-treatment eliminates the cells which lack *hprt* expression from the population *(194)*.

The effect of AGT on mechlorethamine-induced mutagenicity in the *hprt* gene was first examined by comparison of CHO cells over-expressing human AGT and the corresponding controls transfected with an empty vector (*Figure 5.2*). While no significant difference was observed in terms of cytotoxicity at the drug concentrations tested (*panel A*), the *hprt* mutation frequency observed in the CHO-AGT cell line was 2 to 3-fold higher than that in the CHO-EV cell line (*panel B*). Despite this small difference, it is possible that other factors such as genetic differences between the two cell lines may have been contributing to the observed effect.

To address this potential problem, a second experiment was performed in which mechlorethamine-induced mutagenicity was examined in AGT-expressing CHO cells in the presence and in the absence of AGT inhibitor O^6-BG. As O^6-BG is a potent inactivator of AGT, any contribution that this repair protein has towards mechlorethamine-mediated cytotoxicity/mutagenicity should be negated in the presence of O^6-BG. As shown in *Figure 5.3*, treatment with O^6-BG resulted in a negligible difference in cytotoxicity (*panel A*). Interestingly, the number of mechlorethamine-induced mutants detected in the O^6-BG-treated cells was greater than in the untreated cells, suggesting that AGT has a protective effect against mechlorethamine-mediated DNA damage in this cell system (*panel B*).

Figure 5.2 Effect of AGT expression on the cytotoxicity and mutagenicity induced by mechlorethamine. CHO-AGT (*blue*) or CHO-EV (*red*) cells were treated with mechlorethamine (0-0.5 μM) for 1 h at 37 °C. Mechlorethamine-induced cytotoxicity (**A**) was comparable between the two cell lines while the number of *hprt* mutants was slightly higher in the AGT-expressing cell line (**B**).

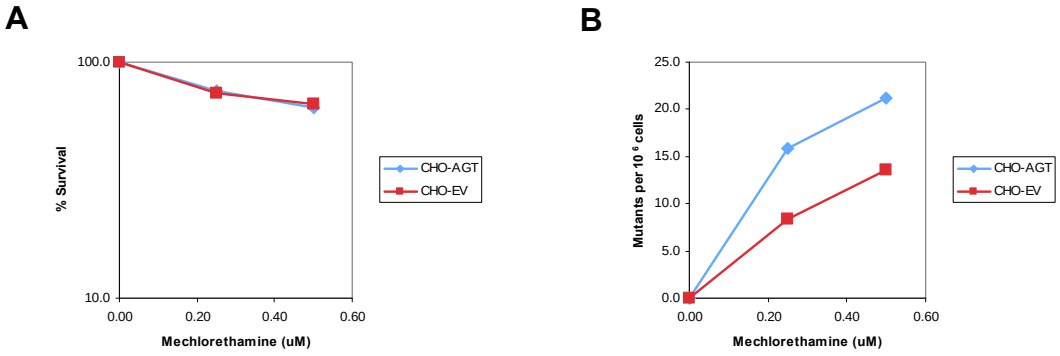

Figure 5.3 Effect of AGT activity on the cytotoxicity and mutagenicity induced by mechlorethamine. CHO-AGT cells were treated with mechlorethamine (0-0.5 μM) for 1 h at 37 ^{o}C in the presence (*green*) and absence (*violet*) of O^6-BG. Mechlorethamine-induced cytotoxicity (**A**) and mutation frequency (**B**) was seemingly unaffected by AGT inhibition.

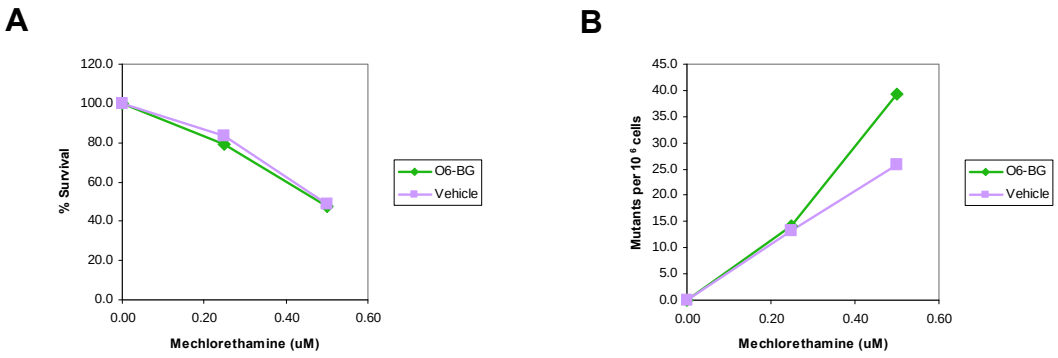

5.5 Discussion

Due to the overexpression of AGT in many tumor types, AGT-mediated drug resistance must be considered when pursuing chemotherapy with alkylating agents. Numerous studies have demonstrated AGT's protective effects against DNA methylating and chloroethylating agents including procarbazine, dacarbazine, streptozotocin, temozolomide, carmustine, and lomustine *(107)*. Because these agents selectively alkylate the O^6 position of guanine, the resulting lesions are substrates for direct repair by AGT. Could AGT expression influence the efficacy of other clinically-useful alkylating drugs that do not specifically target the O^6 position of guanine?

In one study, the role of AGT in protecting against the genotoxic effects of several alkylating agents employed in cancer chemotherapy (streptozotocin, carmustine, lomustine, nimustine, elmustine, chlorambucil, melphalan, cyclophosphamide, ifosfamide, cis- and transplatin) was examined by comparing the cytotoxicity and recombination potency in CHO and HeLa cells *(179)*. While cells expressing AGT were resistant to streptozotocin and the nitrosoureas, the presence of AGT did not effect cytotoxicity of other drugs. Likewise, AGT afforded protection against sister-chromatid exchange following treatment with nitrosoureas tested. No AGT-mediated protection from sister-chromatid exchange was observed with the other drugs with the exception of cis- and transplatin. Because the protective effect observed with the platinum compounds was abolished *via* treatment with O^6-benzyguanine, this suggests that some cis- and trasplatin-induced lesions may be substrates for AGT repair.

The ability of AGT to protect CHO cells from the cytotoxic and mutagenic effects of cyclophosphamide has also been reported *(177)*. Following treatment of CHO cells

with 4-hydroperoxycyclophosphamide (an activated derivative of cyclophosphamide), AGT-expressing cells were 7-fold less sensitive in terms of cytotoxicity and displayed a 4-fold lower mutation frequency in the *hprt* locus. In contrast, cells treated with phosphoramide mustard displayed similar survival curves and exhibited no difference in mutation frequency. This suggests that the contribution of AGT activity in protecting against the genotoxic effects of cyclophosphamide is due to solely to the effects of acrolein, a reactive metabolite of cyclophosphamide. Later studies in CHO cells confirmed that AGT expression protects against acrolein-induced cytotoxicity and that AGT is not simply acting as a "molecular scavenger" since DNA binding is required for the repair of acrolein adducts *(178)*. While AGT expression resulted in obvious protection against the cytotoxic effects of cyclophosphamide in cell culture, no difference was observed *in vivo* using AGT knock-out mice *(198;199)*.

In contrast to previous reports of increased cytotoxicity and mutagenicity of *bis*-electrophiles in bacterial systems expressing AGT *(153;154)*, we found that AGT expression in CHO cells has little to no effect on the cytotoxicity and mutagenicity of DEB and nitrogen mustards.

VI. IDENTIFICATION OF ADDITIONAL CELLULAR PROTEINS THAT CROSS-LINK DNA IN THE PRESENCE OF *BIS*-ELECROPHILES

6.1 Abstract

Nitrogen mustard drugs are a class of antitumor agents used clinically for the treatment of a variety of neoplastic conditions. The biological activity of these compounds is attributed to their ability to induce DNA-DNA cross-links and DPCs by consecutive alkylation of two nucleophilic sites within cellular biomolecules. However, DPC formation by nitrogen mustards is not well characterized because of its inherent structural complexity and the insufficient specificity and sensitivity of previous methodologies. In the present work, we employed affinity capture in combination with mass spectrometry-based proteomics to identify mammalian proteins that form covalent cross-links to DNA in the presence of mechlorethamine. Following incubation of biotinylated DNA duplexes with nuclear protein extracts from CHO and HeLa cells, DPCs were isolated *via* affinity capture on streptavidine beads, and the cross-linked proteins were identified *via* HPLC-ESI$^+$-MS/MS analysis of tryptic peptides. We found that mechlorethamine treatment resulted in the formation of DPC lesions with multiple proteins encompassing a broad range of cellular functions including chromatin regulation, DNA replication and repair, cell cycle control, transcription regulation, and architectural/structural roles. Western blot analysis using commercial antibodies against specific protein targets was employed to confirm protein identities and to quantify the extent of drug-mediated DNA-protein cross-linking. The structures of mechlorethamine-induced cross-links were elucidated by mass spectrometry of amino acid-nucleobase

conjugates. The DPCs were shown to form *via* alkylation of the N7 position of guanine in duplex DNA and cysteine thiols within the identified proteins. Despite its affinity for DNA, histone H4 did not participate in nitrogen mustard-mediated cross-linking *in vitro*. Because the formation of DPCs interferes with crucial cellular processes such as DNA replication and transcription, our findings suggest that DPC formation is likely to contribute to the cytotoxicity and antitumor activity of nitrogen mustards in mammalian cells.

6.2 Introduction

DPCs are conjugates formed upon covalent modification of DNA and proteins by *bis*-electrophiles *(1)*. DPCs form following cellular exposure to a wide variety of cytotoxic, mutagenic, and carcinogenic agents, including ionizing radiation *(11)*, metals and metalloids *(1)*, endogenous and exogenous aldehydes *(19)*, and chemotherapeutic drugs *(36;100)*. The half-lives of DPCs *in vivo* range from hours to days, depending on their chemical stability and their ability to be recognized by repair proteins *(1)*. Because of the propensity of DPCs to persist within a cell, they could play an important role in the antitumor activity of DNA-alkylating drugs used in cancer chemotherapy as well as in spontaneous mutagenesis, cytotoxicity, and aging.

Due to their inherent complexity, DPCs have received far less attention compared to other types of DNA damage, and their biological consequences are not well understood. Due to the bulky nature of these helix-distorting lesions, DPCs are expected to block the binding and progression of protein complexes involved in crucial cellular processes, including replication, transcription, DNA repair, recombination, and chromatin

remodeling *(1)*. If not repaired, DPCs are likely to contribute to the cytotoxic and mutagenic effects of *bis*-electrophiles, such as antitumor nitrosoureas, cisplatin, and nitrogen mustards.

Nitrogen mustards comprise a class of bifunctional alkylating agents used clinically in the treatment of a wide variety of cancers *(170)*. Drugs of this class (including mechlorethamine, chlorambucil, and melphalan) contain two reactive chloroethyl groups, allowing for sequential alkylation of two nucleophilic sites within biomolecules. As shown in *Scheme 6.1*, the high reactivity of these compounds is due to the formation of positively-charged aziridinium ions, which react readily with amino and sulfhydryl groups in DNA and proteins to form both monoadducts and cross-linked lesions *(170)*. Historically, the antitumor activity of these drugs has been attributed to their ability to form DNA-DNA cross-links *(85;171)*. However, they can also form bulky DNA-protein conjugates potentially contributing to their target and off-target cytotoxicity.

As described in *Chapter III*, we previously employed a mass spectrometry-based approach to demonstrate that human recombinant AGT is readily cross-linked to DNA in the presence of two representative nitrogen mustards, mechlorethamine and chlorambucil *(38)*. Mass spectrometric analyses of tryptic peptides revealed thatthe cross-linking sites included two active site residues, Cys^{145} and Cys^{150}. Western blot analysis revealed that AGT-DNA cross-linking was concentration-dependent and occurred in the presence of other cellular proteins *(38)*.We hypothesized that DNA-binding proteins other than AGT can participate in DPC formation in the presence of nitrogen mustards. In the present work, we employed affinity capture methodology coupled with shotgun proteomics

Scheme 6.1 Formation of DNA-protein cross-links by nitrogen mustards

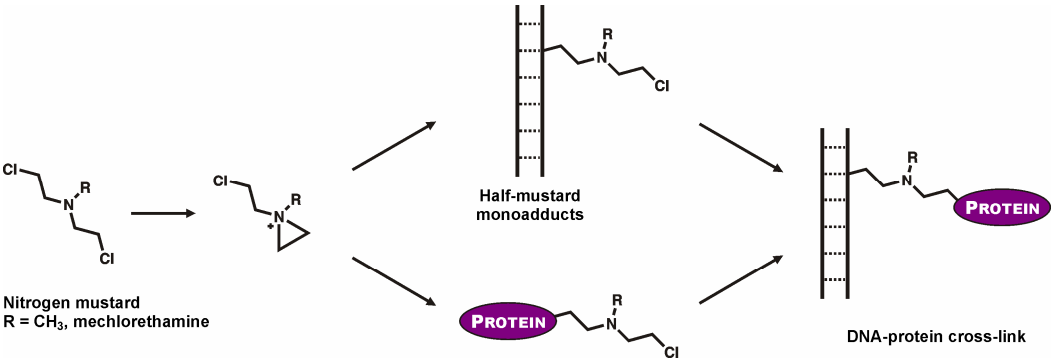

and Western blot analysis to identify mammalian nuclear proteins that form covalent cross-links to DNA in the presence of mechlorethamine. Mechlorethamine-induced DPCs were then shown to involve the N7 position of guanine in DNA and the side chain sulfhydryls of cysteine residues within the identified proteins.

6.3 Materials and Methods

Cell Culture. Chinese hamster ovary (CHO) cells expressing human recombinant AGT were generously provided by Dr. Anthony E. Pegg (Pennsylvania State University) and maintained as exponentially growing monolayer cultures in α-MEM supplemented with 9% FBS and G418 (1 mg/mL) in a humidified incubator at 37 ^{o}C with 5% CO_2 *(183)*. HeLa cells were a generous gift from Dr. Jonathan Marchand (University of Minnesota). The cells were maintained as exponentially growing monolayer cultures in DMEM supplemented with 9% FBS in a humidified incubator at 37°C with 5% CO_2.

Preparation of Nuclear Extracts. Nuclear protein extracts were prepared as described previously *(184)*. Briefly, ~ 10^8 cells were harvested, washed with phosphate-buffered saline, and suspended in hypotonic buffer (10 mM TRIS-HCl - pH 7.4/10 mM $MgCl_2$/10 mM KCl/1 mM dithiothreitol). Phenylmethylsulfonyl fluoride was added (1 mM), and the cells were broken by 20 strokes in a Dounce homogenizer. The resulting mixture was centrifuged at 2,600 rpm for 8 min, and the pelleted nuclei were resuspended in hypotonic buffer containing 350 mM NaCl. Following the addition of protease inhibitors (pepstatin, leupeptin, aprotinin, and phenylmethylsulfonyl fluoride), the nuclei were incubated at 0 ^{o}C for 1 h. The extracted nuclei were centrifuged at 70,000 rpm at 4 °C for

30 min, and the nuclear proteins were isolated from the clear supernatant. Extracts were dialyzed overnight at 4 ^{o}C against 10 mM TRIS-HCl (pH 7.4) using Slide-A-Lyzer dialysis cassettes from Pierce Biotechnology (3.5 kDa molecular weight cut-off, Rockford, IL). Protein concentrations were determined *via* a colorimetric assay *(185)*.

DNA-Protein Cross-Linking and Biotin Capture. 5'-Biotinylated double-stranded oligodeoxynucleotides (5'-GGA GCT CGT GGC CTA-3' (+) strand, 3.12 nmol) were combined with CHO-AGT or HeLa nuclear extracts (500 μg total protein) in 10 mM TRIS-HCl – pH 7.4 in the absence or in the presence of mechlorethamine (0–1000 μM, 1 mL total volume) at 37 ^{o}C for 3 h to induce cross-linking. To select for proteins covalently bound to the biotinylated oligodeoxynucleotides, Streptavidin Sepharose High Performance beads (GE Healthcare, Piscataway, NJ) were used to capture the biotinylated DNA along with any DPCs. To remove non-covalently bound proteins, the beads were washed with 1% SDS, 4 M urea, and 1 M NaCl. Biotinylated DNA was released from the beads by heating in the presence of 4X SDS-PAGE loading buffer (90 ^{o}C for 15 min). Cross-linked proteins were analyzed by HPLC-ESI^{+}-MS/MS and Western blotting as described below.

Protein Identification by Mass Spectrometry. Cross-linking reactions were performed as described above. Following elution from the beads, DPCs were separated by 10% SDS-PAGE. The gels were stained with SimplyBlue SafeStain (Invitrogen, Carlsbad, CA) to visualize proteins. Gel lanes were cut into 5 slices encompassing the entire molecular weight range, then further into 1 mm pieces prior to washing with 100 mM ammonium bicarbonate. Each fraction was subjected to reduction with DTT and alkylation with

iodoacetaminde as described previously *(186)*. To initiate proteolytic digestion, gel pieces were dehydrated with acetonitrile, dried under vacuum, and reconstituted in 25 mM ammonium bicarbonate containing 10 μg proteomics grade trypsin (Trypsin Gold – Promega, Madison, WI). The samples were digested overnight at 37 ^{o}C. Tryptic peptides were extracted from the gel pieces using 0.1% aqueous formic acid/60% acetonitrile, evaporated to dryness, and resuspended in 0.1% aqueous formic acid prior to analysis. All analyses were performed on a Thermo LTQ linear ion trap MS system equipped with a Thermo Surveyor solvent delivery system and a microelectrospray source. Peptides were resolved on a 100 μm x 11 cm fused silica capillary column packed with 5 μm, 300 Å Jupiter C18 (Phenomenex, Torrence, CA) eluted at 0.6 μL/min with 0.1 formic acid in water (A) and 0.1% formic acid in acetonitrile (B). The column temperature was maintained at 25 ^{o}C. Solvent composition was held at 2% B for the first 15 min, followed by a linear increase to 25% B over the next 35 min and further to 90% B in the next 15 min where it was held constant for the remaining 10 min. MS/MS spectra of peptides were acquired using data-dependent scanning, in which a single full MS spectrum (400-2000 *m/z*) was followed by four MS/MS spectra. Spectra were recorded using dynamic exclusion of previously analyzed precursors for 60 s. The MS/MS spectra were searched against human and *Cricetulus griseus* (Chinese hamster) database sequences using the SEQUEST algorithm *(60)*. *S*-Carboxamidomethylation at cysteine (+57 Da), oxidation of methionine (+16 Da), and mechlorethamine-induced alkylation at cysteine (hydrolyzed monoadduct: +102 Da, guanine cross-link: +234 Da) were specified as dynamic modifications to identify spectra of adducted peptides. Parsimony analysis of the MS/MS

data was performed to derive a minimal protein list, thus enhancing the confidence levels of protein identification *(200)*.

Western Blot Analysis of Identified Proteins. Primary polyclonal antibodies to mammalian actin, nucleolin, poly (ADP-ribose) polymerase (PARP), DNA-(apurinic or apyrimidinic site) lyase (Ref-1), glyceraldehyde-3-phosphate dehydrogenase (GAPDH), and elongation factor 1-alpha 1 (EF-1α1) were obtained from Santa Cruz Biotechnology (SantaCruz, CA). The primary polyclonal antibody to the ATP-dependent DNA helicase subunit 2 (Ku) and the monoclonal antibody against X-ray repair cross-complementary protein 1 (XRCC1) were purchased from Lab Vision/NeoMarkers (Fremont, CA). Alkaline phosphatase-conjugated anti-mouse and anti-rabbit IgG secondary antibodies were purchased from Sigma (St. Louis, MO). CHO and HeLa nuclear extracts were exposed to 0-1000 μM mechlorethamine in the presence of the biotinylated oligonucleotide to induce cross-linking as described above. Following biotin capture, the DNA-protein cross-links were separated by 10 or 12% SDS-PAGE. Proteins were transferred to nitrocellulose membranes (Bio-Rad, Hercules, CA) and immediately blocked in Tris-buffered saline containing 5% bovine serum albumin. Following a 2 h incubation with primary antibody at room temperature, the blots were washed 3 times with Tris-buffered saline and incubated with the corresponding secondary antibody (1-2 h at room temperature or 4 ^{o}C overnight). After washing with Tris-buffered saline to remove unbound antibodies, the blots were developed with SIGMA Fast BCIP/NBT (Bio-Rad, Hercules, CA). The developed blots were scanned as image files, and the optical densities of the bands in the resulting image files were quantified using the

ImageJ software/shareware available free of charge from the NIH (www.ncbi.nlm.nih.gov). The extent of cross-linking for each protein was estimated by comparing the band intensities of cross-linked samples to that present in a known amount of nuclear extract.

HPLC-ESI$^+$-MS/MS Analysis of a Mechlorethamine-Induced Cysteine-Guanine Cross-Link. Double-stranded oligodeoxynucleotides (5'-GGA GCT CGT GGC CTA-3' (+) strand, 9.36 nmol) were incubated with HeLa nuclear extracts (1.5 mg total protein) in 10 mM TRIS-HCl – pH 7.4 in the presence and absence of mechlorethamine (0 or 1000 μM, 1 mL total volume) for 3 h at 37 ^{o}C to induce cross-linking. The samples were heated to 80 ^{o}C for 30 min to release N7 alkylguanine lesions from the DNA backbone, followed by complete proteolytic digestion with trypsin, carboxypeptidase Y, and proteinase K. The resulting mixtures were purified by HPLC to selectively enrich for Cys-N7G-EMA using an Agilent Technologies HPLC system (1100 model) incorporating a variable wavelength UV detector and a semi-micro UV cell. A Supelcosil LC-18-DB column (4.6 mm x 250 mm, 5 μm) was eluted with 20 mM ammonium acetate, pH 4.9 (A) and acetonitrile (B) at a flow rate of 1 mL/min. The gradient program began at 0% B, followed by a linear increase to 24% B in 24 min, and further to 60% B in 6 min. Under these conditions, Cys-N7G-EMA eluted as a sharp peak at ~9 min. For the purification of HeLa total digest samples, fractions corresponding to the elution time of Cys-N7G-EMA (8-10 min) were collected, dried in a speed-vac concentrator, and reconstituted in buffer A prior to HPLC-ESI$^+$-MS/MS analysis.

A Waters nanoAQUITY UPLC system interfaced to a Thermo-Finnigan TSQ Quantum Ultra mass spectrometer was used for the detection of Cys-N7G-EMA in HeLa total digests. Chromatographic separation was achieved using a Phenomenex Synergi C18 column (250 mm x 0.5 mm, 4 μm) eluted with15 mM ammonium acetate, pH 5.0 (A) and methanol (B) at a flow rate of 12 μL/min. Employing a linear gradient of 2-14% B over the course of 15 min, Cys-N7G-EMA eluted as a broad peak at ~10 min. ESI^+ was achieved at a spray voltage of 3.2 kV and a capillary temperature of 250 ^oC. CID was performed with Ar as a collision gas (1.0 mTorr) and a collision energy of 18 V. The mass spectrometer parameters were optimized for maximum response during infusion of a standard solution of Cys-N7G-EMA. Analyses were performed in the selected reaction monitoring (SRM) mode corresponding to the neutral loss of guanine from protonated molecules of Cys-N7G-EMA (*m/z* 356.1 → 205.1).

Detection of Nitrogen Mustard-Induced DPCs Involving Histone H4 by Denaturing PAGE. DNA 18-mer, 5'-GGA GCT GGT GGC GTA GGC-3' (200 pmol), was 5'-end labeled with ^{32}P in the presence of [γ-^{32}P]ATP/T4 polynucleotide kinase. The resulting [γ-^{32}P] 5'-end labeled oligodeoxynucleotide was purified by 12% denaturing PAGE and desalted by SPE using Waters SepPak C18 cartridges. Following spiking with the corresponding unlabeled DNA (12 nmol), the radiolabeled (+) strand was annealed to its complimentary strand (12.2 nmol) and dissolved in buffer containing 50 mM TRIS - pH 7.6, and 0.1 mM EDTA. The ^{32}P-labeled duplex (0.93 nmol) was incubated with bovine histone H4 (2.0 μg, 0.177 nmol) in the presence of 50, 100, and 200 molar equivalents of mechlorethamine or chlorambucil (8.9, 17.7, and 35.4 nmol respectively). Following a 3

h incubation at 37 °C, the reaction mixtures were separated by 12% SDS-PAGE and the radiolabeled products were visualized using a Bio-Rad Molecular Imager FX.

Treatment of Histone H4 with the Guanine Half-Mustards of Chlorambucil and Mechlorethamine. Calf thymus histone H4 (30 μg, 2.7 nmol) was reacted with 50 molar equivalents of N7G-PBA-Cl or N7G-EMA-Cl (133.5 nmol) in 10 mM Tris-HCl buffer (pH 7.2) at 37 °C for 48 h. Following incubation, aliquots from each reaction mixture were set aside for HPLC-ESI^+-MS analysis of the intact protein. The remaining alkylated protein (~24 μg) was dried, reconstituted in 100 mM ammonium bicarbonate buffer (pH 7.9), and trypsin (3 μg) was added to initiate digestion. The resulting solutions were incubated at 37 ^oC for 24 h. Once dried, the tryptic peptides were reconstituted in 0.5% formic acid/0.01% TFA in water and subjected to HPLC-ESI^+-MS/MS analysis. Total digestion of guanine half mustard-treated histone H4 to amino acids was performed to look for half mustard-induced amino acid-guanine conjugates. Histone H4 tryptic peptides (from ~20 μg protein) were dried, resuspended in water, filtered through Microcon YM-10 membrane filters to remove trypsin, and carboxypeptidase Y (1 μg) and proteinase K (1 μg) were added to the filtrate to initiate digestion. The samples were incubated at room temperature for 24 h. Prior to HPLC-ESI^+-MS/MS analysis, the samples were dried and reconstituted in 15 mM ammonium acetate buffer, pH 5.0.

Mass Spectrometric Analysis of Alkylated Histone H4. Analysis of half mustard-treated histone H4 was performed using an Agilent 1100 capillary HPLC-ion trap MS system employing similar methods to those used for the analysis of modified hAGT as described in *Chapter III*.

Preparation of HeLa Whole Cell Extract. Confluent cultures of HeLa cells (~ 5 x 10^6 cells) were harvested, washed with phosphate-buffered saline, and suspended in 2 mL cell lysis buffer containing 20 mM TRIS – pH 7.8/50 mM KCl/0.2% NP-40/1 mM phenylmethylsulfonyl fluoride/1 μg/mL leupeptin/1 μg/mL pepstatin/5% glycerol. The cell suspension was sonicated three times (15 sec/each) on ice. The resulting solution was then centrifuged at 10,000 x *g* for 15 min at 4 ^{o}C. The protein concentration of supernatant was determined *via* colormetric assay *(185)*.

Western Blot Analysis of DPCs Involving Histone H4: Whole Cell Lysates. 5'-Biotinylated double-stranded oligodeoxynucleotides (5'-GGA GCT CGT GGC CTA-3' (+) strand, 3.12 nmol) were combined with HeLa whole cell extract (500 μg total protein) in 10 mM TRIS-HCl – pH 7.4 in the absence and presence of mechlorethamine (0, 500, and 1000 μM – 1 mL total volume). The reaction mixtures were incubated at 37 ^{o}C for 3 h to induce cross-linking. To select for proteins covalently bound to the biotinylated oligodeoxynucleotides, streptavidin beads were used to capture the biotinylated DNA/DPCs. To remove non-covalently bound proteins, the beads were washed with 1% SDS, 4 M urea, and 1 M NaCl. Biotinylated DNA was released from the beads by heating in the presence of 4X SDS-PAGE loading buffer (90 ^{o}C for 15 min). Protein mixtures were separated by 15% SDS-PAGE prior to Western blot analysis using the primary polyclonal antibody to histone H4 (Millipore, Temecula, CA). Human recombinant histone H4 (Millipore) served as a positive control.

6.4 Results

6.4.1 Mass Spectrometric Identification of Cross-Linked Proteins

We employed an affinity-based approach to capture proteins that form cross-links to DNA in the presence of mechlorethamine (*Scheme 6.2*). Nuclear protein extracts from transgenic CHO cells expressing human recombinant AGT protein or from human cervical carcinoma (HeLa) cells were incubated with synthetic DNA duplexes containing a 5'-biotin tag [5'-GGAGCTGGTGGCGTAGGC-3', (+) strand] in the presence or in the absence of mechlorethamine. Streptavidin beads were then used to capture biotinylated DNA along with any DPCs. Following stringent washing procedures to remove any non-covalently bound proteins, DNA-protein cross-links were eluted *via* heating in a gel loading buffer and separated by SDS-PAGE. Analysis of proteins captured following exposure to 0, 250, 500, 750, or 1000 μM mechlorethamine revealed a concentration dependent formation of mechlorethamine-induced cross-links in both CHO and HeLa nuclear extracts (*Figure 6.1, panels A and B respectively*). To identify cross-linked proteins, subsequent experiments were performed in triplicate by treating CHO and HeLa nuclear extracts with 0 or 500 μM of mechlorethamine in the presence of biotinylated DNA. Following biotin capture, the resulting DPCs were separated by SDS-PAGE and stained with SimplyBlue. Gel bands encompassing the entire molecular weight range were excised for identification of cross-linked proteins by mass spectrometry (*Figures 6.2 and 6.3*). As shown in *panel A* of *Figure 6.2* and *Figure 6.3*, little to no protein was

Scheme 6.2 Detection of DNA-protein cross-links in nuclear protein extracts: Biotin capture enrichment

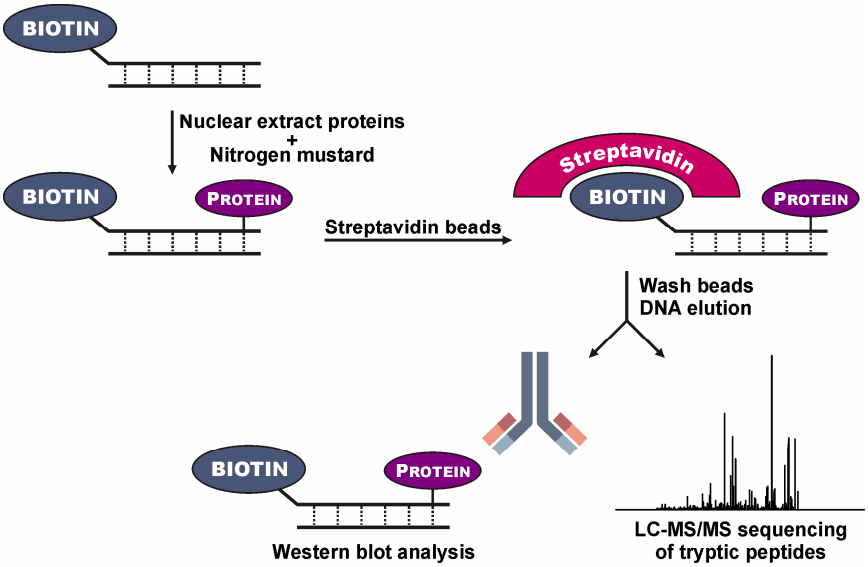

Figure 6.1 Concentration-dependent formation of DNA-protein cross-links in CHO (**A**) and HeLa (**B**) nuclear extracts following exposure to mechlorethamine. Nuclear extract proteins and 5'-biotinylated double-stranded oligodeoxynucleotides were incubated with 0-1000 μM mechlorethamine (lanes 3-8), subjected to biotin capture enrichment, and resolved by 10% SDS-PAGE. The gels were stained with SimplyBlue SafeStain to visualize cross-linked proteins.

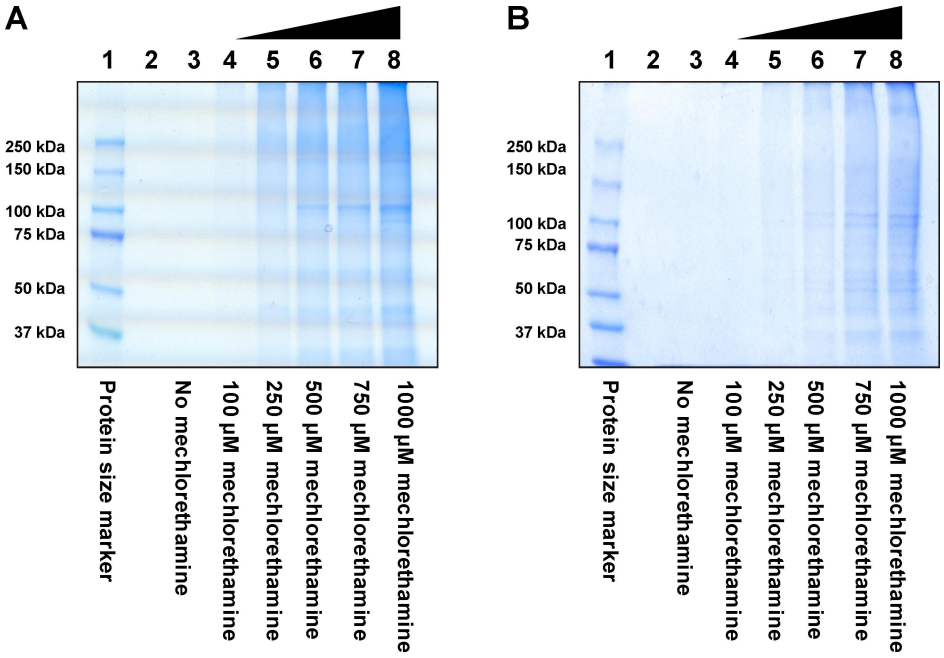

Figure 6.2 SDS-PAGE analysis of mechlorethamine-induced DNA-protein cross-links in CHO nuclear extracts. CHO nuclear extract proteins and 5'-biotinylated double-stranded oligodeoxynucleotides were incubated in triplicate with 0 (**A**) or 500 μM (**B**) mechlorethamine. Following biotin capture enrichment, cross-linked proteins were resolved by 10% SDS-PAGE and visualized with SimplyBlue SafeStain. Each lane was cut into 5 sections, and the proteins present in each piece were subjected to in-gel tryptic digestion prior to HPLC-ESI$^+$-MS/MS analysis.

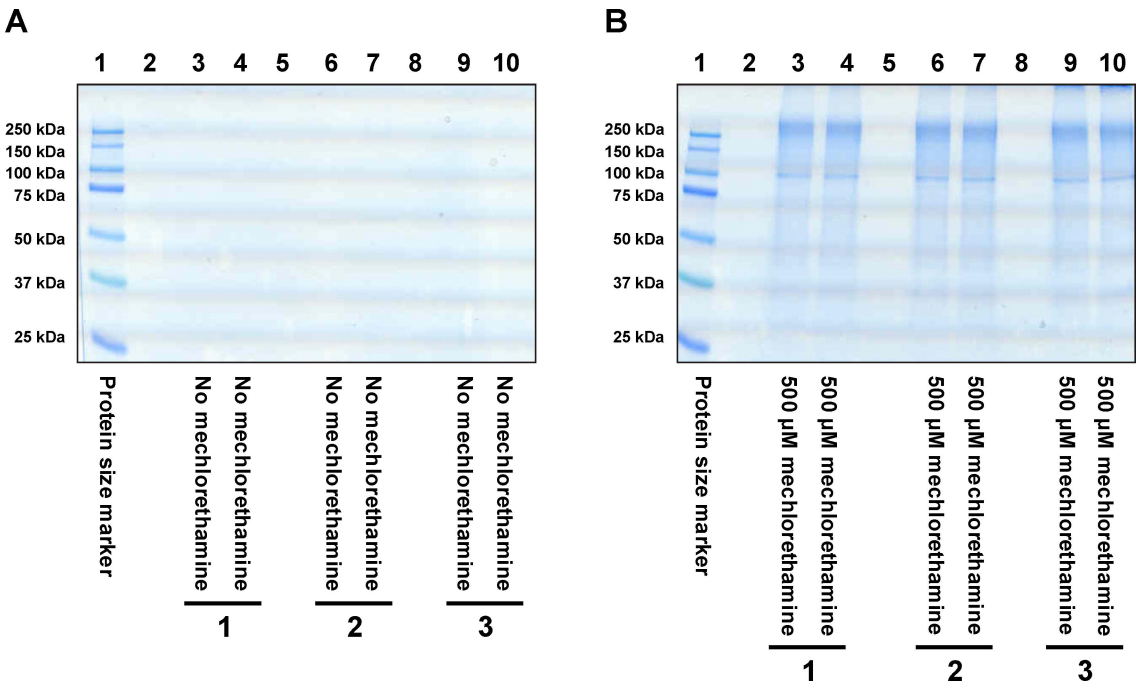

Figure 6.3 SDS-PAGE analysis of mechlorethamine-induced DNA-protein cross-links in HeLa nuclear protein extracts. Nuclear extract proteins from HeLa cells were incubated in triplicate with 0 (**A**) or 500 μM (**B**) mechlorethamine in the presence of 5'-biotinylated double-stranded oligodeoxynucleotides. Following biotin capture enrichment, cross-linked proteins were resolved by 10% SDS-PAGE, visualized with SimplyBlue SafeStain, and sample lanes were cut into sections prior to in-gel tryptic digestion. The resulting peptides were analyzed by HPLC-ESI$^+$-MS/MS.

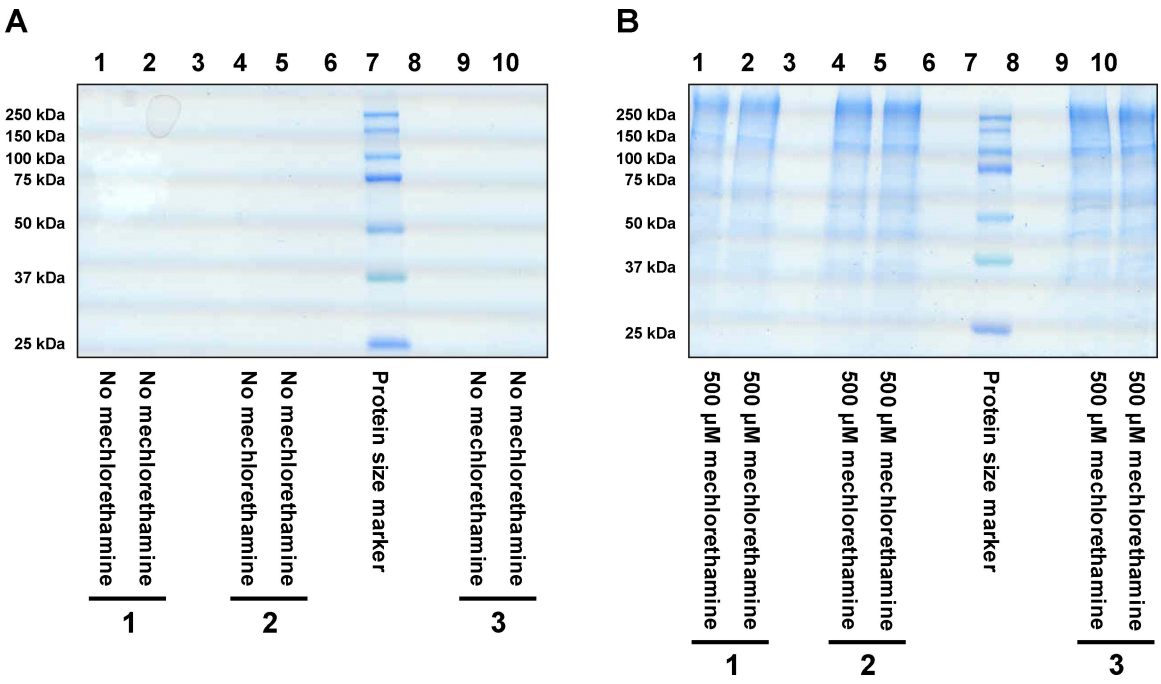

visible in the untreated cross-link samples. In contrast, significant staining was observed in the mechlorethamine-treated samples (*panel B of Figures 6.2 and 6.3*), indicating that DNA-protein cross-linking had taken place. Upon excision from the gel, the cross-linked proteins were subjected to reduction and alkylation prior to in-gel tryptic digestion. The recovered peptides were analyzed by HPLC-ESI$^+$-MS/MS for protein identification (*see Figure 6.4 for examples of MS/MS spectra of peptides*).

Parsimony analysis of the spectral data yielded minimal protein lists for both sets of cross-link samples (*Tables 6.1 and 6.2*). Statistical analyses were performed to ensure that the levels of protein identified in mechlorethamine-treated samples were significantly higher than in the untreated controls. There was obvious overlap between the lists of HeLa and CHO nuclear proteins participating in DPC formation, with the CHO and HeLa extracts yielding 15 and 53 cross-linked proteins, respectively (Tables 6.1 and 6.2, respectively).

6.4.2 Confirmation of Individual Proteins that Cross-Link DNA by Western Blot Analysis

The identities of the proteins participating in DPC formation in the presence of mechlorethamine were confirmed *via* Western blotting using commercially-available antibodies. These experiments also allowed us to perform relative quantitation regarding the extent of DNA-protein cross-linking in CHO and HeLa nuclear protein extracts exposed to 0, 500, or 1000 μM mechlorethamine, followed by affinity capture and SDS-PAGE analysis as described above. The samples were transferred to nitrocellulose

Figure 6.4 HPLC-ESI$^+$-MS/MS identification of tryptic peptides resulting from biotin capture of mechlorethamine-induced DNA-protein cross-links involving GAPDH (**A**), PARP (**B**), and nucleolin (**C**).

A

Seq	#	b	y	(+1)
L	1	114.1	1763.8	14
I	2	227.2	1650.7	13
S	3	314.2	**1537.6**	12
W	4	500.3	**1450.6**	11
Y	5	**663.4**	**1264.5**	10
D	6	**778.4**	**1101.5**	9
N	7	**892.4**	**986.4**	8
E	8	**1021.5**	**872.4**	7
F	9	**1168.5**	**743.3**	6
G	10	**1225.6**	**596.3**	5
Y	11	**1388.6**	**539.3**	4
S	12	**1475.6**	**376.2**	3
N	13	**1589.7**	**289.2**	2
R	14	1745.8	175.1	1

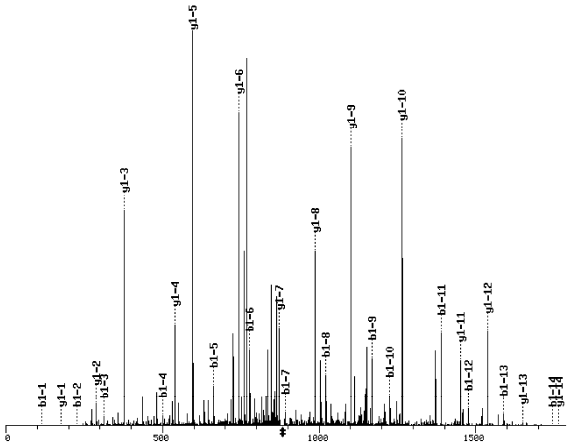

B

Seq	#	b	y	(+1)
V	1	100.1	1361.8	13
F	2	**247.1**	1262.7	12
S	3	**334.2**	**1115.7**	11
A	4	**405.2**	**1028.6**	10
T	5	506.3	**957.6**	9
L	6	**619.3**	**856.6**	8
G	7	676.4	**743.5**	7
L	8	**789.5**	686.4	6
V	9	**888.5**	**573.4**	5
D	10	**1003.5**	**474.3**	4
I	11	**1116.6**	**359.3**	3
V	12	**1215.7**	**246.2**	2
K	13	1343.8	147.1	1

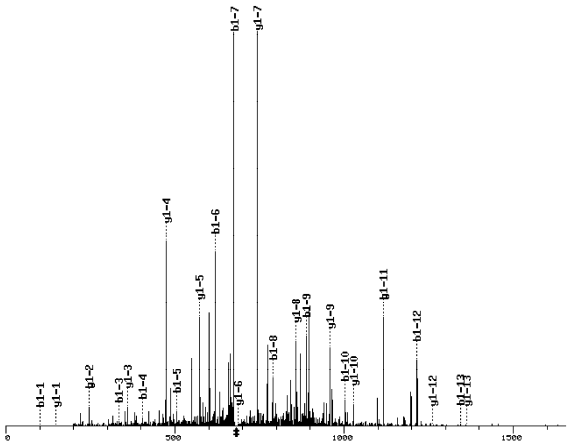

C

Seq	#	b	y	(+1)
G	1	58.0	1594.7	14
Y	2	221.1	1537.7	13
A	3	**292.1**	**1374.7**	12
F	4	**439.2**	**1303.6**	11
I	5	**552.3**	**1156.6**	10
E	6	**681.3**	**1043.5**	9
F	7	**828.4**	**914.4**	8
A	8	**899.4**	**767.4**	7
S	9	**986.5**	**696.3**	6
F	10	**1133.5**	**609.3**	5
E	11	**1262.6**	**462.2**	4
D	12	**1377.6**	**333.2**	3
A	13	**1448.6**	218.2	2
K	14	1576.7	147.1	1

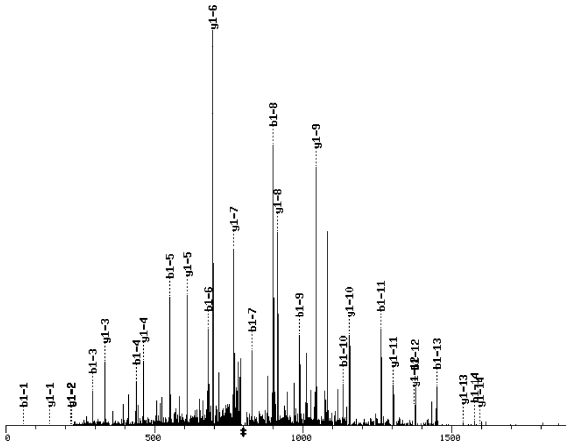

Table 6.1 CHO nuclear extract proteins that form DPCs in the presence of mechlorethamine

Swiss-Prot ID	Protein	Cellular Localization	Peptide Sequences	Spectra	Classification
P48975	Actin	Cyt	19	276	Architectural/Structural
P69893	Beta tubulin	Cyt	24	144	
P68361	Alpha tubulin	Cyt	15	125	
P68362	Alpha tubulin II	Cyt	14	103	
Q9J155	Plectin-1	Cyt	23	34	
Q60399	Nucleolin (C23)	Nuc	22	255	Chromatin Regulators
P17244	Glyceraldehyde-3-phosphate dehydrogenase	Cyt	9	109	Cellular Homeostasis/Cell Cycle
P46633	Heat shock protein HSP 90-alpha	Cyt, Nuc	24	154	
P19378	Isoform 1 of Heat shock cognate 71 kDa protein	Cyt, Nuc	19	133	
P62629	Elongation factor 1-alpha 1	Cyt	23	196	Transcription Regulators/RNA Splicing
P09445	Elongation factor 2	Cyt	23	98	
Q07050	DNA topoisomerase 1	Nuc	14	69	DNA Replication/Repair
P16455	Methylated-DNA--protein-cysteine methyltransferase (AGT)	Nuc	4	41	
P41515	DNA topoisomerase 2-alpha	Cyt, Nuc	18	34	
Q9R152	Poly [ADP-ribose] polymerase 1 (PARP)	Nuc	11	18	

Table 6.2 HeLa nuclear extract proteins that form DPCs in the presence of mechlorethamine

Swiss-Prot ID	Protein	Cellular Localization	Peptide Sequences	Spectra	Classification
P60709	Actin	Cyt	12	109	Architectural/Structural
P02545	Isoform A of Lamin-A/C	Nuc	25	98	
Q9BQE3	Tubulin alpha-1C chain	Cyt	9	49	
Q14978	Isoform Beta of Nucleolar phosphoprotein p130	Cyt, Nuc	7	39	
P19338	Nucleolin (C23)	Nuc	18	197	Chromatin Regulators
Q9Y5B9	FACT complex subunit SPT16	Nuc	35	127	
Q08945	FACT complex subunit SSRP1	Nuc	20	116	
Q01105	Isoform 1 of Protein SET	Cyt, ER, Nuc	7	54	
Q13283	Ras GTPase-activating protein-binding protein 1	Cyt, Nuc	8	43	
Q9UQE7	Structural maintenance of chromosomes protein 3	Nuc	22	43	
P04406	Glyceraldehyde-3-phosphate dehydrogenase	Cyt	9	109	Cellular Homeostasis/Cell Cycle
Q09666	AHNAK nucleoprotein isoform 1	Nuc	48	97	
Q9P258	Protein RCC2	Nuc	14	74	
Q92688	Isoform 1 of Acidic leucine-rich nuclear phosphoprotein 32 family member B	Nuc	7	60	
Q99459	Cell division cycle 5-like protein	Cyt, Nuc	16	52	
P11142	Isoform 1 of Heat shock cognate 71 kDa protein	Cyt, Nuc	12	47	
P07900	Heat shock protein HSP 90-alpha	Cyt, Nuc	12	40	
Q16666	Isoform 1 of Gamma-interferon-inducible protein Ifi-16	Nuc	11	35	
P49736	DNA replication licensing factor MCM2	Nuc	8	17	
P61978	Isoform 2 of Heterogeneous nuclear ribonucleoprotein K	Cyt, Nuc	22	254	Transcription Regulators/RNA Splicing
P06748	Isoform 2 of Nucleophosmin	Nuc	11	217	
Q15233	Non-POU domain-containing octamer-binding protein	Nuc	27	189	
P52272	Isoform 1 of Heterogeneous nuclear ribonucleoprotein M	Nuc	36	167	
Q08211	ATP-dependent RNA helicase A	Cyt, Nuc	44	148	
P23246	Isoform Long of Splicing factor, proline- and glutamine-rich	Nuc	20	132	
P26599	Isoform 1 of Polypyrimidine tract-binding protein 1	Nuc	20	132	
Q92841	DEAD box polypeptide 17 isoform 1	Nuc	27	116	
P09651	Isoform A1-B of Heterogeneous nuclear ribonucleoprotein A1	Cyt, Nuc	14	115	

Q12906	Interleukin enhancer-binding factor 3	Nuc	26	89	
P60842	Eukaryotic initiation factor 4A-I	Cyt, Nuc	22	82	
O43390	Heterogeneous nuclear ribonucleoprotein R	Nuc	17	78	
O60506	Isoform 3 of Heterogeneous nuclear ribonucleoprotein Q	Nuc	20	77	
P22626	Isoform B1 of Heterogeneous nuclear ribonucleoproteins A2/B1	Nuc	12	75	
P68104	Elongation factor 1-alpha 1	Cyt	9	71	
P31943	Heterogeneous nuclear ribonucleoprotein H	Nuc	9	57	
Q15459	Splicing factor 3 subunit 1	Nuc	13	55	
P17844	Probable ATP-dependent RNA helicase DDX5	Nuc	18	54	
Q16630	Isoform 1 of Cleavage and polyadenylation specificity factor subunit 6	Nuc	10	39	
P43243	Matrin-3	Nuc	7	20	
P12956	ATP-dependent DNA helicase 2 subunit 1 (Ku70)	Nuc	26	186	DNA Replication/Repair
P27695	DNA-(apurinic or apyrimidinic site) lyase (Ref-1)	Nuc	14	128	
P13010	ATP-dependent DNA helicase 2 subunit 2 (Ku86)	Nuc	24	117	
P11388	DNA topoisomerase 2-alpha	Cyt, Nuc	39	91	
P11387	DNA topoisomerase 1	Nuc	22	80	
Q02880	DNA topoisomerase 2-beta	Cyt, Nuc	26	70	
P09874	Poly [ADP-ribose] polymerase 1 (PARP)	Nuc	28	69	
P39748	Flap endonuclease 1	Nuc	6	24	
Q16531	DNA damage-binding protein 1	Cyt, Nuc	15	23	
Q9Y230	RuvB-like 2	Nuc	8	20	
P43246	DNA mismatch repair protein Msh2	Nuc	7	19	
P49959	Isoform 1 of Double-strand break repair protein MRE11A	Nuc	7	18	
P16455	Methylated-DNA--protein-cysteine methyltransferase (AGT)	Nuc	2	5	
O60216	Double-strand-break repair protein rad21 homolog	Nuc	2	5	

membranes and probed with antibodies against actin, nucleolin, histone H4, PARP, Ref-1, GAPDH, Ku, elongation factor 1-alpha 1, and XRCC1. As shown in *panel A* of *Figure 6.5*, mechlorethamine-induced cross-linking of actin, nucleolin, and PARP was confirmed *via* Western blot analysis of CHO nuclear extracts. For each of the three proteins, the extent of cross-linking increased with increased drug concentration, with actin displaying the highest cross-link levels (6.9% of total protein at 1000 μM mechlorethamine, *Figure 6.5, panel B*). Cross-linking of these same three proteins also occurred upon treatment of HeLa nuclear protein extracts with mechlorethamine in the presence of DNA (*Figure 6.6, panel A*). In addition, Ref-1, Ku, elongation factor 1-alpha 1, and GAPDH were also identified in the biotin capture fractions from the nuclear protein extracts from human cells. While no cross-linked protein was observed in the untreated controls, significant levels (4-12%) were observed upon exposure to both 500 and 1000 μM mechlorethamine.

Although not identified during MS analysis of cross-linked proteins, XRCC1 was detected in the biotin capture fractions of both CHO and HeLa nuclear extracts exposed to mechlorethamine using immunological methods (*Figure 6.7*). Cross-linking of XRCC1 to DNA in the presence of mechlorethamine ranged from 4-7%, with little to no protein was observed in the untreated controls. Taken together, these results confirm the identities of cross-linked proteins, as well as demonstrate that cross-linking does not occur in the absence of drug.

Figure 6.5 Western blot analysis of mechlorethamine-induced DNA-protein cross-links in CHO nuclear extracts. (**A**) Nuclear extract proteins from CHO cells were incubated with 0 (lane 1), 500 µM (lane 2), or 1000 µM mechlorethamine in the presence of 5'-biotinylated double-stranded oligodeoxynucleotides. Following biotin capture enrichment, cross-linked proteins were resolved by 10 or 12% SDS-PAGE, transferred to nitrocellulose membranes, and blotted using primary antibodies to actin, nucleolin, and poly (ADP-ribose) polymerase (PARP) and alkaline phosphatase-conjugated secondary antibodies. Untreated nuclear extract (~25 µg) was loaded as a positive control (lane 4). (**B**) Once developed, volume analysis was performed on each blot to determine % cross-linking of each protein.

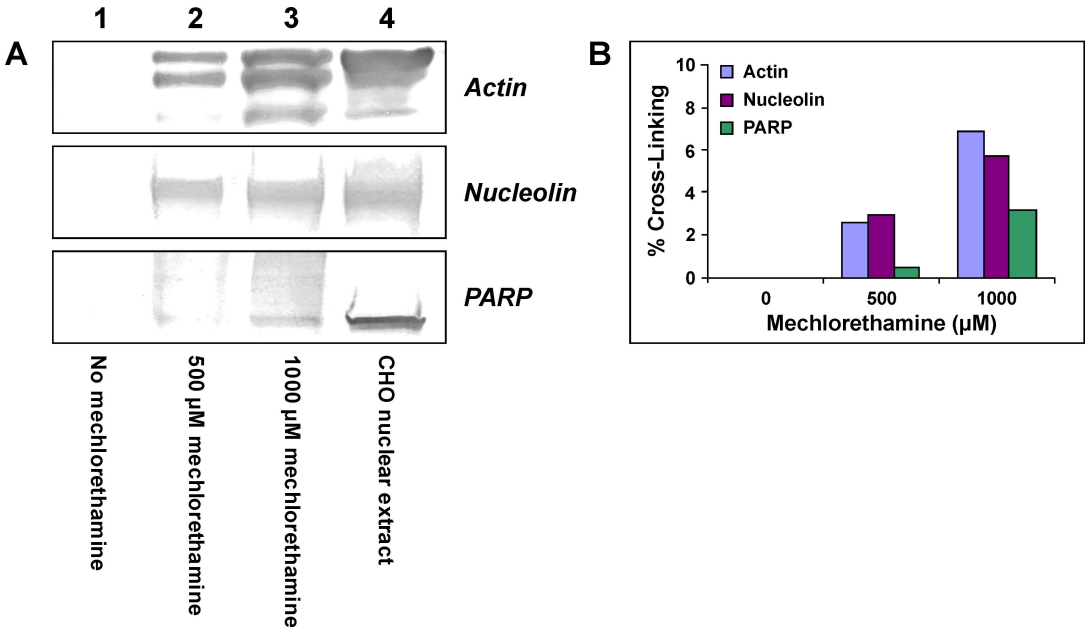

Figure 6.6 Western blot analysis of mechlorethamine-induced DNA-protein cross-links in nuclear protein extracts from HeLa human cervical carcinoma cells. (**A**) HeLa nuclear extract proteins were incubated with 5'-biotinylated double-stranded oligodeoxynucleotides in the presence of 0 (lane 1), 500 μM (lane 2), or 1000 μM mechlorethamine. Following affinity capture enrichment, cross-linked proteins were resolved by 10 or 12% SDS-PAGE, transferred to nitrocellulose membranes, and blotted using primary antibodies to actin, nucleolin, poly (ADP-ribose) polymerase (PARP), DNA-(apurinic or apyrimidinic site) lyase (Ref-1), glyceraldehyde-3-phosphate dehydrogenase (GAPDH), ATP-dependent DNA helicase subunit 2 (Ku), O^6-alkylguanine DNA alkyltransferase (AGT), and elongation factor 1-alpha 1 (EF-1α1). Use of alkaline phosphatase-conjugated secondary antibodies allowed for facile development of the blots. Untreated nuclear extract (~25 μg) was loaded as a positive control (lane 4). (**B**) Upon development of the blots, volume analysis was performed to determine % cross-linking of each protein relative to the amount of protein present in the untreated extract.

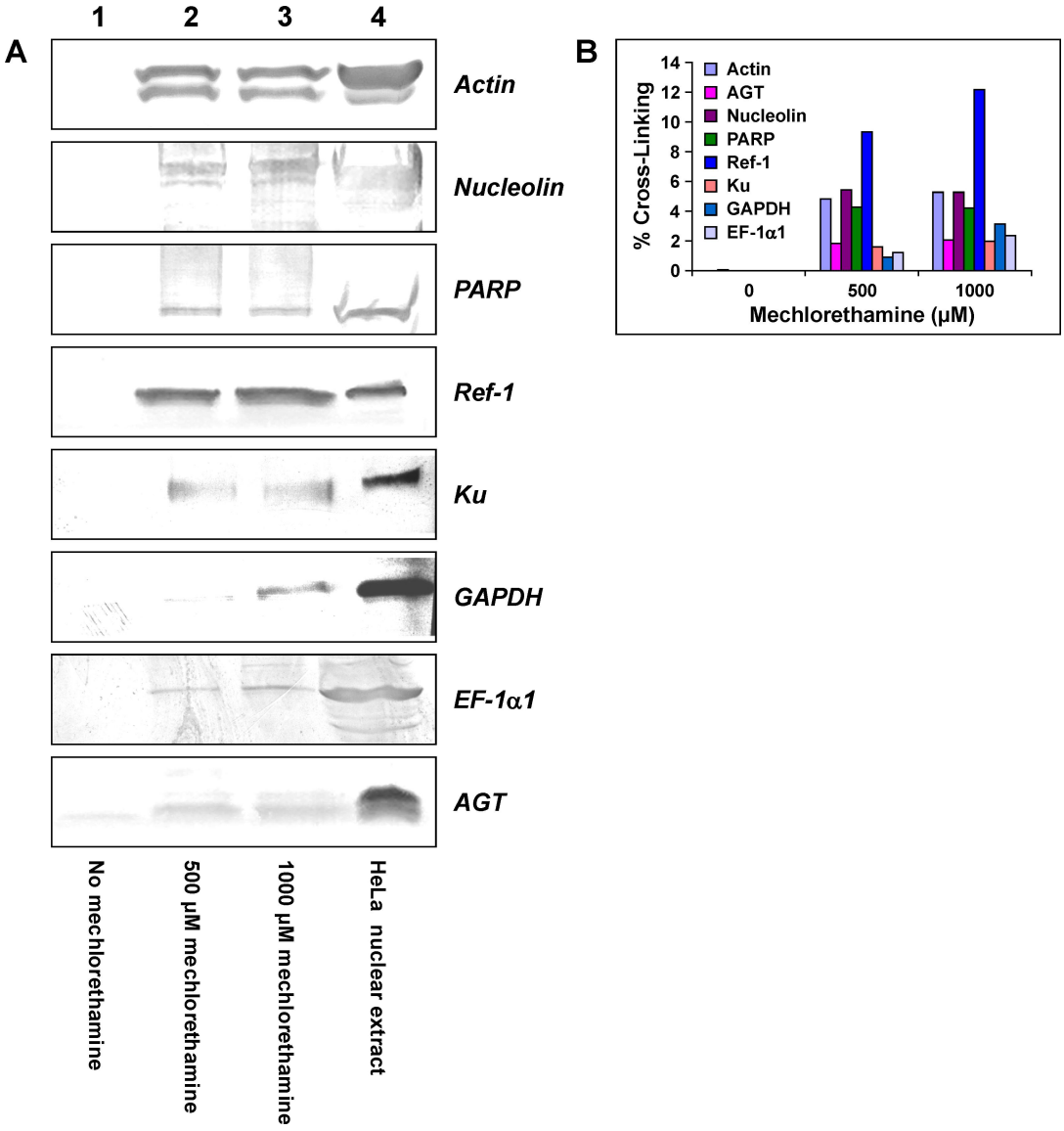

Figure 6.7 Western blot analysis of mechlorethamine-induced DNA-protein cross-links involving XRCC1 in CHO and HelLa protein extracts. (**A**) CHO and HeLa nuclear extract proteins were incubated with 5'-biotinylated double-stranded oligodeoxynucleotides in the presence of 0 (lane 1), 500 μM (lane 2), or 1000 μM (lane 3) mechlorethamine. Following biotin capture enrichment, cross-linked proteins were resolved by 10% SDS-PAGE. Once transferred to nitrocellulose membranes, the proteins were incubated with the primary antibody against X-ray repair cross-complementary protein 1 (XRCC1) followed by treatment with an alkaline phosphatase-conjugated secondary antibody. Untreated nuclear extracts (~25 μg each) were loaded as positive controls (lane 4). (**B**) Upon development, volume analysis was performed on each blot to determine % cross-linking of XRCC1.

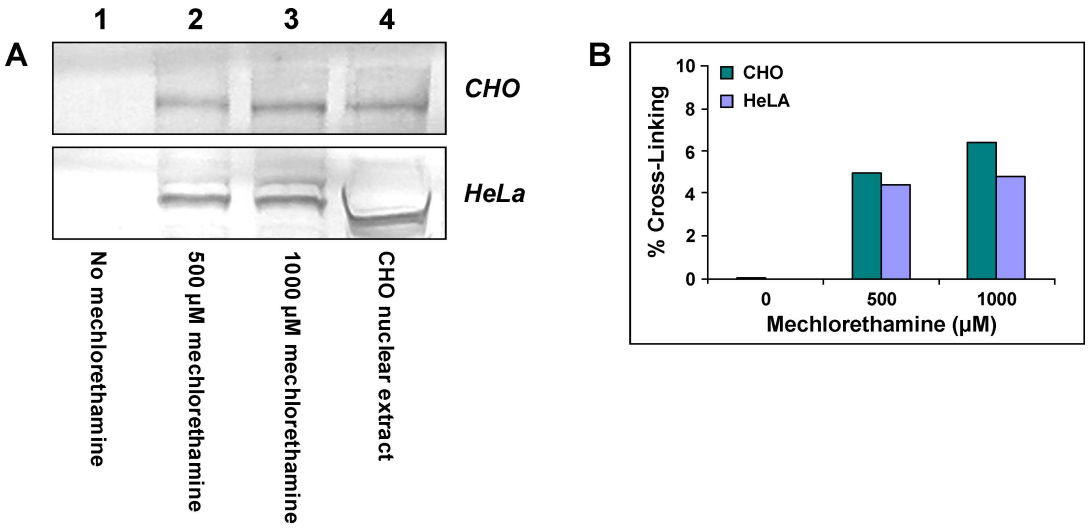

6.4.3 Covalent DPC Formation: Detection of a Mechlorethamine-Induced Cysteine-Guanine Cross-Link

To confirm that mechlorethamine exposure results in the formation of covalent DNA-protein complexes, HeLa nuclear protein extracts which had been incubated with double-stranded DNA in the presence or absence of mechlorethamine were subjected to neutral thermal hydrolysis and proteolytic digestion. Detection of mechlorethamine-induced amino acid-nucleobase conjugates in the resulting mixtures was achieved *via* capillary HPLC-ESI$^+$-MS/MS using a triple quadrupole mass spectrometer operated in SRM mode. Based upon our previous work with AGT protein (*Chapter III*), our efforts focused on the detection of Cys-N7G-EMA, the only mechlorethamine-induced cross-link observed in that study.

As shown in *Figure 6.8*, mechlorethamine treatment resulted in the formation of a cysteine-guanine conjugate that displayed the same HPLC retention time and MS/MS fragmentation as synthetic *N*-[2-[*S*-cysteinyl]ethyl]-N-[2-(guan-7-yl)ethyl]methylamine (*panels A, C, and D*). In contrast, no peak was detected in the untreated control (*panel B*). Not only does this result imply that mechlorethamine-induced DPCs are covalent in nature, it also demonstrates that this bifunctional drug reacts with the N7 position of guanine in duplex DNA and with the side chain sulfhydryl of cysteine residues within proteins to form a covalent, drug-induced complex.

6.4.4 Histone H4 Is Not Involved in Mechlorethamine-Induced DPC Formation

Due to their involvement in cellular packaging of DNA, it was hypothesized that histone proteins may become cross-linked to DNA in the

Figure 6.8 HPLC-ESI$^+$-MS/MS analysis of Cys-N7G-EMA in HeLa nuclear extracts. Synthetic Cys-N7G-EMA, *m/z* 356.1 $[M + H]^+$ (**A**); Cys-N7G-EMA present in enzymatic digests of HeLa nuclear protein extracts following incubation with 0 (**B**) and 1000 μM (**C**) mechlorethamine in the presence of double-stranded DNA; and mechlorethamine-treated total digest spiked with Cys-N7G-EMA (**D**).

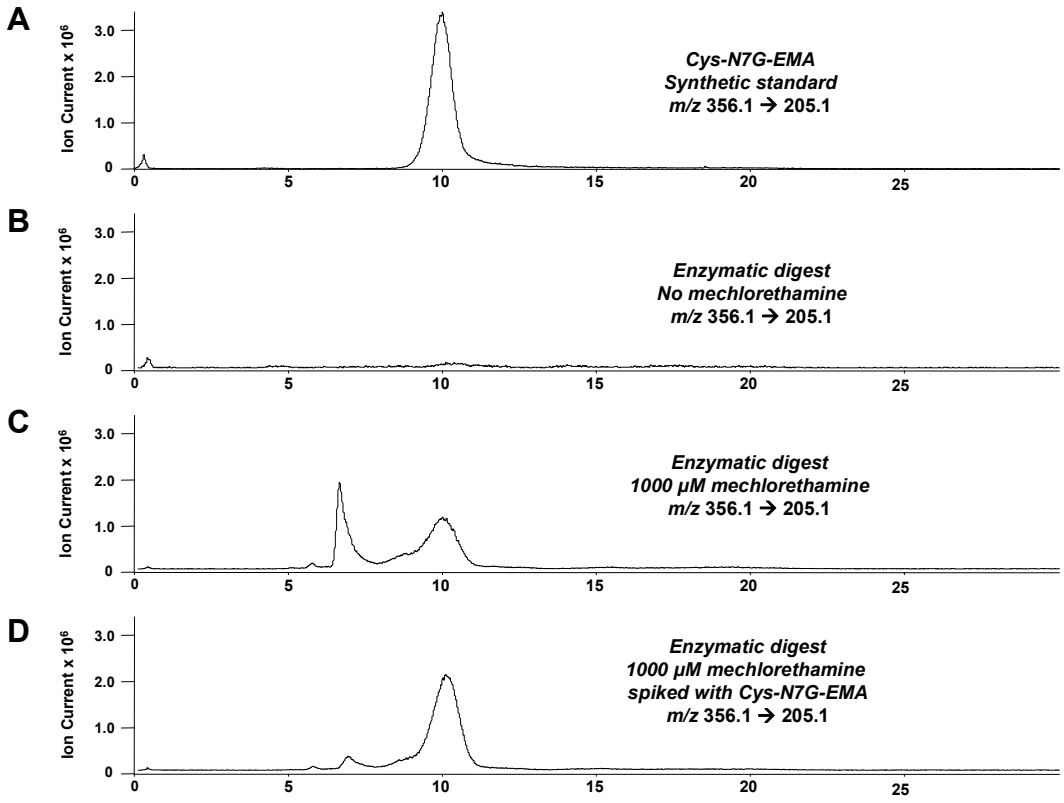

presence of *bis*-electrophiles. To assess the ability of proteins from this family to form nitrogen mustards-mediated DPCs, experiments were performed to examine cross-linking of histone H4 (*Table 6.3*) to DNA following exposure to mechlorethamine and chlorambucil. The ability of purified bovine histone H4 to become cross-linked to double-stranded oligodeoxynucleotides in the presence of these two drugs was first examined by denaturing PAGE. Upon incubation of histone H4 with ^{32}P-endlabled DNA duplexes in the presence of increasing amounts of mechlorethamine or chlorambucil, no additional DNA bands were observed to support the formation of a covalent histone-DNA complex (*Figure 6.9*). This result is in contrast to what was observed when the same experiment was performed with human recombinant AGT (*Chapter III, section 3.4.1*).

We then set out to look for evidence of half mustard-induced alkylation of histone H4. HPLC-ESI$^+$-MS analysis of N7G-PBA-Cl-treated protein led to the identification of several ions corresponding to numerous post-translational modifications and oxidation states of histone H4, but no cross-links to guanine (*Figure 6.10*). Likewise, histone H4 treated with the guanine half-mustard of mechlorethamine yielded the same deconvoluted spectrum (*Figure 6.11)*, again suggesting that no cross-linking had taken place. Although no guanine cross-links were detected, several post-translational modifications were identified through HPLC-ESI$^+$-MS/MS analysis of tryptic peptides (*Table 6.4*). Histone proteins undergo several post-translational modifications which determine whether or not the protein is active. For example, transcription is activated when histone H4 is becomes acetylated at Lys^8 *(201)*. Histone acetyl transferases (HATs) are involved in transcription

Table 6.3 Amino acid sequence of histone H4

Histone H4
SGRGKGGKGL GKGGAKRHRK VLRDNIQGIT KPAIRRLARR GGVKRISGLI YEETRGVLKV FLENVIRDAV TYTEHAKRKT VTAMDVVYAL KRQGRTLYGF GG
MW (average mass): 11236.2 Da / MW (monoisotopic mass): 11229.4 Da
Observed Masses: 11310 Da (MW + Acet + 2Me); 11352 Da (MW + 2Acet + 2Me); 11326 Da (MW + Acet + 2Me + O); and 11368 Da (MW + 2 Acet + 2 Me + O)

Figure 6.9 12% SDS-PAGE analysis of ^{32}P-end labeled DNA duplexes (5'-GGA GCT GGT GGC GTA GGC, (+) strand) following incubation with increasing amounts of mechlorethamine (lanes 1-3) or chlorambucil (lane 5-7) in the presence of histone H4. Lanes 4 and 8 containing no nitrogen mustard serve as negative controls, as do lanes 9 and 10 lacking protein or DNA.

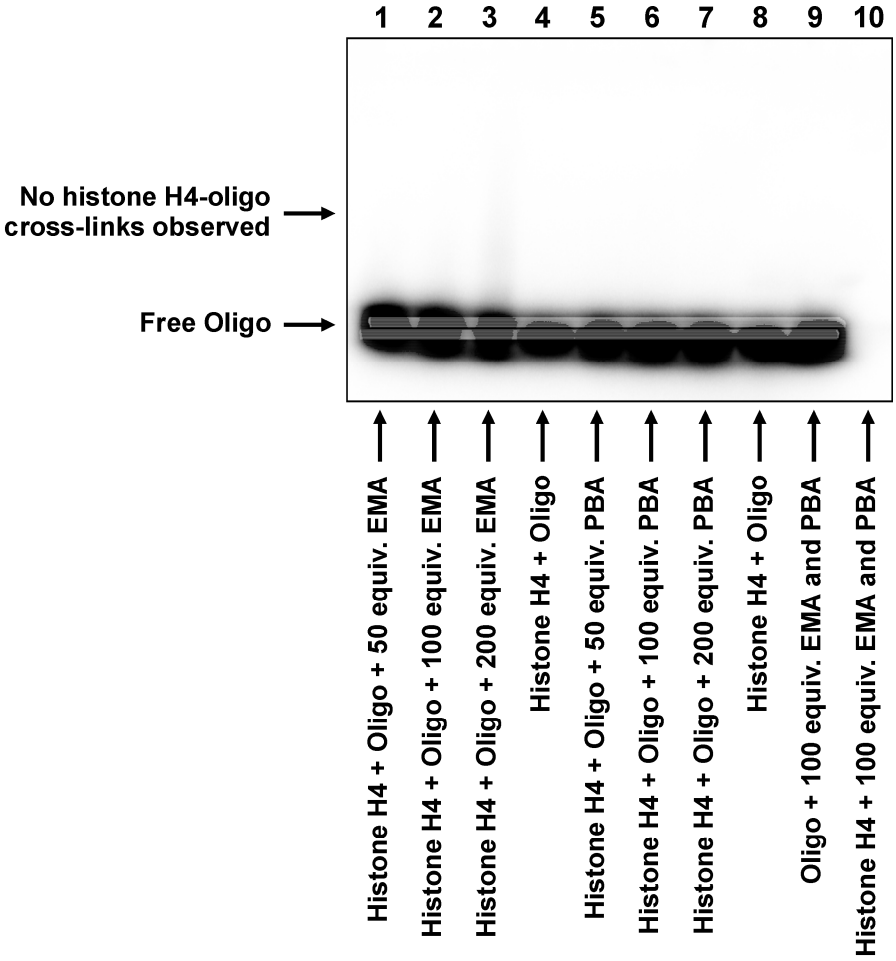

Figure 6.10 Whole protein MS analysis of histone H4 treated with N7G-PBA-Cl.*Top*: Total ion chromatogram; *Bottom left*: ESI^+ mass spectrum of 16.9 min protein peak; *Inset:* Deconvoluted mass spectrum of the 16.9 min protein peak: *A* = histone H4 + Acet + 2Me + O (calculated *M* = 11 326 Da, observed *M* = 11 326 Da), *B* = histone H4 + 2Acet + 2Me + O (calculated *M* = 11 368 Da, observed *M* = 11 368 Da); *Bottom right*: ESI^+ mass spectrum of 19.9 min protein peak; *Inset*: Deconvoluted mass spectrum of the 19.9 min protein peak: *A* = histone H4 + Acet + 2Me (calculated *M* = 11 310 Da, observed *M* = 11 310 Da), *B* = histone H4 + 2Acet + 2Me (calculated *M* = 11 352 Da, observed *M* = 11 352 Da).

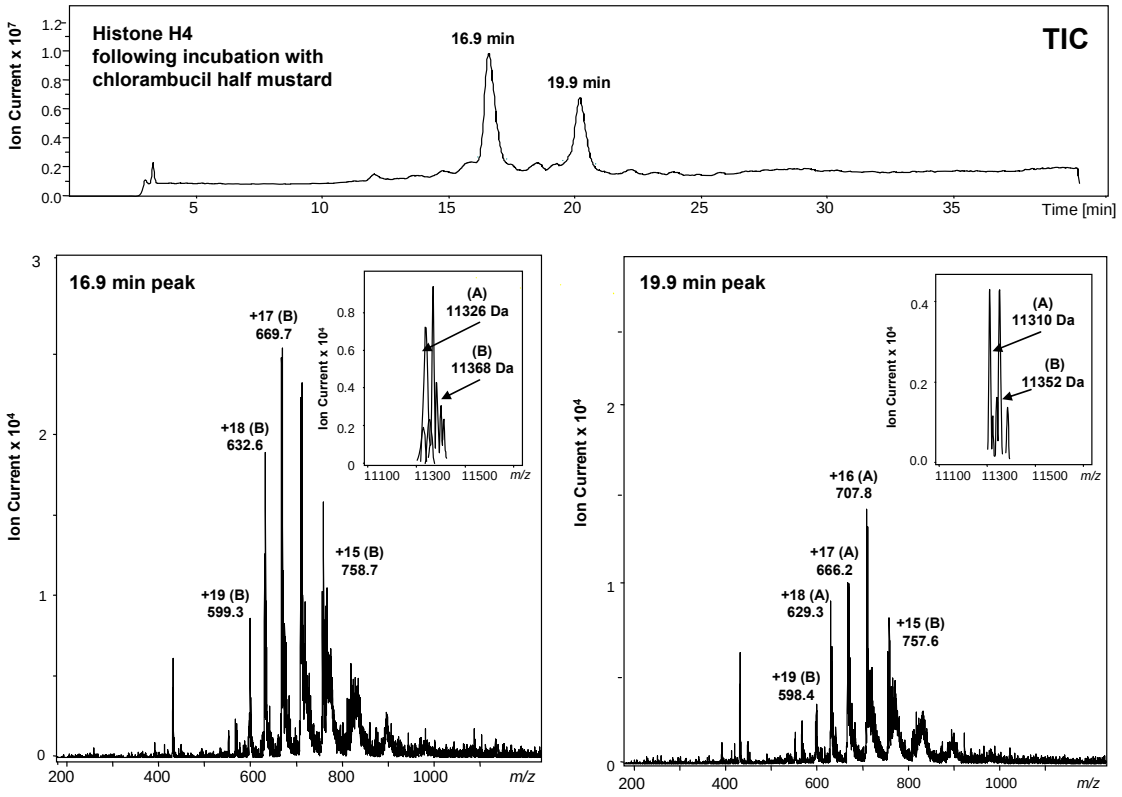

Figure 6.11 Whole protein MS analysis of histone H4 treated with N7G-EMA-Cl. *Top*: Total ion chromatogram; *Bottom left*: ESI^+ mass spectrum of 16.9 min protein peak; *Inset:* Deconvoluted mass spectrum of the 16.9 min protein peak: *A* = histone H4 + Acet + 2Me + O (calculated *M* = 11 326 Da, observed *M* = 11 326 Da), *B* = histone H4 + 2Acet + 2Me + O (calculated *M* = 11 368 Da, observed *M* = 11 368 Da); *Bottom right*: ESI^+ mass spectrum of 19.9 min protein peak; *Inset*: Deconvoluted mass spectrum of the 19.9 min protein peak: *A* = histone H4 + Acet + 2Me (calculated *M* = 11 310 Da, observed *M* = 11 310 Da), *B* = histone H4 + 2Acet + 2Me (calculated *M* = 11 352 Da, observed *M* = 11 352 Da).

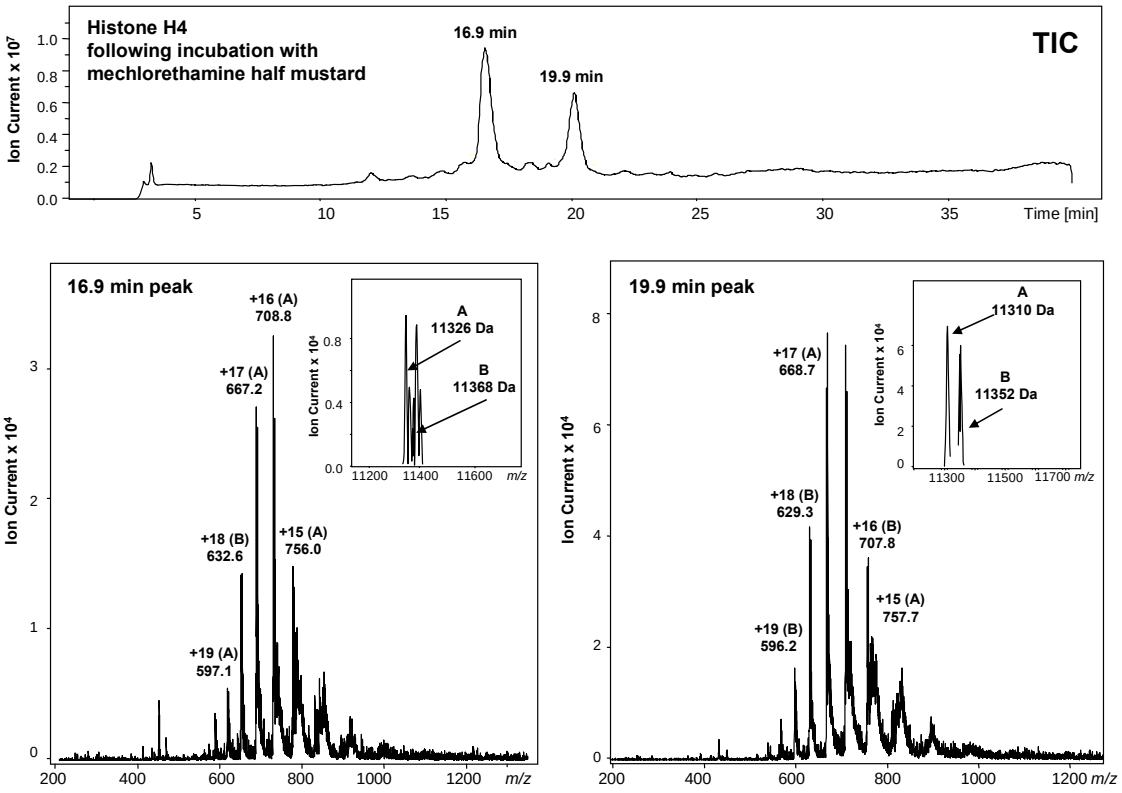

Table 6.4 Histone H4 tryptic peptides

Position	Peptide	$[M+H]^{+}_{calculated}$	$[M+2H]^{2+}_{calculated}$	Observed Ions
1-8	SGRGKGGK	746.43	373.72	746.8, 374.3
4-16 + 2Me	GKGG^{Me}KGLG^{Me}KGGAK	1142.6	571.8	1142.6, 571.8
6-16 + 2Acet	GG^{Acet}KGLG^{Acet}KGGAK	1014.55	507.28	1014.7
17-19	RHR	468.3	234.65	ND
20-23	KVLR	515.4	257.7	515.4, 258.1
24-35	DNIQGITKPAIR	1325.75	663.38	1325.8, 663.6
36-39	RLAR	515.64	258.32	ND
40-45	RGGVKR	672.43	336.72	672.5, 336.8
46-55	ISGLIYEETR	1180.62	590.81	1180.6, 590.9
56-59	GVLK	416.54	208.77	416.3
60-67	VFLENVIR	989.58	495.29	989.6, 495.3
68-77	DAVTYTEHAK	1134.54	567.77	1134.5, 567.9
78-79	RK	303.39	170.2	ND
80-91 + Oxygen	TVTAMDVVYALK	1326.7	663.85	1326.0, 663.7
92-95	RQGR	516.3	258.65	ND
96-102	TLYGFGG	714.35	357.68	714.5

activation as they are responsible for the acetylation of histones at N-terminal lysine residues *(202)*. In our analysis of histone H4, we observed acetylation of N-terminal lysines 8 and 12. Kasprzak and colleagues have documented damage of histone H2B when its methionine residues are oxidized to sulfoxides *(202)*. We observed oxidized histone H4 in both whole protein and peptide mass spectrometric analysis (*Figures 6.10-6.11 and Table 6.4*). Histone H4 contains only one methionine, Met^{84}, which is located in the oxidized peptide $T^{80}VTAMDVVYALK^{91}$.

Lastly, the ability of histone H4 in HeLa whole cell extracts to become cross-linked to 5'-biotinylated oligodeoxynucleotides by mechlorethamine was examined by Western blotting. Following biotin capture enrichment, cross-linked proteins were separated by 15% SDS-PAGE and a polyclonal antibody against human histone H4 was used to detect any captured protein. While histone H4 was detected in the whole cell extract (*Figure 6.12, lane 4*), no evidence of histone-DNA cross-linking was observed (*lanes 1-3*). A known amount of human recombinant histone H4 (Millipore, Billerica, MA) was analyzed in parallel to determine the limit of detection (*lane 5*). Based upon the amount of histone H4 present in the reaction mixtures, the formation of histone-DNA cross-links at ~1% cross-linking efficiency or greater would be detectable by this method.

6.5 Discussion

Despite the known ability of *bis*-electrophiles to cross-link nucleophilic sites within DNA and proteins, research into the biological consequences of DNA-protein lesions is still in its infancy. As a result, little is known about the identities of these lesions and their potential cytotoxic and mutagenic effects. Due to their high reactivity towards

Figure 6.12 Western blot analysis of mechlorethamine-induced DNA-protein cross-links involving histone H4. HeLa whole cell extracts were incubated with 5'-biotinylated double-stranded oligodeoxynucleotides in the presence of 0 (*lane 1*), 500 μM (*lane 2*), or 1000 μM (*lane 3*) mechlorethamine. Following biotin capture enrichment, cross-linked proteins were resolved by 15% SDS-PAGE. Once transferred to nitrocellulose membranes, proteins were incubated with the primary antibody against histone H4 followed by incubation with an alkaline phosphatase-conjugated secondary antibody. Untreated HeLa whole cell extract (~25 μg) was loaded as a positive control (*lane 4*), as was 100 ng of human recombinant histone H4 (*lane 5*).

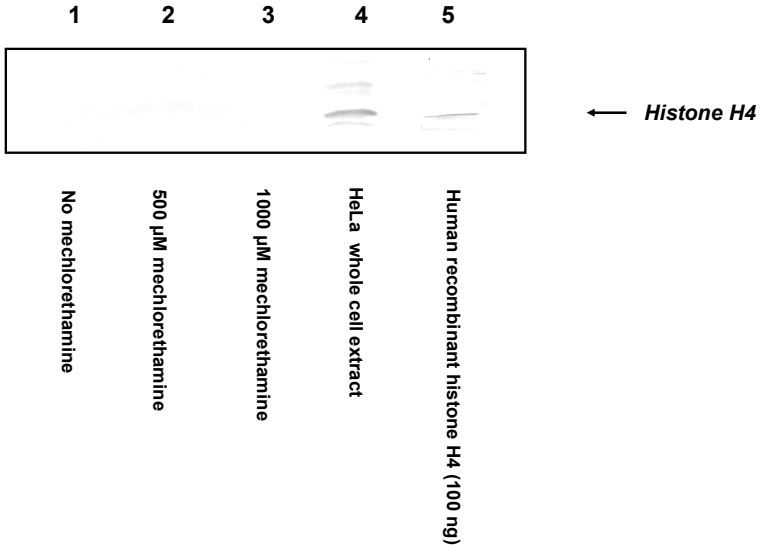

nucleophilic sites in biomolecules, antitumor nitrogen mustards are likely to form DPCs in drug-treated cells.

Previous work in our laboratory has demonstrated the ability of the nitrogen mustards mechlorethamine and chlorambucil to form DPCs involving the human DNA repair protein AGT to DNA *in vitro (38)*. Within a cell, AGT is responsible for the repair of promutagenic O^6-alkylguanine lesions in DNA *via* transfer of the alkyl group to an active site cysteine residue *(101)*. In the process of restoring normal guanine, AGT is inactivated and subsequently degraded by the ubiquitin-proteosome pathway *(117;155)*. As AGT is over-expressed in many types of tumors, it could mediate the cytotoxicity of nitrogen mustards *via* formation of AGT-DNA cross-links. However, due to the vast number of proteins that interact with DNA, we hypothesized that AGT was not the only protein within the cell capable of becoming cross-linked to DNA in the presence of nitrogen mustards.

DPCs induced by other agents are well established, with the catalogued proteins displaying great diversity in terms of cellular function *(1)*. For example, following exposure of CHO cells to ionizing radiation, tandem mass spectrometry was used to identify 29 proteins that had become cross-linked to DNA *(11)*. Among those identified were structural/nuclear matrix proteins (actin and vimentin), spliceosome components (hnRNPs and protein-associated splicing factor), stress response proteins (HSP10 and GRP78), and proteins involved in chromatin regulation/remodeling (histones H1, H2A, H2B, H3, H4 and chromatin remodeling protein CGI-55).

Similarly, the proteins identified in our study of mechlorethamine-mediated DNA-protein cross-links display great diversity. They include structural proteins,

transcription regulators, proteins involved in cell cycle control and homeostasis, DNA repair proteins, and chromatin regulators (*Tables 6.1 and 6.2*). While the overall distribution of proteins varied between the two lines in terms of cellular function (*Figure 6.13*), there was significant overlap in terms of the proteins identified (*Tables 6.1 and 6.2*).

In the category of architectural and structural proteins, actin dominated in terms of unique peptide sequences and MS/MS spectra (*Tables 6.1 and 6.2*). This is not surprising since this high abundance protein has previously been shown to become cross-linked DNA in the presence of chromium, cisplatin, mitomycin C, and pyrrolizidine alkaloids *(203;204)*. Although it is predominantly known for its role in cell motility, actin is also thought to play regulatory roles in chromatin remodeling, DNA replication, and transcription *(205;206)*. Involvement in these types of processes would help explain how actin could come in close enough proximity to DNA to undergo cross-linking.

Glyceraldehyde-3-phosphate dehydrogenase (GAPDH) was another protein that was identified with high confidence in both cellular systems. Although it is most notable for catalyzing the sixth step of glycolysis, GAPDH is also implicated in non-metabolic functions including transcription activation, initiation of apoptosis, and ER to golgi vesicle shuttling *(206-210)*. In *Schizosaccharomyces pombe*, GAPDH (along with actin) has been shown to associate with the Rpb7 subunit of RNA polymerase II *(206)*. In human cells, GAPDH has been identified as a key component of a coactivator complex for histone H2B transcription *(209)*. In both cases, the potential involvement of GAPDH

Figure 6.13 Cellular functions of identified proteins: CHO vs. HeLa

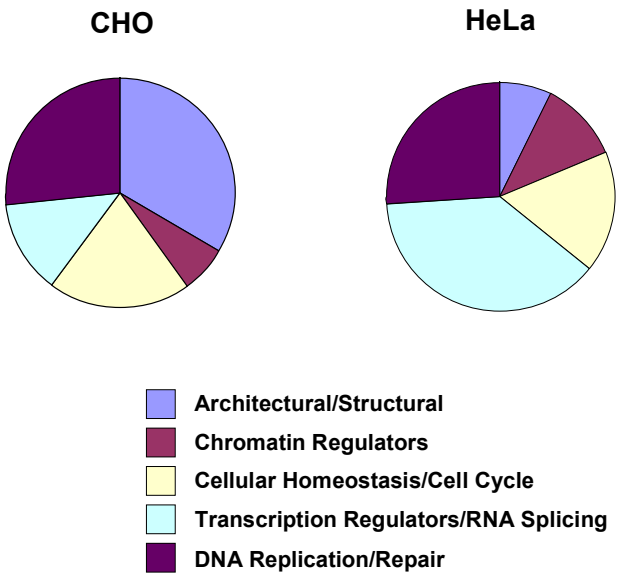

in transcription regulation would place this protein in the nucleus, making cross-linking to DNA highly probable.

Nucleolin, the most abundant nucleolar protein, was also found to cross-link DNA in the presence of mechlorethamine in both the CHO and HeLa nuclear extracts. Although it is better known for its roles in ribosome biogenesis, nucleolin is also believed to mediate interactions between histone H1 and double-stranded DNA *(211)*. By inducing chromatin decondensation through binding to histone H1, nucleolin can be regarded as a protein of the high mobility group (HMG) type.

In the category of transcription regulators/RNA splicing, two proteins were identified upon analysis of mechlorethamine-treated CHO extracts, Elongation factors 1-alpha 1 and 2 (*Table 6.1*). In contrast, 20 proteins of this type were identified following MS analysis of the HeLa extracts (*Table 6.2*). As proteins involved in DNA transcription and RNA processing bind nucleic acids, it is not surprising that they would become covalently bound to DNA in the presence of nitrogen mustards.

Because of their high affinity for duplex DNA, DNA-binding proteins involved in replication and repair are likely candidates to cross-link DNA in the presence of *bis*-electrophiles. Using tandem mass spectrometry, we were able to identify numerous proteins that fit this description, including DNA topoisomerases, DNA helicases, and several DNA repair enzymes. Among the proteins identified were AGT, ATP-dependent DNA helicase 2 subunit 2 (Ku), poly (ADP-ribose) polymerase (PARP), and DNA-(apurinic or apyrimidinic site) lyase (Ref-1).

Ku, which is also known as ATP-dependent DNA helicase 2 and X-ray repair cross-complementary protein 5 (XRCC5), is an abundant nuclear protein that works in

conjunction with DNA ligase IV and XRCC4 to repair DNA double-strand breaks *via* non-homologous end-joining and V(D)J recombination *(212-214)*. Ku binds to the ends of double-stranded DNA, acting as the DNA-binding component of a DNA-dependent protein kinase *(213)*. Rodents with mutations in the *XRCC5* gene are sensitive to ionizing radiation as they lack the ability to repair/rejoin radiation-induced DNA double-strand breaks *(212)*.

Another DNA-binding protein that was identified as cross-linking DNA in the presence of mechlorethamine was poly (ADP-ribose) polymerase (PARP). One of the most abundant proteins in the nucleus, PARP is implicated in both DNA repair and transcription regulation *(215;216)*. Catalytically, PARP acts as a DNA damage sensing and signaling molecule, with the zinc fingers of PARP recognizing single- and double-stranded DNA breaks. Within the nucleus, PARP interacts with numerous proteins involved in the single-strand break repair (SSRB) and base-excision repair (BER) pathways including XRCC1, DNA ligase III, and DNA polymerase-β. Upon sensing a DNA break, the damage signal is translated and amplified by PARP *via* poly (ADP-ribosyl)ation of histones H1 and H2B. This results in the relaxation of chromatin structure, allowing repair proteins to access the site of the DNA break. Upon recruitment of XRCC1 and assembly of the SSRB repair complex, end processing ensues, followed by gap filling and ligation courtesy of DNA polymerase-β and DNA ligase III. PARP has also been shown to be involved in transcription *via* regulation of DNA methylation and participation in enhancer/promoter-binding complexes.

Like PARP, DNA-(apurinic or apyrimidinic site) lyase (or Ref-1) is a nuclear protein involved in both DNA repair and transcription regulation *(217-219)*. As a class II

A/P endonuclease, mammalian Ref-1 catalyzes the repair of oxidative DNA damage (primarily abasic sites but also 3' replication-blocking lesions) *via* the BER pathway *(220)*. Ref-1 hydrolytically cleaves 5' to the abasic site, producing nucleotide-3'-hydroxyl and 5'-deoxyribose-5-phosphate residues on opposite sides of the nick. In addition to its roles in DNA repair, Ref-1 regulates transcription of Fos and Jun though a redox-dependent mechanism involving reduction of a conserved cysteine within the protein's DNA binding domain *(219)*.

In light of their involvement in DNA replication, repair, and transcription regulation, our finding that AGT, Ku, PARP, and Ref-1 form cross-links to DNA in the presence of mechlorethamine is not surprising. But what about other important repair proteins? Is it possible that our MS analysis could have missed one/some? To confirm our MS results as well as to determine the extent of cross-linking, Western blot analysis was performed targeting many of the identified proteins: actin, nucleolin, GAPDH, AGT, Ref-1, PARP, Ku, and elongation factor 1-alpha 1. In addition, antibodies against histone H4 and X-ray repair cross-complementary protein 1 (XRCC1) were used to look for immunological evidence of cross-linking. As shown previously with AGT, mechlorethamine-induced cross-linking of actin, nucleolin, GAPDH, Ref-1, PARP, elongation factor 1-alpha 1, and Ku to DNA displayed dose-dependence, with little to no protein detected in control samples lacking drug (*Figures 6.5 and 6.6*). While no cross-links involving histone H4 were detected (*Figures 6.9-6.11*), XRCC1 present in CHO and HeLa nuclear extracts was found to form cross-links to DNA in the presence of mechlorethamine (*Figure 6.7*). In complex with DNA ligase III, PARP, and DNA polymerase-β, XRCC1 functions in the repair of single-strand DNA breaks as described

above *(215;216;221)*. Defects in the XRCC1 gene result in sensitivity to ionizing radiation and methylating agents and increased levels of single-strand DNA breaks and sister chromatid exchange *(221)*.

Through the HPLC-ESI$^+$-MS/MS detection of Cys-N7G-EMA in reaction mixtures in which HeLa nuclear protein extracts had been incubated with double-stranded oligodeoxynucleotides in the presence of mechlorethamine prior to neutral thermal hydrolysis and complete proteolytic digestion (*Figure 6.8*), we demonstrate that mechlorethamine-mediated DPCs are covalent in nature, involving the N7 position of guanine in duplex DNA and the side chain sulfhydryl of cysteine residues within nuclear proteins. While cross-linking involving other amino acids cannot be ruled out, cysteine-guanine conjugates were the major types of mechlorethamine-induced DPC observed in studies with recombinant proteins *(38)*.

Although the contribution of DPCs towards the cytotoxicity of nitrogen mustard drugs is currently unknown, it is likely that this type of DNA damage may enhance the antitumor activity of these compounds. Work is currently underway in our laboratory to examine DNA-protein cross-linking in mechlorethamine-treated cells (*see Chapter VIII*).

VII. SUMMARY AND CONCLUSIONS

While the genotixic effects of *bis*-electrophiles are generally attributed to the formation of DNA-DNA interstrand cross-links, the contribution of DPCs to cytotoxicity and mutagenicity of these agents is less clear *(170)*. Because of their size, DPCs are expected to interfere with the binding and progression of protein complexes involved in DNA replication, transcription, and other important cellular processes *(1)*. Proteins which recognize and repair monoalkylated DNA lesions can become covalently bound to their DNA substrate in the presence of *bis*-electrophiles, resulting in the formation of bulky, helix-distorting DNA lesions and possible depletion of cellular pools of DNA repair proteins. In this work, the ability of *bis*-electrophiles DEB and the antitumor nitrogen mustards mechlorethamine and chlorambucil to induce DPCs was analyzed *in vitro* using a combination of mass spectrometry, gel-shift assays, NMR spectroscopy, UV spectrophotometry, and immunological techniques.

In a previous study, Pegg and colleagues demonstrated DBE-mediated DPC formation involving the active site cysteine residue (Cys^{145}) of human AGT and the N7 position guanine in duplex DNA *(57)*. We hypothesized that similar AGT-DNA cross-linking can be observed in the presence of the genotoxic *bis*-epoxide, DEB. AGT-DNA cross-linking was first detected by SDS-PAGE when ^{32}P-labeled double-stranded oligodeoxynucleotides were exposed to DEB in the presence the human recombinant AGT protein and an active site AGT mutant (C145A AGT, *Figure 2.1*). This experiment clearly demonstrated the formation of DEB-mediated AGT-DNA cross-links *via* two separate sites including Cys^{145}, but provided us with no structural information about the resulting DPC lesion. To gain insight into the chemical nature of DEB-mediated AGT-

DNA cross-links, a mass spectrometry-based approach was employed to identify the cross-linking sites within the protein and to elucidate the covalent structures of DEB-induced amino acid-nucleobase conjugates (*Scheme 2.2*). HPLC-ESI$^+$-MS/MS analysis of AGT-guanine cross-links obtained upon incubation of AGT with dG monoepoxide (a synthetic model of monoalkylated DNA) or with double-stranded oligodeoxynucleotides in the presence of DEB followed by tryptic digestion resulted in the identification of peptide-guanine cross-links involving cysteines 145 and 150 of the human repair protein. Subsequent analysis of amino acid-nucleobase conjugates resulting from total digestion of AGT-DNA cross-linking reactions revealed the structure of the cross-linked lesion as 1-(*S*-cysteinyl)-4-(guan-7-yl)-2,3-butanediol.

Similar methods were employed to investigate the formation of AGT-DNA cross-links induced by the nitrogen mustard drugs mechlorethamine and chlorambucil (*Scheme 3.2*). Like DEB, both nitrogen mustards produced AGT-DNA cross-links involving cysteines 145 and 150 of AGT and the N7 position of guanine in duplex DNA. HPLC-ESI$^+$-MS/MS was employed for comparative analysis of cysteine-guanine conjugates obtained upon total digestion of cross-linked proteins to synthetically-prepared cross-link standards, confirming the structures of nitrogen mustard-induced lesions as *N*-(2-[*S*-cysteinyl]ethyl)-*N*-(2-[guan-7-yl]ethyl)methylamine and *N*-(2-[*S*-cysteinyl]ethyl)-*N*-(2-[guan-7-yl]ethyl)-*p*-aminophenylbutyric acid. Interestingly, mechlorethamine was also found to induce an intermolecular protein cross-link, covalently bridging Cys^{145} and Cys^{150} (*Figure 3.20*).

Based upon our analysis, AGT-DNA cross-linking by DEB and nitrogen mustards favored cross-link formation at Cys^{145} over Cys^{150} (~3:1). This was not surprising due to

the high reactivity of this catalytic residue *(113)*. However, the large extent of cross-link formation at Cys^{150} observed was unexpected. While previous studies with DBE did detect cross-linking at Cys^{150}, it was only observed under extreme conditions and comprised a very small fraction of total cross-links *(57)*. A potential explanation for enhanced cross-linking at Cys^{150} involves the sequence of events leading up to cross-link formation. Unlike DEB and nitrogen mustards, DBE does not readily react with DNA. Thus, AGT-DNA cross-linking is believed to result from the initial alkylation of AGT to form a reactive AGT half-mustard which then binds DNA to initiate cross-linking (*Scheme 2.1*) *(153)*. Because DEB and nitrogen mustards readily alkylate DNA, AGT-DNA cross-linking could result from the binding of AGT to DNA containing a monoalkylated lesion containing a reactive epoxide or chloroethyl group (*Scheme 2.1*). This could very well explain the enhanced formation of cross-links involving Cys^{150}, a residue located near the DNA-protein interface (*Figure 2.10*). In a recent report, Kalapila *et al.* show that DEB-induced AGT-DNA cross-links do in fact arise following an initial reaction of DEB with DNA, and that cross-linking is likely to occur in this manner due to the hydrolytic instability of AGT monoalkylated lesions *(222)*.

After establishing that DEB and nitrogen mustards induce AGT-DNA cross-links in experiments with purified protein, we set out to determine if AGT-DNA cross-linking could occur in a more complex system. Thus, the ability of AGT present in mammalian nuclear protein extracts to form mechlorethamnine-mediated DPCs was examined by mass spectrometry and immunological methods. Due to the low numbers of DPCs formed, a novel biotin/streptavidin enrichment strategy was developed to improve our chances of detecting cross-linked proteins (*Scheme 4.1*). Briefly, cross-linking reactions

were carried out using double-stranded oligodeoxynucleotides containing a 5'-biotin tag, allowing for the capture of all DNA and DNA-protein cross-links on Streptavidin beads. This allowed us to remove all non-covalently bound proteins prior to analysis, thus improving detection by reducing the background levels and eliminating false positives. Using this technique, we were able to demonstrate that AGT does cross-link DNA in the presence of other cellular proteins. But what does this mean? Can DEB and nitrogen mustards induce AGT-DNA cross-links in treated cells? Could AGT expression influence the cytotoxicity and mutagenicity of these agents *in vivo*? More importantly, could AGT expression in tumor cells sensitize them to the therapeutic effects of bifunctional alkylating drugs?

Previous studies in *E. coli* and *Salmonella* species have shown that the expression of AGT enhances the cytotoxic and mutagenic effects of numerous *bis*-electrophiles, including DBE and DEB *(153;154)*. To determine if the same was true in mammalian cells, CHO cells expressing human recombinant AGT and their empty vector counterpart were obtained from the laboratory of Dr. Pegg (Pennsylvania State University) and the effect of AGT expression on the cytotoxicity and mutagenicity of DEB, mechlorethamine, and chlorambucil was examined. Contrary to what was observed in bacteria, AGT expression had little to no effect on the cytotoxicity and mutagenicity of these agents (*Figures 5.1-5.3*), suggesting that AGT expression does not significantly influence the genotoxic effects of *bis*-electrophiles in mammalian cells.

Due to the high reactivity of DEB and nitrogen mustards towards cellular nucleophiles, we hypothesize that AGT is not the only protein capable of becoming cross-linked to DNA. To identify other cellular proteins that form cross-links to DNA in

the presence of *bis*-electrophiles, biotin capture enrichment coupled with tandem mass spectrometry was employed as previously described. Because it is the most efficient cross-linker in our arsenal, mechlorethamine was selected for these analyses. As depicted in *Scheme 6.2*, biotin capture enrichment was utilized to select for cross-linked proteins prior to analysis. Using HPLC-ESI$^+$-MS/MS analysis of peptides resulting from in-gel tryptic digests of cross-linked proteins, numerous proteins were identified that had become cross-linked to DNA in the presence of mechlorethamine (*Tables 6.1 and 6.2*). The identified proteins displayed great diversity in terms of cellular function, with roles in chromatin regulation, DNA replication and repair, cell cycle control, transcription regulation, and architectural/structural support. The identities of a number of proteins observed during mass spectrometric analysis were later confirmed *via* Western blotting using commercially-available antibodies. Due to their close proximity to DNA and their roles in chromosomal processing, cross-linking of many of the proteins identified was not unexpected. Interestingly, histone H4 did not participate in nitrogen mustard-mediated DPC formation, despite their known affinity for DNA and involvement in DNA packaging. Histones have previously been shown to cross-link DNA in the presence of other agents, including formaldehyde and ionizing radiation *(2;11)*. The lack of reactivity of histone proteins towards DEB and nitrogen mustards suggests agent-specific selectivity in DPC formation. As histone H4 contains no cysteine residues, this suggests the importance of sulfhydryl groups in DEB and nitrogen mustard-induced protein alkylation.

In summary, DEB and nitrogen mustards are capable of inducing DPCs in addition to DNA-DNA cross-links, and both types of lesions are likely to contribute to

the genotoxic effects of these agents. Further work is necessary to obtain a greater understanding in regards to the biological relevance of these diverse DNA lesions.

VIII. FUTURE WORK

8.1 Detection of DPCs in Cells Exposed to *Bis*-Electrophiles

Although our results presented above establish that DPCs can form *in vitro* following incubation of nuclear protein extracts and DNA in the presence of DEB and nitrogen mustards, questions still remain whether similar cross-linking occurs in intact cells treated with *bis*-electrophiles. To detect DPC formation *in vivo*, one must devise a plan to isolate genomic DNA along with covalently-bound proteins and remove any non-covalently bound proteins. These cross-linked proteins can then be identified using mass spectrometry and immunological approaches.

Previous studies employed the commercial reagent DNAzol (Invitrogen, Carlsbad, CA) to isolate DPCs from cells *(59)*. DNAzol is a novel reagent used for the isolation of genomic DNA from both solid and liquid samples of animal, plant, or bacterial origin. Through the use of a proprietary guanidine-detergent lysing solution, the fast, selective precipitation of DNA from the cell lysate is achieved *(59)*.
Our preliminary studies attempted to use DNAzol to isolate mechlorethamine-induced DPCs. Unfortunately, poor results were obtained due to the poor solubility of chromosomal DNA following the SDS/urea/sodium chloride washing steps (results not shown).

An alternative strategy to isolate DPCs from cells could employ phenol/chloroform extraction and anion exchange chromatography to isolate DNA along with any covalently attached proteins (*Scheme 8.1*). Following drug treatment, cells will be lysed using a buffer containing TRIS, EDTA, and SDS. Phenol/chloroform extraction will be used to remove proteins that are not associated with DNA. Cellular DNA and

Scheme 8.1 Detection of DNA-protein cross-links in treated cells

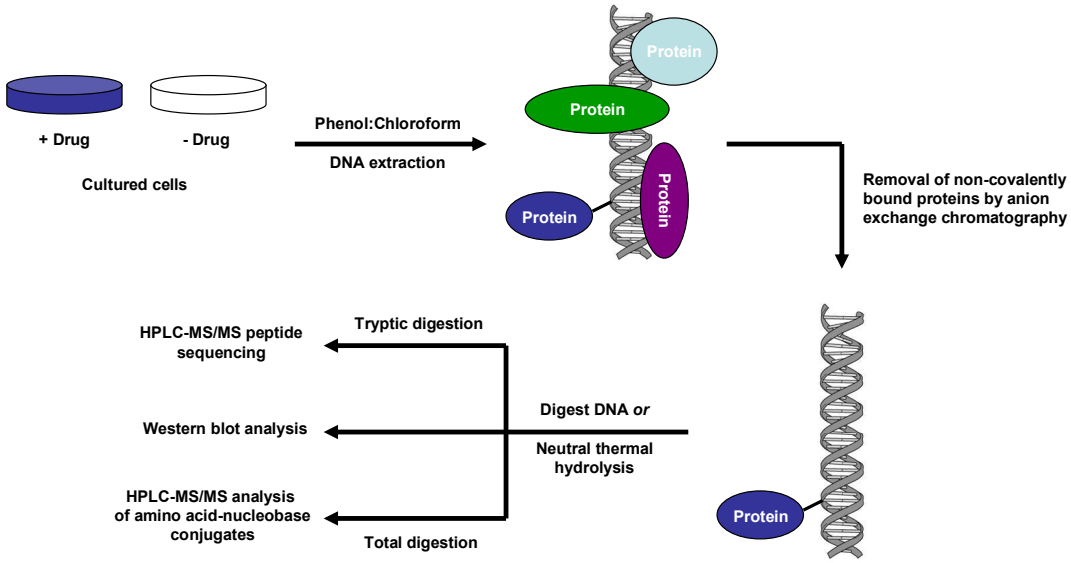

DPCs will then undergo further purification *via* anion exchange chromatography on Nucleobond AX cartridges (Macherey-Nagel, Düren). Following elution from the column and ethanol precipitation, the resulting DNA will be digested with nuclease P1. Proteins will be identified by SDS-PAGE/Western blotting or SDS-PAGE/MS analysis of tryptic peptides. Further information about adduct structures will be obtained from HPLC-ESI$^+$-MS/MS analysis of amino acid-guanine conjugates obtained from total digests of DPCs with trypsin, carboxypeptidase Y, and proteinase K.

8.2 Determine the Genotoxic Effects of DPCs in Mammalian Cells

In previous studies of DPCs induced by bifunctional alkylating agents, some of the results are difficult to interpret because of the propensity of these agents produce other types of damage, including monoalkylated lesions to DNA and proteins, DNA-DNA cross-links, single- and double-stranded DNA breaks, and abasic sites *(1)*. In order to assess the contribution of DPCs to cytotoxicity and mutagenicity of *bis*-electrophiles, methods are needed to selectively introduce DPCs into cells. One way of achieving this involves nuclear translocation of a protein/peptide containing a reactive group capable of reacting with chromosomal DNA to induce DPCs.

While large biomolecules (proteins/peptides, DNA/oligodeoxynucleotides) are not readily taken up by cells since they do not efficiently cross the plasma membrane, several techniques (electroporation, liposome encapsulation, and microinjection) have been developed which aid in this process *(223)*. Unfortunately, transfer efficiency associated with these methods is generally low and can result in cytotoxicity. More

recently, several peptides have been identified that can aid in the cellular uptake of biomolecules *(224)*.

Human immunodeficiency virus (HIV) contains several *trans*-acting regulatory genes, including *tat*, which encodes for a 14 kDa protein that acts to stimulate viral gene expression *(224)*. The Tat protein is efficiently taken up by cells, and a region of the protein centered on a cluster of basic amino acids (RKKRRQRRR) is critical for the translocation activity. Studies in which this sequence of basic amino acids was fused onto the N-terminus of various other proteins resulted in their nuclear translocation *(223)*.

Capitalizing on its propensity for cellular uptake, we propose to transfect cells with a Tat-derived peptide (YGRKKRRQRRRC) containing an N-terminal fluorescent tag and a monoalkyled lesion at the cysteine sulfhydryl (*Scheme 8.2*). Upon synthesis of the fluorescently-labeled peptide, the monoalkylated form will be prepared *via* incubation of the peptide with the corresponding *bis*-electrophile, followed by HPLC purification. Due to its ability to withstand HPLC purification, initial studies will focus on the ability of DEB to induce DPCs through the preparation of a peptide containing a DEB-mediated monoepoxide lesion. Because we are interested in the genotoxic contributions of DPCs, removal of excess cross-linker is essential.

HeLa cells will then be incubated with the monoalkylated peptide or with the unmodified Tat peptide. Because of the presence of the fluorescent tag, we can determine the extent of peptide accumulation in the nucleus by confocal microscopy. By treating cells with various concentrations of both the monoalkylated Tat peptide and the unmodified control, the effect this peptide (and thus DPC formation) has in terms of cytotoxicity and mutagenicity can be established (*see Chapter V*).

Scheme 8.2 Determine the genotoxic effects of DNA-protein cross-links in cells: Tat peptide

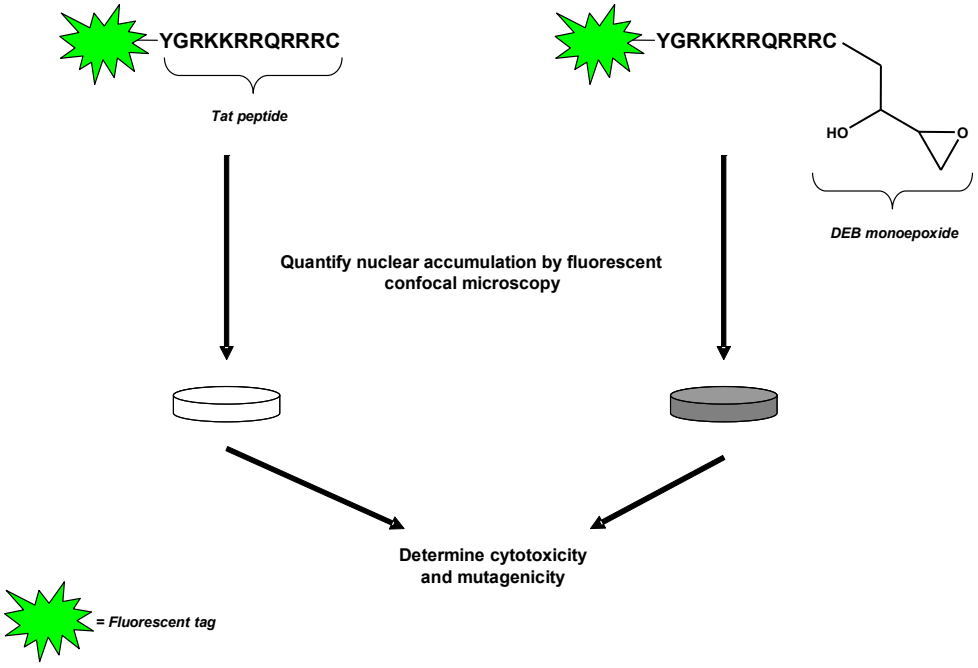

8.3 Examine DPC Repair *In Vitro* and *In Cultured Cells*

As DPCs are likely to disrupt normal DNA-protein interactions by blocking important cellular functions including DNA replication and transcription, their elimination from chromatin is essential for cell survival. Previous studies looking at DPC repair provided conflicting/incomplete information regarding which DNA repair systems are involved in the removal of DPCs. While NER-coupled proteolysis and HRR have both been implicated in DPC repair *(26;29)*, the relative contributions of each pathway towards the removal of DPCs is unclear. The hypothesis that DPCs are preferentially eliminated by a particular repair system based upon their size, the nature of the cross-linking agent involved, and the protein's identity is also yet to be systematically tested.

To identify the molecular mechanism(s) responsible for the recognition and removal of DPCs in mammalian cells, synthetic DNA substrates containing structurally-defined DPC lesions will be prepared by hybridizing and subsequently ligating a series of single-stranded oligodeoxynucleotides containing the reactive nucleotide analog 8-oxo-dG at a specified site which can then undergo photooxidation in the presence of various target proteins (*Figure 8.1*) *(16)*.

To examine DPC repair *in vitro*, synthetic DNA substrates containing DPCs will be radiolabeled and incubated with nuclear protein extracts from HeLa cells. The resulting excision products will then be analyzed by gel electrophoresis. Because different repair mechanisms (NER, BER, double-strand break repair) generate different length excision products, we will be able to determine which pathway is facilitating DPC repair. The contribution of proteolytic degradation in DPC removal can also be assessed *via* a similar approach in which the DPC substrate is incubated with nuclear protein

Figure 8.1 Oxidative DNA-protein cross-linking *via* 8-oxo-dG

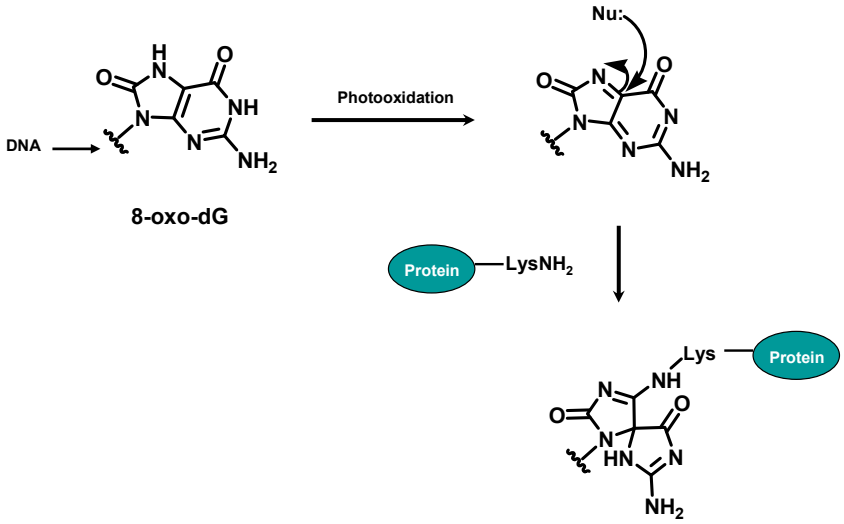

extract in the presence of a commercially-available proteasome inhibitor followed by SDS-PAGE of radiolabeled products.

To study DPC repair in cultured cells, the same 8-ox-dG-containing duplex mentioned above will be ligated into a plasmid, photooxidized in the presence of protein to induce DPC formation, and the entire vector will be electroporated into cells. Similar to the *in vitro* assay, DPC repair will be assessed based upon the fate of the DNA, this time in terms of plasmid function *via* gene expression. As the presence of the DPC will block expression of a reporter gene, its removal will ultimately restore gene function, allowing for a quantitative means of detecting DPC repair.

IX. BIBLIOGRAPHY

(1) Barker, S., Weinfeld, M., and Murray, D. (2005) DNA-protein crosslinks: their induction, repair, and biological consequences. *Mutat. Res.* **589**(2), 111-135.

(2) Quievryn, G., and Zhitkovich, A. (2000) Loss of DNA-protein crosslinks from formaldehyde-exposed cells occurs through spontaneous hydrolysis and an active repair process linked to proteosome function. *Carcinogenesis* **21**(8), 1573-1580.

(3) Crosby, R. M., Richardson, K. K., Craft, T. R., Benforado, K. B., Liber, H. L., and Skopek, T. R. (1988) Molecular analysis of formaldehyde-induced mutations in human lymphoblasts and E. coli. *Environ. Mol. Mutagen.* **12**(2), 155-166.

(4) Heck, H. D., Casanova, M., and Starr, T. B. (1990) Formaldehyde toxicity--new understanding. *Crit Rev. Toxicol.* **20**(6), 397-426.

(5) Shaham, J., Bomstein, Y., Meltzer, A., Kaufman, Z., Palma, E., and Ribak, J. (1996) DNA--protein crosslinks, a biomarker of exposure to formaldehyde--in vitro and in vivo studies. *Carcinogenesis* **17**(1), 121-125.

(6) Merk, O., and Speit, G. (1998) Significance of formaldehyde-induced DNA-protein crosslinks for mutagenesis. *Environ. Mol. Mutagen.* **32**(3), 260-268.

(7) Dunnick, J. K., Elwell, M. R., Radovsky, A. E., Benson, J. M., Hahn, F. F., Nikula, K. J., Barr, E. B., and Hobbs, C. H. (1995) Comparative carcinogenic effects of nickel subsulfide, nickel oxide, or nickel sulfate hexahydrate chronic exposures in the lung. *Cancer Res.* **55**(22), 5251-5256.

(8) Zhitkovich, A., Voitkun, V., Kluz, T., and Costa, M. (1998) Utilization of DNA-protein cross-links as a biomarker of chromium exposure. *Environ. Health Perspect.* **106 Suppl 4**, 969-974.

(9) Chen, C. J., Chen, C. W., Wu, M. M., and Kuo, T. L. (1992) Cancer potential in liver, lung, bladder and kidney due to ingested inorganic arsenic in drinking water. *Br. J. Cancer* **66**(5), 888-892.

(10) Mattagajasingh, S. N., and Misra, H. P. (1999) Analysis of EDTA-chelatable proteins from DNA-protein crosslinks induced by a carcinogenic chromium(VI) in cultured intact human cells. *Mol. Cell Biochem.* **199**(1-2), 149-162.

(11) Barker, S., Weinfeld, M., Zheng, J., Li, L., and Murray, D. (2005) Identification of mammalian proteins cross-linked to DNA by ionizing radiation. *J. Biol. Chem.* **280**(40), 33826-33838.

(12) Weir Lipton, M. S., Fuciarelli, A. F., Springer, D. L., and Edmonds, C. G. (1996) Characterization of radiation-induced thymine-tyrosine crosslinks by electrospray ionization mass spectrometry. *Radiat. Res.* **145**(6), 681-686.

(13) Zhang, H., and Wheeler, K. T. (1993) Radiation-induced DNA damage in tumors and normal tissues. I. Feasibility of estimating the hypoxic fraction. *Radiat. Res.* **136**(1), 77-88.

(14) Zhang, H., and Wheeler, K. T. (1994) Radiation-induced DNA damage in tumors and normal tissues. II. Influence of dose, residual DNA damage and physiological factors in oxygenated cells. *Radiat. Res.* **140**(3), 321-326.

(15) Zhang, H., Koch, C. J., Wallen, C. A., and Wheeler, K. T. (1995) Radiation-induced DNA damage in tumors and normal tissues. III. Oxygen dependence of the formation of strand breaks and DNA-protein crosslinks. *Radiat. Res.* **142**(2), 163-168.

(16) Hickerson, R. P., Chepanoske, C. L., Williams, S. D., David, S. S., and Burrows, C. J. (1999) Mechanism-Based DNA-Protein Cross-Linking of MutY via Oxidation of 8-Oxoguanosine. *J. Am. Chem. Soc.* **121**(42), 9901-9902.

(17) Johansen, M. E., Muller, J. G., Xu, X., and Burrows, C. J. (2005) Oxidatively induced DNA-protein cross-linking between single-stranded binding protein and oligodeoxynucleotides containing 8-oxo-7,8-dihydro-2'-deoxyguanosine. *Biochemistry* **44**(15), 5660-5671.

(18) Xu, X., Fleming, A. M., Muller, J. G., and Burrows, C. J. (2008) Formation of tricyclic [4.3.3.0] adducts between 8-oxoguanosine and tyrosine under conditions of oxidative DNA-protein cross-linking. *J. Am. Chem. Soc.* **130**(31), 10080-10081.

(19) Murata-Kamiya, N., and Kamiya, H. (2001) Methylglyoxal, an endogenous aldehyde, crosslinks DNA polymerase and the substrate DNA. *Nucleic Acids Res.* **29**(16), 3433-3438.

(20) Roberts, M. J., Wondrak, G. T., Laurean, D. C., Jacobson, M. K., and Jacobson, E. L. (2003) DNA damage by carbonyl stress in human skin cells. *Mutat. Res.* **522**(1-2), 45-56.

(21) Zwelling, L. A., Anderson, T., and Kohn, K. W. (1979) DNA-protein and DNA interstrand cross-linking by cis- and trans-platinum(II) diamminedichloride in L1210 mouse leukemia cells and relation to cytotoxicity. *Cancer Res.* **39**(2 Pt 1), 365-369.

(22) Masuda, K., Nakamura, T., Mizota, T., Mori, J., and Shimomura, K. (1988) Interstrand DNA-DNA and DNA-protein cross-links by a new antitumor antibiotic, FK973, in L1210 cells. *Cancer Res.* **48**(18), 5172-5177.

(23) Ewig, R. A., and Kohn, K. W. (1978) DNA-protein cross-linking and DNA interstrand cross-linking by haloethylnitrosoureas in L1210 cells. *Cancer Res.* **38**(10), 3197-3203.

(24) Cupo, D. Y., and Wetterhahn, K. E. (1985) Binding of chromium to chromatin and DNA from liver and kidney of rats treated with sodium dichromate and chromium(III) chloride in vivo. *Cancer Res.* **45**(3), 1146-1151.

(25) Oleinick, N. L., Chiu, S. M., Ramakrishnan, N., and Xue, L. Y. (1987) The formation, identification, and significance of DNA-protein cross-links in mammalian cells. *Br. J. Cancer Suppl* **8**, 135-140.

(26) Baker, D. J., Wuenschell, G., Xia, L., Termini, J., Bates, S. E., Riggs, A. D., and O'Connor, T. R. (2007) Nucleotide excision repair eliminates unique DNA-protein cross-links from mammalian cells. *J. Biol. Chem.* **282**(31), 22592-22604.

(27) Reardon, J. T., Cheng, Y., and Sancar, A. (2006) Repair of DNA-protein cross-links in mammalian cells. *Cell Cycle* **5**(13), 1366-1370.

(28) Thompson, L. H. (1996) Evidence that mammalian cells possess homologous recombinational repair pathways. *Mutat. Res.* **363**(2), 77-88.

(29) Nakano, T., Morishita, S., Katafuchi, A., Matsubara, M., Horikawa, Y., Terato, H., Salem, A. M., Izumi, S., Pack, S. P., Makino, K., and Ide, H. (2007) Nucleotide excision repair and homologous recombination systems commit differentially to the repair of DNA-protein crosslinks. *Mol. Cell* **28**(1), 147-158.

(30) Reynolds, M., Peterson, E., Quievryn, G., and Zhitkovich, A. (2004) Human nucleotide excision repair efficiently removes chromium-DNA phosphate adducts and protects cells against chromate toxicity. *J. Biol. Chem.* **279**(29), 30419-30424.

(31) Murray, D., and Meyn, R. E. (1986) Cell cycle-dependent cytotoxicity of alkylating agents: determination of nitrogen mustard-induced DNA cross-links and their repair in Chinese hamster ovary cells synchronized by centrifugal elutriation. *Cancer Res.* **46**(5), 2324-2329.

(32) Murray, D., Vallee-Lucic, L., Rosenberg, E., and Andersson, B. (2002) Sensitivity of nucleotide excision repair-deficient human cells to ionizing radiation and cyclophosphamide. *Anticancer Res.* **22**(1A), 21-26.

(33) Meyn, R. E., Vanankeren, S. C., and Jenkins, W. T. (1987) The induction of DNA-protein crosslinks in hypoxic cells and their possible contribution to cell lethality. *Radiat. Res.* **109**(3), 419-429.

(34) Murray, D., and Rosenberg, E. (1996) The importance of the ERCC1/ERCC4[XPF] complex for hypoxic-cell radioresistance does not appear to derive from its participation in the nucleotide excision repair pathway. *Mutat. Res.* **364**(3), 217-226.

(35) Kasparkova, J., Novakova, O., Vrana, O., Intini, F., Natile, G., and Brabec, V. (2006) Molecular aspects of antitumor effects of a new platinum(IV) drug. *Mol. Pharmacol.* **70**(5), 1708-1719.

(36) Kloster, M., Kostrhunova, H., Zaludova, R., Malina, J., Kasparkova, J., Brabec, V., and Farrell, N. (2004) Trifunctional dinuclear platinum complexes as DNA-protein cross-linking agent. *Biochemistry* **43**(24), 7776-7786.

(37) Loeber, R., Rajesh, M., Fang, Q., Pegg, A. E., and Tretyakova, N. (2006) Cross-linking of the human DNA repair protein O^6-alkylguanine DNA alkyltransferase to DNA in the presence of 1,2,3,4-diepoxybutane. *Chem. Res. Toxicol.* **19**(5), 645-654.

(38) Loeber, R., Michaelson, E., Fang, Q., Campbell, C., Pegg, A. E., and Tretyakova, N. (2008) Cross-linking of the DNA repair protein Omicron6-alkylguanine DNA alkyltransferase to DNA in the presence of antitumor nitrogen mustards. *Chem. Res. Toxicol.* **21**(4), 787-795.

(39) Kohn, K. W. (1981) DNA damage in mammalian cells. *BioScience* **31**(8), 593-597.

(40) Ewig, R. A., and Kohn, K. W. (1978) DNA-protein cross-linking and DNA interstrand cross-linking by haloethylnitrosoureas in L1210 cells. *Cancer Res.* **38**(10), 3197-3203.

(41) Ross, W. E., Ewig, R. A., and Kohn, K. W. (1978) Differences between melphalan and nitrogen mustard in the formation and removal of DNA cross-links. *Cancer Res.* **38**(6), 1502-1506.

(42) Thomas, C. B., Kohn, K. W., and Bonner, W. M. (1978) Characterization of DNA-protein cross-links formed by treatment of L1210 cells and nuclei with bis(2-chloroethyl)methylamine (nitrogen mustard). *Biochemistry* **17**(19), 3954-3958.

(43) Merk, O., Reiser, K., and Speit, G. (2000) Analysis of chromate-induced DNA-protein crosslinks with the comet assay. *Mutat. Res.* **471**(1-2), 71-80.

(44) Merk, O., and Speit, G. (1999) Detection of crosslinks with the comet assay in relationship to genotoxicity and cytotoxicity. *Environ. Mol. Mutagen.* **33**(2), 167-172.

(45) Zhitkovich, A., and Costa, M. (1992) A simple, sensitive assay to detect DNA-protein crosslinks in intact cells and in vivo. *Carcinogenesis* **13**(8), 1485-1489.

(46) Costa, M., Zhitkovich, A., Harris, M., Paustenbach, D., and Gargas, M. (1997) DNA-protein cross-links produced by various chemicals in cultured human lymphoma cells. *J. Toxicol. Environ. Health* **50**(5), 433-449.

(47) Costa, M., Zhitkovich, A., Toniolo, P., Taioli, E., Popov, T., and Lukanova, A. (1996) Monitoring human lymphocytic DNA-protein cross-links as biomarkers of biologically active doses of chromate. *Environ. Health Perspect.* **104 Suppl 5**, 917-919.

(48) Park, S., Anderson, C., Loeber, R., Seetharaman, M., Jones, R., and Tretyakova, N. (2005) Interstrand and intrastrand DNA-DNA cross-linking by 1,2,3,4-diepoxybutane: role of stereochemistry. *J. Am. Chem. Soc.* **127**(41), 14355-14365.

(49) Goggin, M., Loeber, R., Park, S., Walker, V., Wickliffe, J., and Tretyakova, N. (2007) HPLC-ESI+-MS/MS analysis of N7-guanine-N7-guanine DNA cross-links in tissues of mice exposed to 1,3-butadiene. *Chem. Res. Toxicol.* **20**(5), 839-847.

(50) Balcome, S., Park, S., Quirk Dorr, D. R., Hafner, L., Phillips, L., and Tretyakova, N. (2004) Adenine-containing DNA-DNA cross-links of antitumor nitrogen mustards. *Chem. Res. Toxicol.* **17**(7), 950-962.

(51) Hoes, I., Van, D. W., Lemiere, F., Esmans, E. L., Van, B. D., and Berneman, Z. N. (2000) Comparison between capillary and nano liquid chromatography-electrospray mass spectrometry for the analysis of minor DNA-melphalan adducts. *J. Chromatogr. B Biomed. Sci. Appl.* **748**(1), 197-212.

(52) Wang, Y., Zhang, Q., and Wang, Y. (2004) Tandem mass spectrometry for the determination of the sites of DNA interstrand cross-link. *J. Am. Soc. Mass Spectrom.* **15**(11), 1565-1571.

(53) Smith, J. C., Lambert, J. P., Elisma, F., and Figeys, D. (2007) Proteomics in 2005/2006: developments, applications and challenges. *Anal. Chem.* **79**(12), 4325-4343.

(54) Wong, D. L., Pavlovich, J. G., and Reich, N. O. (1998) Electrospray ionization mass spectrometric characterization of photocrosslinked DNA-EcoRI DNA methyltransferase complexes. *Nucleic Acids Res.* **26**(2), 645-649.

(55) Wong, D. L., and Reich, N. O. (2000) Identification of tyrosine 204 as the photo-cross-linking site in the DNA-EcoRI DNA methyltransferase complex by electrospray ionization mass spectrometry. *Biochemistry* **39**(50), 15410-15417.

(56) Steen, H., Petersen, J., Mann, M., and Jensen, O. N. (2001) Mass spectrometric analysis of a UV-cross-linked protein-DNA complex: tryptophans 54 and 88 of E. coli SSB cross-link to DNA. *Protein Sci.* **10**(10), 1989-2001.

(57) Liu, L., Hachey, D. L., Valadez, G., Williams, K. M., Guengerich, F. P., Loktionova, N. A., Kanugula, S., and Pegg, A. E. (2004) Characterization of a mutagenic DNA adduct formed from 1,2-dibromoethane by O6-alkylguanine-DNA alkyltransferase. *J. Biol. Chem.* **279**(6), 4250-4259.

(58) Olinski, R., Nackerdien, Z., and Dizdaroglu, M. (1992) DNA-protein cross-linking between thymine and tyrosine in chromatin of gamma-irradiated or H2O2-treated cultured human cells. *Arch. Biochem. Biophys.* **297**(1), 139-143.

(59) Barker, S., Murray, D., Zheng, J., Li, L., and Weinfeld, M. (2005) A method for the isolation of covalent DNA-protein crosslinks suitable for proteomics analysis. *Anal. Biochem.* **344**(2), 204-215.

(60) Eng, J. K., McCormack, A. L., and Yates, J. R. (1994) An approach to correlate tandem mass spectral data of peptides with amino acid sequences in a protein database. *Journal of the American Society for Mass Spectrometry* **5**(11), 976-989.

(61) Huff, J. E., Melnick, R. L., Solleveld, H. A., Haseman, J. K., Powers, M., and Miller, R. A. (1985) Multiple organ carcinogenicity of 1,3-butadiene in B6C3F1 mice after 60 weeks of inhalation exposure. *Science* **227**(4686), 548-549.

(62) Birch, S. F. (1929) Preparation of Butadiene. *Industrial and Engineering Chemistry* **20**(5), 474.

(63) Fred, C., Haglund, J., Alsberg, T., Rydberg, P., Minten, J., and Tornqvist, M. (2004) Characterization of alkyl-cobalamins formed on trapping of epoxide metabolites of 1,3-butadiene. *J. Sep. Sci.* **27**(7-8), 607-612.

(64) Pelz, N., Dempster, N. M., and Shore, P. R. (1990) Analysis of low molecular weight hydrocarbons including 1,3-butadiene in engine exhaust gases using an aluminum oxide porus-layer open-tubular fused-silica column. *J. Chromatogr. Sci.* **28**(5), 230-235.

(65) Brunnemann, K. D., Kagen, M. R., Cox, J. E., and Hoffmann, D. (1990) Analysis of 1,3-butadiene and other selected gas-phase componentsin cigarette mainstream and sidestream smoke by gas chromatography-mass selective detection. *Carcinogenesis* **11**(10), 1863-1868.

(66) Hecht, S. S. (1999) Tobacco smoke carcinogens and lung cancer. *J. Natl. Cancer Inst.* **91**(14), 1194-1210.

(67) Merritt, W. K., Nechev, L. V., Scholdberg, T. A., Dean, S. M., Kiehna, S. E., Chang, J. C., Harris, T. M., Harris, C. M., Lloyd, R. S., and Stone, M. P. (2005) Structure of the 1,4-bis(2'-deoxyadenosin-N6-yl)-2R,3R-butanediol cross-link arising from alkylation of the human N-ras codon 61 by butadiene diepoxide. *Biochemistry* **44**(30), 10081-10092.

(68) Ward, J. B., Jr., Ammenheuser, M. M., Whorton, E. B., Jr., Bechtold, W. E., Kelsey, K. T., and Legator, M. S. (1996) Biological monitoring for mutagenic effects of occupational exposure to butadiene. *Toxicology* **113**(1-3), 84-90.

(69) Sram, R. J., Rossner, P., Peltonen, K., Podrazilova, K., Mrackova, G., Demopoulos, N. A., Stephanou, G., Vlachodimitropoulos, D., Darroudi, F., and Tates, A. D. (1998) Chromosomal aberrations, sister-chromatid exchanges, cells with high frequency of SCE, micronuclei and comet assay parameters in 1, 3-butadiene-exposed workers. *Mutat. Res.* **419**(1-3), 145-154.

(70) de Meester, C. (1988) Genotoxic properties of 1,3-butadiene. *Mutat. Res.* **195**(3), 273-281.

(71) Macaluso, M., Larson, R., Delzell, E., Sathiakumar, N., Hovinga, M., Julian, J., Muir, D., and Cole, P. (1996) Leukemia and cumulative exposure to butadiene, styrene and benzene among workers in the synthetic rubber industry. *Toxicology* **113**(1-3), 190-202.

(72) de Meester, C., Poncelet, F., Roberfroid, M., and Mercier, M. (1980) The mutagenicity of butadiene towards Salmonella typhimurium. *Toxicol. Lett.* **6**(3), 125-130.

(73) Malvoisin, E., and Roberfroid, M. (1982) Hepatic microsomal metabolism of 1,3-butadiene. *Xenobiotica* **12**(2), 137-144.

(74) Verly, W. G., Brakier, L., and Feit, P. W. (1971) Inactivation of the T7 coliphage by the diepoxybutane stereoisomers. *Biochim. Biophys. Acta* **228**(2), 400-406.

(75) Matagne, R. (1969) Induction of chromosomal aberrations and mutations with isomeric forms of L-threitol-I,4-bismethanesulfonate in plant materials. *Mutat. Res.* **7**(2), 241-247.

(76) Bianchi, A., and Contin, M. (1962) Mutagenic activity of isomeric forms of diepoxybutane in maize. *J. Heredity* **53**, 277-281.

(77) Runowicz, C. D., Fields, A. L., and Goldberg, G. L. (1995) Promising new therapies in the treatment of advanced ovarian cancer. *Cancer* **76**(10 Suppl), 2028-2033.

(78) Hartley, J. A., O'Hare, C. C., and Baumgart, J. (1999) DNA alkylation and interstrand cross-linking by treosulfan. *Br. J. Cancer* **79**(2), 264-266.

(79) Schmidmaier, R., Oellerich, M., Baumgart, J., Emmerich, B., and Meinhardt, G. (2004) Treosulfan-induced apoptosis in acute myeloid leukemia cells is accompanied by translocation of protein kinase C delta and enhanced by bryostatin-1. *Exp. Hematol.* **32**(1), 76-86.

(80) Sasiadek, M., Norppa, H., and Sorsa, M. (1991) 1,3-Butadiene and its epoxides induce sister-chromatid exchanges in human lymphocytes in vitro. *Mutat. Res.* **261**(2), 117-121.

(81) Cochrane, J. E., and Skopek, T. R. (1994) Mutagenicity of butadiene and its epoxide metabolites: I. Mutagenic potential of 1,2-epoxybutene, 1,2,3,4-diepoxybutane and 3,4-epoxy-1,2- butanediol in cultured human lymphoblasts. *Carcinogenesis* **15**(4), 713-717.

(82) Park, S., and Tretyakova, N. (2004) Structural Characterization of the Major DNA-DNA Cross-Link of 1,2,3,4-Diepoxybutane. *Chem. Res. Toxicol.* **17**(2), 129-136.

(83) Park, S., Hodge, J., Anderson, C., and Tretyakova NY. (2004) Guanine-adenine cross-linking by 1,2,3,4-diepoxybutane: potential basis for biological activity. *Chem. Res. Toxicol.* **17**, 1638-1651.

(84) Lawley, P. D., and Brookes, P. (1967) Interstrand cross-linking of DNA by difunctional alkylating agents. *J. Mol. Biol.* **25**(1), 143-160.

(85) Lawley, P. D., and Brookes, P. (1965) Molecular mechanism of the cytotoxic action of difunctional alkylating agents and of resistance to this action. *Nature* **206**(983), 480-483.

(86) Antsypovich, S., Quirk Dorr, D., Pitts, C., and Tretyakova, N. (2007) Site specific N^6-(2-hydroxy-3,4-epoxybuty-1-yl)adenine oligodeoxynucleotide adducts of 1,2,3,4-diepoxybutane: synthesis and stability at physiological pH. *Chem. Res. Toxicol.* **20**, 641-649.

(87) Dirven, H. A., van Ommen, B., and van Bladeren, P. J. (1996) Glutathione conjugation of alkylating cytostatic drugs with a nitrogen mustard group and the role of glutathione S-transferases. *Chem. Res. Toxicol.* **9**(2), 351-360.

(88) Hall, A. G., and Tilby, M. J. (1992) Mechanisms of action of, and modes of resistance to, alkylating agents used in the treatment of haematological malignancies. *Blood Rev.* **6**(3), 163-173.

(89) Gilman, A., and Philips, F. S. (1946) The Biological Actions and Therapeutic Applications of the B-Chloroethyl Amines and Sulfides. *Science* **103**(2675), 409-436.

(90) Gamcsik, M. P., Hamill, T. G., and Colvin, M. (1990) NMR studies of the conjugation of mechlorethamine with glutathione. *J. Med. Chem.* **33**(3), 1009-1014.

(91) Dulik, D. M., Colvin, O. M., and Fenselau, C. (1990) Characterization of glutathione conjugates of chlorambucil by fast atom bombardment and thermospray liquid chromatography/mass spectrometry. *Biomed. Environ. Mass Spectrom.* **19**(4), 248-252.

(92) Bank, B. B., Kanganis, D., Liebes, L. F., and Silber, R. (1989) Chlorambucil pharmacokinetics and DNA binding in chronic lymphocytic leukemia lymphocytes. *Cancer Res.* **49**(3), 554-559.

(93) Goldenberg, G. J., Lam, H. Y., and Begleiter, A. (1979) Active carrier-mediated transport of melphalan by two separate amino acid transport systems in LPC-1 plasmacytoma cells in vitro. *J. Biol. Chem.* **254**(4), 1057-1064.

(94) Chang, T. K., Weber, G. F., Crespi, C. L., and Waxman, D. J. (1993) Differential activation of cyclophosphamide and ifosphamide by cytochromes P-450 2B and 3A in human liver microsomes. *Cancer Res.* **53**(23), 5629-5637.

(95) Draeger, U., and Hohorst, H. J. (1976) Permeation of cyclophosphamide (NSC-26271) metabolites into tumor cells. *Cancer Treat. Rep.* **60**(4), 423-427.

(96) Kohn, K. W., Hartley, J. A., and Mattes, W. B. (1987) Mechanisms of DNA sequence selective alkylation of guanine-N7 positions by nitrogen mustards. *Nucleic Acids Res.* **15**(24), 10531-10549.

(97) Rink, S. M., Solomon, M. S., Taylor, M. J., Rajur, S. B., McLaughlin, L. W., and Hopkins, P. B. (1993) Covalent structure of a nitrogen mustard-induced DNA interstrand cross-link: An N^7-to-N^7 linkage of deoxyguanosine residues at the duplex sequence 5'-d(GNC). *J. Am. Chem. Soc.* **115**, 2551-2557.

(98) Osborne, M. R., Wilman, D. E., and Lawley, P. D. (1995) Alkylation of DNA by the nitrogen mustard bis(2-chloroethyl)methylamine. *Chem. Res. Toxicol.* **8**(2), 316-320.

(99) Haapala, E., Hakala, K., Jokipelto, E., Vilpo, J., and Hovinen, J. (2001) Reactions of N,N-bis(2-chloroethyl)-p-aminophenylbutyric acid (chlorambucil) with 2'-deoxyguanosine. *Chem. Res. Toxicol.* **14**(8), 988-995.

(100) Ewig, R. A., and Kohn, K. W. (1977) DNA damage and repair in mouse leukemia L1210 cells treated with nitrogen mustard, 1,3-bis(2-chloroethyl)-1-nitrosourea, and other nitrosoureas. *Cancer Res.* **37**(7 Pt 1), 2114-2122.

(101) Pegg, A. E. (2000) Repair of O^6-alkylguanine by alkyltransferases. *Mutat. Res.* **462**(2-3), 83-100.

(102) Dumenco, L. L., Allay, E., Norton, K., and Gerson, S. L. (1993) The prevention of thymic lymphomas in transgenic mice by human O6-alkylguanine-DNA alkyltransferase. *Science* **259**(5092), 219-222.

(103) Lim, I. K., Park, T. J., Jee, J. W., Lee, M. S., and Paik, W. K. (1999) Differential expression of O6-methylguanine-DNA methyltransferase during diethylnitrosamine-induced carcinogenesis and liver regeneration in Sprague-Dawley male rats. *J. Cancer Res. Clin. Oncol.* **125**(8-9), 493-499.

(104) Peterson, L. A., Thomson, N. M., Crankshaw, D. L., Donaldson, E. E., and Kenney, P. J. (2001) Interactions between methylating and pyridyloxobutylating agents in A/J mouse lungs: implications for 4-(methylnitrosamino)-1-(3-pyridyl)-1- butanone-induced lung tumorigenesis. *Cancer Res.* **61**(15), 5757-5763.

(105) Zaidi, N. H., Pretlow, T. P., O'Riordan, M. A., Dumenco, L. L., Allay, E., and Gerson, S. L. (1995) Transgenic expression of human MGMT protects against azoxymethane-induced aberrant crypt foci and G to A mutations in the K-ras oncogene of mouse colon. *Carcinogenesis* **16**(3), 451-456.

(106) Gerson, S. L. (2004) MGMT: its role in cancer aetiology and cancer therapeutics. *Nat. Rev. Cancer* **4**(4), 296-307.

(107) Gerson, S. L. (2002) Clinical relevance of MGMT in the treatment of cancer. *J. Clin. Oncol.* **20**(9), 2388-2399.

(108) Daniels, D. S., Mol, C. D., Arvai, A. S., Kanugula, S., Pegg, A. E., and Tainer, J. A. (2000) Active and alkylated human AGT structures: a novel zinc site, inhibitor and extrahelical base binding. *EMBO J* **19**(7), 1719-1730.

(109) Moore, M. H., Gulbis, J. M., Dodson, E. J., Demple, B., and Moody, P. C. (1994) Crystal structure of a suicidal DNA repair protein: the Ada O6-methylguanine-DNA methyltransferase from E. coli. *EMBO J.* **13**(7), 1495-1501.

(110) Daniels, D. S., Woo, T. T., Luu, K. X., Noll, D. M., Clarke, N. D., Pegg, A. E., and Tainer, J. A. (2004) DNA binding and nucleotide flipping by the human DNA repair protein AGT. *Nat. Struct. Mol. Biol.* **11**(8), 714-720.

(111) Pegg, A. E., Dolan, M. E., and Moschel, R. C. (1995) Structure, function, and inhibition of O6-alkylguanine-DNA alkyltransferase. *Prog. Nucleic Acid Res. Mol. Biol.* **51**, 167-223.

(112) Goodtzova, K., Kanugula, S., Edara, S., and Pegg, A. E. (1998) Investigation of the role of tyrosine-114 in the activity of human O6-alkylguanine-DNA alkyltranferase. *Biochemistry* **37**(36), 12489-12495.

(113) Guengerich, F. P., Fang, Q., Liu, L., Hachey, D. L., and Pegg, A. E. (2003) O^6-alkylguanine-DNA alkyltransferase: low pKa and high reactivity of cysteine 145. *Biochemistry* **42**(37), 10965-10970.

(114) Daniels, D. S., and Tainer, J. A. (2000) Conserved structural motifs governing the stoichiometric repair of alkylated DNA by O(6)-alkylguanine-DNA alkyltransferase. *Mutat. Res.* **460**(3-4), 151-163.

(115) Rasimas, J. J., Pegg, A. E., and Fried, M. G. (2003) DNA-binding mechanism of *O^6*-alkylguanine-DNA alkyltransferase. Effects of protein and DNA alkylation on complex stability. *J. Biol. Chem* **278**(10), 7973-7980.

(116) Coulter, R., Blandino, M., Tomlinson, J. M., Pauly, G. T., Krajewska, M., Moschel, R. C., Peterson, L. A., Pegg, A. E., and Spratt, T. E. (2007) Differences in the rate of repair of O6-alkylguanines in different sequence contexts by O6-alkylguanine-DNA alkyltransferase. *Chem. Res. Toxicol.* **20**(12), 1966-1971.

(117) Rasimas, J. J., Dalessio, P. A., Ropson, I. J., Pegg, A. E., and Fried, M. G. (2004) Active-site alkylation destabilizes human O^6-alkylguanine DNA alkyltransferase. *Protein Sci.* **13**(1), 301-305.

(118) Xu-Welliver, M., and Pegg, A. E. (2002) Degradation of the alkylated form of the DNA repair protein, O(6)-alkylguanine-DNA alkyltransferase. *Carcinogenesis* **23**(5), 823-830.

(119) Pauly, G. T., Hughes, S. H., and Moschel, R. C. (1994) Response of repair-competent and repair-deficient Escherichia coli to three O6-substituted guanines and involvement of methyl-directed mismatch repair in the processing of O6-methylguanine residues. *Biochemistry* **33**(31), 9169-9177.

(120) Rossi, S. C., and Topal, M. D. (1991) Mutagenic frequencies of site-specifically located O6-methylguanine in wild-type Escherichia coli and in a strain deficient in ada-methyltransferase. *J. Bacteriol.* **173**(3), 1201-1207.

(121) Tong, W. P., Kirk, M. C., and Ludlum, D. B. (1982) Formation of the cross-link 1-[N3-deoxycytidyl),2-[N1-deoxyguanosinyl]ethane in DNA treated with N,N'-bis(2-chloroethyl)-N-nitrosourea. *Cancer Res.* **42**(8), 3102-3105.

(122) Zaidi, N. H., Liu, L., and Gerson, S. L. (1996) Quantitative immunohistochemical estimates of O6-alkylguanine-DNA alkyltransferase expression in normal and malignant human colon. *Clin. Cancer Res.* **2**(3), 577-584.

(123) Redmond, S. M., Joncourt, F., Buser, K., Ziemiecki, A., Altermatt, H. J., Fey, M., Margison, G., and Cerny, T. (1991) Assessment of P-glycoprotein, glutathione-based detoxifying enzymes and O6-alkylguanine-DNA alkyltransferase as potential indicators of constitutive drug resistance in human colorectal tumors. *Cancer Res.* **51**(8), 2092-2097.

(124) Moriwaki, S., Nishigori, C., Takebe, H., and Imamura, S. (1992) O6-alkylguanine-DNA alkyltransferase activity in human malignant melanoma. *J. Dermatol. Sci.* **4**(1), 6-10.

(125) Lee, S. M., Rafferty, J. A., Elder, R. H., Fan, C. Y., Bromley, M., Harris, M., Thatcher, N., Potter, P. M., Altermatt, H. J., Perinat-Frey, T., and . (1992) Immunohistological examination of the inter- and intracellular distribution of O6-alkylguanine DNA-alkyltransferase in human liver and melanoma. *Br. J. Cancer* **66**(2), 355-360.

(126) Kokkinakis, D. M., Ahmed, M. M., Delgado, R., Fruitwala, M. M., Mohiuddin, M., and bores-Saavedra, J. (1997) Role of O6-methylguanine-DNA methyltransferase in the resistance of pancreatic tumors to DNA alkylating agents. *Cancer Res.* **57**(23), 5360-5368.

(127) Citron, M., Schoenhaus, M., Graver, M., Hoffman, M., Lewis, M., Wasserman, P., Niederland, M., Kahn, L., White, A., and Yarosh, D. (1993) O6-methylguanine-DNA methyltransferase in human normal and malignant lung tissues. *Cancer Invest* **11**(3), 258-263.

(128) Bobola, M. S., Berger, M. S., Ellenbogen, R. G., Roberts, T. S., Geyer, J. R., and Silber, J. R. (2001) O6-Methylguanine-DNA methyltransferase in pediatric primary brain tumors: relation to patient and tumor characteristics. *Clin. Cancer Res.* **7**(3), 613-619.

(129) Silber, J. R., Blank, A., Bobola, M. S., Ghatan, S., Kolstoe, D. D., and Berger, M. S. (1999) O6-methylguanine-DNA methyltransferase-deficient phenotype in human gliomas: frequency and time to tumor progression after alkylating agent-based chemotherapy. *Clin. Cancer Res.* **5**(4), 807-814.

(130) Chen, Z. P., Yarosh, D., Garcia, Y., Tampieri, D., Mohr, G., Malapetsa, A., Langleben, A., and Panasci, L. C. (1999) Relationship between O6-methylguanine-DNA methyltransferase levels and clinical response induced by chloroethylnitrosourea therapy in glioma patients. *Can. J. Neurol. Sci.* **26**(2), 104-109.

(131) Belanich, M., Randall, T., Pastor, M. A., Kibitel, J. T., Alas, L. G., Dolan, M. E., Schold, S. C., Jr., Gander, M., Lejeune, F. J., Li, B. F., White, A. B., Wasserman, P., Citron, M. L., and Yarosh, D. B. (1996) Intracellular Localization and intercellular heterogeneity of the human DNA repair protein O(6)-methylguanine-DNA methyltransferase. *Cancer Chemother. Pharmacol.* **37**(6), 547-555.

(132) Citron, M., Decker, R., Chen, S., Schneider, S., Graver, M., Kleynerman, L., Kahn, L. B., White, A., Schoenhaus, M., and Yarosh, D. (1991) O6-methylguanine-DNA methyltransferase in human normal and tumor tissue from brain, lung, and ovary. *Cancer Res.* **51**(16), 4131-4134.

(133) Watts, G. S., Pieper, R. O., Costello, J. F., Peng, Y. M., Dalton, W. S., and Futscher, B. W. (1997) Methylation of discrete regions of the O6-methylguanine DNA methyltransferase (MGMT) CpG island is associated with heterochromatinization of the MGMT transcription start site and silencing of the gene. *Mol. Cell Biol.* **17**(9), 5612-5619.

(134) Esteller, M., Hamilton, S. R., Burger, P. C., Baylin, S. B., and Herman, J. G. (1999) Inactivation of the DNA repair gene O6-methylguanine-DNA methyltransferase by promoter hypermethylation is a common event in primary human neoplasia. *Cancer Res.* **59**(4), 793-797.

(135) Kang, G. H., Lee, S., Kim, W. H., Lee, H. W., Kim, J. C., Rhyu, M. G., and Ro, J. Y. (2002) Epstein-barr virus-positive gastric carcinoma demonstrates frequent aberrant methylation of multiple genes and constitutes CpG island methylator phenotype-positive gastric carcinoma. *Am. J. Pathol.* **160**(3), 787-794.

(136) Dolan, M. E., Moschel, R. C., and Pegg, A. E. (1990) Depletion of mammalian O6-alkylguanine-DNA alkyltransferase activity by O6-benzylguanine provides a means to evaluate the role of this protein in protection against carcinogenic and therapeutic alkylating agents. *Proc. Natl. Acad. Sci. U. S. A* **87**(14), 5368-5372.

(137) Spiro, T. P., Gerson, S. L., Liu, L., Majka, S., Haaga, J., Hoppel, C. L., Ingalls, S. T., Pluda, J. M., and Willson, J. K. (1999) O6-benzylguanine: a clinical trial establishing the biochemical modulatory dose in tumor tissue for alkyltransferase-directed DNA repair. *Cancer Res.* **59**(10), 2402-2410.

(138) Schilsky, R. L., Dolan, M. E., Bertucci, D., Ewesuedo, R. B., Vogelzang, N. J., Mani, S., Wilson, L. R., and Ratain, M. J. (2000) Phase I clinical and pharmacological study of O6-benzylguanine followed by carmustine in patients with advanced cancer. *Clin. Cancer Res.* **6**(8), 3025-3031.

(139) Friedman, H. S., Kokkinakis, D. M., Pluda, J., Friedman, A. H., Cokgor, I., Haglund, M. M., Ashley, D. M., Rich, J., Dolan, M. E., Pegg, A. E., Moschel, R. C., McLendon, R. E., Kerby, T., Herndon, J. E., Bigner, D. D., and Schold, S. C., Jr. (1998) Phase I trial of O6-benzylguanine for patients undergoing surgery for malignant glioma. *J. Clin. Oncol.* **16**(11), 3570-3575.

(140) Dolan, M. E., Roy, S. K., Fasanmade, A. A., Paras, P. R., Schilsky, R. L., and Ratain, M. J. (1998) O6-benzylguanine in humans: metabolic, pharmacokinetic, and pharmacodynamic findings. *J. Clin. Oncol.* **16**(5), 1803-1810.

(141) Long, L., and Dolan, M. E. (2001) Role of cytochrome P450 isoenzymes in metabolism of O(6)-benzylguanine: implications for dacarbazine activation. *Clin. Cancer Res.* **7**(12), 4239-4244.

(142) Friedman, H. S., Pluda, J., Quinn, J. A., Ewesuedo, R. B., Long, L., Friedman, A. H., Cokgor, I., Colvin, O. M., Haglund, M. M., Ashley, D. M., Rich, J. N., Sampson, J., Pegg, A. E., Moschel, R. C., McLendon, R. E., Provenzale, J. M., Stewart, E. S., Tourt-Uhlig, S., Garcia-Turner, A. M., Herndon, J. E., Bigner, D. D., and Dolan, M. E. (2000) Phase I trial of carmustine plus O6-benzylguanine for patients with recurrent or progressive malignant glioma. *J. Clin. Oncol.* **18**(20), 3522-3528.

(143) Reese, J. S., Qin, X., Ballas, C. B., Sekiguchi, M., and Gerson, S. L. (2001) MGMT expression in murine bone marrow is a major determinant of animal survival after alkylating agent exposure. *J. Hematother. Stem Cell Res.* **10**(1), 115-123.

(144) Crone, T. M., Kanugula, S., and Pegg, A. E. (1995) Mutations in the Ada O6-alkylguanine-DNA alkyltransferase conferring sensitivity to inactivation by O6-benzylguanine and 2,4-diamino-6-benzyloxy-5-nitrosopyrimidine. *Carcinogenesis* **16**(8), 1687-1692.

(145) Loktionova, N. A., and Pegg, A. E. (1996) Point mutations in human O6-alkylguanine-DNA alkyltransferase prevent the sensitization by O6-benzylguanine to killing by N,N'-bis (2-chloroethyl)-N-nitrosourea. *Cancer Res.* **56**(7), 1578-1583.

(146) Davis, B. M., Koc, O. N., and Gerson, S. L. (2000) Limiting numbers of G156A O(6)-methylguanine-DNA methyltransferase-transduced marrow progenitors repopulate nonmyeloablated mice after drug selection. *Blood* **95**(10), 3078-3084.

(147) Kreklau, E. L., Pollok, K. E., Bailey, B. J., Liu, N., Hartwell, J. R., Williams, D. A., and Erickson, L. C. (2003) Hematopoietic expression of O(6)-methylguanine DNA methyltransferase-P140K allows intensive treatment of human glioma xenografts with combination O(6)-benzylguanine and 1,3-bis-(2-chloroethyl)-1-nitrosourea. *Mol. Cancer Ther.* **2**(12), 1321-1329.

(148) Zielske, S. P., and Gerson, S. L. (2002) Lentiviral transduction of P140K MGMT into human CD34(+) hematopoietic progenitors at low multiplicity of infection confers significant resistance to BG/BCNU and allows selection in vitro. *Mol. Ther.* **5**(4), 381-387.

(149) Zielske, S. P., Reese, J. S., Lingas, K. T., Donze, J. R., and Gerson, S. L. (2003) In vivo selection of MGMT(P140K) lentivirus-transduced human NOD/SCID repopulating cells without pretransplant irradiation conditioning. *J. Clin. Invest* **112**(10), 1561-1570.

(150) Ragg, S., Xu-Welliver, M., Bailey, J., D'Souza, M., Cooper, R., Chandra, S., Seshadri, R., Pegg, A. E., and Williams, D. A. (2000) Direct reversal of DNA damage by mutant methyltransferase protein protects mice against dose-intensified chemotherapy and leads to in vivo selection of hematopoietic stem cells. *Cancer Res.* **60**(18), 5187-5195.

(151) Bowman, J. E., Reese, J. S., Lingas, K. T., and Gerson, S. L. (2003) Myeloablation is not required to select and maintain expression of the drug-resistance gene, mutant MGMT, in primary and secondary recipients. *Mol. Ther.* **8**(1), 42-50.

(152) Koc, O. N., Reese, J. S., Davis, B. M., Liu, L., Majczenko, K. J., and Gerson, S. L. (1999) DeltaMGMT-transduced bone marrow infusion increases tolerance to O6-benzylguanine and 1,3-bis(2-chloroethyl)-1-nitrosourea and allows intensive therapy of 1,3-bis(2-chloroethyl)-1-nitrosourea-resistant human colon cancer xenografts. *Hum. Gene Ther.* **10**(6), 1021-1030.

(153) Liu, L., Pegg, A. E., Williams, K. M., and Guengerich, F. P. (2002) Paradoxical enhancement of the toxicity of 1,2-dibromoethane by O6-alkylguanine-DNA alkyltransferase. *J. Biol. Chem.* **277**(40), 37920-37928.

(154) Valadez, J. G., Liu, L., Loktionova, N. A., Pegg, A. E., and Guengerich, F. P. (2004) Activation of bis-electrophiles to mutagenic conjugates by human O6-alkylguanine-DNA alkyltransferase. *Chem. Res. Toxicol.* **17**(7), 972-982.

(155) Federwisch, M., Hassiepen, U., Bender, K., Dewor, M., Rajewsky, M. F., and Wollmer, A. (1997) Recombinant human O^6-alkylguanine-DNA alkyltransferase (AGT), Cys145-alkylated AGT and Cys145 --> Met145 mutant AGT: comparison by isoelectric focusing, CD and time-resolved fluorescence spectroscopy. *Biochem. J.* **324 (Pt 1)**, 321-328.

(156) Dolan, M. E., Pegg, A. E., Biser, N. D., Moschel, R. C., and English, H. F. (1993) Effect of O6-benzylguanine on the response to 1,3-bis(2-chloroethyl)-1-nitrosourea in the Dunning R3327G model of prostatic cancer. *Cancer Chemother. Pharmacol.* **32**(3), 221-225.

(157) Dolan, M. E., Mitchell, R. B., Mummert, C., Moschel, R. C., and Pegg, A. E. (1991) Effect of O6-benzylguanine analogues on sensitivity of human tumor cells to the cytotoxic effects of alkylating agents. *Cancer Res.* **51**(13), 3367-3372.

(158) Wanner, M. J., Koch, M., and Koomen, G. J. (2004) Synthesis and antitumor activity of methyltriazene prodrugs simultaneously releasing DNA-methylating agents and the antiresistance drug O(6)-benzylguanine. *J. Med. Chem.* **47**(27), 6875-6883.

(159) Guengerich, F. P. (2005) Principles of covalent binding of reactive metabolites and examples of activation of bis-electrophiles by conjugation. *Arch. Biochem. Biophys.* **433**(2), 369-378.

(160) Melnick, R. L., and Kohn, M. C. (1995) Mechanistic data indicate that 1,3-butadiene is a human carcinogen. *Carcinogenesis* **16**(2), 157-163.

(161) Rice, J. M., and Boffetta, P. (2001) 1,3-Butadiene, isoprene and chloroprene: reviews by the IARC monographs programme, outstanding issues, and research priorities in epidemiology. *Chem. Biol. Interact.* **135-136**, 11-26.

(162) Himmelstein, M. W., Turner, M. J., Asgharian, B., and Bond, J. A. (1996) Metabolism of 1,3-butadiene: inhalation pharmacokinetics and tissue dosimetry of butadiene epoxides in rats and mice. *Toxicology* **113**(1-3), 306-309.

(163) Krause, R. J., and Elfarra, A. A. (1997) Oxidation of butadiene monoxide to meso- and (+/-)-diepoxybutane by cDNA-expressed human cytochrome P450s and by mouse, rat, and human liver microsomes: evidence for preferential hydration of meso-diepoxybutane in rat and human liver microsomes. *Arch. Biochem. Biophys.* **337**(2), 176-184.

(164) Henderson, R. F., Thornton-Manning, J. R., Bechtold, W. E., and Dahl, A. R. (1996) Metabolism of 1,3-butadiene: species differences. *Toxicology* **113**(1-3), 17-22.

(165) Jelitto, B., Vangala, R. R., and Laib, R. J. (1989) Species differences in DNA damage by butadiene: role of diepoxybutane. *Arch. Toxicol. Suppl.* **13**, 246-249.

(166) Liu, L., Xu-Welliver, M., Kanugula, S., and Pegg, A. E. (2002) Inactivation and degradation of O^6-alkylguanine-DNA alkyltransferase after reaction with nitric oxide. *Cancer Res.* **62**(11), 3037-3043.

(167) Edara, S., Kanugula, S., Goodtzova, K., and Pegg, A. E. (1996) Resistance of the human O6-alkylguanine-DNA alkyltransferase containing arginine at codon 160 to inactivation by O6-benzylguanine. *Cancer Res.* **56**(24), 5571-5575.

(168) Sambrook, J., Fritsch, E. F., and Maniatis, T. *Molecular Cloning: A Laboratory Manual* (1989) Cold Spring Harbor Press.

(169) Tretyakova, N. Y., Sangaiah, R., Yen, T. Y., and Swenberg, J. A. (1997) Synthesis, characterization, and *in vitro* quantitation of N-7-guanine adducts of diepoxybutane. *Chem. Res. Toxicol.* **10**(7), 779-785.

(170) Rajski, S. R., and Williams, R. M. (1998) DNA Cross-Linking Agents as Antitumor Drugs. *Chem Rev.* **98**(8), 2723-2796.

(171) Osborne, M. R., and Lawley, P. D. (1993) Alkylation of DNA by melphalan with special reference to adenine derivatives and adenine-guanine cross-linking. *Chem. Biol. Interact.* **89**(1), 49-60.

(172) Copeland, K. D., Lueras, A. M., Stemp, E. D., and Barton, J. K. (2002) DNA cross-linking with metallointercalator-peptide conjugates. *Biochemistry* **41**(42), 12785-12797.

(173) Kurbanyan, K., Nguyen, K. L., To, P., Rivas, E. V., Lueras, A. M., Kosinski, C., Steryo, M., Gonzalez, A., Mah, D. A., and Stemp, E. D. (2003) DNA-protein cross-linking via guanine oxidation: dependence upon protein and photosensitizer. *Biochemistry* **42**(34), 10269-10281.

(174) Javanmard, S., Loktionova, N. A., Fang, Q., Pauly, G. T., Pegg, A. E., and Moschel, R. C. (2007) Inactivation of O(6)-Alkylguanine-DNA Alkyltransferase by Folate Esters of O(6)-Benzyl-2'-deoxyguanosine and of O(6)-[4-(Hydroxymethyl)benzyl]guanine. *J. Med. Chem.* **50**(21), 5193-5201.

(175) Chemotherapy of Malignant Tumors (1995) In *Drug Actions: Basic Principles and Therapeutic Aspects* (Mutschler, E., and Derendorf, H., Eds.) pp 600-601, Medpharm Scientific Publishers, Stuttgart.

(176) Friedman, H. S., Pegg, A. E., Johnson, S. P., Loktionova, N. A., Dolan, M. E., Modrich, P., Moschel, R. C., Struck, R., Brent, T. P., Ludeman, S., Bullock, N., Kilborn, C., Keir, S., Dong, Q., Bigner, D. D., and Colvin, O. M. (1999) Modulation of cyclophosphamide activity by O6-alkylguanine-DNA alkyltransferase. *Cancer Chemother. Pharmacol.* **43**(1), 80-85.

(177) Cai, Y., Wu, M. H., Ludeman, S. M., Grdina, D. J., and Dolan, M. E. (1999) Role of O6-alkylguanine-DNA alkyltransferase in protecting against cyclophosphamide-induced toxicity and mutagenicity 1. *Cancer Res.* **59**(13), 3059-3063.

(178) Hansen R.J., Ludeman, S. M., Pegg, A. E., and Dolan, M. E. (2007) Role of MGMT in protecting against cyclophosphamide-Induced toxicity in cells and animals. *DNA Repair* **6**, 1145-1154.

(179) Preuss, I., Thust, R., and Kaina, B. (1996) Protective effect of O6-methylguanine-DNA methyltransferase (MGMT) on the cytotoxic and recombinogenic activity of different antineoplastic drugs. *Int. J. Cancer* **65**(4), 506-512.

(180) D'Incalci, M., Bonfanti, M., Pifferi, A., Mascellani, E., Tagliabue, G., Berger, D., and Fiebig, H. H. (1998) The antitumour activity of alkylating agents is not correlated with the levels of glutathione, glutathione transferase and O6-alkylguanine-DNA-alkyltransferase of human tumour xenografts. EORTC SPG and PAMM Groups. *Eur. J. Cancer* **34**(11), 1749-1755.

(181) Salmelin, C., Hovinen, J., and Vilpo, J. (2000) Polymyxin permeabilization as a tool to investigate cytotoxicity of therapeutic aromatic alkylators in DNA repair-deficient Escherichia coli strains. *Mutat. Res.* **467**(2), 129-138.

(182) Hansen R.J., Nagasubramanian, R., Delaney, S. M., Samson, L. D., and Dolan, M. E. (2007) Role of O6-methylguanine-DNA methyltransferase in protecting from alkylating agent-induced toxicity and mutations in mice. *Carcinogenesis* **28**(5), 1111-1116.

(183) Cai, Y., Wu, M. H., Xu-Welliver, M., Pegg, A. E., Ludeman, S. M., and Dolan, M. E. (2000) Effect of O^6-benzylguanine on alkylating agent-induced toxicity and mutagenicity in Chinese hamster ovary cells expressing wild-type and mutant O^6-alkylguanine-DNA alkyltransferases. *Cancer Res.* **60**(19), 5464-5469.

(184) Jessberger, R., and Berg, P. (1991) Repair of deletions and double-strand gaps by homologous recombination in a mammalian in vitro system. *Mol. Cell Biol.* **11**(1), 445-457.

(185) Bradford, M. M. (1976) A rapid and sensitive method for the quantitation of microgram quantities of protein utilizing the principle of protein-dye binding. *Anal. Biochem.* **72**(1-2), 248-257.

(186) Shin, N. Y., Liu, Q., Stamer, S. L., and Liebler, D. C. (2007) Protein targets of reactive electrophiles in human liver microsomes. *Chem. Res. Toxicol.* **20**(6), 859-867.

(187) Gerson, S. L., Trey, J. E., Miller, K., and Berger, N. A. (1986) Comparison of O6-alkylguanine-DNA alkyltransferase activity based on cellular DNA content in human, rat and mouse tissues. *Carcinogenesis* **7**(5), 745-749.

(188) Gerson, S. L., Berger, N. A., Arce, C., Petzold, S. J., and Willson, J. K. (1992) Modulation of nitrosourea resistance in human colon cancer by O6-methylguanine. *Biochem. Pharmacol.* **43**(5), 1101-1107.

(189) Gerson, S. L., and Willson, J. K. (1995) O6-alkylguanine-DNA alkyltransferase. A target for the modulation of drug resistance. *Hematol. Oncol. Clin. North Am.* **9**(2), 431-450.

(190) Grillari, J., Katinger, H., and Voglauer, R. (2007) Contributions of DNA interstrand cross-links to aging of cells and organisms. *Nucleic Acids Res.* **35**(22), 7566-7576.

(191) Akkari, Y. M., Bateman, R. L., Reifsteck, C. A., Olson, S. B., and Grompe, M. (2000) DNA replication is required To elicit cellular responses to psoralen-induced DNA interstrand cross-links. *Mol. Cell Biol.* **20**(21), 8283-8289.

(192) Pegg, A. E. (1990) Properties of mammalian O^6-alkylguanine-DNA transferases. *Mutat. Res.* **233**(1-2), 165-175.

(193) Dolan, M. E., McRae, B. L., Ferries-Rowe, E., Belanich, M., van Seventer, G. A., Guitart, J., Pezen, D., Kuzel, T. M., and Yarosh, D. B. (1999) O6-alkylguanine-DNA alkyltransferase in cutaneous T-cell lymphoma: implications for treatment with alkylating agents. *Clin. Cancer Res.* **5**(8), 2059-2064.

(194) Freshney, R. I. *Culture of animal cells; a manual of basic techniques* (1994) John Wiley and Sons, Inc., Hoboken.

(195) Stout, J. T., and Caskey, C. T. (1985) HPRT: gene structure, expression, and mutation. *Annu. Rev. Genet.* **19**, 127-148.

(196) Nelson, J. A., Carpenter, J. W., Rose, L. M., and Adamson, D. J. (1975) Mechanisms of action of 6-thioguanine, 6-mercaptopurine, and 8-azaguanine. *Cancer Res.* **35**(10), 2872-2878.

(197) Cole, P. D., Drachtman, R. A., Smith, A. K., Cate, S., Larson, R. A., Hawkins, D. S., Holcenberg, J., Kelly, K., and Kamen, B. A. (2005) Phase II trial of oral aminopterin for adults and children with refractory acute leukemia. *Clin. Cancer Res.* **11**(22), 8089-8096.

(198) Shiraishi, A., Sakumi, K., and Sekiguchi, M. (2000) Increased susceptibility to chemotherapeutic alkylating agents of mice deficient in DNA repair methyltransferase. *Carcinogenesis* **21**(10), 1879-1883.

(199) Glassner, B. J., Weeda, G., Allan, J. M., Broekhof, J. L., Carls, N. H., Donker, I., Engelward, B. P., Hampson, R. J., Hersmus, R., Hickman, M. J., Roth, R. B., Warren, H. B., Wu, M. M., Hoeijmakers, J. H., and Samson, L. D. (1999) DNA repair methyltransferase (Mgmt) knockout mice are sensitive to the lethal effects of chemotherapeutic alkylating agents. *Mutagenesis* **14**(3), 339-347.

(200) Zhang, B., Chambers, M. C., and Tabb, D. L. (2007) Proteomic parsimony through bipartite graph analysis improves accuracy and transparency. *J. Proteome. Res.* **6**(9), 3549-3557.

(201) Waterborg, J. H. (2001) Dynamics of histone acetylation in *Saccharomyces cerevisiae*. *Biochemistry* **40**(8), 2599-2605.

(202) Karaczyn, A. A., Golebiowski, F., and Kasprzak, K. S. (2005) Truncation, deamidation, and oxidation of histone H2B in cells cultured with nickel(II). *Chem. Res. Toxicol.* **18**(12), 1934-1942.

(203) Miller, C. A., III, Cohen, M. D., and Costa, M. (1991) Complexing of actin and other nuclear proteins to DNA by cis-diamminedichloroplatinum(II) and chromium compounds. *Carcinogenesis* **12**(2), 269-276.

(204) Coulombe, R. A., Jr., Drew, G. L., and Stermitz, F. R. (1999) Pyrrolizidine alkaloids crosslink DNA with actin. *Toxicol. Appl. Pharmacol.* **154**(2), 198-202.

(205) Zhao, K., Wang, W., Rando, O. J., Xue, Y., Swiderek, K., Kuo, A., and Crabtree, G. R. (1998) Rapid and phosphoinositol-dependent binding of the SWI/SNF-like BAF complex to chromatin after T lymphocyte receptor signaling. *Cell* **95**(5), 625-636.

(206) Mitsuzawa, H., Kimura, M., Kanda, E., and Ishihama, A. (2005) Glyceraldehyde-3-phosphate dehydrogenase and actin associate with RNA polymerase II and interact with its Rpb7 subunit. *FEBS Lett.* **579**(1), 48-52.

(207) Tarze, A., Deniaud, A., Le, B. M., Maillier, E., Molle, D., Larochette, N., Zamzami, N., Jan, G., Kroemer, G., and Brenner, C. (2007) GAPDH, a novel regulator of the pro-apoptotic mitochondrial membrane permeabilization. *Oncogene* **26**(18), 2606-2620.

(208) Hara, M. R., Agrawal, N., Kim, S. F., Cascio, M. B., Fujimuro, M., Ozeki, Y., Takahashi, M., Cheah, J. H., Tankou, S. K., Hester, L. D., Ferris, C. D., Hayward, S. D., Snyder, S. H., and Sawa, A. (2005) S-nitrosylated GAPDH initiates apoptotic cell death by nuclear translocation following Siah1 binding. *Nat. Cell Biol.* **7**(7), 665-674.

(209) Zheng, L., Roeder, R. G., and Luo, Y. (2003) S phase activation of the histone H2B promoter by OCA-S, a coactivator complex that contains GAPDH as a key component. *Cell* **114**(2), 255-266.

(210) Tisdale, E. J., and Artalejo, C. R. (2007) A GAPDH mutant defective in Src-dependent tyrosine phosphorylation impedes Rab2-mediated events. *Traffic.* **8**(6), 733-741.

(211) Erard, M. S., Belenguer, P., Caizergues-Ferrer, M., Pantaloni, A., and Amalric, F. (1988) A major nucleolar protein, nucleolin, induces chromatin decondensation by binding to histone H1. *Eur. J. Biochem.* **175**(3), 525-530.

(212) Chen, D. J., Park, M. S., Campbell, E., Oshimura, M., Liu, P., Zhao, Y., White, B. F., and Siciliano, M. J. (1992) Assignment of a human DNA double-strand break repair gene (XRCC5) to chromosome 2. *Genomics* **13**(4), 1088-1094.

(213) Taccioli, G. E., Gottlieb, T. M., Blunt, T., Priestley, A., Demengeot, J., Mizuta, R., Lehmann, A. R., Alt, F. W., Jackson, S. P., and Jeggo, P. A. (1994) Ku80: product of the XRCC5 gene and its role in DNA repair and V(D)J recombination. *Science* **265**(5177), 1442-1445.

(214) Tuteja, N., Tuteja, R., Ochem, A., Taneja, P., Huang, N. W., Simoncsits, A., Susic, S., Rahman, K., Marusic, L., Chen, J., and . (1994) Human DNA helicase II: a novel DNA unwinding enzyme identified as the Ku autoantigen. *EMBO J.* **13**(20), 4991-5001.

(215) Nguewa, P. A., Fuertes, M. A., Valladares, B., Alonso, C., and Perez, J. M. (2005) Poly(ADP-ribose) polymerases: homology, structural domains and functions. Novel therapeutical applications. *Prog. Biophys. Mol. Biol.* **88**(1), 143-172.

(216) Jagtap, P., and Szabo, C. (2005) Poly(ADP-ribose) polymerase and the therapeutic effects of its inhibitors. *Nat. Rev. Drug Discov.* **4**(5), 421-440.

(217) Demple, B., and Harrison, L. (1994) Repair of oxidative damage to DNA: enzymology and biology. *Annu. Rev. Biochem.* **63**, 915-948.

(218) Levin, J. D., and Demple, B. (1990) Analysis of class II (hydrolytic) and class I (beta-lyase) apurinic/apyrimidinic endonucleases with a synthetic DNA substrate. *Nucleic Acids Res.* **18**(17), 5069-5075.

(219) Xanthoudakis, S., and Curran, T. (1996) Redox regulation of AP-1: a link between transcription factor signaling and DNA repair. *Adv. Exp. Med. Biol.* **387**, 69-75.

(220) Beernink, P. T., Segelke, B. W., Hadi, M. Z., Erzberger, J. P., Wilson, D. M., III, and Rupp, B. (2001) Two divalent metal ions in the active site of a new crystal form of human apurinic/apyrimidinic endonuclease, Ape1: implications for the catalytic mechanism. *J. Mol. Biol.* **307**(4), 1023-1034.

(221) Marintchev, A., Mullen, M. A., Maciejewski, M. W., Pan, B., Gryk, M. R., and Mullen, G. P. (1999) Solution structure of the single-strand break repair protein XRCC1 N-terminal domain. *Nat. Struct. Biol.* **6**(9), 884-893.

(222) Kalapila, A. G., Loktionova, N. A., and Pegg, A. E. (2008) Alkyltransferase-mediated toxicity of 1,3-butadiene diepoxide. *Chem. Res. Toxicol.* **21**(9), 1851-1861.

(223) Vives, E., Brodin, P., and Lebleu, B. (1997) A truncated HIV-1 Tat protein basic domain rapidly translocates through the plasma membrane and accumulates in the cell nucleus. *J. Biol. Chem.* **272**(25), 16010-16017.

(224) Ruben, S., Perkins, A., Purcell, R., Joung, K., Sia, R., Burghoff, R., Haseltine, W. A., and Rosen, C. A. (1989) Structural and functional characterization of human immunodeficiency virus tat protein. *J. Virol.* **63**(1), 1-8.